Geological Society of America Memoirs

Framework and petrogenesis of the northern Peninsular Ranges batholith, southern California

D.M. Morton, F.K. Miller, R.W. Kistler, W.R. Premo, C-T.A. Lee, V.E. Langenheim, J.L. Wooden, L.W. Snee, B.L. Clausen and P. Cossette

Geological Society of America Memoirs 2014;211;61-143
doi: 10.1130/2014.1211(03)

The Geological Society of America
Memoir 211
2014

Framework and petrogenesis of the northern Peninsular Ranges batholith, southern California

D.M. Morton
U.S. Geological Survey and Department of Earth Sciences, University of California, Riverside, California 92521, USA

F.K. Miller
U.S. Geological Survey, Spokane, Washington 99201, USA

R.W. Kistler
U.S. Geological Survey, Menlo Park, California 94025, USA

W.R. Premo
U.S. Geological Survey, Denver, Colorado 80225, USA

C-T.A. Lee
Department of Earth Sciences, Rice University, Houston, Texas 77005, USA

V.E. Langenheim
U.S. Geological Survey, Menlo Park, California 94025, USA

J.L. Wooden
Department of Geological and Environmental Sciences, Stanford University, California 94305, USA

L.W. Snee
Global Gems and Minerals, Denver, Colorado 80235, USA

B.L. Clausen
Geoscience Research Institute and Department of Earth and Biological Sciences, Loma Linda University, Loma Linda, California 92350, USA

P. Cossette
U.S. Geological Survey, Spokane, Washington 99201, USA

Morton, D.M., Miller, F.K., Kistler, R.W., Premo, W.R., Lee, C-T.A., Langenheim, V.E., Wooden, J.L., Snee, L.W., Clausen, B.L., and Cossette, P., 2014, Framework and petrogenesis of the northern Peninsular Ranges batholith, southern California, *in* Morton, D.M., and Miller, F.K., eds., Peninsular Ranges Batholith, Baja California and Southern California: Geological Society of America Memoir 211, p. 61–143, doi:10.1130/2014.1211(03).

ABSTRACT

The Peninsular Ranges batholith north of latitude 33°N consists of five distinctive longitudinal batholith zones. Four zones are autochthonous—a western zone, western transition zone, eastern transition zone, and an eastern zone. The fifth zone, the upper-plate zone, is allochthonous. The western zone, western transition zone, eastern transition zone, and eastern zone are contiguous products of Cretaceous subduction transitioning from a Mesozoic oceanic-arc setting to continental margin arc setting. Within the autochthonous zones, the nature and geochemistry of plutons record changes reflecting subduction proceeding from west to east over a 35 m.y. period. The allochthonous upper-plate zone is structurally located above the regional Eastern Peninsular Ranges mylonite zone. Host rocks for the western zone, western transition zone, and eastern transition zone are mostly Mesozoic, and host rocks of the eastern zone are Paleozoic. The composition of the plutons reflects changes in magma originating in shallow oceanic crust in the western zone to a deeper continental marginal setting in the eastern zone and upper-plate zone. Several aspects of the upper-plate zone rocks set them apart from the autochthonous batholithic rocks.

Western zone magmatism occurred during an extensional subduction phase that involved Mesozoic oceanic crust. Plutons were emplaced passively from 126 Ma to 108 Ma, forming 47.9% of the area of the autochthonous batholith at a rate of 2.7% per million years. Geochemical variation is greater in the western zone than it is in the other zones. Rock compositions range from gabbro to high-SiO_2 granites; plutons in this zone contain magnetite as an accessory mineral. Most plutonic rocks have initial $^{87}Sr/^{86}Sr$ (Sr_i) values <0.7045, initial $^{206}Pb/^{204}Pb$ (Pb_i) <19, $\delta^{18}O$ <9‰, and positive initial epsilon Nd (ε_{Ndi}).

By 111 Ma, conditions for pluton emplacement began to change radically from extensional to compressional as subduction encountered older continental crust. The boundary between the western zone and western transition zone is marked clearly by a change in the magnetic properties, which are highly magnetic in the western zone to weakly magnetic in the transition zones. Western transition zone plutons, which have affinities with the western zone plutons, constitute 13.5% by area of the autochthonous batholith and formed over 13 m.y. at a decreased rate of batholith formation, 1% per million years. Plutons of the western transition zone are characterized by Sr_i values of 0.7045–0.7050, $\delta^{18}O$ <9‰, and positive ε_{Ndi}. Deformation of the prebatholithic rocks was intense at 100 Ma, as the plutonism of the western transition zone ended and emplacement in the eastern transition zone began. From 99 to 93 Ma, the rate of magma emplacement accelerated, forming 2.4% per million years by area of the northern part of the autochthonous batholith. The eastern transition zone plutons, having affinities with the eastern zone plutons, have Sr_i values of 0.7051–0.7057, $\delta^{18}O$ >9‰, and negative ε_{Ndi}. Most eastern transition zone plutons were emplaced in a less dynamic setting than the western transition zone plutons.

By 98 Ma, subduction had transitioned eastward as plutons were emplaced in continental crust. The rate of magma emplacement increased to form the eastern zone over 7 m.y., or a rate of batholith growth of 3.4% per million years by area. There is considerable temporal overlap in the magma emplacement of the eastern transition zone and the eastern zone. Combined eastern transition zone and eastern zone magmatism produced 39% (by area) of the autochthonous batholith in 8 m.y. at a rate of ~5% per million years. The 102 Ma gabbro body is not considered in this analysis. Eastern zone plutons are characterized by Sr_i >0.7060, mostly in the range of 0.7061–0.7076, Pb_i >19, $\delta^{18}O$ >9‰, and a large negative ε_{Ndi}.

The allochthonous granitic sheets that constitute the upper-plate zone include batholithic rocks ranging in age from 92 to 75 Ma; most are in the range of 86–75 Ma. These granitic rocks have a more restricted range of geochemistry than those in the other zones; they are magnetite-bearing rocks, unlike the ilmenite-bearing granitic

rocks of the transition zones and eastern zone, and they have large negative ε_{Ndi}, and Sr_i in the range of 0.7076–0.7084. During the Late Cretaceous, the Eastern Peninsular Ranges mylonite zone developed in the eastern part of the Peninsular Ranges Province, deforming granitic rocks of the eastern part of the eastern zone. Following mylonitization, westward displacement on a series of low-angle thrust faults placed sheets of metamorphic and plutonic rock above the Eastern Peninsular Ranges mylonite zone, forming the upper-plate zone.

Compatible elements decrease west to east across the batholith, and incompatible elements increase. Geochemical variation shows that magma forming the western part of the batholith had a shallow and primitive source compared with the eastern part, which had a deeper and more-evolved continental component. The frequency distribution of Sr_i in the batholith is bimodal, having a peak of 0.7038 in the western zone, reflecting the oceanic crustal source, and a peak of 0.7072 in the eastern zone, reflecting increased incorporated continental crust sources. Only a small part of the batholith has Sr_i values between 0.7055 and 0.7065, indicating a relatively sharp boundary between oceanic and continental crust. Linear arrays on Harker diagram indicate that geochemical variation within the batholith is from magma mixing and not magmatic differentiation. Our data are most simply explained by the Cretaceous arc transitioning from a Mesozoic oceanic-arc setting to a continental margin setting.

INTRODUCTION

The Mesozoic Sierra Nevada and Peninsular Ranges batholiths of California and Baja California are considered stereotypic examples of subduction-related magmatism. Large numbers of papers have interpreted various segments of the Cretaceous batholiths in plate-tectonic models (e.g., Bateman, 1992; Busby, 2004; papers in Johnson et al., 2003; Lackey et al., 2012; Silver and Chappell, 1988; Wenner and Coleman, 2004). Here, detailed field and analytical data are presented for a geologic transect across the northern part of the Cretaceous Peninsular Ranges batholith, primarily for the area north of latitude 33°30′N (Fig. 1). In addition to field and analytical data, the transect study includes descriptions of both prebatholithic and batholithic rocks. Regional geochemical and potential field data extend south to 33°N (Fig. 2 [available on the CD-ROM accompanying this volume and in the GSA Data Repository[1]), coinciding with the northern boundary of the geologic transect described by Todd et al. (2003). Our isotopic data set south of latitude 33°30′N is not as complete as it is to the north. In addition to the general features of the batholith, several individual plutons, considered characteristic of various parts of the batholith, are described. The various data sets are interpreted in a subduction magmatic model.

Unless otherwise cited, detailed geologic maps of prebatholithic rock bodies and individual plutons are by D.M. Morton. Regional geochemical and isotope data are from systematically collected samples of the late A.K. Baird and E.E. Welday, Pomona College, California (Baird et al., 1974, 1979; Baird and Miesch, 1984), augmented with 60 samples from selected parts of the batholith where greater detail was needed. The Baird samples are all composite samples collected on a predesigned and tested grid to mitigate heterogeneity and sampling bias at individual sample sites; the augmented samples are single rock samples. The sampling method used by Baird and Welday is described in the Appendix. These systematically collected samples allow an

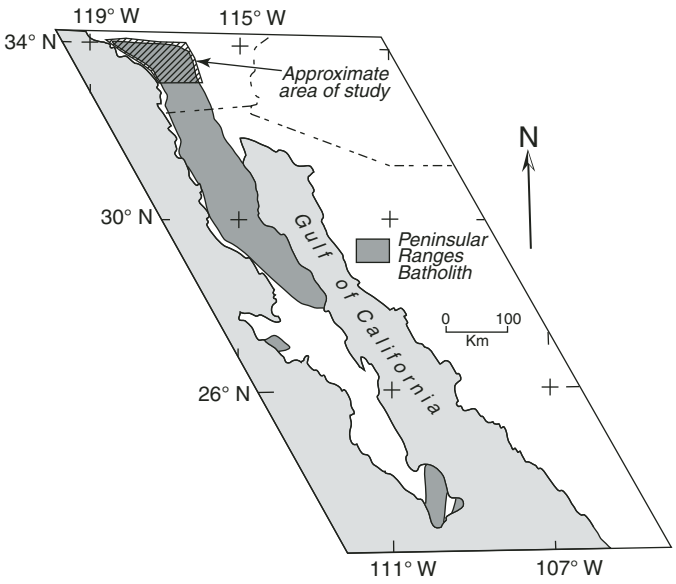

Figure 1. Index map of the Peninsular Ranges batholith; cross-ruled area shows outline of the northern part of the batholith covered in this paper.

[1]GSA Data Repository Item 2014040—Table 2: Major oxides and trace elements of Northern Peninsular Ranges batholith; Table 5: Major oxides and trace elements of Box Springs plutonic complex; and detailed, enlargeable versions of Figures 2, 3, 18, and 68—is available at www.geosociety.org/pubs/ft2014.htm, or on request from editing@geosociety.org or Documents Secretary, GSA, P.O. Box 9140, Boulder, CO 80301-9140, USA.

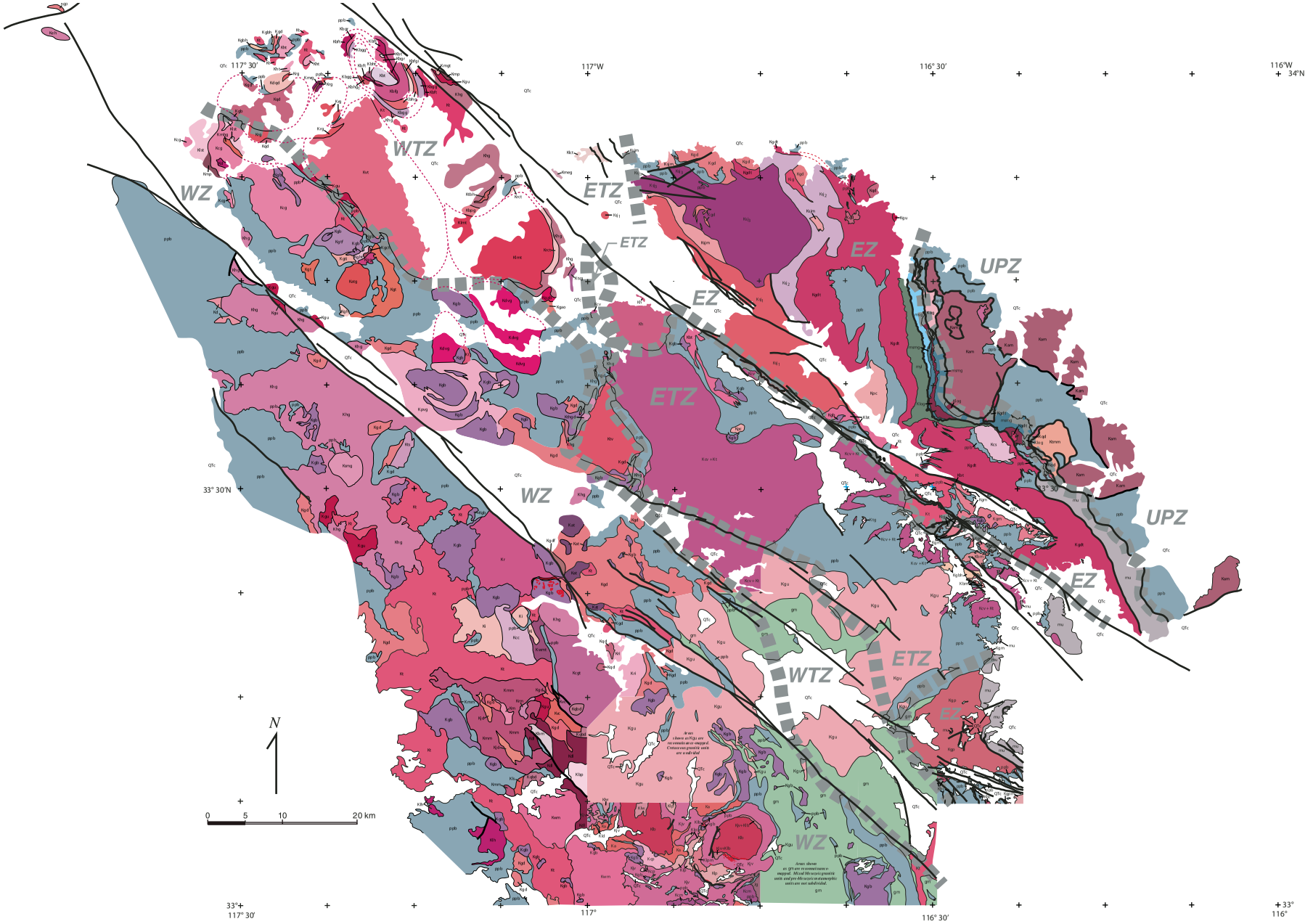

Figure 2. Generalized geologic map for the northern Peninsular Ranges batholith showing boundaries for the five batholith zones. Detailed version of this map and list of map units are on the accompanying CD-ROM (see text footnote 1). Compilation sources for the map are on the list of map units. WZ—western zone; WTZ—western transition zone; ETZ—eastern transition zone; EZ—eastern zone; UPZ—upper-plate zone.

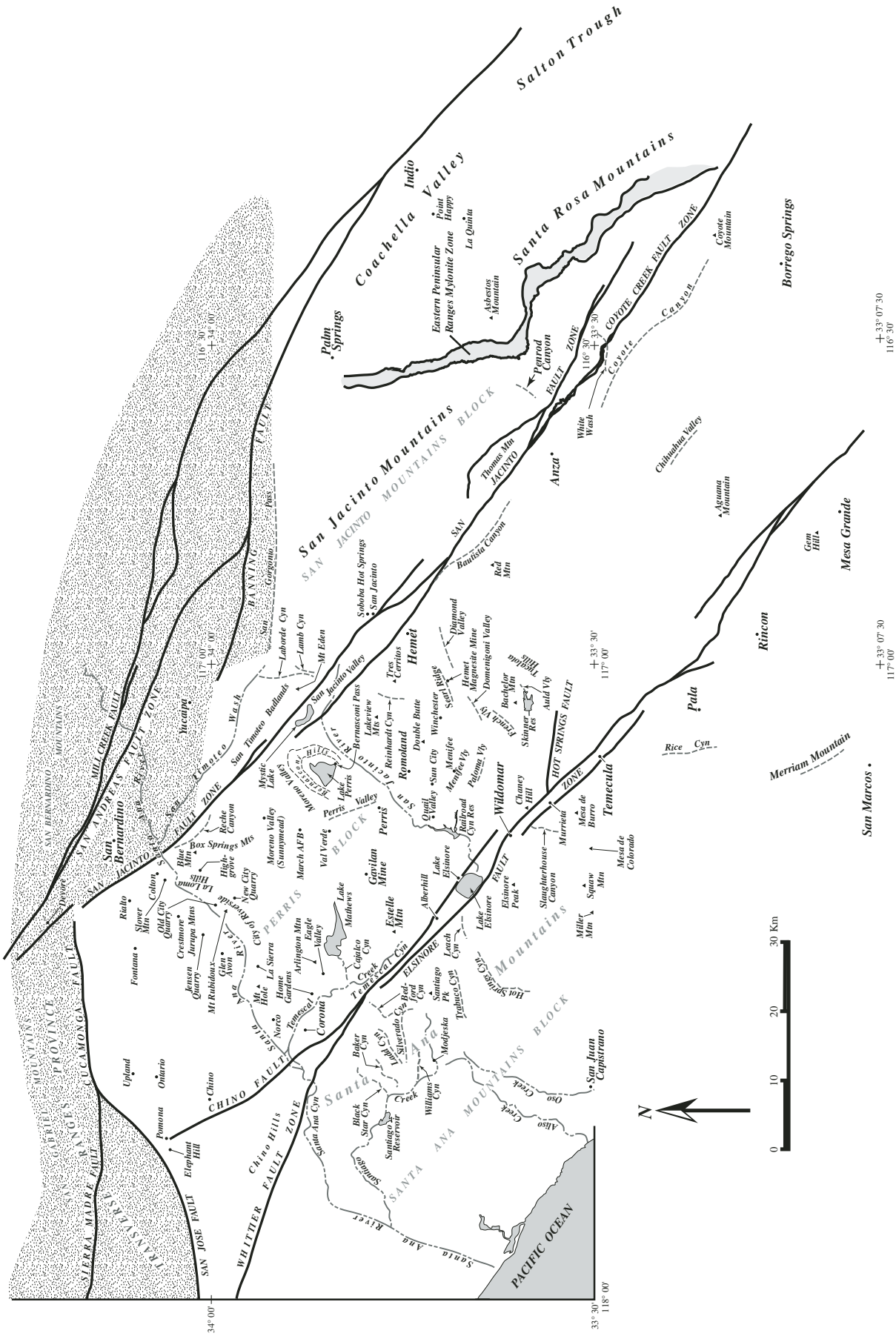

Figure 3. Map of the northern Peninsular Ranges showing locations and place names mentioned in the text. An enlargeable version is on accompanying CD-ROM (see text footnote 1). AFB—Air Force base; Vly—valley; Cyn—canyon; Res—Reservoir.

accurate quantitative estimation of the composition of this part of the Peninsular Ranges batholith. We know of no other batholith that has been sampled in such a complete and systematic fashion as the northern Peninsular Ranges batholith, thanks to the Baird-Welday collection.

All samples were analyzed in U.S. Geological Survey (USGS) laboratories, Denver, Colorado, using standard techniques. Major elements were analyzed by X-ray fluorescence analysis, and trace elements were analyzed by inductively coupled plasma mass spectrometry (ICP-MS) analysis. Major-element analyses were done by Dave Siems, and trace-element analyses were done by Fred Lichte and Jim Budahn.

U/Pb zircon and monazite ages, unless otherwise cited, were determined by W.R. Premo and J.L. Wooden. Isotope dilution U-Pb ages on zircons are indicated by the subscript "id," and ion probe ages are indicated with the subscript "ip." Premo et al. (this volume, Chapter 4) provide a detailed description and analytical data for ages cited here. Additional U-Pb zircon ages from gabbroic rocks are from D.L. Kimbrough, San Diego State University (2010, written commun.). Sr, Rb, Pb, and O isotope data are from R.W. Kistler, and J.L. Wooden (Kistler et al., 2003, this volume). Kistler et al. (2003, this volume) provide detailed analytical descriptions for Sr, Rb, Nd, Pb, and O isotopes and initial $^{87}Sr/^{86}Sr$ (Sr_i). Additional Sr and Rb isotopic data are from R.J. Fleck, U.S. Geological Survey (2011, written commun.). All Sr, Rb, Nd, Pb, and O isotopes and initial $^{87}Sr/^{86}Sr$ (Sr_i) values are whole-rock values. The $^{40}Ar/^{39}Ar$ data, unless otherwise indicated, are from L.W. Snee. Conventional K/Ar ages are from F.K. Miller, who gives detailed descriptions and analytical data in this volume (Miller et al., this volume). Conventional K/Ar, and $^{40}Ar/^{39}Ar$ ages of hornblende, biotite, and K-feldspar, with one exception, are interpreted as cooling ages. Also, unless otherwise indicated, hornblende geobarometry data are from D.K. Smith (Smith et al., 1991; Smith, 1991, written commun.). Locations of place names mentioned in the text are given in Figure 3.

We have subdivided the batholith into five zones. The subdivisions are defined on the basis of field characteristics, geochemistry, age, stable and radiogenic isotopes, and geophysics. Specific features and properties characterizing the zones are summarized in Figure 4. From west to east, these zones are (1) western zone, (2) western transition zone, (3) eastern transition zone, (4) eastern zone, and (5) upper-plate zone. The first four zones are autochthonous, and the fifth is allochthonous. Although each of these batholith zones is distinct from the others based on the above combination of properties, because of the transitional nature of the processes controlling batholith emplacement, in some cases there is overlap and/or gradation between zones. For example, north of 33°22′N, rock fabric is a key element used to distinguish the western zone from the western transition zone. Although most measured properties discussed in this report and

	Western Zone (WZ)	Western Transition Zone (WTZ)	Eastern Transition Zone (ETZ)	Eastern Zone (EZ)	Upper Plate Zone (UPZ)
Characteristic range of emplacement ages	126-108 Ma	109-98 Ma	96-93 Ma	98-91 Ma	85-75 Ma
Average emplacement age	115 Ma	103 Ma	95 Ma	96 Ma	84 Ma
Mode of emplacement	Passive	Dynamic	Dynamic	Dynamic	Unknown
Characteristic fabric	Isotropic	Well foliated	Moderately well foliated	Moderately well foliated	Well foliated
Mafic enclaves	Equidimensional	Thin discoidal to plate-like	Thin discoidal	Thin discoidal	Thin discoidal
Range of characteristic Sr_i	0.7032-0.7040	0.7045-0.7050	0.7050-0.7054	0.7060-0.7075	0.7077-0.7082
Average Sr_i	0.7039	0.7049	0.7053	0.7070	0.7079
Range of characteristic $^{206}Pb/^{204}Pb$	18.650-18.980	18.760-18.870	18.830-18.900	19.045-19.300	19.220-19.450
Average $^{206}Pb/^{204}Pb$	18.783	18.841	18.880	19.198	19.336
Range of characteristic $\delta^{18}O$	6.0-8.0	7.6-8.6	9.0-10.9	9.2-12.0	8.6-9.1
Average $\delta^{18}O$	6.97	8.11	9.74	10.22	8.73
Average εNd	2.9	1.7	-2.6	-2.8	-6.65
Potential field	Intensely magnetic	Nonmagnetic	Nonmagnetic	Nonmagnetic	Moderately magnetic
Depth of emplacement (kb)	2 to 3	4 to 6	4 to 5	4 to 4.5	6 to 6.5

Figure 4. Comparison of selected zone characteristics, listing features and properties that typify the five batholith zones.

used to define the zone boundaries are surface properties, some properties reflect depth within the batholith (e.g., aeromagnetic); this leads to some differences between the surface zone boundary and a parameter that reflects the boundary at depth (e.g., surface rock textures at the western zone–western transition zone boundary compared with aeromagnetic data that reflect conditions at 10 km depth).

In reporting results of their geochemical studies, Baird et al. (1979) subdivided the northern part of the batholith into three Pleistocene postbatholith structural blocks, which are, from west to east, the Santa Ana Mountains block, the Perris block, and the San Jacinto Mountains block. The Santa Ana Mountains and Perris blocks are separated by the Elsinore fault zone, and the Perris and San Jacinto Mountains blocks are separated by the San Jacinto fault zone. For descriptive and locational purposes, we recognize and utilize this structural subdivision scheme, which is independent of the fivefold scheme described herein based on geochemical, isotopic, and geophysical batholith criteria.

BATHOLITH SETTING

Introduction

The boundaries and the nature of the boundaries of the northern part of the Peninsular Ranges batholith, chiefly north of latitude 33°30′N, are extremely varied and complex, being in places intrusive, depositional, and structural. The Peninsular Ranges Province, and the included Peninsular Ranges batholith, is structurally terminated on the north by the Transverse Ranges Province (Fig. 3). At the present level of erosion, boundaries of the western part of the batholith in and west of the Santa Ana Mountains are both intrusive and depositional by overlapping younger sedimentary rocks. The eastern limit of batholith exposures includes intrusive contacts with metamorphic rocks in the eastern San Jacinto Mountains, and overlapping Quaternary and Tertiary sedimentary deposits of the western Coachella Valley and Salton Trough (Fig. 3).

The northwesternmost exposures of the batholith consist of a few isolated outcrops surrounded by sedimentary materials in the Pomona area (Fig. 3), 3 km south of an isolated exposure of Transverse Ranges Province granitic rocks (see Premo et al., this volume, Chapter 4). East of Pomona, in the Jurupa Mountains and Slover Mountain areas (Fig. 3), batholithic rocks occur in isolated but more extensive exposures. East of Riverside, the northern part of the batholith is covered by extensive Tertiary and Quaternary sedimentary deposits of the San Timoteo Badlands (Fig. 5) and San Gorgonio Pass. In the San Gorgonio Pass area, the northern part of the Peninsular Ranges batholith is structurally overridden by Transverse Ranges Province basement by displacement on the reverse San Gorgonio Pass faults (Morton and Matti, 1993). South and southeast of San Gorgonio Pass, Peninsular Ranges batholith rocks core the San Jacinto and Santa Rosa Mountains (Fig. 3).

In the Santa Monica Mountains, which are the southwestern part of the Transverse Ranges, both the plutonic and metamorphic rocks have affinities with Peninsular Ranges batholith rocks but not with plutonic and metamorphic rocks elsewhere in the Transverse Ranges (e.g., Miller and Morton, 1980). These Santa Monica Mountains basement rocks were probably detached during the mid-Tertiary from the western Peninsular Ranges Province basement. Although they were probably originally part of the Peninsular Ranges batholith, our field and analytical data are insufficient to evaluate them, and therefore they are not considered further here.

Host rocks for the Cretaceous batholith range in age from Jurassic to probably early Paleozoic and, in general, are increasingly older eastward across the Peninsular Ranges Province. Jurassic batholithic rocks, well documented farther south (e.g., Shaw et al., 2003), have not been confidently documented in this area by geochronology. However, based on high initial $^{87}Sr/^{86}Sr$ ratios and foliated fabric, some deformed plutonic rocks north of the city of San Jacinto in the central part of the northern Peninsular Ranges are undoubtedly Jurassic. These rocks are shown as gr-m on the Santa Ana 1:250,000 scale quadrangle (Rogers, 1965). Farther south, in the Palomar Mountain area (Fig. 3), two samples from the south-central part of the batholith have high initial $^{87}Sr/^{86}Sr$ (Sr_i) values of 0.7120 and 0.7133 (Kistler et al., 2003) and are undoubtedly Jurassic granitic rocks (Shaw et al., 2003). Even though Jurassic granitic rocks are well documented by isotopic dating south of the area sampled for this study, only the Cretaceous batholith is considered in this paper.

Foliation in prebatholithic metamorphic rocks is oriented northwest, except at the northern edge of the batholith and except for local deflections around some western transition zone, eastern transition zone, and eastern zone plutons. In the northern San Jacinto Mountains and the Jurupa Mountains–Riverside areas, foliation is oriented east-west. In the Jurupa Mountains, granitic rocks have two planar fabrics, an older northwest foliation and

Figure 5. Tonalite of Lamb Canyon and overlying Pliocene sediments of the San Timoteo Badlands, north end of Lamb Canyon.

a younger east-striking foliation (Morton, 2003a). The younger east-striking planar fabric lacks brittle or protoclastic textures and appears to have formed when the granitic rocks were still ductile. South of Riverside, tonalite in the northern part of the Val Verde pluton (Fig. 2) commonly has an older northwest-oriented planar fabric and a younger east to northeast planar fabric. Based on the widespread eastward-oriented planar fabrics in both prebatholithic and batholithic rocks of the north-central and northeastern parts of the Peninsular Ranges batholith, these areas may be approaching the northern termination of the entire batholith.

Paleozoic Prebatholithic Rocks

Metasedimentary rocks that include thick sections of marble and quartzite occur in the San Jacinto and Santa Rosa Mountains in the eastern part of the Peninsular Ranges batholith, and at the north end in the Riverside-Colton area. These rocks are considered to be Paleozoic based on general lithologic affinities with dated Paleozoic rocks further to the south in the Peninsular Ranges (Morton and Miller, 2006). The size and thickness of marble bodies are considerably greater than those in the Jacumba Mountains sequence. Ordovician conodonts have been recovered from similar carbonate rocks in the Coyote Mountains in western Imperial County (Dockum, 1982; Dockum and Miller, 1982; Miller and Dockum, 1983); in northern Baja California, Permian fossils have been found in similar carbonate rocks (Gastil and Miller, 1981). All of these marble and quartzite sections appear to differ in various ways from Paleozoic sections found north of the Peninsular Ranges in the Great Basin, Mojave Desert, and San Bernardino Mountains.

In the northern San Jacinto Mountains, west of the Eastern Peninsular Ranges mylonite zone, marble, quartzite, and schist sequences are commonly termed the Windy Point group, and in the southern San Jacinto Mountains, they are termed the Desert Divide group (e.g., Brown, 1968; Hill, 1984). These two groups of rocks are probably correlative; both include thick sections of quartzite and marble, interlayered with amphibolite-grade biotite schist and gneiss. Sillimanite-biotite schist is common, and garnet-sillimanite-biotite schist is less common. Corundum-biotite gneiss occurs very locally in the northern San Jacinto Mountains (Murdoch and Webb, 1942). Chemical analyses of both Desert Divide and Windy Point samples are given in Hill (1988b). East of the Eastern Peninsular Ranges mylonite zone, Erskine (1986a), following the usage of Miller (1946), termed metasedimentary rocks the Palm Canyon Complex for allochthonous rocks in the Palm Springs area. The intensely deformed metasedimentary rocks of the Palm Canyon Complex include marble bodies but appear to lack the quartzite sections of the Windy Point–Desert Divide groups.

Probable Paleozoic metasedimentary rocks in the Riverside-Colton area include biotite schist, gneiss, quartzite, calc-silicate rocks, and marble. Mineral assemblages are of mostly pyroxene hornfels facies, but include hornblende hornfels facies assemblages at Slover Mountain (Fig. 2). No fossils have been recovered from these rocks due to the high degree of metamorphism and penetrative deformation.

Most occurrences of these metasedimentary rocks in the Riverside-Colton area consist of two marble layers and an intervening silicate layer. Two thick marble layers separated by a section of schist occur at Slover Mountain (Fig. 6), Crestmore (Burnham, 1959), Jensen, and the Old City (Riverside) Quarries (Morton, 2003a; Morton and Cox, 2001a, 2001b), suggesting that the same sequence of rocks may occur at each locality. Although the marble and schist appear to be structurally simple, they are pervasively deformed (Figs. 7 and 8). At Slover Mountain, marble blocks occur in tonalite near a marble-tonalite contact, and locally tonalite has been emplaced along layering in the marble. The uniform orientation of lineations within the marble extends to the contact with the tonalite, indicating deformation was synchronous with the emplacement of the tonalite.

At the New City (Riverside) Quarry (Fig. 9), marble layers are separated by a section of meta-quartzite and pyroxenite. Boudins are common in the pyroxenite layers (Fig. 10), and discontinuous lenticular biotite-hornblende tonalite bodies are interleaved with the metasedimentary units. The marble consists of massive, coarse-grained to extremely coarse-grained calcite, calcite-dolomite, and predazzite marble. A wide variety of skarns is found in the contact zones between marble and plutonic rocks, including ludwigite-paigeite magnetite skarn. Oxygen isotope analyses of garnet and clinopyroxene skarn show high $\delta^{18}O$ values (7‰–11‰) in the New City Quarry skarns, indicating that magmatic fluids driving formation of the skarns were buffered to high-$\delta^{18}O$ values by the surrounding carbonates (J.S. Lackey, 2012, written commun.). Other examples of marble and thick quartzite units occur in the central Jurupa Mountains and the Glen Avon area (Fig. 3) (Morton, 2003a; Morton and Cox, 2001b).

In the Santa Rosa Mountains and southern and eastern San Jacinto Mountains areas, the Paleozoic metasedimentary rocks strike northwest, but in the northern San Jacinto Mountains, they veer westward. In the Jurupa Mountains and Glen Avon area, the foliation strikes west. Paleozoic rocks in the Santa Rosa and San Jacinto Mountains are located within the eastern part of the batholith, whereas those in the Jurupa Mountains and Glen Avon areas are located in the western part of the batholith. Restoration of strike-slip displacement on the San Jacinto fault closely aligns the Paleozoic rocks of the northern San Jacinto Mountains with those of the Riverside-Colton area. This alignment suggests major pre–105 Ma deformation and bending of the Paleozoic rocks from northwest to west orientation in this area.

Mesozoic and Paleozoic(?) Prebatholithic Rocks

Rocks of Jacumba Mountains

West of the Paleozoic rocks, there are discontinuous masses of schist and gneiss, minor quartzite, and marble containing local small masses of skarn, and amphibole- and pyroxene-bearing rocks. We interpret this assemblage to be the northward extension

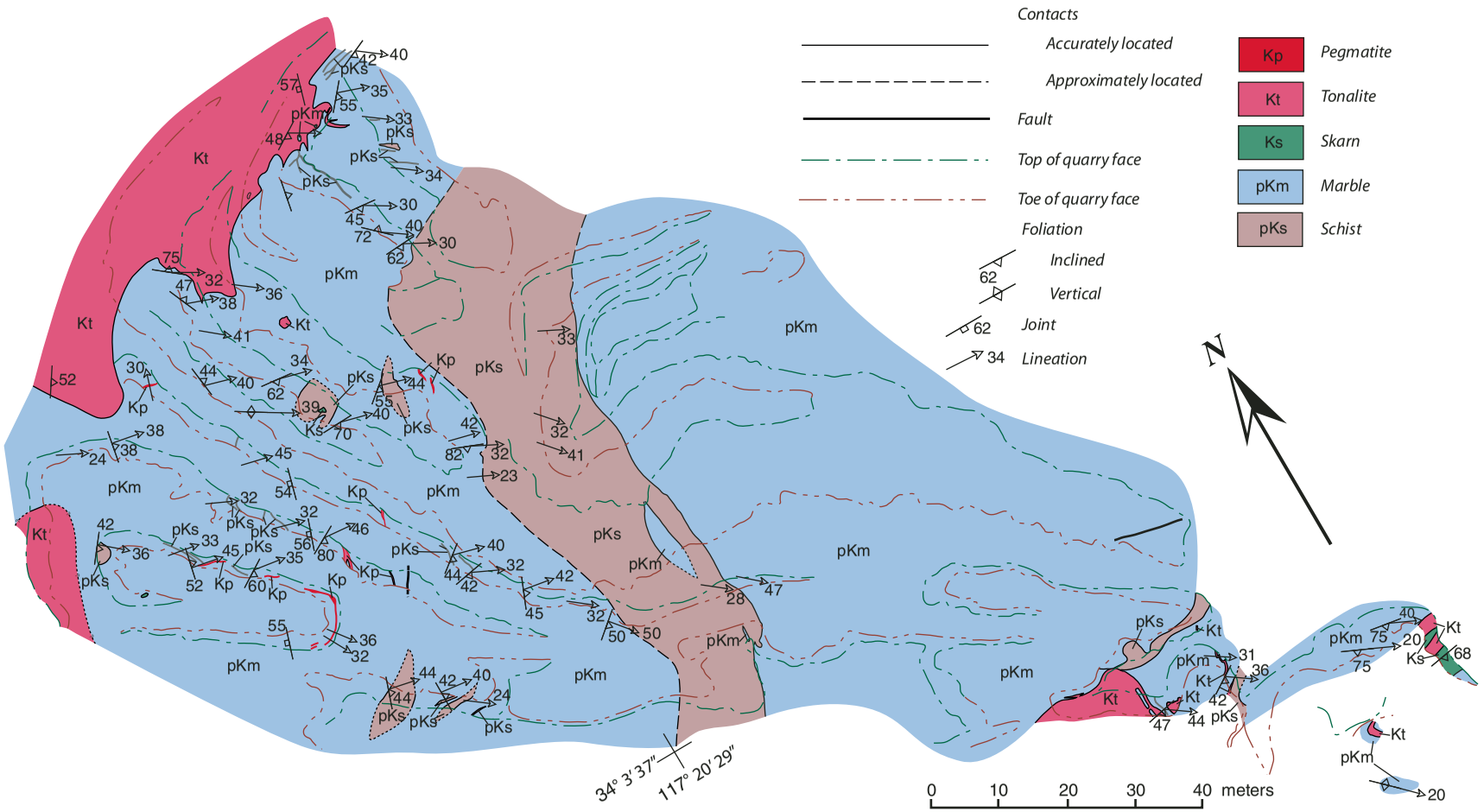

Figure 6. Geologic map of Slover Mountain, Colton. Two intensely deformed Paleozoic(?) marble layers separated by a biotite schist layer are intruded by biotite-hornblende tonalite. Some detached blocks of marble are included in the marginal part of the tonalite, and a few isolated schist bodies are included in the marble.

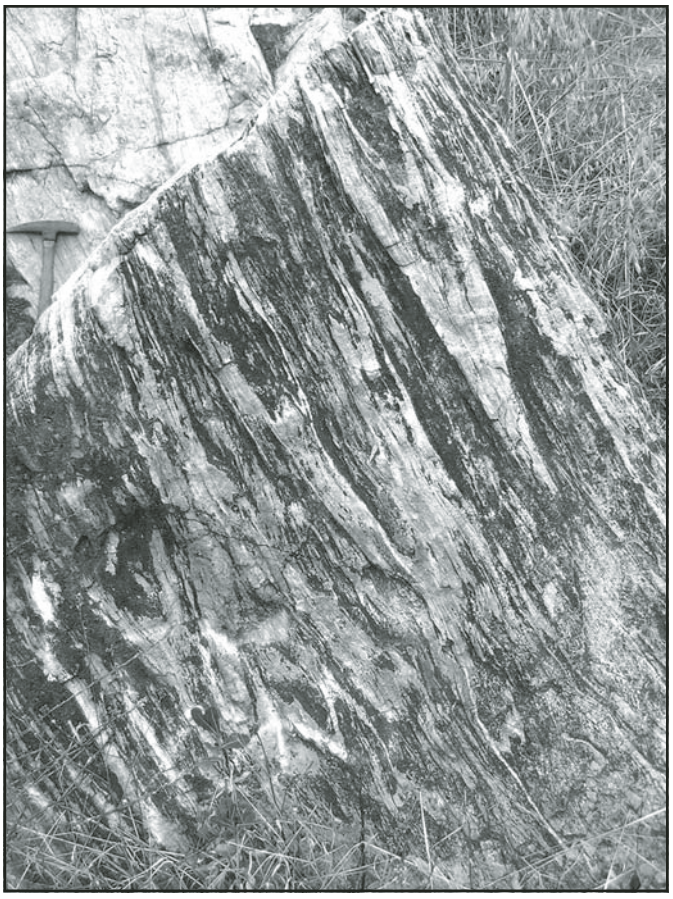

Figure 7. Intensely slip-folded, metamorphosed siliceous calcareous metasedimentary rocks containing diopside and wollastonite, Old City Quarry, Riverside. Light-colored layers are discontinuous layers of quartzite and wollastonite. Pick for scale.

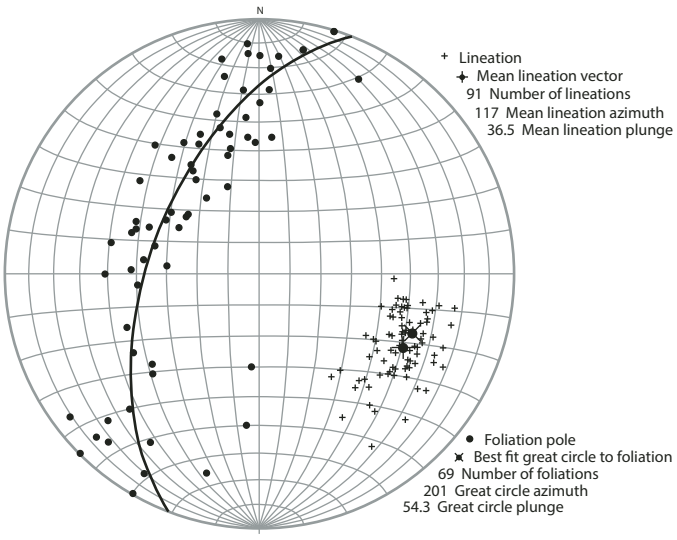

Figure 8. Stereoplot of minor folds and lineations in marble and schist, Slover Mountain, Colton. Foliation is penetrative planar fabric in marble and mineral foliation in schist. Lineations are penetrative mineral orientation and minor folds in marble and schist.

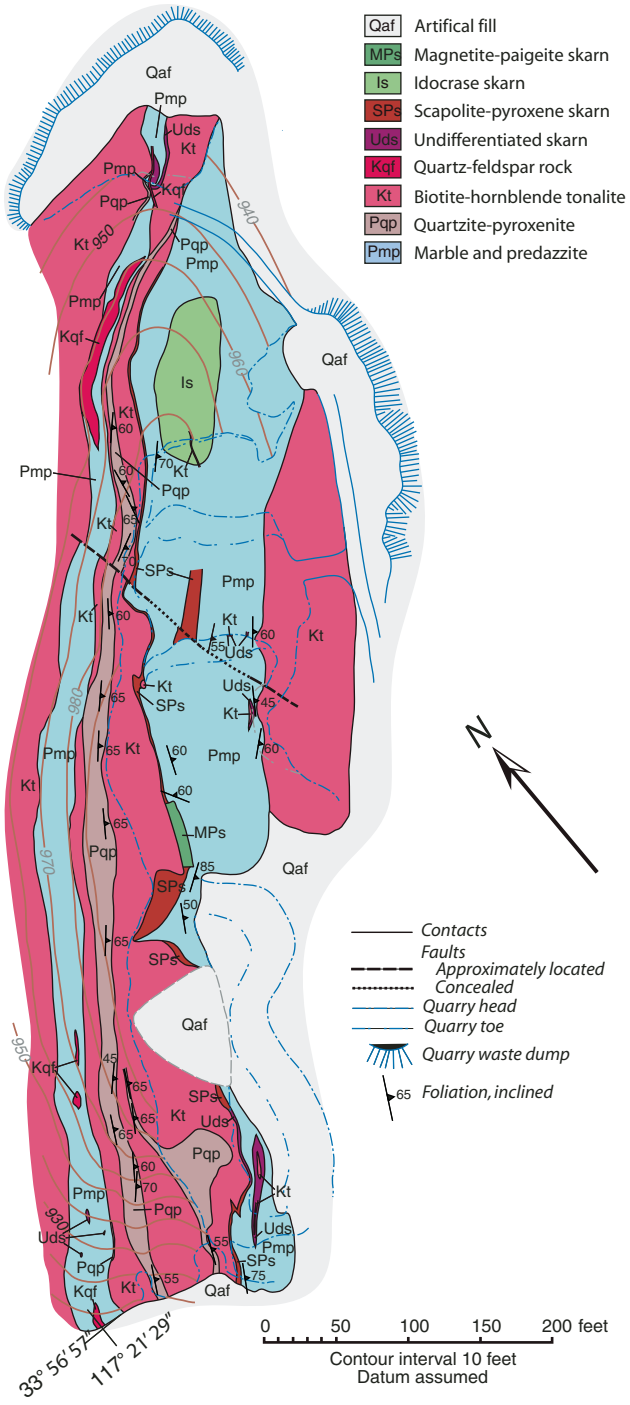

Figure 9. Geologic map of the New City Quarry, Riverside. Paleozoic(?) marble-predazzite (Pmp) layers are separated by an intervening quartzite-pyroxenite layer (Pqp); both units are intruded by biotite-hornblende tonalite (Kt). Nature of contacts indicates that tonalite was forcefully emplaced mostly along contact between the marble-predazzite and quartzite-pyroxenite layers.

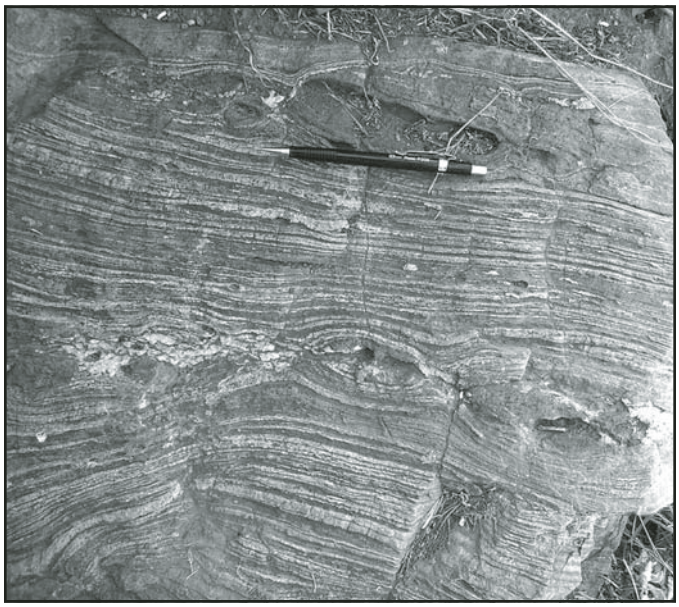

Figure 10. Boudinaged pyroxenite layers in the interlayered quartzite-pyroxenite unit, New City Quarry, Riverside. Pencil for scale.

of the Mesozoic and Paleozoic(?) rocks of the Jacumba Mountains of Todd (2004).

Included in the schist and gneiss are relatively thin, discontinuous marble layers that occur as discontinuous bodies on the east side of the Lakeview Mountains, in the area between Mount Eden and Soboba Hot Springs (Figs. 3 and 11), and as a large heterogeneous body from the mouth of Bautista Canyon south to Anza (Sharp, 1967). These rocks are dominantly biotite schist and gneiss, containing minor amphibolite and variable small amounts of marble and skarn. A few pod-like and variable (but small in amount) marble and calc-silicate rock bodies occur with sillimanite-biotite schist and gneiss in the easternmost Lakeview Mountains and in the hills north of Lakeview. In the Mount Eden–Soboba Hot Springs area, predominant sillimanite-biotite schist and gneiss commonly contain marble bodies and sparse amphibolite and rare gabbro. Within this unit north of the town of San Jacinto, gneissic biotite monzogranite and biotite-hornblende tonalite are widespread. Based on the nature and intensity of deformation, the monzogranite and tonalite are probably Jurassic. The metamorphic rocks are intruded by a distinctive garnet-bearing granitic rock, the granite of Mount Eden (Morton and Miller, 2006). Similar schist and gneiss, the Bautista complex of Sharp (1967), extend from the mouth of Bautista Canyon to Anza. Within the Bautista complex, there are bodies of garnet-bearing monzogranite that resemble the Mount Eden monzogranite, as well as foliated biotite monzogranite and gabbro. East of Anza, the Burnt Valley complex of Sharp (1967) is the continuation of the Bautista complex offset by the San Jacinto fault. South of 33°30′N, the large Tule Canyon complex of Sharp (1967) is probably also part of the Jacumba Mountains sequence. The widespread sillimanite indicates all metamorphism is in excess of 500 °C and therefore at least amphibolite facies.

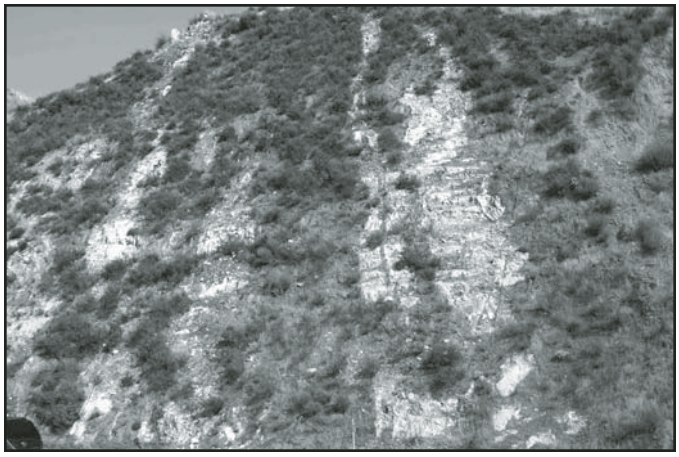

Figure 11. Thick (1–4 m) marble layers in sillimanite-biotite schist and gneiss, Lamb Canyon; unit is interpreted to be part of rocks of Jacumba Mountains of Todd (2004).

Triassic Prebatholithic Rocks

Rocks of Menifee Valley

Larsen (1948) considered the metasedimentary rocks east of the Santa Ana Mountains, in the western part of the Perris block, to be part of the Bedford Canyon Formation, and those in the eastern part of the Perris block to be Paleozoic in age. Schwarcz (1969) interpreted the rocks Larsen assigned to the Paleozoic to be Mesozoic and named them the French Valley Formation. He retained Larsen's terminology of Bedford Canyon Formation for the rocks in the western Perris block. Both Larsen and Schwarcz noted lithologic differences between the Bedford Canyon Formation on the Perris block and the Bedford Canyon Formation at its type locality in the Santa Ana Mountains. Schwarcz's Mesozoic age was based on his observations that "….The French Valley Formation interfingers with the Bedford Canyon Formation at their contact…." (Schwarcz, 1969, p. 22). Based on mapping in the Winchester area, Morton (2003b; Morton et al., this volume) interpreted this as structural interfingering of S_1 fabric rocks. Because of this, all of Larsen's and Schwarcz's Bedford Canyon Formation on the Perris block and all but the easternmost part of Schwarcz's French Valley Formation are here included in rocks of Menifee Valley as defined by Morton and Miller (2006). The easternmost part of Schwarcz's French Valley Formation is here interpreted as the northward extent of the metavolcanic and metasedimentary unit of Todd (2004). Schwarcz (1960, 1969) described a remarkable Buchan-type metamorphic gradient of greenschist to upper amphibolite facies within the rocks of the eastern part of his French Valley Formation.

Age. Larsen's (1948) Paleozoic age assignment for the Perris block rocks was based upon a report (Webb, 1939a) of a single Mississippian coral from the waste dump of the Hemet (Winchester) magnesite mine (Fig. 3). Larsen (1948, p. 16)

characterized the coral as "Carboniferous (Mississippian) fossils in the interbedded limestone near the old magnesite quarry …." Schwarcz (1969), however, clearly showed that the coral specimen cited by Larsen, which was found as float by a mineral collector, could not have originated where it was found.

M.A. Murphy (1966, personal commun.) collected poorly preserved deformed fossils from a calc-silicate rock included in the rocks of Menifee Valley, east of Menifee (previously Sun City). Included in the collection were large crinoid stems and pelecypods. A latex impression of a pelecypod was examined by G.E.G. Westerman (personal commun.), who reported "… This is a poorly preserved, obviously distorted specimen which cannot be identified at the generic or specific level. I dare only the following: Right valve of the Bivalvia family *Aviculepectinidae*; possible ?? *Claraia* ex. gr. *C. himaica* (Bittner) and *C.(?) occidentalis* (Whiteaves) which would be late Lower Triassic. However, almost any age within the Triassic or even Permian is possible…." Based on Westerman's comments, Morton and Miller (2006) considered the rocks of Menifee Valley as Triassic. Samples from the western part of the rocks of Menifee Valley on Searl Ridge contain no post–210–205 Ma detrital zircons (Premo and Morton, this volume).

Lithology. Almost all bedding in the rocks of Menifee Valley was pervasively transposed to S_1 foliation before 134 Ma, the age of the oldest dated undeformed volcanic rocks in the region (Anderson, 1991). The structural transposition producing the S_1 fabric was probably Jurassic in age. Bedding is locally preserved in the hinges of folds, in addition to thin, mostly subcentimeter layers that contain relic cross-bedding showing alternating top directions.

Phyllite, containing some discontinuous sequences of metagraywacke, dominates in the western part of the rocks of Menifee Valley. Metagraywacke, impure quartzite, and interlayered quartzite and phyllite are increasingly abundant eastward. Thick sequences of impure quartzite, including calcareous quartzite, form extensive sections in the Quail Valley and Menifee City areas (Morton, 2003b; Morton and Weber, 2003)(Fig. 3). East of Elsinore, a 9-km-thick section of S_1 foliated phyllite, containing some interlayered metagraywacke, and minor tremolite-bearing marble and manganese-bearing siliceous rocks, locally contains small tabular aggregates of white mica that appear to be pseudomorphs after chiastolite. Tremolite-bearing marble, which is dissimilar to the block-like limestone bodies in the Bedford Canyon Formation, occurs as a few thin elongate layers in this sequence (Morton, 2003b). Manganese-bearing siliceous rocks are sparse but widespread in the Railroad Canyon area and also occur in a single layer in the Winchester area. Rhodonite is common, as are manganese oxides and hydroxides in these manganese-bearing siliceous rocks.

Metagraywacke forms thick S_1 layers, many of which contain small phyllite fragments. Many of these phyllite fragments are deformed into irregularly to uniformly oriented tabular bodies. Some metagraywacke sections contain discontinuous phyllite layers, and some in the Menifee and Winchester areas contain interlayered quartzite and phyllite (Morton, 2003b, 2003c). Sedimentary structure in sporadically occurring 8- to 24-cm-thick quartzite beds in fold hinges is interpreted as relic bedding, contrasting with 5- to 7-cm-thick S_1 quartzite layers on the flanks of the folds (Fig. 12).

On Searl Ridge (Fig. 3), the eastern 4.5 km of the rocks of Menifee Valley are within the transition zones of the northern batholith (for details of the structure and mineralogy of these metamorphic rocks, see Morton et al., this volume). Metamorphism of this 5-km-thick section increases from west to east, from greenschist grade to lower granulite grade. Schwarcz (1969) and Morton et al. (this volume) give detailed descriptions of the mineralogy of the metamorphic gradient; Premo and Morton (this volume) give Ar-Ar ages, and temperature and

Figure 12. Interlayered quartzite and phyllite of the Triassic(?) rocks of the Menifee Valley (Morton and Miller, 2006) and relic bedding, S_0, in hinges of slip folds (arrows) in the upper left and upper center of the photograph. Dominant layering is first-generation transposed bedding, S_1. For scale, arrows are ~33 cm long. Hill east of the city of Menifee Valley.

pressure data are provided by Miggins et al. (this volume). Metamorphic zircon rims on detrital zircons from these rocks have an age range of 103–97 Ma, which dates the time of deformation and metamorphism. Structures related to deformation within the transition zones include, west to east, three progressive structural transpositions. In the western part of Searl Ridge, the regional S_1 layering and schistosity were transposed to S_2, which in turn was transposed to S_3; in turn, $S_3$was transposed to S_4. Mineralogic changes are evident over a 3.5-km-wide zone on the ridge, as thermal effects of the structural transitions produced a low-pressure–high-temperature, Buchan-type metamorphic gradient. Progressive changes in mineral assemblages containing andalusite, cordierite, sillimanite, garnet, and K-feldspar reflect changes from greenschist facies to lower granulite facies.

In the eastern part of the multiply deformed rocks of Menifee Valley, several meta-serpentinite and related rock bodies are discontinuously exposed over a strike length of 14 km. These ultramafic and related rocks are most abundant on Searl Ridge, where the least-altered meta-serpentinite is composed of olivine-talc rock, in which some talc crystals are more than 5 cm in diameter. Several bodies of meta-serpentinite are thoroughly altered to a mixture of clay minerals containing numerous veinlets of magnesite. At and near the outer margins of most of the meta-serpentinite bodies, there is a layer consisting mostly of enstatite, which in some places grades outward to a few-centimeter-thick layer of spinel (Table 1).

Jurassic Prebatholithic Rocks

Bedford Canyon Formation

The name Bedford Canyon Formation has been loosely applied to a wide variety of metasedimentary rocks in the northern Peninsular Ranges Province. At the type locality in Bedford Canyon, northern Santa Ana Mountains, it consists of a thick and structurally complex metasedimentary section of mostly well-indurated lithologies. For a history of the nomenclature used for the Bedford Canyon Formation, see Morton and Miller (2006). Here, the name Bedford Canyon Formation is restricted to the rocks contiguously exposed in the northern Santa Ana Mountains (Fig. 3).

Age. Based on fossil evidence, the Bedford Canyon Formation is considered to be Jurassic (Imlay, 1963, 1964, 1980; Silberling et al., 1961), but a Triassic age for some of the unit cannot be ruled out. Criscione et al. (1978), based on Rb-Sr isotopes from fine-grained lithologies within the Bedford Canyon Formation, interpreted two ages of deposition: a Jurassic age of 175.8 ± 3.2 Ma and a Triassic age of 228 ± 4.3 Ma. The ages were based on analysis of 14 samples collected between Silverado and Ladd Canyons near Bedford Canyon (Fig. 2). The Bedford Canyon Formation is unconformably overlain by the Cretaceous Santiago Peak Volcanics (see Herzig et al., this volume).

Lithology. Exposures of the Bedford Canyon Formation are commonly thoroughly fractured, complexly folded sequences of brown to black and gray interbedded shale or mudstone (argillite), graywacke, conglomerate, impure quartzite, and minor scattered limestone (Fig. 13). At the type locality, the Bedford Canyon Formation consists of well-indurated lithologies containing a variety of sedimentary structures including ripple marks and cross-bedding. Exposures of the unit are generally nonexistent in the chaparral-covered slopes of the Santa Ana Mountains, except along roads and in scoured canyon bottoms. Most limestone bodies are blocky and have no appreciable length. Brachiopods identified as *Anarhynchia gabbi* Ager collected from one of these limestone bodies are interpreted to typify a cold-seep paleoenvironment (Sandy and Campbell, 2003). Dark-gray conglomerate layers are massive and contain subangular clasts of a wide variety of lithologies. Massive graywacke, lithic graywacke, and arkosic arenites consist of subangular quartz, feldspar, and rock fragments. Some gray-colored beds appear to be tuffaceous. Impure quartzite consists of fine- to medium-grained, subrounded to subangular quartz and a small amount of feldspar. Thickness of most beds is on the order of a few centimeters, but locally, beds are up to about 1 m thick.

West of Lake Elsinore, the southern part of the Bedford Canyon Formation is mostly massive quartz-rich metasandstone and impure quartzite (Morton and Miller, 2006). West of Murrieta-Temecula (Fig. 3), a large area is underlain by unnamed metasedimentary rocks that include thick sections of black, impure quartzite commonly containing disseminated pyrite. These rocks are unlike the rocks of the Bedford Canyon Formation to the north.

Although most of the Bedford Canyon Formation is intensely deformed, primary sedimentary features are commonly preserved (e.g., Gray, 1961; Schoellhamer et al., 1981). Bedding (S_0) in parts of the formation is incipiently to moderately transposed to S_1 layering; many outcrops show mixed bedding and transposed S_1 layering. Typically, in the northern part of the unit, primary sedimentary structures are pristine, and the rocks appear as a folded section of indurated sedimentary rocks. South

TABLE 1. MAJOR OXIDES (%) AND SELECTED TRACE ELEMENTS (PPM) OF WINCHESTER MAGNESITE MINE MAFIC ROCKS

		SiO_2	Al_2O_3	Fe_2O_3*	MgO	CaO	Na_2O	K_2O	TiO_2	P_2O_5	MnO	Cr	Ni
MM-109	Metaserpentinite	31.4	24	10.37	29.3	0.27	0.15	0.03	1.08	0.19	0.193	140	90
MM-110	Metaserpentinite	31.9	16.75	8.81	30.29	0.26	0.18	0.03	0.9	0.18	0.13	430	550
MM-111	Metaserpentinite	33.7	15.5	8.34	31.16	0.19	0.15	0.02	0.88	0.11	0.078	100	330
MM-108	Spinel-rich metaserpentinite	19.67	40.7	10.34	18	5.78	0.75	0.15	1.99	0.58	0.221	210	140
MM-112	Pyroxenite	55.25	1.76	7.11	32	0.09	0.12	0.02	0.07	0.02	0.093	2810	2200
MM-113	Pyroxenite	55.23	0.88	6.58	32.84	0.15	0.1	0.11	0.05	0.06	0.071	2970	1560
MM-114	Pyroxenite	50.21	1.06	7.29	36.52	0.2	0.1	0.01	0.05	0.02	0.088	2450	1970

*Total Fe expressed as Fe_2O_3.

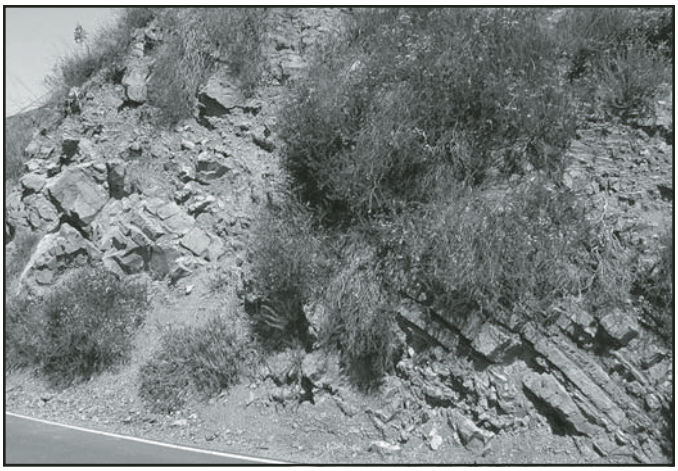

Figure 13. Interbedded argillite and graywacke, Jurassic Bedford Canyon Formation, near the mouth of Silverado Canyon, northern Santa Ana Mountains. Argillite beds are recessive and do not show well in the photograph. Unit also includes immature, poorly sorted pebble conglomerate beds.

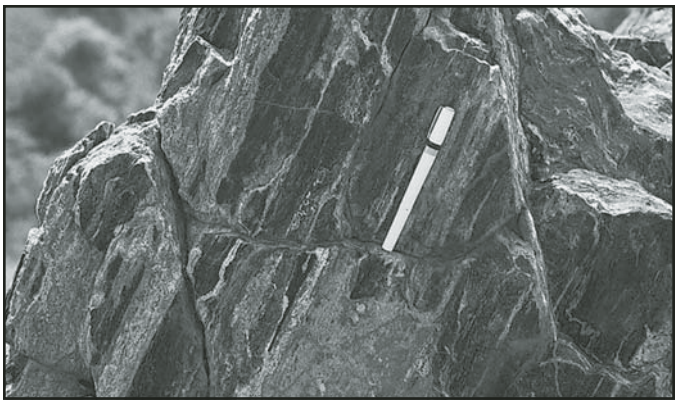

Figure 14. Discontinuous black amphibolite layers in Cretaceous–Jurassic metavolcanic and metasedimentary unit of Todd (2004). Peak metamorphism is inferred to be in the upper amphibolite facies. Location is near east end of Searl Ridge.

and east from Bedford Canyon, primary sedimentary structures appear to be progressively obliterated, largely by structural transposition. Bedding in many places is transposed, and the extent of transposition ranges from slight to intense. Flexural slip folds are common in the areas where bedding is intact (e.g., Gray, 1961; Schoellhamer et al., 1981).

Jurassic and Cretaceous Prebatholithic Rocks

Metavolcanic and Metasedimentary Unit of Todd (2004)

South from the Hemet-Winchester area through the Magee Hills (Fig. 3), and extending to at least 30°30′N, there is a sequence of schist, gneiss, and amphibolite. These rocks are interpreted to be the northward extension of the Cretaceous–Jurassic metavolcanic and metasedimentary unit (KJvs) of Todd (2004).

It is assumed that the age of the prograde metamorphism producing the schist and gneiss is the same as the pre–134 Ma regional metamorphism of the Triassic rocks of Menifee Valley unit, which is described later herein. Rims on detrital zircons from this unit, where it is adjacent to younger deformed and metamorphosed rocks north of 30°30′N, give ages of 100 Ma (Premo and Morton, this volume), which are interpreted as the age KJvs was metamorphosed. Older detrital zircons from the KJvs unit range in age from 250 Ma to ca. 120 Ma, and 1710 Ma to ca. 1040 Ma (Premo and Morton, this volume). On Searl Ridge (Fig. 3), the eastern 600 m section of rocks with S_4 fabrics was derived from this unit. The S_4 fabric rocks there grade eastward into older prograde gneissic foliation.

The metavolcanic and metasedimentary unit is dominantly biotite schist and gneiss that contains numerous elongate bodies and layers of black amphibolite (Fig. 14). The amphibolite bodies range in size from a few centimeters to several hundred meters in length. Sillimanite-biotite gneiss is common, and, although present, garnet-sillimanite-biotite gneiss is subordinate. Much of the gneiss is anatectic, containing thin rheomorphic stringers of quartz and feldspar (Fig. 15). This unit is distinct from the Triassic rocks of Menifee Valley in that it lacks the thick sections of pelitic rocks that are abundant in the latter, and it generally lacks thick sections of graywacke, which are also characteristic of that unit. In addition, the numerous and widespread black amphibolite bodies within the metavolcanic and metasedimentary unit do not occur in the rocks of Menifee Valley. Rocks of the metavolcanic and metasedimentary unit contain Mesozoic inherited and metamorphic zircons having ages of 200–250 Ma and 103–123 Ma, respectively (Premo et al., 2002; Premo and Morton, this volume).

Cretaceous Rocks Coeval with the Batholith

Early Cretaceous Sedimentary Rocks

Sedimentary rocks coeval with the batholith are locally exposed within the Gavilan plutonic ring complex (Fig. 2). In the southern part of the Gavilan ring complex, there is a sequence of volcanic, interbedded volcanic and sedimentary, and sedimentary rocks. The sedimentary rocks are well indurated and undeformed and include granitic pebble conglomerate, quartzite, and black, thin-bedded siliceous rocks (Fig. 16). The volcanic rocks are part of the Estelle Mountain volcanics of Herzig (1991; Herzig et al., this volume). West of Lake Mathews (Fig. 3), siliceous sedimentary rocks also associated with the Estelle Mountain volcanics are considered to be of Early Cretaceous age (Morton and Weber, 2001).

Cretaceous Volcanic and Hypabyssal Rocks

A large area of the Santa Ana Mountains and adjacent parts of the Perris block are underlain by Cretaceous volcanic rocks and related shallow intrusive rocks. The volcanic rocks include some volcaniclastic and sedimentary rocks. In the Santa Ana

Figure 15. Upper-amphibolite-grade anatectic gneiss of the Cretaceous–Jurassic metavolcanic and metasedimentary unit of Todd (2004). Location is near east end of Searl Ridge.

Mountains, these volcanic rocks were originally termed the Black Mountain volcanics by Hanna (1926), but the name was preempted, and Larsen (1948) renamed them the Santiago Peak volcanics for exposures in the vicinity of Santiago Peak, northern Santa Ana Mountains (Fig. 3). The Santiago Peak volcanics, which range in composition from basaltic andesite to rhyolite, rest unconformably on the Jurassic Bedford Canyon Formation. Zircon ages range from 134 to 123 Ma, indicating they are at least partly coeval with older granitic rocks of the Peninsular Ranges batholith (Anderson, 1991). Included in the Santiago Peak volcanics in the Santa Ana Mountains block is a small serpentinite body and associated carbonate-silicate rock (Gray, 1961).

Cretaceous volcanic rocks of the Perris block are in general more silicic than those of the Santa Ana Mountains block and were named the Temescal dacite-porphyry by Dudley (1935) and Temescal Wash quartz latite porphyry by Larsen (1948). Based on a more recent detailed study, Herzig (1991) described and named these rocks the Estelle Mountain volcanics after their extensive distribution in the Estelle Mountain area in the western part of the Perris block (Fig. 3). Included in the Estelle Mountain volcanics is relatively homogeneous rhyolite, and in southeastern

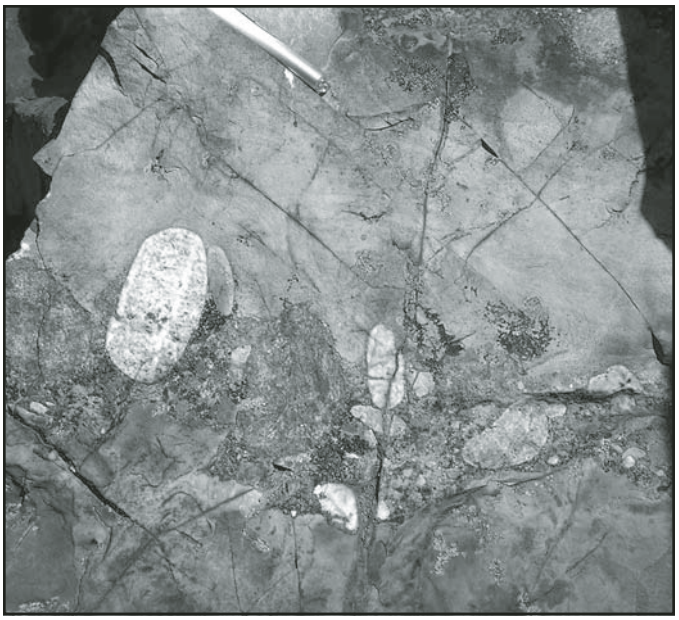

Figure 16. Well-indurated Cretaceous conglomeratic quartzite interbedded with Estelle Mountain volcanics of Herzig (1991), Arroyo del Toro Canyon. Clasts include leucogranite.

exposures, siliceous layered rocks, some of which have primary folds (Morton and Weber, 2003) (Fig. 17). A U-Pb zircon age from the Estelle Mountain volcanics just west of Lake Mathews is 125.8 Ma (Anderson, 1991).

Interlayered volcanic and well-indurated sedimentary rocks along the southwest and south sides of the Arroyo del Toro pluton (Fig. 2) are not included in the Estelle Mountain volcanics. The sedimentary rocks of this sequence, in which primary bedding features are well preserved, consist of conglomerate and thinly bedded, very fine-grained sedimentary rocks.

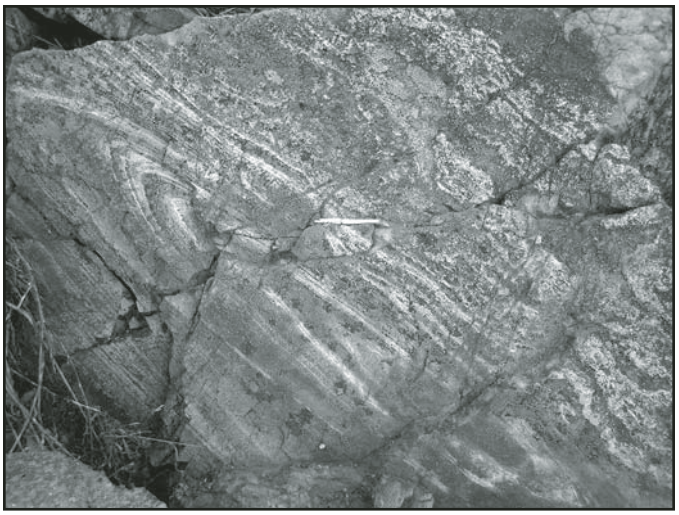

Figure 17. Fold in volcanic rocks, Estelle Mountain volcanics of Herzig (1999), east side of Arroyo del Toro Canyon. Pen for scale.

Early descriptions of the Santiago Peak volcanics and Estelle Mountain volcanics suggested they had been subject to low-grade metamorphism. Herzig (1991), in a thorough examination at the Santiago Peak "type" area, determined that mineral assemblages previously considered to be the result of low-grade regional metamorphism were produced by hydrothermal activity associated with the volcanism; see also Wetmore et al. (2003). To the south, in San Diego County, sedimentary rocks interbedded with volcanic rocks, which had been correlated with the Santiago Peak volcanics, have yielded Late Jurassic fossils (Fife et al., 1967; see Kimbrough et al., this volume). The San Diego County Jurassic volcanic rocks may be related to the Jurassic batholithic rocks south of 33°30′N. These volcanics obviously do not correlate with the Cretaceous Santiago Peak volcanics.

NORTHERN PART OF THE PENINSULAR RANGES BATHOLITH

Previous Work

Early descriptions of portions of the northern part of the batholith include those by Dudley (1935), Osborn (1939), Merriam (1946), Miller (1946), and Engel (1959). An early and very detailed investigation of the modal mineralogy and structure of the tonalite of Val Verde pluton was done by Osborn (1939). The first major synthesis of the batholith was by Larsen (1948), who conducted field work discontinuously from 1906 to 1938 in the central and western parts of the batholith. Jahns (1954) provided an overview of the entire southern California part of the batholith. Recently, Todd et al. (2003) provided an excellent analysis of the batholith immediately south of the area considered here. Most recent batholithic investigations have centered largely on topical aspects (e.g., Baird et al., 1974, 1979; Krummenacher et al., 1975; Taylor and Silver, 1978; Baird and Miesch, 1984; Gromet and Silver, 1987; Silver and Chappell, 1988; DePaolo, 1981; Premo et al., 1998), and on individual plutons (e.g., Hill, 1988a, 1988b; Jenney, 1968; Joshi, 1967; Menzie, 1962; Miesch and Morton, 1977; Morton, 1969; Morton et al., 1969; Morton and Baird, 1976; Sims, 1960).

Because systematic variations across the Peninsular Ranges batholith were recognized very early, previous workers have subdivided it into various longitudinal zones based on a variety of parameters, including age, chemistry, isotopes, and potential field data, (e.g., Baird et al., 1974, 1979; Taylor and Silver, 1978; Baird and Miesch, 1984; Gromet and Silver, 1987; Silver and Chappell, 1988; Todd et al., 1988; Gastil et al., 1990; Langenheim et al., 2004). Most agree on a basic twofold subdivision of the batholith, generally termed the western and eastern zones. This twofold subdivision has been variously attributed to (1) a change in plate motions, (2) two magmatic arcs, or (3) a single arc transitioning from oceanic to continental crust. Kimbrough et al. (2001) calculated, for the 800 km length of the batholith north of 28°N, that the western half constitutes 53% of the batholith and the eastern half 47%. Their western half ranged in age from ca. 140 to 105 Ma, and their eastern half from 99 to 92 Ma.

Based on sparsely spaced samples, Taylor and Silver (1978) described a linear step of $\delta^{18}O$ from +8.5‰ to +9‰ from latitude 31°30′N to the north end of the batholith. Baird and Miesch (1984) developed a mixing model having four end members the northern part of the batholith, based on major-element geochemistry. They interpreted the western part of the batholith to have been largely derived from oceanic crust and the eastern part largely from continental crust. As determined by Baird and Miesch (1984), the boundary between the two is essentially coincident with the $\delta^{18}O$ step of Taylor and Silver (1978). Gromet and Silver (1987) divided the batholith into three zones based on rare earth elements. Similar to Baird and Miesch (1984), they interpreted the western part of the batholith as being derived from largely oceanic materials and the eastern part from continental materials. Kistler et al. (2003) recorded a major step in initial $^{87}Sr/^{86}Sr$ ratio (Sr_i) that does not coincide with the $\delta^{18}O$ step of Taylor and Silver (1978). Based on a combination of geochemistry and age, Silver and Chappell (1988) divided the batholith into six, mostly longitudinal, zones. Five of their zones occur in the area north of 33°N. Todd et al. (1988) summarized the various subdivisions of the batholith. While conducting paleomagnetic studies in the batholith, Erskine (1982) noted systematic variation in magnetic properties, which led to subdividing the batholith into a magnetically high western part and a magnetically low eastern part (Gastil et al., 1990). This difference in magnetic properties between the western and eastern parts of the batholith shows as a marked change on aeromagnetic maps (e.g., Langenheim et al., this volume).

The five batholith zones we have established are based on a combination of field and analytical data. Field data consist chiefly of fabric, structure, enclave shape and configuration, mode of emplacement, and to some degree, contrasting rock types. Analytical data include geochemistry, age, stable and radiogenic isotopes, and geophysics. Specific features and properties characterizing the zones are summarized in Figure 4. The five batholith zones are distinct from one another, but because of the transitional nature of the processes controlling batholith emplacement, and a combination of surface and subsurface measured properties, in some cases there is overlap and/or gradation between the zones. Chemistry of the five batholith zones is given in Table 2 (on CD-ROM accompanying this volume and in the GSA Data Repository [see footnote 1]).

General Features

Relatively shallowly emplaced western zone plutons have sharp, discordant contacts and passively intrude Mesozoic-age rocks. Pluton compositions range from olivine gabbro to high-silica monzogranite. Typically, mafic enclave shapes are equidimensional, not exhibiting the dynamically modified shapes common in varying degrees in zones to the east. Except for some rocks in the northern part of the western zone, Sr_i values are typically between 0.7032 and 0.7040. In the northern Santa Ana Mountains and the northwestern Perris block, most Sr_i values are between 0.7044 and 0.7047, except for seven samples that

range from 0.7052 to 0.7075. Samples from the Jurupa Mountains, including the sample having a Sr_i of 0.7075 (sample DMM 94–13), are in an area of Paleozoic (?) metasedimentary rocks. Some of these samples may be anomalous due to interaction with these metasedimentary host rocks.

Aeromagnetic data clearly show a major twofold division of the autochthonous batholith consisting of an intensely magnetic western part, essentially coincident with the western zone, and a mildly magnetic part to the east (Fig. 18 [available on the CD-ROM accompanying this volume and in the GSA Data Repository]). The upper-plate zone is more magnetic than the eastern zone. This twofold magnetic division of the autochthonous part of the Peninsular Ranges batholith extends for the length of the batholith (Gastil et al., 1990). As the aeromagnetic data reflect magnetic properties to a depth of ~10 km, deviation between surface-collected data and the aeromagnetic data is to be expected. See Langenheim et al. (this volume) for a geophysical overview of the batholith.

The boundary between the western zone and western transition zone in the northern Peninsular Ranges batholith is marked by a change in rock fabric from isotropic to foliated. In the western transition zone, pluton emplacement is dynamic, producing concordant, in places gradational, contacts with the Mesozoic host rocks. Where detailed mapping exists, the change from western zone discordant pluton contacts to concordant western transition zone contacts is very obvious (e.g., Morton and Miller, 2006). In contrast to the equidimensional mafic enclaves in western zone plutons, mafic enclaves in the western transition zone are ellipsoidal- to pancake-shaped. All but the northern part of western zone–western transition zone boundary coincides with the Sr_i 0.7045 isopleth. Most initial epsilon Nd (ε_{Ndi}) values are slightly positive. Magnetite-bearing plutons of the western zone contrast with ilmenite-bearing plutons in the western transition zone; the contrast is especially noticeable in aeromagnetic data. A few zoned ilmenite-magnetite plutons occur in the western transition zone (e.g., Lakeview Mountains pluton; Fig. 3). Western transition zone plutons have a range of chemistry similar to that of the western zone but with Sr_i consistently greater than 0.7045, and positive ε_{Ndi} values.

Host rock for the eastern transition zone is largely Mesozoic, but it includes some probable Paleozoic rocks. The eastern transition zone plutons, mostly larger than those of the western transition zone, have less-well-developed planar fabrics than the typical western transition zone plutons. Sr_i values are more uniform and slightly higher in the eastern transition zone than they are in the western transition zone. Similar to those in the eastern zone, rocks in the eastern transition zone have more negative ε_{Ndi}, and $\delta^{18}O$ >9‰. The eastern transition zone has geochemical similarities to the eastern zone, just as the western transition zone has geochemical similarities to the western zone. All four zones collectively show an irregular, but distinct gradation of properties across the batholith.

Eastern zone plutons, emplaced into Paleozoic rocks, have initial $^{206}Pb/^{204}Pb$ (Pb_i) > 19 and Sr_i > 0.7060, with most Sr_i values in the range of 0.7076–0.7084. Textural changes between the eastern transition zone and eastern zone are less obvious than those between the western transition zone and eastern transition zone, but the presence of megascopically noticeable sphene in eastern zone rocks is highly distinctive. The range in rock compositions is more narrowly restricted in eastern zone plutons than in those of the western part of the batholith. Gabbro is sparse and is found in only the western part of the zone. The eastern zone is terminated on the east by the regional Late Cretaceous Eastern Peninsular Ranges mylonite zone, which is bounded almost everywhere on its east side by younger east-dipping thrust faults. These thrust faults place the easterly derived allochthonous upper-plate zone rocks above the Eastern Peninsular Ranges mylonite zone and the eastern zone.

Upper-plate zone plutons are distinctly younger and more magnetic than those in the eastern zone. Major-element chemistry of upper-plate zone rocks has a narrower range, and the average silica value is lower than that of eastern zone rocks, disrupting the trend of higher silica values from west to east in the allochthonous zones. Sr_i also has a narrow range, averaging 0.7079, which is considerably higher than the 0.7067 average of the eastern zone. $\delta^{18}O$ values are decidedly lower than in the eastern zone.

Based on collective structural, chemical, and isotopic data, the western zone, western transition zone, eastern transition zone, and eastern zone are interpreted to have developed as subduction transitioned from oceanic-arc setting to a continental margin arc setting. Western zone plutons were emplaced into Mesozoic oceanic crust. Western transition zone and eastern transition zone plutons were emplaced at the interface between oceanic and continental crust. The eastern zone plutons were emplaced into older continental crust, and granitic rocks, originating east of the eastern zone, were subsequently thrust westward on low-angle faults to form the upper-plate zone.

In general, our western transition zone corresponds to the "…older, western static arc…" of Silver et al. (1979), the western Peninsular Ranges batholith of Silver and Chappell (1988), and the western plutonic zone of Kimbrough et al. (2001) and Todd et al. (2003). Our combined western transition zone, eastern transition zone, eastern zone, and upper-plate zone corresponds in general to the "…younger migrating arc…" of Silver et al. (1979, p. 92), the eastern Peninsular Ranges batholith of Silver and Chappell (1988), and the eastern zone of Kimbrough et al. (2001) and Todd et al. (2003). Our upper-plate zone may be included in the eastern part of the eastern zone of Kimbrough et al. (2001) and the eastern batholith of Todd et al. (2003), and it appears to be the same as the chemical domain F of Silver and Chappell (1988). The upper-plate zone granitic rocks are exposed only north of 33°22.5′N. South of 33°22.5′N to 33°15′N, any upper-plate zone rocks are covered by postbatholithic sedimentary rocks (Fig. 2).

Some Batholith-Wide Rock Types

Pegmatites

The northern Peninsular Ranges batholith is well known for a large number of complex pegmatites that include a number

of world-class gem- and lithium-bearing pegmatites. With one exception, all of these complex pegmatites are located within the western zone, western transition zone, and eastern transition zone. Essentially all complex pegmatites in the northern Peninsular Ranges occur within plutonic rocks of the Peninsular Ranges batholith. The largest and best-known gem- and lithium-bearing pegmatite districts are Pala (Jahns and Wright, 1951), Mesa Grande (Jahns, 1979), and Rincon (Hanley, 1951). Smaller districts include Aguanga Mountain, Chihuahua Valley, and Red Mountain, and the single occurrence in the eastern zone, Thomas Mountain (Fig. 3). An overview of the gem-bearing pegmatites in San Diego County was given in Weber (1963) and Foord et al. (1991). Most of the complex pegmatites, including the gem- and lithium-bearing pegmatites, are hosted by mafic plutonic rocks, gabbro, diorite, and mafic tonalite (e.g., Jahns, 1979; Foord et al., 1991).

Thin pegmatite dikes, many with planar-sided walls, are ubiquitous throughout the northern part of the batholith. They consist of symmetrical border and wall zones composed of biotite, sodic plagioclase, K-feldspar, and quartz. Graphic textures within these dikes are common. Larger dikes have an intermediate zone that includes schorl, garnet, muscovite, sodic plagioclase, K-feldspar, and quartz, and, where present, a core zone consists of quartz and K-feldspar. The productive gem- and lithium-bearing pegmatites have miarolitic cavities in the core zone, or less commonly, in intermediate zones (Fig. 19), both of which are crystal-lined and contain loose euhedral crystals in the interior of the pockets (Fig. 20). Most shallow-dipping Pala district pegmatites have a low K-feldspar, aplitic-textured footwall rock, termed “line rock” that generally includes alternating layers of garnet and tourmaline (Jahns and Wright, 1951). The 50-m-thick Stewart pegmatite, the largest complex pegmatite in the area, contains a complex of multiple zones. At the roof of the Coahuila Valley pluton, in the Chihuahua Valley area, a greisen-like lithium-bearing rock contains lithium-bearing gem minerals. The northernmost pegmatite district, Lakeview Mountains, consists of complex, rare-earth–bearing pegmatites (see Morton et al., this volume).

Based on isotopic data from two plutons that host complex pegmatites, the Pala gabbro and the Lakeview Mountains pluton, the pegmatites and mafic host rocks are essentially the same and have essentially the same Sr_i. At Pala, western zone gabbro that hosts the lithium-bearing Stewart pegmatite has a U-Pb zircon age of 104 Ma, and muscovite from the pegmatite has a $^{40}Ar/^{39}Ar$ age of 100.4 Ma. Sr_i of the Pala Stewart pegmatite is 0.7040, similar to the host gabbro value of 0.7034. Three tonalite samples from the western transition zone Lakeview Mountains pluton, collected from the oldest to youngest parts of the pluton, have zircon ages of 97.4–100.6 Ma; monazite from a complex rare earth element (REE) pegmatite in the pluton has a sensitive high-resolution ion microprobe (SHRIMP) age of 103 Ma and an isotope dilution–thermal ionization mass spectrometry (ID-TIMS)

Figure 19. Core zone of the Stewart pegmatite, Pala, containing abundant lath-shaped crystals of converted spodumene that now consists of petalite, spodumene, quartz, tridymite, heulandite, and stilbite in a matrix of albite, petalite intergrown with heulandite, altered elbaite, and amblygonite-montebrasite.

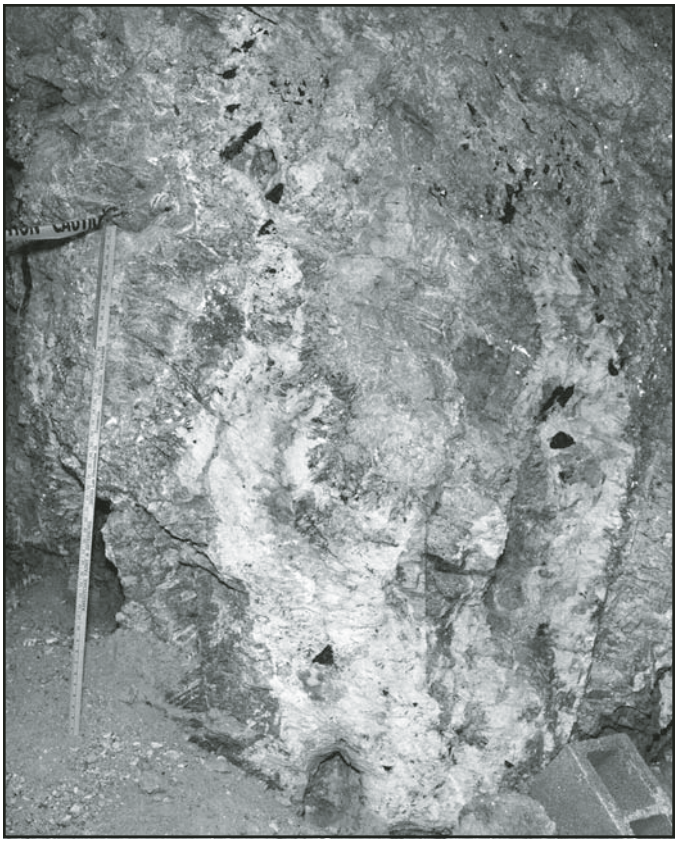

Figure 20. Metasomatic chimney containing miarolitic cavities in an intermediate zone of the Stewart pegmatite, Pala. The upward-tapering chimney replaces perthite and consists of an outer zone of albite, quartz, and muscovite and a core of albite that contains miarolitic cavities.

age of 99.6 (Morton et al., this volume). Sr_i values for the Lakeview Mountains tonalite range from 0.7045 to 0.7051 and have an average value of 0.7048. Sr_i values for perthite from two pegmatites are both 0.7049. The complex pegmatites appear to be the products of immiscible residues from mafic host rock, and not products of foreign fluids derived from some nearby fertile granite as generally interpreted (e.g., Jahns and Wright, 1951; Hanley, 1951; Jahns, 1979; Foord et al., 1991; Walawender, 2003).

Gabbro

Gabbro bodies, originally called the San Marcos Gabbro by Larsen (1948), occur in all zones except the upper-plate zone, decreasing in volume from west to east. A few small gabbro bodies occur in the western part of the eastern zone, but they are not present in the eastern part. Most of our chemical and isotopic data are from gabbro in the western zone. The Sr_i values of 18 gabbro samples from the western zone range from 0.7031 to 0.7043 and have an average of 0.7037, which is slightly less than the 0.7039 average value for all samples from the western zone. A troctolite from the western transition zone, the Green Acres gabbro, has a Sr_i value of 0.7046. Two samples from an eastern transition zone gabbro body, collected only 100 m apart, have Sr_i values of 0.7034 and 0.7050. The eastern zone easternmost gabbro, an olivine gabbro from a small body adjacent to the San Jacinto pluton, has a Sr_i value of 0.7057. Based on these few samples from the western transition zone, eastern transition zone, and eastern zone, a systematic increase in Sr_i from the western zone into the eastern zone is apparent, just as is true for granitic plutons. Rb/Sr ratios are very similar; all samples have Rb under 12 ppm, except for one containing 36 ppm Rb. Gabbros from all four zones in which gabbro occurs have REE patterns that are similar to each other (Fig. 21) and to those reported by Todd et al. (2003) farther to the south. Most of the gabbros have a positive Eu anomaly.

Early workers in the northern Peninsular Ranges batholith stated or implied that gabbro was the oldest component of the batholith (e.g., Jahns, 1954, 1979; Larsen, 1948). Zircon ages by David Kimbrough (D. Kimbrough, 2009, personal commun.) clearly demonstrate that gabbro bodies are not the oldest part of the batholith but are of varying ages, which, in general, decrease from west to east. In the northern part of the Peninsular Ranges batholith, the westernmost gabbro of the western zone has a U-Pb zircon age of 110.5 ± 0.7 Ma. The U-Pb zircon age of gabbro from Rice Canyon, just west of Pala, is 112 ± 0.6 Ma, and at Pala, the gabbro is 104 Ma (both localities are also in the western zone). Gabbro at Thomas Mountain, adjacent to the 94 Ma San Jacinto pluton, yields a U-Pb zircon age of 101.4 ± 1.7 Ma. Todd et al. (2003) described commingling of gabbroic and granitic rocks indicating coexisting gabbroic and granitic magmas.

Mafic Enclaves

Mafic enclaves having relatively uniform mineralogic composition are moderately abundant to very abundant in most northern Peninsular Ranges batholith granitic rocks of all zones. Most enclaves have a higher biotite and hornblende content than the host rock (e.g., Larsen, 1948). The parentage for most mafic enclaves is either unclear or undetermined, although earlier workers invoked a gabbroic parentage for many of them (e.g., Larsen, 1948; Schwarcz, 1960). This interpretation is probably in large part due to an early study by Hurlbut (1935), who clearly demonstrated that mafic xenoliths in a tonalite pluton in San Diego County were derived from gabbro. In a few places, enclave parentage is recognizable. Larsen (1948, p. 162) noted that "… The typical inclusions were in almost perfect equilibrium with the magma, and they would probably persist a very long time in a stagnant magma without mixing with the magma to give a homogeneous rock…"

Mixing of magmas having distinctly different compositions has been described from granitic rocks of the Bernasconi Hills area (Mason and Cohen, 1990), the San Jacinto pluton (Hill, 1984), and by Todd et al. (2003) for granitic rocks farther south in the batholith.

It appears that, regardless of initial composition, mafic enclaves attain a composition in equilibrium with the enclosing host rock, probably through grain-boundary advection of magmatic fluids because a positive correlation exists between the silica content of an enclave and that of the enclosing host rock. Within the western zone Domenigoni Valley pluton, stoped calcareous quartzite xenoliths are progressively transformed to the composition of typical mafic enclaves. The silica content of the country rock of the Domenigoni Valley pluton is consistently greater than that of the transformed mafic xenoliths. In an apophasis of the Domenigoni Valley pluton, the transformation of calcareous quartzite xenoliths (SiO_2 = 80%), derived from the country rock, to typical mafic enclaves (SiO_2 = 57%) within the apophasis tonalite (SiO_2 = 65%) clearly demonstrates that the initial silica content of the xenolith is not the controlling factor

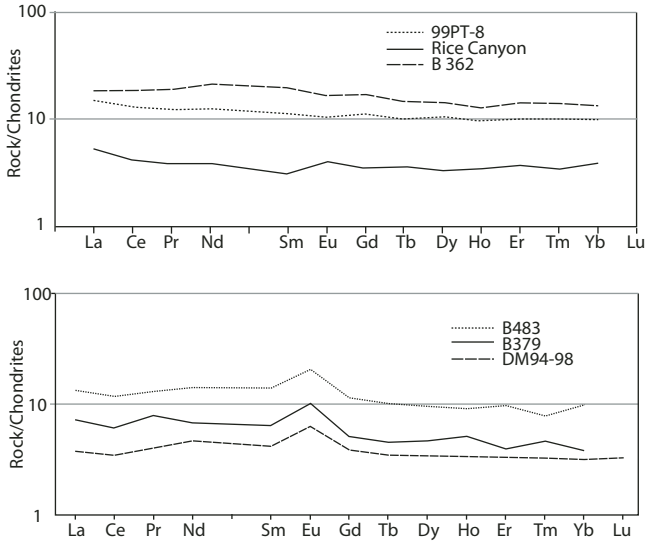

Figure 21. Chondrite-normalized rare earth element (REE) spider diagrams for representative gabbro bodies. Note the relatively strong positive Eu anomalies in B379 and B483.

regarding the final silica content of the enclave, but rather the final silica content is a function of the silica content of the host rock. In the northern part of the batholith, the relationship between the silica content of mafic enclaves and host rock holds for the western transition zone Lakeview Mountains pluton (Morton et al., 1969) and the western transition zone Box Springs Mountains pluton (Morton et al., this volume) (Fig. 22). The parentage of mafic enclaves in these two plutons is not known, but adjacent older rocks suggest it was not gabbro. The average silica content of enclaves increases with an increase in silica content of the host rock. For a host rock of 60% silica, the average silica content of the enclaves is 10% less. This difference increases to an average of 13% for enclaves in a 75% silica host rock.

To determine the chemical variability of enclaves at the outcrop scale, eight enclaves were collected from a 1 m^2 outcrop in the Lakeview Mountains pluton. The silica content of the host tonalite is 58%. The silica content of the enclaves ranged from 46.7% to 50.8%, or 7.2%–11.3% less than the silica content of the tonalite; enclave silica average is 48.8%, or 9.2% less than the silica content of the tonalite.

Enclaves appear to be passive participants in the structural evolution of the granitic plutons. Shape, orientation, and fabric of most enclaves are dependent on the mode of pluton emplacement. Enclaves in passively emplaced western zone plutons are mainly angular and commonly equant. Borrowing terminology for structural designation of metamorphic tectonites, these enclaves are referred to as primary, or first-generation enclaves, E_0. Xenoliths that retain or largely retain their initial composition (e.g., quartzite, phyllite, and schist) have more angular shapes than those that have reached, or largely reached, equilibrium with the host rock (Fig. 23). Some E_0 enclaves may show some degree of alignment, but they are not physically (dynamically) shaped.

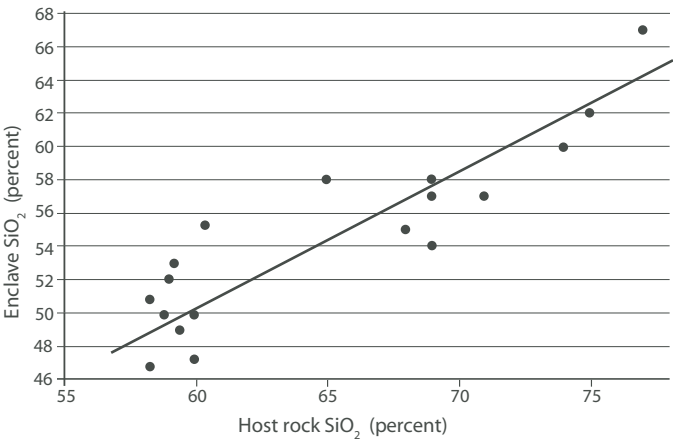

Figure 22. SiO_2 value in host rocks compared to SiO_2 values in the mafic enclaves within the host rocks. As the SiO_2 value of host rock increases, the SiO_2 value of mafic enclaves likewise increases. Analyses are of representative host rock and mafic enclaves from the western zone Domenigoni Valley pluton and western transition zone Lakeview Mountains pluton and Box Springs Mountains plutonic complex.

Xenoliths in the Domenigoni Valley pluton typify morphology of first-generation enclaves, E_0 (Fig. 23). In western transition zone, eastern transition zone, eastern zone, and upper-plate zone plutons, mafic enclaves were dynamically shaped during pluton emplacement, reflecting movement in the host magma. These enclaves are referred to as transposed enclaves, E_1. The degree of enclave attenuation is a function of several variables, including, but not limited to, the amount of movement within the host rock and its viscosity. Enclaves in the Lakeview Mountains and Val Verde plutons, and the Bernasconi monzogranite are typical E_1 enclaves.

E_1 enclaves that have undergone deformation after pluton emplacement are termed E_2 enclaves. Shape alone cannot be used to define whether an enclave is E_1 or E_2. The clearest case of transposition of E_1 to E_2 enclaves occurs when E_1 enclaves are only partly transposed to E_2 or in outcrops that show alternating $E_1$and E_2 enclave zones. Enclaves in the mixed granitic rocks south of the Lakeview Mountains pluton are examples of E_1 enclaves partly transposed to E_2 (Figs. 24 and 25). Lacking the presence of partly transposed E_1 enclaves, the determination of whether extremely attenuated enclaves are E_1 or E_2 is questionable. The uniform attenuated mafic enclaves in the Reinhardt Canyon pluton (Fig. 26), which are interpreted as deformed by an expanding Lakeview Mountains pluton (see Morton et al., this volume), are an example of E_2 enclaves.

Western Zone Plutons

Most western zone plutons are moderate sized, have discordant contacts, are exposed at shallow levels, and were passively emplaced into Jurassic and Triassic metasedimentary rocks. The plutons were emplaced from 126 to 108 Ma in an early extensional phase of subduction in a back-arc setting (e.g., Lee et al., 2007). Exposed levels of plutons crystallized at pressures of 1.5–3 kbar (Ague and Brimhall, 1988; Smith et al., 1991; Hammarstrom, 1992). Included in the western zone north of 33°N are three distinct ring complexes: the Paloma Valley ring complex (Morton and Baird, 1976), the Gavilan ring complex described here, and the Ramona ring complex, described in detail by Todd et al. (this volume). These ring complexes are commonly interpreted to be roots of calderas. The location of the ring structures in the western part of the Peninsular Ranges batholith is similar to the location of ring structures in the westernmost part of the Sierra Nevada batholith (e.g., Lackey et al., 2008).

Lithologies of western zone plutons range from olivine gabbro to monzogranite. Granitoids that make up the western zone plutons are visually characterized by isotropic fabric and equidimensional mafic enclaves. These plutons have a broader range of compositions than found in the plutons of the other four batholith zones. Silica content averages 64.8% and ranges from 42.5% to 76.8%. Most Sr_i values are between 0.7034 and 0.7040. The $\delta^{18}O$ values range from +2.3‰ to +9.0‰ and average +6.9‰. Pb_i values have an average of 18.753. Based on 14 samples, ε_{Ndi} values average +2.8, with ranges between +0.3 and +5.6, except for a

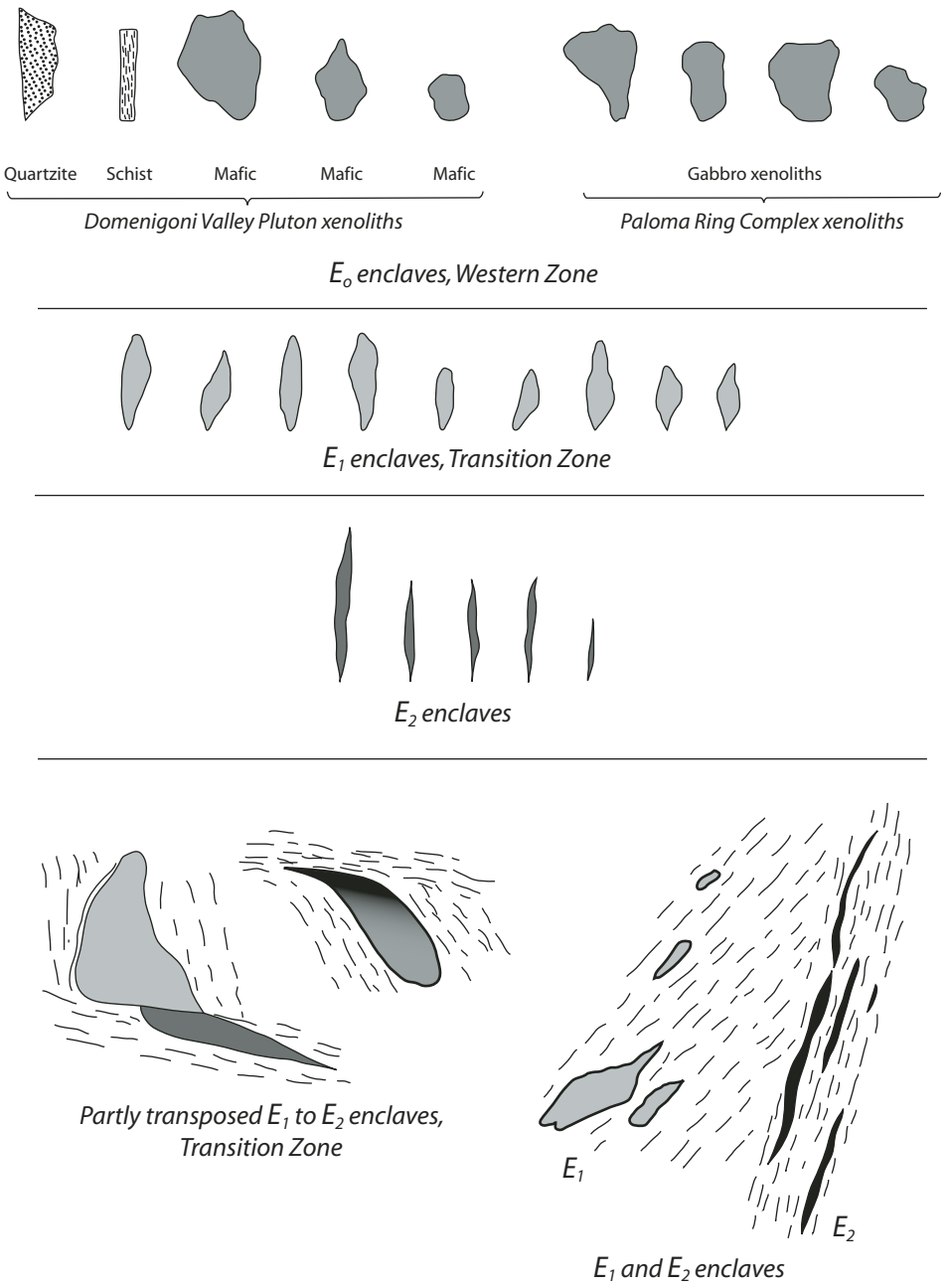

Figure 23. Mafic enclaves, northern Peninsular Ranges batholith, showing characteristic enclave shapes related to passive emplacement (E_0), dynamic emplacement (E_1), and late and post emplacement deformation (E_2).

single negative ε_{Ndi} of –0.97 or –1.0 at the contact of a granodiorite pluton at Hot Springs Canyon on the west side of the northern Santa Ana Mountains (Fig. 3). A sample from the same pluton 500 m away from the contact has a ε_{Ndi} of + 2.7 (see Premo et al., this volume, Chapter 4). The negative ε_{Ndi} sample also has an anomalously high Pb_i value of 19.092.

Northern Santa Ana Mountains

Detailed studies of plutonic rocks in the northern Santa Ana Mountains have not been undertaken due to a combination of exceedingly poor exposure and thick brush. Much of the area has been mapped only in reconnaissance, and many plutonic rocks have been mapped as undifferentiated granitic rocks (e.g., Morton and Miller, 2006). Pluton compositions range from gabbro to monzogranite. Granitic rocks are mostly isotropic-textured biotite granodiorite containing various amounts of equidimensional mafic enclaves. Although most plutonic rocks have typical hypidiomorphic-granular textures, some hypabyssal granitic rocks are located in the Santiago Peak area (Fig. 3).

The westernmost sample from Hot Springs Canyon (Fig. 3.) near the contact of granodiorite and Bedford Canyon Formation has a U-Pb zircon age of 119.2 Ma_{id} and 117.4 Ma_{ip}; a sample collected 1 km east of the contact has a U-Pb zircon age of 119.9 Ma_{ip}. In the vicinity of Elsinore Peak (Fig. 3), a large area is underlain by

Figure 24. E_1 enclaves transposed and others partly transposed to E_2 enclaves, western transition zone tonalite from mixed granitic rock unit south of the Lakeview Mountains pluton, central Perris block.

homogeneous granodiorite that has a U-Pb zircon age of 125 Ma_{ip}. South of Elsinore Peak, intermixed gabbro, granodiorite-tonalite, and monzogranite plutons are common. Within these intermixed plutonic rocks, there is the Squaw Mountain pluton (Fig. 3), a well-defined, small (5 km^2), equant-shaped monzogranite pluton. The Squaw Mountain pluton has an age similar to the Elsinore Peak granodiorite, with U-Pb zircon ages of 120.4 Ma_{id} and 122.8 Ma_{ip}. It consists of isotropic biotite monzogranite, some of which is semiporphyritic. East of the Squaw Mountain pluton, on the Santa Rosa Plateau, a hornblende tonalite pluton has U-Pb zircon dates of 122.0 Ma_{id} and 126.0 Ma_{ip}. In the northern Santa Ana Mountains, most REE patterns for generic granodiorite, commonly referred to as Woodson Mountain granodiorite (e.g., Larsen, 1948), have moderate negative Eu anomalies and have slight increases in heavy REEs (Fig. 27).

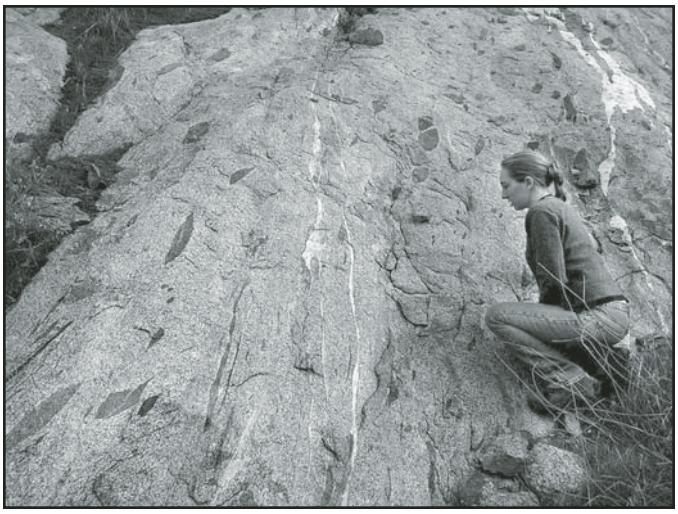

Figure 25. Tonalite outcrop showing both E_1 and E_2 enclaves. Tonalite with extremely attenuated E_2 enclaves in central part of photograph (area with narrow light streaks of quartz) is bordered by a zone in the tonalite that contains noticeably less-attenuated E_1 enclaves. Mixed western transition zone granitic rocks south of the Lakeview Mountains pluton, central Perris block.

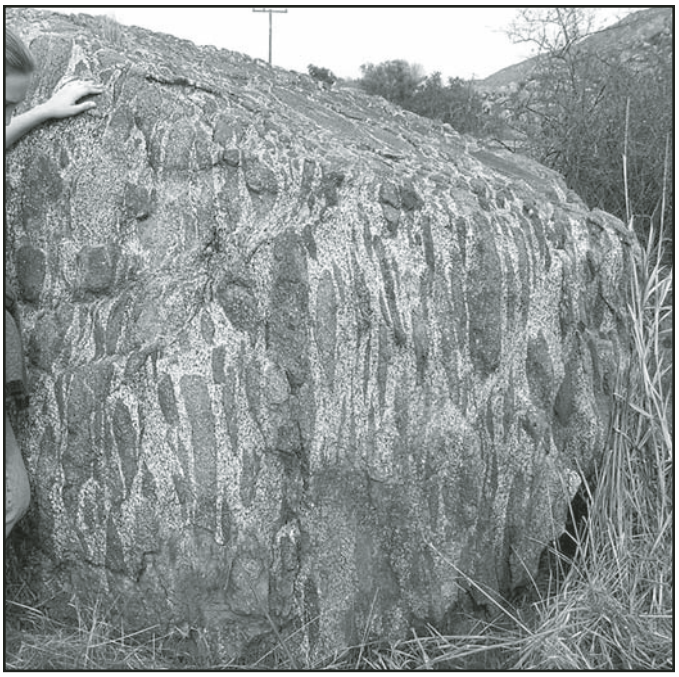

Figure 26. Attenuated mafic enclaves in the western transition zone Reinhardt Canyon pluton are interpreted to be E_2 enclaves. Attenuation is interpreted to be the result of upward and outward expansion of the adjacent Lakeview Mountains pluton. Note pair of postenclave deformation shears extending to the left from the central-upper part of the outcrop to the middle of the left side of outcrop.

Perris Block

Western zone plutons are much better exposed on the Perris block than those in the Santa Ana Mountains. Three western zone

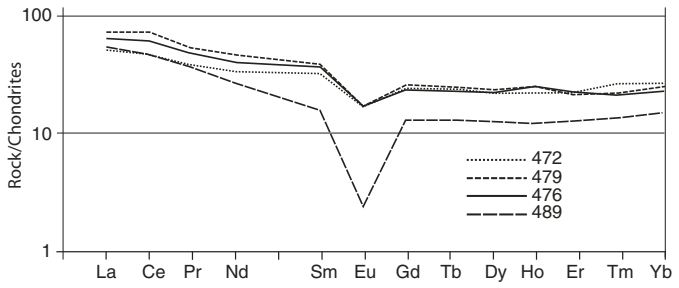

Figure 27. Chondrite-normalized rare earth element (REE) spider diagrams for western zone Woodson Mountain granodiorite, showing consistent negative Eu anomalies, particularly strong for sample 489. All samples are from the Baird-Welday collection.

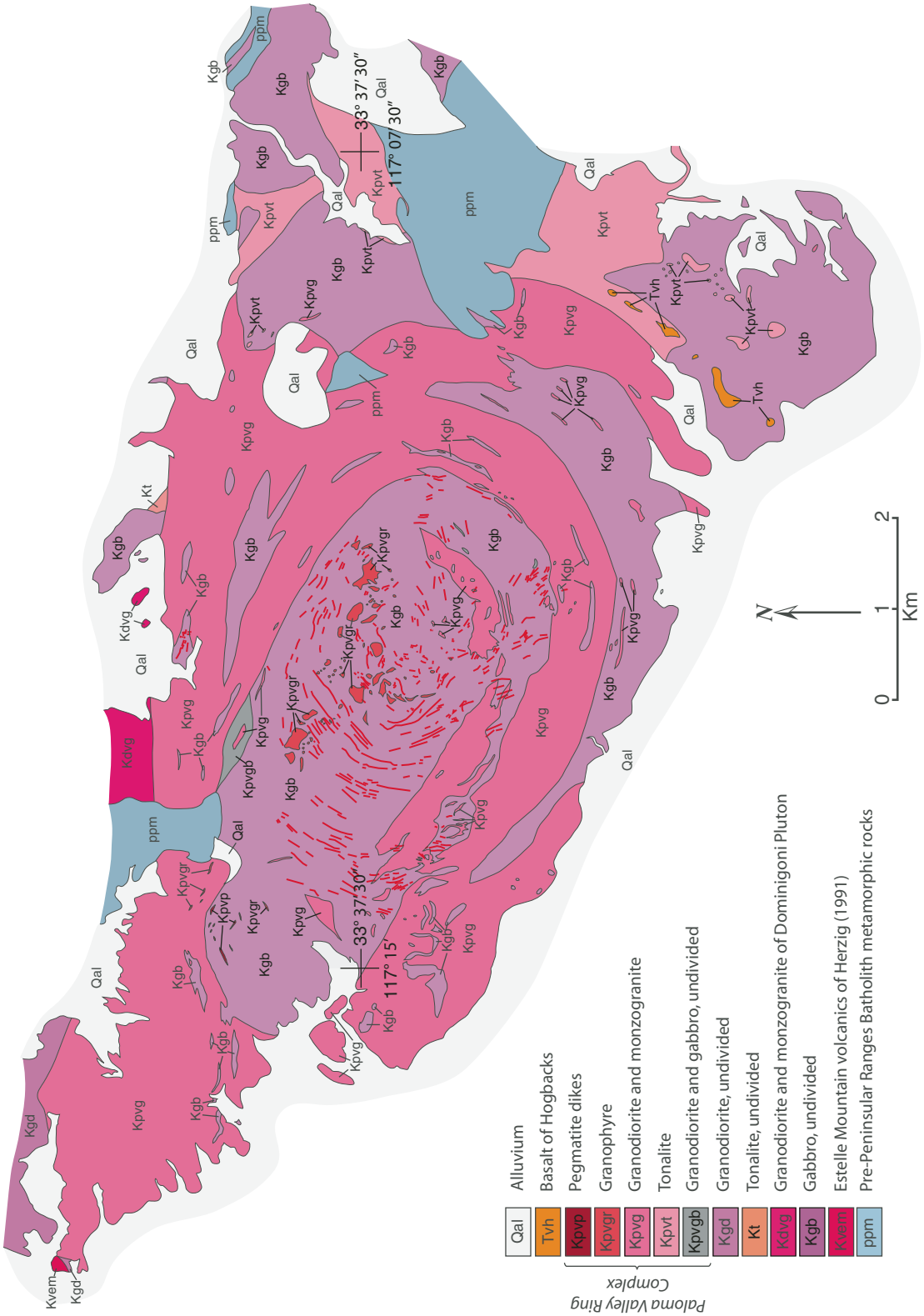

Figure 28. Generalized geologic map of the western zone Paloma Valley ring complex, Paloma Valley area, Perris block. The older outer ring dike of granodiorite and monzogranite was emplaced by magmatic stoping of gabbro. The younger inner pegmatitic ring dike complex fills domal-shaped fractures that resulted from cauldron subsidence. Aphanitic granophyre bodies in the center of the complex are products of pressure-quenched pegmatitic fluids.

plutons have been studied in detail: the Paloma Valley ring complex (Morton and Baird, 1976), the Domenigoni Valley pluton (Morton et al., this volume), and the Ramona ring dike (Todd et al., this volume).

Paloma Valley ring complex. The Paloma Valley ring complex (Fig. 28) is a composite ring complex consisting of an outer granodiorite ring dike, emplaced by magmatic stoping in gabbro, and an inner set of slightly younger pegmatitic and granitoid dikes, most of which were emplaced in the gabbro core of the older dike (Morton and Baird, 1976). The outer granodiorite ring dike is composed of massive granodiorite and monzogranite that grade to tonalite in the eastern part of the complex. In some places, a faintly developed planar fabric, produced by oriented biotite crystals, parallels the geometry of the ring dike. The elliptical in plan outer ring dike, and several subsidiary short-arc dikes, are steep walled. Continuity of the outer dike is interrupted in its northwest part for 0.5 km by the southeast end of a mass of metasedimentary rock that was apparently more resistant to stoping than the gabbro.

The outer granodiorite dike was emplaced into gabbro by ring fracturing and magmatic stoping. Stoped masses of gabbro are common to abundant in much of the dike; locally, the amounts of granodiorite dike rock and stoped gabbro are subequal (Fig. 29). Based on the low magnesium content of the granodiorite, however, only a few percent of gabbro could have been assimilated by the granodiorite magma (Morton and Baird, 1976). The larger, stoped gabbro blocks are up to 3 km in length. Many of these large stoped gabbro blocks are plate-like or elliptical. Most of the elliptically shaped blocks are oriented with the long axes vertical, although a few are oriented with the long axes near horizontal. U-Pb zircon ages of atypical hornblende-bearing granodiorite from the western part of the outer dike are 121.3 Ma_{id} and 121.2 Ma_{ip}. The $^{40}Ar/^{39}Ar$ ages of hornblende and biotite are 117.7 and 118.8 Ma, respectively. More typical granodiorite of the unit, from the eastern part of the outer dike, has a U-Pb zircon age of 119.3 Ma_{ip}.

Figure 29. Stoped gabbro blocks in the granodiorite of the older outer ring dike, Paloma Valley ring complex, north side of the ring dike where it is exposed in road cuts on Scott Road, west of U.S. Interstate 215.

The inner and younger part of the ring dike complex consists of hundreds of thin, relatively short-arc granitic pegmatite and interlayered pegmatitic-textured and coarse-grained granite dikes. These dikes define a domal structure composed of steeply dipping outer dikes that shallow progressively to subhorizontal in the center of the complex (Fig. 28). Most pegmatite dikes are 30 cm to 1 m thick and are texturally and compositionally zoned. Mineralogy of the dikes is simple: Outer zones of coarse-grained granite are composed of quartz, perthite, and sodic plagioclase, and, locally, biotite and minor amounts of magnetite. Pegmatite inner zones consist of pegmatitic perthite, sodic plagioclase, quartz, biotite, and/or muscovite. Some pegmatite dikes have accessory magnetite, schorl, garnet, and epidote, and some larger dikes contain small miarolitic cavities lined with quartz crystals. Graphic intergrowths of quartz and perthite are common in rock transitional between coarse-grained granite and pegmatitic granite. Dikes that lack pegmatitic cores consist entirely of coarse- to extremely coarse-grained granitoid textured rock, with or without graphic intergrowths. Based on their domal arrangement, the dikes of the younger ring complex dikes are interpreted as products of volatile-charged magma that filled a domal set of fractures developed during cauldron subsidence attendant to the emplacement of the outer dike.

Horizontal and near-horizontal floored masses of granophyre occur in the central part of the ring complex. Where fresh, the granophyre is pale gray, but it typically weathers to form reddish-brown outcrops due to oxidation of pyrite, a ubiquitous accessory mineral. The very fine-grained porphyritic granophyre consists of phenocrysts of altered plagioclase in a groundmass of granophyric intergrowths of quartz within K-feldspar and sodic plagioclase. A network of pegmatitic stringers averaging 2.5 cm thick cuts much of the granophyre. These pegmatitic stringers are compositionally and texturally zoned and have fine-grained margins and coarse-grained interiors. Vertically and steeply dipping pegmatite stringers are symmetrically zoned, whereas horizontal or gently dipping stringers are asymmetrically zoned. The asymmetrically zoned pegmatite stringers have plagioclase crystals growing upward from the base and K-feldspar crystals growing and increasing in size downward from the top of the dike. The granophyre is interpreted as the product of pressure-quenched granitic pegmatite magma. The potassium content of the granophyre is lower than that of the granitic pegmatites, and the calcium content is higher. The lower potassium content is interpreted as due to a loss of volatiles, including potassium, accompanied by the decrease in pressure during cauldron subsidence. Less-mobile calcium remained in the pressure-quenched granophyre (Fig. 30).

Gavilan ring complex. The discontinuously exposed, elliptical-in-plan, composite Gavilan ring complex consists of granitic rocks ranging from hypersthene monzogranite to biotite-hornblende tonalite (Morton, 2001; Morton and Weber, 2003). Located in the core of the ring complex, but not part of

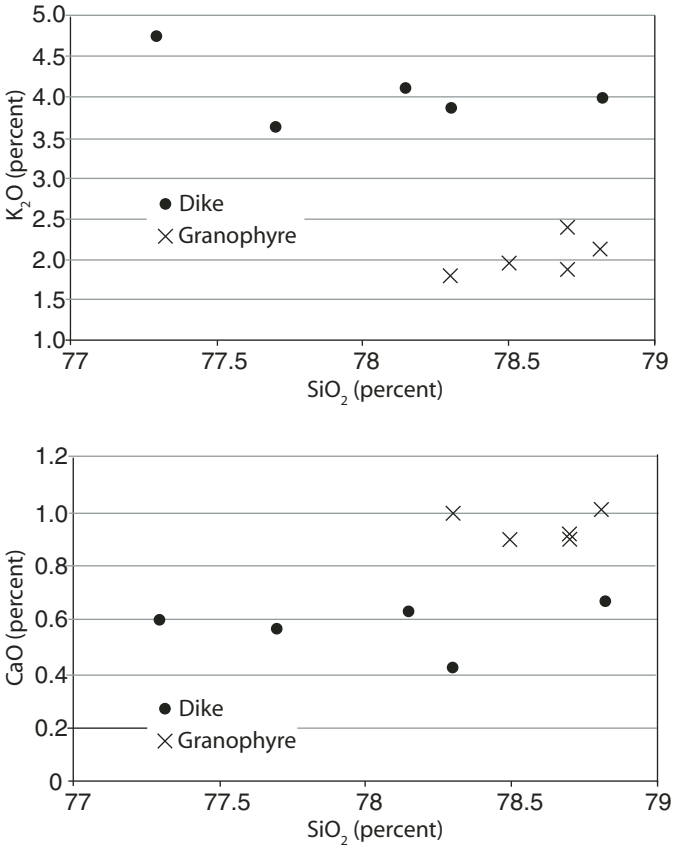

Figure 30. Comparison of K_2O and CaO values of younger ring dike rocks and granophyre of the Paloma Valley ring complex. Lower value of K_2O in the granophyre is interpreted to be the result of potassium leaving the young ring dike magma when pressure was reduced during caldron subsidence.

it, is the near-circular Arroyo del Toro pluton (Fig. 31). Interlayered Estelle Mountain volcanics and well-indurated sedimentary rocks are the country rocks on the west side of the complex; rocks of Menifee Valley are the host rocks in the eastern part.

In the southeastern part of the complex, the level of exposure is at the complex roof, giving rise to irregular traces of contacts with the rocks of Menifee Valley. Textures within the ring complex grade from hypabyssal in the west to hypautomorphic-granular in the central and eastern parts. Based on textural differences and country rock relations, the ring complex was tilted up on the east, and the near-horizontal erosion surface exposes progressively deeper levels of the complex from west to east. The hypabyssal rocks in the western part of the body grade topographically upward into volcanic-textured rocks that were previously mapped as intrusive rocks related to the Santiago Peak volcanics (Weber, 1976).

Hypersthene is a characteristic mineral for most of the complex. A feature restricted to the northern part of the complex is a distinctive brown weathering, massive, hypautomorphic-granular hypersthene-bearing biotite-hornblende tonalite. It contains equidimensional mesocratic-to-melanocratic enclaves. The northeastern part of the complex consists of hypersthene monzogranite. This black monzogranite weathers to form slopes covered with distinctive dark-brown outcrops. The monzogranite contains hypersthene, clinopyroxene, hornblende, and biotite, as well as sparse small mafic enclaves that are commonly lighter colored than the fresh monzogranite. This part of the complex, with its widely spaced joints, has been quarried for stone, marketed as black granite (Fig. 32).

Medium-grained biotite-hornblende tonalite and moderately fine-grained tonalite in the northern part of the complex have a faint, poorly developed foliation and contain abundant, small platy mesocratic enclaves. In the northeastern part of the complex, a relatively small body of coarse-grained, relatively light-colored biotite-hornblende tonalite resembles a schlieren-free tonalite in the western transition zone Lakeview Mountains pluton. This tonalite weathers to form giant core stones. Chemical analyses of the major rock types of the complex are given in Table 2 (on CD-ROM accompanying this volume and in the GSA Data Repository [see footnote 1]).

Several gold mines in the Gavilan ring complex comprise the Pinacate mining district (Sampson, 1935). The largest producer was the Goodhope Mine, located in the southeastern part of the complex. The gold occurred in arsenopyrite-bearing quartz veins that are spatially restricted to the complex.

U-Pb zircon ages for the complex have a spread of 5.3 m.y., ranging from 112.9 to 107.6 Ma. U-Pb zircon ages of the hypersthene tonalite are 112.9 Ma_{id} and 112.7 Ma_{ip}. The $^{40}Ar/^{39}Ar$ age of biotite and K-feldspar in the same rock is 106.2 Ma and 95–103.5 Ma, respectively. U-Pb zircon ages for the black hypersthene monzogranite are 109.0 Ma_{id} and 107.6 Ma_{ip}. The $^{40}Ar/^{39}Ar$ age of biotite is 104.5 Ma, and the age of K-feldspar is 98–100.5 Ma. U-Pb zircon ages for the fine-grained tonalite in the northern part of the complex are 108.5 Ma_{id} and 109.1 Ma_{ip}, and the U-Pb age of sphene is 103.9 Ma_{id}. The $^{40}Ar/^{39}Ar$ ages of hornblende, biotite, and K-feldspar from this rock are 106.4 Ma, 103.1 Ma, and 101–97 Ma, respectively.

Arroyo del Toro pluton. Located in the center of the Gavilan ring complex, the nearly circular Arroyo del Toro pluton geometrically resembles a resurgent dome (Fig. 31). The pluton intrudes Estelle Mountain volcanics and well-indurated Cretaceous sedimentary rocks on the west and rocks of Menifee Valley on the east. The pluton is spatially related to the Gavilan ring complex, but because its chemistry and mineralogy are so different from those of the ring complex units, it is not considered to be related petrogenetically to the complex. Chemically, the Arroyo del Toro pluton is higher in Na_2O and SiO_2 and lower in MgO and Fe_2O_3 than the Gavilan ring complex. The pluton is composed of light-gray, medium-grained, very homogeneous isotropic biotite-hornblende granodiorite. Where exposed, the contact with surrounding rocks is very sharp (Fig. 33). Some of the granodiorite in the western part of the pluton is subporphyritic. Small equidimensional mafic enclaves are rare. The granodiorite typically weathers to form large boulders (Fig. 34). Based on the

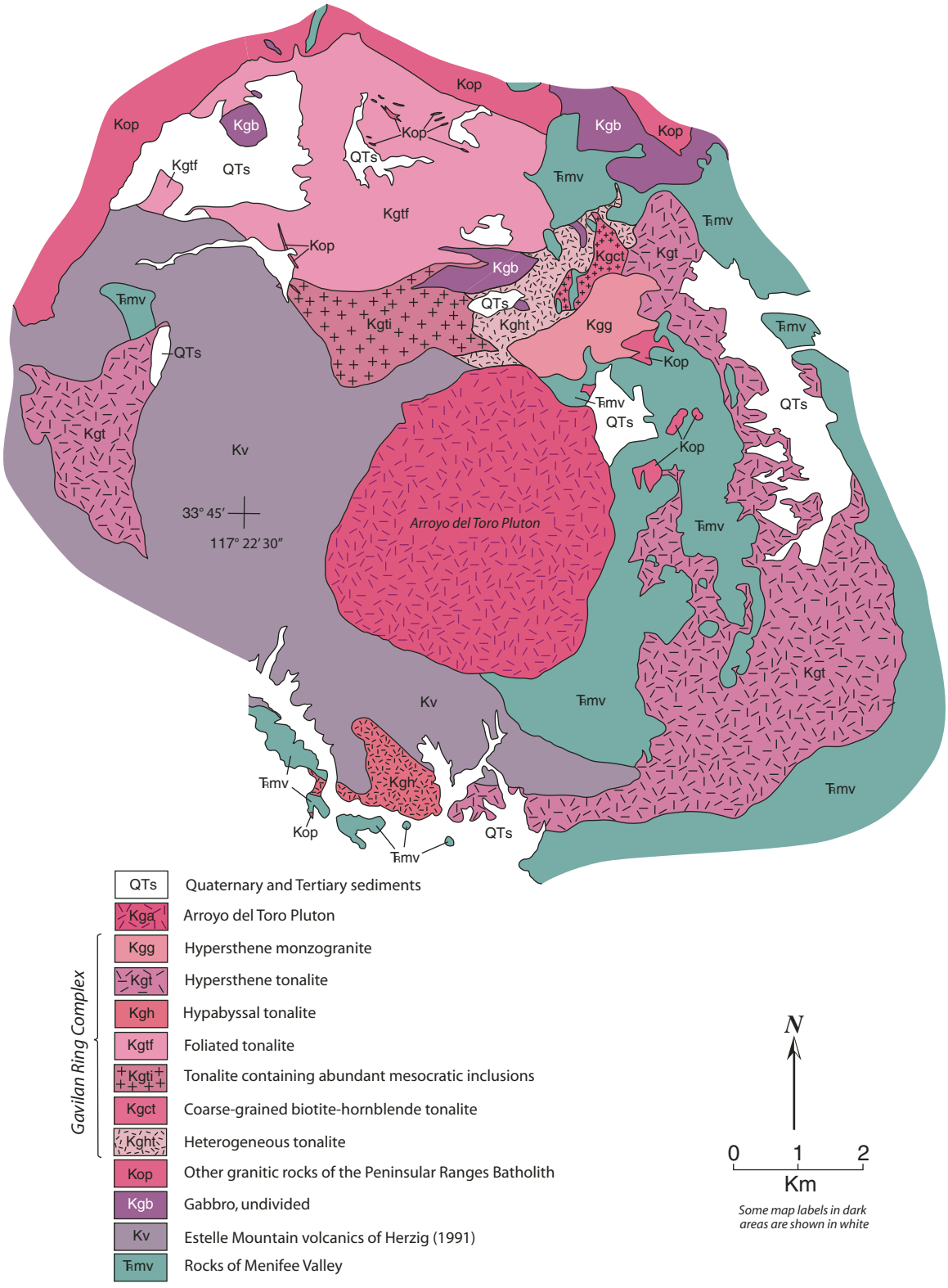

Figure 31. Generalized geologic map of the western zone Gavilan ring complex and the Arroyo del Toro pluton, Perris block. Despite its locational and temporal coincidence with the Gavilan ring complex, on the basis of geochemical and isotopic properties, the Arroyo del Toro pluton is considered to be petrogenetically unrelated to the Gavilan complex.

Figure 32. Quarry in massive-textured, hypersthene-bearing monzogranite (Kgg unit); Kgg is cut by widely spaced joints, northeastern part of the Gavilan ring complex. Kgg was quarried and marketed under the name "Black Granite."

specific gravity of 20 samples collected across the pluton, it is very homogeneous, with values ranging from 2.621 to 2.66, and a mean value of 2.647. The specific gravity range of 0.039 is considerably less than the 0.191 range in the Lakeview Mountains tonalite or the 0.07 range in the Domenigoni Valley pluton. The emplacement age of the Arroyo del Toro pluton is the same as that of the Gavilan ring complex. U-Pb zircon ages are 108.6 Ma_{id} and 113.4 Ma_{ip}. The $^{40}Ar/^{39}Ar$ age of biotite is 104.3 Ma, and K-feldspar age is 94–102.5 Ma. Although apparently not sharing a petrogenetic relationship to the Gavilan ring complex, because of its location and similarity in age, the Arroyo del Toro pluton almost certainly shares an emplacement history with the Gavilan

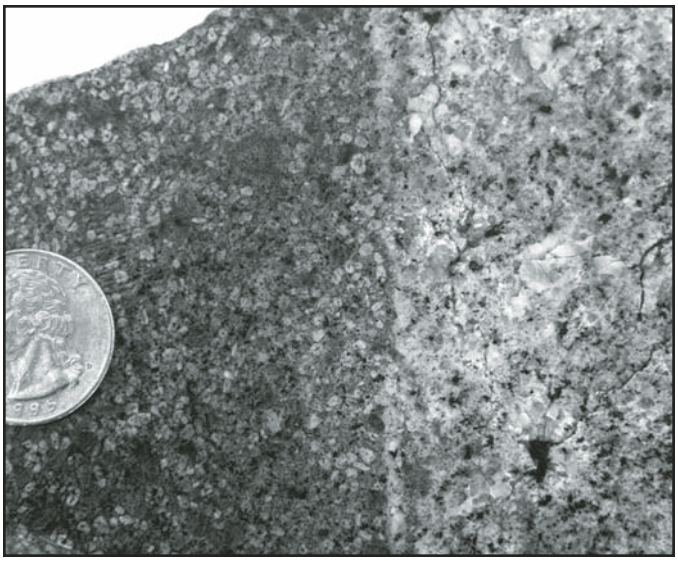

Figure 33. Hand sample showing sharp contact between the Estelle Mountain volcanics of Herzig (1991) and granodiorite of the Arroyo del Toro pluton. Where seen, western zone pluton contacts are typically very sharp.

Figure 34. Boulder-covered slopes underlain by the Arroyo del Toro pluton stand in contrast to the rubbly, brush-covered slopes underlain by the Estelle Mountain volcanics of Herzig (1991). Southwestern contact of the Arroyo del Toro pluton.

ring complex. Chemical analysis of granodiorite of the pluton is given in Table 2 (on CD-ROM accompanying this volume and in the GSA Data Repository [see footnote 1]).

Domenigoni Valley pluton. At the present level of exposure, the pluton consists of two roughly elliptical in plan, noncontiguous bodies separated by a septum composed of Triassic (?) metasedimentary rocks, Cretaceous gabbro, and minor Cretaceous granitic rock (Fig. 35). The eastern body, which is ~11 km long and 8 km wide, underlies an area of ~88 km^2; the western body underlies an area of ~24 km^2. Subsurface, beneath the intervening septum, the two parts of the pluton are inferred to be joined and have a combined areal extent of ~160 km^2. Two small apophyses of Domenigoni Valley–type granitic rocks intrude calcareous quartzite within the septum; one apophysis is well exposed in a highway cut on Interstate 215. Several irregularly shaped apophyses, with very discordant contacts, are poorly exposed within quartzite west of the pluton (Fig. 35). The pluton contact is steeply dipping, except where the eastern extent of the pluton is within the western transition zone. Displacement in the western transition zone has deformed and elevated the eastern edge of the pluton, forming a shallow-dipping contact with rocks of Menifee Valley. The degree of deformation in the tonalite ranges from closely spaced fractures to gneissic-textured tonalite (Morton et al., this volume).

The pluton was passively emplaced into low- to intermediate-metamorphic-grade metasedimentary rocks of the Triassic-age (?) rocks of Menifee Valley (Morton and Miller, 2006). The metasedimentary rocks consist mainly of impure quartzite, calcareous quartzite, phyllite, interlayered quartzite and phyllite, and metagraywacke. Where seen, the contact with country rock is extremely sharp with little or no observable chemical or textural change in the country rock at the contact (Fig. 36). The

pluton contact is conspicuously discordant in all but the southern part of the pluton, where it is structurally concordant with foliation in phyllite. The contact between this part of the pluton and the phyllite is not exposed.

The pluton is composed of massive, isotropic, gray, medium-grained, biotite-hornblende tonalite, minor granodiorite, and some faintly foliated rock in the southeastern part of the pluton. Biotite in the northeastern part of the pluton consists of felted aggregates. Common accessory minerals include zircon, sphene, apatite, and magnetite-ilmenite. Minute, oriented rutile crystals impart a faint blue opalescence to the quartz. Small masses of epidote and/or tourmaline rock occur locally and replace the granodiorite-tonalite. The tonalite-granodiorite contains common-to-abundant equidimensional mafic xenoliths (Fig. 37). Xenoliths are rare or lacking around the margins of the pluton. In the apophasis exposed on I-215, xenoliths range from thermally metamorphosed metasedimentary xenoliths to those in all stages of transformation into the mafic xenoliths that are typical of the pluton.

Two relatively consistent, steeply dipping joint sets are present throughout the pluton; one strikes northeast, and the other strikes northwest. A dacite-quartz latite dike swarm was emplaced along these northwest-striking joints. Most of the dikes are located in the eastern part of the pluton, but a few extend into the surrounding metasedimentary country rock or occur entirely within the metasedimentary rock pendant separating the two halves of the pluton. Almost all of the dikes are foliated and lineated. The foliated texture of the dikes contrasts sharply with the massive texture of the enclosing tonalite. Some dike rocks contain small needle-like hornblende prisms. Streaks of biotite,

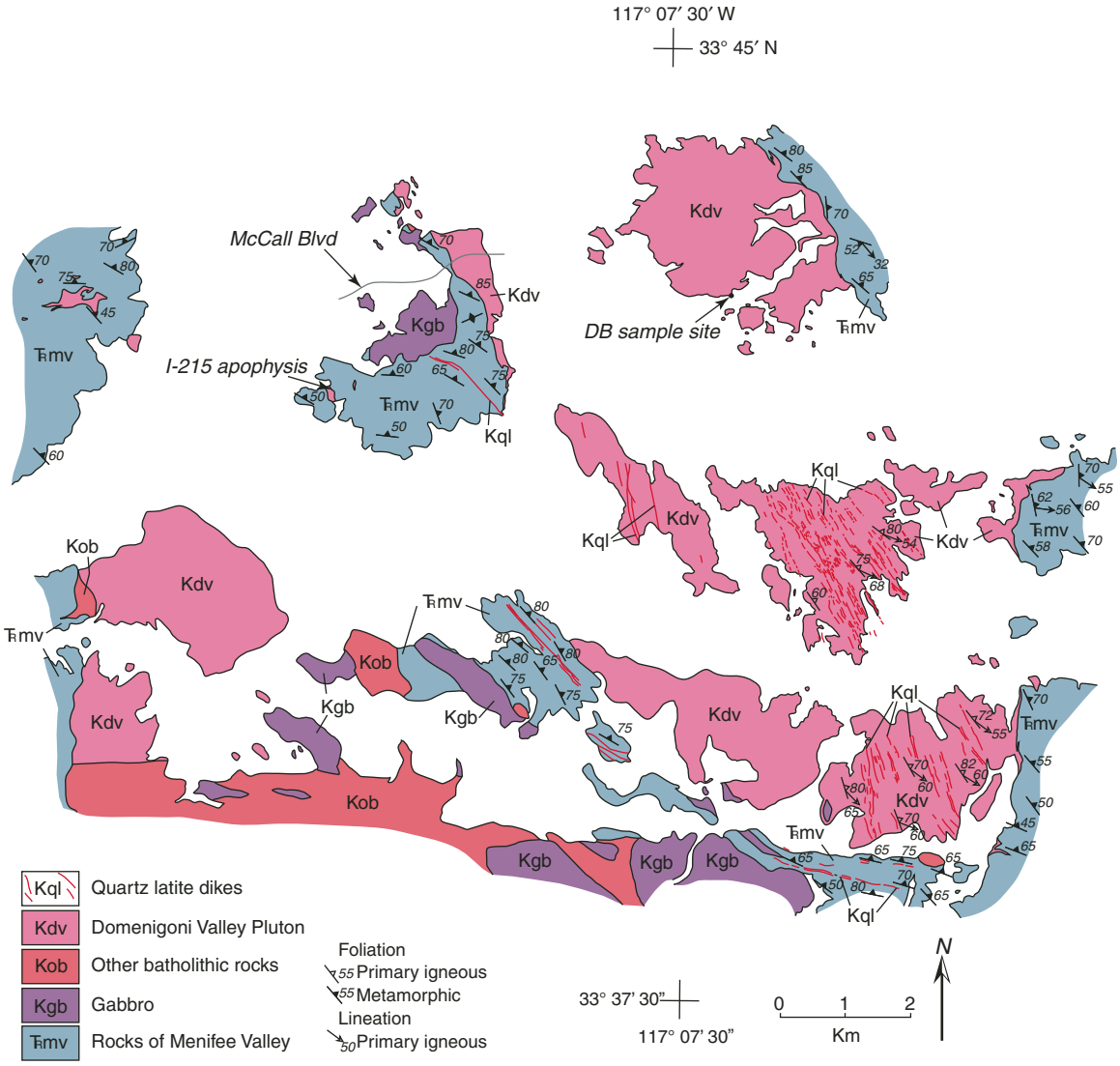

Figure 35. Generalized geologic map of the western zone Domenigoni Valley pluton, Perris block. The McCall Boulevard, I-215 apophasis, and DB sample site localities are discussed in text.

Figure 36. Contact between the Domenigoni Valley pluton and the interlayered quartzite and biotite schist of the rocks of Menifee Valley (Morton and Miller, 2006). No contact effects, structural or chemical, are visible at the contact. Photograph was taken on McCall Boulevard on the east side of the city of Menifee Valley. Keys for scale.

and less commonly, oriented hornblende crystals give rise to a pronounced lineation plunging to the southeast.

Zircons from the western part of the pluton have U-Pb ages of 117.8 Ma_{id} and 123.3 Ma_{ip}. The $^{40}Ar/^{39}Ar$ ages of hornblende, biotite, and K-feldspar from this sample are 122.6 Ma, 103.7 Ma, and 95.5 Ma, respectively. A sample from the northeastern part of the pluton, adjacent to the 100 Ma western transition zone metasedimentary rocks and the 100 Ma, dynamically emplaced Lakeview Mountains pluton, has U-Pb zircon ages of 119 Ma_{id} and 124 Ma_{id} (Premo et al., this volume, Chapter 4). Hornblende and biotite from this sample have $^{40}Ar/^{39}Ar$ ages of 101.3 Ma and 93.7 Ma, respectively. The young $^{40}Ar/^{39}Ar$ ages of hornblende and biotite in the northeastern part of the pluton are interpreted as reset ages along the western part of the western transition zone.

Figure 37. Typical equant- to irregular-shaped mafic xenoliths in isotropic biotite-hornblende tonalite, central part of the western zone Domenigoni Valley pluton, Perris block.

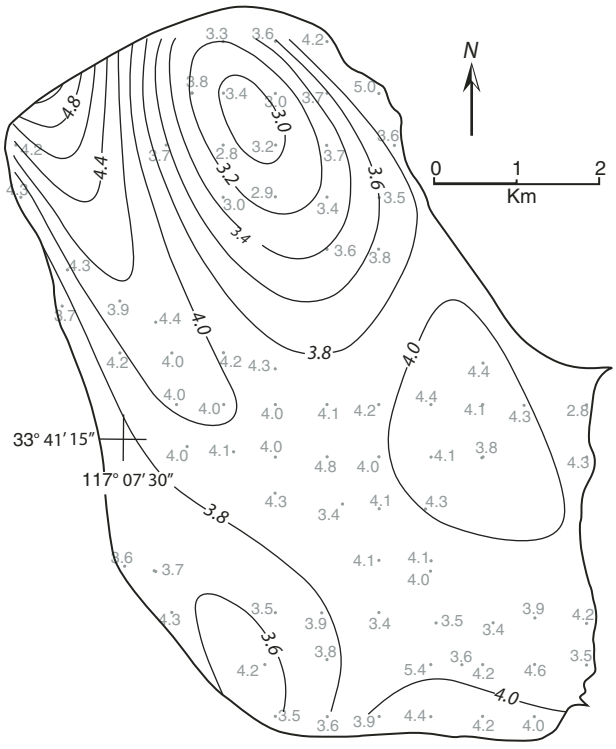

Figure 38. Fifth-degree trend surface map of percent Fe_2O_3 variation in the Domenigoni Valley pluton. Fe_2O_3 is low in the northeast part of the pluton, which is the least $\delta^{18}O$-contaminated part of the pluton (Turi and Taylor, 1971).

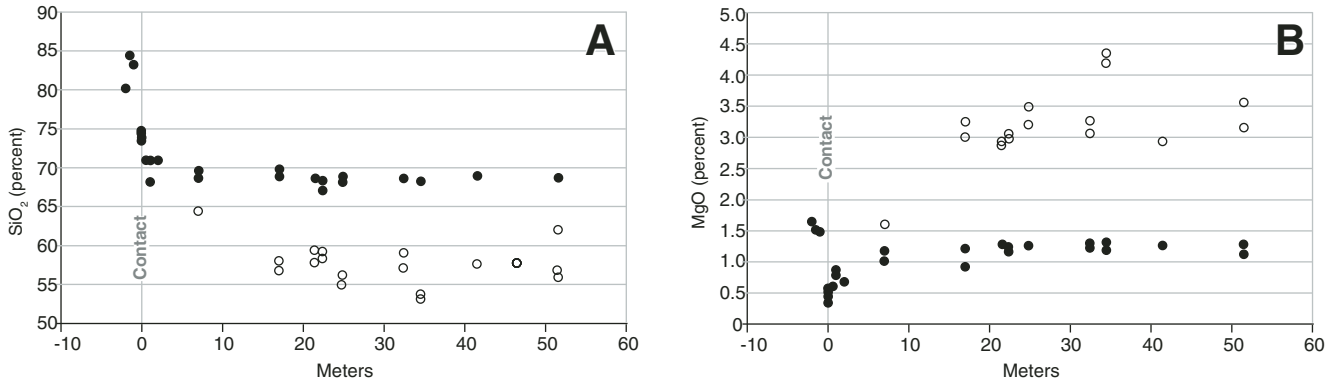

Figure 39. Variation in SiO_2 (A) and MgO (B) at the outer part of the Domenigoni Valley pluton, McCall Boulevard, on the east side of the city of Menifee Valley. Tonalite of the pluton is shown as open circles. The three solid circles outside the pluton contact are rocks of Menifee Valley; the solid circles within the pluton are mafic xenoliths. Note the higher SiO_2 and lower MgO values of the tonalite near the contact.

Like the majority of western zone plutons, the Domenigoni Valley pluton is relatively primitive, with relatively low initial $^{87}Sr/^{86}Sr$ ratios (Sr_i). Sr_i values of six samples from the pluton range from 0.7037 to 0.7045, and average 0.7041 (Kistler et al., 2003, this volume).

Turi and Taylor (1971) found that the eastern body of the pluton has undergone pronounced oxygen and hydrogen isotopic exchange affecting at least 70% of the body. They interpreted elevated isotopic values as evidence of contamination by the metasedimentary country rock. In contrast to the widespread isotopic exchange, major elemental variation shows only the northeastern part of the eastern body having slightly more silicic and less mafic tonalite than the rest of the pluton (Fig. 38). This northeastern area is within a low-$\delta^{18}O$ zone of Turi and Taylor (1971).

A detailed examination of the outer 51.5 m section of the eastern body exposed on McCall Boulevard (Fig. 35), the same location as one of Turi and Taylor's sample traverses, determined the pluton composition to be quite uniform at distances >25 m from the contact. Tonalite at the contact of the pluton has higher SiO_2 and Al_2O_3 contents and a lower contents of CaO, Fe_2O_3, and MgO than tonalite 1 m inside the pluton (Fig. 38). The first xenolith encountered (7 m inside the host rock contact) has slightly higher silica and alumina contents than xenoliths farther from the contact (Fig. 39). Based on detailed chemistry at and near the pluton contact, the pluton magma chamber chemically homogenized within ~25 m of the outer contact, i.e., very different from the oxygen and hydrogen isotope exchange that affects at least 70% of the pluton.

Cajalco pluton. The Cajalco pluton extends from south of Lake Mathews, northwest to the Norco–La Sierra area (Figs. 2 and 3). The pluton was emplaced by magmatic stoping of Estelle Mountain volcanics and volcaniclastic rocks in the western part of the pluton and gabbro in the central and eastern parts. Areas in

TABLE 3. MAJOR OXIDES (%) AND TRACE ELEMENTS (PPM) OF GRANITIC AND TOURMALINIZED ROCKS, CAJALCO PLUTON

Sample	Rock type	SiO_2	Al_2O_3	Fe_2O_3*	MgO	CaO	Na_2O	K_2O	TiO_2	P_2O_5	MnO	Sc	V	Co	Rb	Sr	Y
DMM-94-71	Granodiorite	72.9	13.7	2.47	0.54	2.18	3.49	3.31	0.30	0.11	0.03	4.07	25.16	4.67	157.84	135.23	20.13
DMM-94-72	Granodiorite	72.9	13.7	2.48	0.57	2.16	3.52	3.40	0.30	0.12	0.04	4.13	24.8	3.99	187.9	137	18.55
DMM-94-75	Granodiorite	72.7	13.8	2.61	0.52	1.85	3.51	3.41	0.30	0.12	0.07	4.54	28.29	2.22	178.78	142.78	13.58
DMM-94-78	Monzogranite	75.4	12.9	1.54	0.24	1.45	3.18	4.20	0.19	0.08	0.02	2.98	13.81	1.62	173.58	98.47	33.13
Caj-1	Least tourmalinized	74.3	13.4	2.07	0.35	1.71	3.44	3.79	0.24	0.04	0.03	6	20	2.1	137	116	29.6
Caj-2	Least tourmalinized	75.2	12.9	1.96	0.43	1.7	3.13	3.89	0.23	0.03	0.03	<5	15	2.2	138	124	26.6
Caj-3	Slightly tourmalinized	74.6	13.3	2.1	0.42	1.59	3.59	3.41	0.24	0.04	0.05	<5	18	2.1	118	118	40.3
Caj-4	Slightly tourmalinized	73.7	13.3	1.99	0.41	1.83	3.45	3.64	0.24	0.04	0.02	<5	18	3.4	138	132	24
Caj-5	Moderately tourmalinized	71.8	12.5	8.73	0.32	0.49	0.79	0.04	0.22	0.04	0.03	<5	15	1.5	1.4	52	7.2
Caj-6	Moderately tourmalinized	75.7	11.3	6.83	0.57	0.32	0.6	0.03	0.19	0.04	0.02	<5	14	2.2	1.2	48.5	9.7
Caj-7	Tourmaline	65.6	17.1	6.16	2.23	0.55	0.81	0.31	0.63	0.07	0.03	12	101	7.2	17.3	53.5	41
Caj-8	Tourmaline	36	27.7	17	4.28	1.25	2.06	0.51	0.3	<0.01	0.05	14	56	5.8	38.9	193	33.6

*Total Fe expressed as Fe_2O_3.

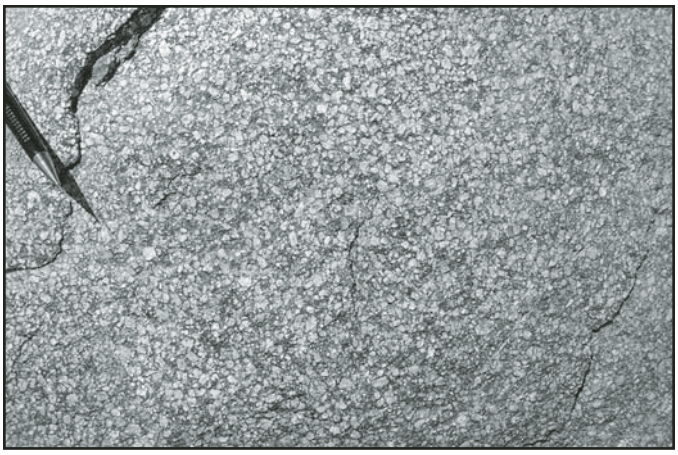

Figure 40. Hypabyssal-textured porphyritic dike that intrudes granodiorite of the western zone Cajalco pluton, south of Lake Mathews, northern Perris block.

the western part of the pluton are underlain by subequal amounts of granodiorite and stoped quartz latite porphyry of the Estelle Mountain volcanics. Small to mappable (1:24,000 scale) stoped blocks of gabbro are abundant north of Lake Mathews, where the pluton consists of about equal volumes of gabbro and granodiorite (Morton and Weber, 2001).

The pluton is composed mostly of biotite and biotite-hornblende monzogranite and granodiorite. Textures in the pluton change from porphyritic and subporphyritic in the shallower western part of the body to hypautomorphic granular in the central and eastern parts. Porphyritic textures are common in the granodiorite near the pluton roof. The west-to-east variation in texture suggests that the pluton, like the Gavilan ring complex, was tilted up on the east. Grain size is quite variable, ranging from fine to coarse grained. Northwest of Lake Mathews, much of the pluton consists of fine-grained leucocratic monzogranite. In the subporphyritic and porphyritic rocks near the pluton roof, quartz phenocrysts have a beta quartz habit. Locally, the subporphyritic and porphyritic rocks contain small miarolitic cavities. In the eastern part of the pluton, monzogranite is subordinate to granodiorite. The granodiorite is mainly medium grained, equigranular, hypautomorphic-granular and contains variable amounts of angular mafic enclaves. Within the pluton, there are a few hypabyssal porphyritic dikes composed of distinctive feldspar phenocrysts in a dark-gray, very fine-grained groundmass (Fig. 40).

Autometamorphic tourmalinized rock is widespread near the pluton roof in the western part of the pluton. Tourmalinization extends into overlying volcanic and volcaniclastic rocks. The tourmalinized rock ranges from incipient fracture-filling films to large masses up to hundreds of meters in length, both consisting of essentially only tourmaline and accessory minerals. These large tourmaline bodies, locally termed "tourmaline blow-outs," consist of very fine-grained to aphanitic schorl that is more erosionally resistant than surrounding granodiorite and stands out as small, bold black hills. Northeast-striking joints are preferential sites for the most tourmalinized rock. In the areas of most intense tourmalinization, the host monzogranite has subporphyritic and porphyritic textures.

The chemistry of the various stages and degree of tourmalinization are given in Table 3 and shown in Figure 41. The first stage of tourmalinization is fracture filling by paper-thin layers of tourmaline (Fig. 41A). Tourmalinization progressively extends beyond fracture filling to replace minerals adjacent to the fracture, first replacing mafic minerals (Fig. 41B) and then feldspar. In moderate tourmalinization, quartz content increases with the increase in tourmaline (Fig. 41C). With further tourmalinization, quartz is progressively replaced by tourmaline. Where quartz

Zr	Nb	Cs	Ba	La	Ce	Pr	Nd	Sm	Eu	Gd	Tb	Dy	Ho	Er	Tm	Yb	Hf	Ta	W	Th	U
106.88	4.42	5.55	631.18	16.61	32.23	3.49	15.97	2.95	0.61	3.16	0.64	3.32	0.73	2.33	0.35	2.12	3.41	0.66	0.76	10.61	2.3
106.02	5.04	5.67	662.37	19.45	38.94	3.94	15.31	3.07	0.7	2.71	0.5	3.22	7	2.14	0.24	1.78	3.24	0.6	0.25	14.56	1.33
116.29	4.52	8.12	717.22	15.67	34.14	3.25	14.94	2.84	0.87	2.49	0.36	2.5	0.47	1.64	0.28	1.45	3.72	0.35	1.06	14.87	4
117.02	5.09	3.76	676.79	32.47	66.92	7	26.43	5.97	0.66	4.73	0.9	5.56	1.19	3.45	0.53	3.35	4.36	0.73	0.58	23.33	3.28
177	6	4.8	863	18.1	33.8	4.32	16.7	3.9	0.77	4.29	0.82	5.18	1.15	3.49	0.54	3.5	6	0.7	0.7	17.9	4.12
142	5	5.2	804	29.6	59.5	6.75	24.7	4.8	0.58	4.66	0.76	5.08	0.98	2.93	0.44	2.9	5	0.6	0.6	20.6	5.49
145	6	2.7	800	29	59	6.77	25.1	5.3	0.75	5.7	1.15	7.53	1.61	4.73	0.74	4.8	5	0.7	0.7	17.1	13.7
160	5	3.8	832	18.9	37.8	4.34	16.4	3.6	0.64	3.45	0.63	4.28	0.88	2.52	0.4	2.9	5	0.5	0.5	14.5	5.16
147	3	0.7	7.2	4.3	8.4	1.03	3.9	0.9	0.12	1.11	0.17	1.05	0.28	0.8	0.11	0.9	5	<0.5	<0.5	15.6	1.91
147	3	0.5	2.4	7.6	15.2	1.83	7	1.3	0.15	1.56	0.26	1.67	0.39	1.03	0.18	1.5	5	<0.5	<0.5	22.3	3.08
93.1	15	0.5	41.5	8.2	12.3	1.99	8.6	2	0.31	3.14	0.67	4.9	1.29	4	0.7	4.1	3	0.8	0.8	6.9	2.98
114	4	1.2	22.3	1.9	3.1	0.4	1.7	0.4	0.12	0.89	0.28	3.46	1.22	5.21	1.07	8.9	4	0.5	0.5	26.8	2.44

is the only remaining mineral of the original rock, the resulting tourmalinized rock is a very distinctive, white-dappled black rock resembling porphyry (Fig. 41D). Brecciated tourmalinized rock is common and occurs in zones as thin as 0.5 cm to tens of meters. Monzogranite clasts in breccia zones show various stages of tourmalinization. Some clasts are zoned, indicating brecciation occurred during tourmalinization (Fig. 41E).

Completely tourmalinized rock contains small amounts of pyrite, and very locally, cassiterite. Cassiterite occurs as branching and anastomosing light-brown veinlets (Fig. 41F) and as small dark-brown masses of zoned crystals (Fig. 41G). Most of the extensively tourmalinized rock has been prospected for tin, which was discovered ca. 1853 within a large body of tourmalinized rock in the Eagle Valley area west of Lake Mathews (Sampson, 1935).

Average silica content of typical Cajalco pluton rock in the western part of the pluton is 73%; moderately tourmalinized rock has slightly higher silica, 74%–75%. Silica content decreases to a range of between 65.6% and 36% in completely tourmalinized rock. With progressive tourmalinization, CaO and K_2O decrease with replacement of feldspar, and Al_2O_3, MgO, and Fe_2O_3 increase with increases in tourmaline (Table 3).

Locally, dumortierite rather than tourmaline occurs, most commonly as large sprays of pink-to-violet acicular to prismatic radiating crystals. An exceptionally large tabular body of dumortierite located in Temescal Canyon (Fig. 3) has been described as a dumortierite dike (Larsen, 1948). Cobbles of tourmalinized rock are locally abundant in the Miocene Lake Mathews Formation and in Quaternary fluvial deposits in the area south of Lake Mathews.

U-Pb zircon ages from the coarse-grained monzogranite of the Cajalco pluton are 109.5 Ma_{id} and 111.5 Ma_{ip}. REE patterns for the Cajalco pluton (Fig. 42) are similar to (1) the generic granodiorite of the western zone plutons, (2) the patterns of Gromet and Silver (1987) for granodiorite of their western region, and (3) the Las Bancas and East Mesa plutonic suites of Todd et al. (2003).

Transition Zone Plutons

The western and eastern transition zones formed (Fig. 2) as subduction transitioned from beneath a Mesozoic oceanic arc to beneath a continental marginal setting overlain by thicker and older continental crust (e.g., Lee et al., 2007). Western transition zone plutons have some geochemical similarities with plutons of the western zone, and similarly, some eastern transition zone plutons are zoned La Posta–type plutons common in the eastern zone. La Posta–type plutons have tonalite outer parts and granodiorite-monzogranite cores, the latter of which are commonly muscovite bearing. Transition zone plutons were emplaced mostly in Mesozoic rocks, but some intruded Paleozoic metamorphic rocks in the eastern part of the eastern transition zone. Pluton contacts are concordant with enclosing country rock, in contrast to the discordant contacts of western zone plutons. The clearest distinction between western zone and transition zone plutons is seen in the western transition zone plutons, which have intense and well-developed planar foliations, slightly positive ε_{Ndi}, and Sr_i >0.7045. Western transition zone plutons are ilmenite bearing, in contrast to the magnetite-bearing western zone plutons. This difference produces a marked change in the aeromagnetic expression of the highly magnetic western zone against the weakly magnetic western transition zone (Fig. 18 [available on the CD-ROM accompanying this volume and in the GSA Data Repository (see footnote 1)]). The slightly positive ε_{Ndi} that characterizes the western transition zone plutons extends to the western transition zone Lakeview Mountains pluton, which is magnetite and ilmenite bearing and has a slightly positive ε_{Ndi}, (+0.4). Values of $\delta^{18}O$ are <9‰ in the western transition zone and >9‰ in the eastern transition zone, and eastern transition zone plutons have distinctively negative ε_{Ndi} values. The eastern transition zone includes large plutons of the La Posta–type that do not occur in the western transition zone but are typical of the eastern zone. La Posta–type plutons of the eastern transition zone are distinguished from those of the eastern zone in having $Sr_i < 0.7060$ and, except for a few samples, Pb_i of <19.

Western Transition Zone Plutons

Western transition zone plutons occur in an irregular zone up to 25 km wide in the northern part of the Perris block. Southeastward, the western transition zone abruptly narrows south of 33°22′N, where a 5 km width of intensely deformed metamorphic rocks, devoid of western transition zone plutons, separates the western zone from the eastern transition zone (Fig. 2). This

Figure 41. Tourmalinized monzogranite, Cajalco pluton, Eagle Valley, northern Perris block. (A) Incipient tourmalinization of semiporphyritic monzogranite containing beta habit quartz. Introduction of tourmaline and quartz is largely restricted to fractures in the monzogranite. Some outward progression of tourmalinization formed the thicker tourmalinized fracture in the center of the photograph. Note development of breccia along the vertical tourmalinized fracture on the right side of the photograph. (B) Pervasive tourmalinization has replaced all mafic minerals in semiporphyritic monzogranite as well as expanding into the monzogranite along fractures. Breccia in thicker tourmalinized rock is visible below the quarter. (C) Monzogranite in which tourmalinization ranges from incipient to complete. Left side of sample is essentially unaltered monzogranite that grades into silica-enriched quartz tourmaline rock, and progressively increases in tourmaline passing into breccia zone on right side of sample. (D) Uniformly tourmalinized monzogranite. All mafic minerals and feldspars have been replaced by tourmaline, leaving only quartz of the original monzogranite. This sample is from a 100-m-wide tourmalinized body. (E) Brecciated tourmalinized monzogranite. Light areas are breccia clasts, not phenocrysts, that are in various stages of tourmalinization. Nolan pick for scale. (F) Vein-like masses of cassiterite in massive aphanitic tourmaline. (G) Zoned cassiterite crystals in massive aphanitic tourmaline. The two largest, prominently zoned crystals just below the center of the photomicrograph are approximately 0.5 mm across.

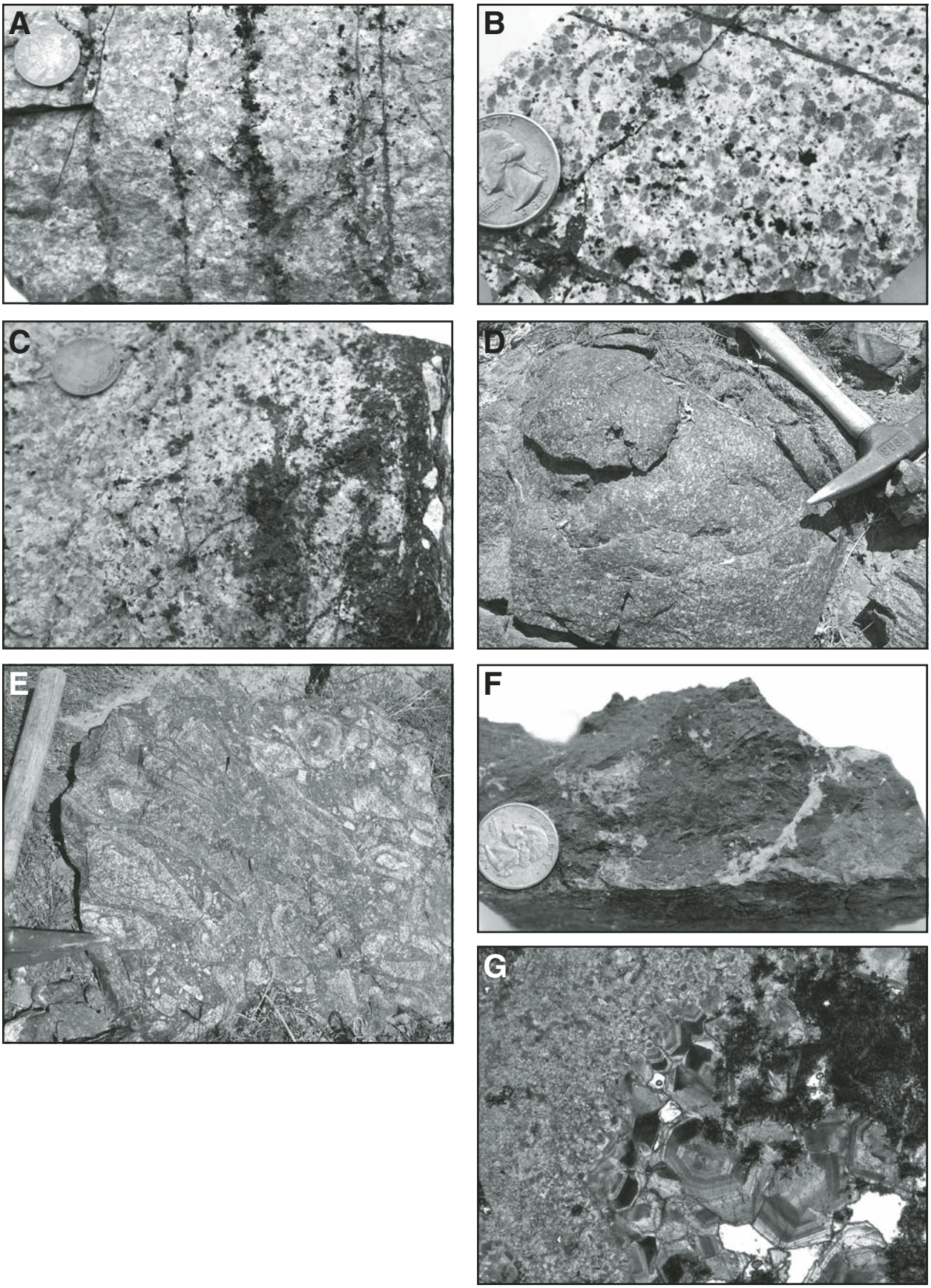

belt of deformed metamorphic rocks, wholly within the western transition zone, continues southward for ~10 km, to the point where it is intruded by a massive to foliated tonalite body, the Tucalota Valley pluton, which may be part of, or related to, a large body of the tonalite of Coahuila Valley to the east. The western transition zone widens around the Tucalota Valley pluton and a kilometer-wide metamorphic screen along its eastern side, and then narrows again to about a width of 2 km just south of the pluton. To the southeast, the western transition zone widens to, and maintains, an average width of ~10 km to at least latitude 33°N. Plutons of the western transition zone south of 33°N have only been mapped in reconnaissance, and although tonalite predominates, the western transition zone consists of a wide range of granitic lithologies that are mixed with large areas of metamorphic rocks.

Western transition zone plutons are eroded at mid- to lower-crustal depths, as indicated by pressures of crystallization ranging from 4.5 to 6.5 kbar (Ague and Brimhall, 1988; Smith et al., 1991). In contrast to the isotropic textured western zone granitic plutons containing equidimensional enclaves, western transition zone plutons consist of well-foliated rock containing ellipsoidal to pancake-shaped enclaves. Locally, some of these enclaves have undergone two periods of deformation (Figs. 22 and 23). Silica content of the western transition zone rocks ranges from 42.9% to 77.1%, and averages 63.8%.

Plutons range in composition from olivine gabbro to monzogranite and are characterized isotopically by moderate Sr_i (0.7045–0.7055), $\delta^{18}O$ (+7‰ to +10‰), and Pb_i average 18.744. The ε_{Ndi} values are positive +0.4 to +2.9. Pluton emplacement age ranges from 111 to 98 Ma.

In addition to discrete plutons, the western transition zone includes significant expanses of heterogeneous granitic rocks, which are commonly gneissic rocks consisting mostly of biotite-hornblende granodiorite and tonalite. These heterogeneous granitic rocks have moderately well-developed planar fabrics and are more mineralogically heterogeneous in close proximity to metamorphic country rock. Northeast of Lakeview (Fig. 3), where they are in contact with the rocks of Jacumba Mountains, these rocks contain abundant thin mafic enclaves. The heterogeneous rock unit bordering the Lakeview Mountains pluton in many places contains complex, composite irregular-to-planar shear zones that appear to be protoclastic. Ellipsoidal mafic enclaves are partly to completely transposed and attenuated where cut by the shear zones. These shear zones are interpreted to have resulted from the outward expansion of the Lakeview Mountains pluton (Morton et al., this volume).

Gabbro is less common in the western transition zone than in the western zone, but this contrasts with the near absence of gabbro farther east in the batholith. Most of the gabbro in the western transition zone is hornblende gabbro with lesser amounts of olivine gabbro. Three plutons, the Val Verde, the Lakeview Mountains, and the Box Springs Mountains plutonic complex, comprise most of the northern part of the western transition zone, in addition to some small plutons in the Bernasconi Hills (Fig. 3). Extensive alluvial cover in the Riverside–Jurupa Mountains area obscures much of the geometry and intrusive relationships of the plutons at the north end of the western transition zone. Chemical analyses for all western transition zone units are given in Table 2 (on CD-ROM accompanying this volume and in GSA Data Repository [see footnote 1]).

Granitic rocks at the northern edge of the batholith. The northwesternmost Peninsular Ranges batholith exposures are a few isolated outcrops of biotite-hornblende tonalite in the Elephant Hill area west of Pomona (Fig. 3), only 3 km south of an exposure of Transverse Ranges granitic rock (see Premo et al., this volume, Chapter 2). The tonalite at Elephant Hill has U-Pb zircon ages of 98.3 Ma_{id} and 100 Ma_{ip}. The Sr_i of the tonalite is 0.7055, and ε_{Ndi} is 0.4.

To the east, exposures of granitic rocks in the Jurupa Mountains (Fig. 3) include gabbro, tonalite, and granodioritic bodies, and common granitic pegmatite dikes, emplaced in probable Paleozoic metasedimentary rocks. Some bodies are elongate in a western Transverse Ranges orientation, while others are in a more typical northwest Peninsular Ranges orientation. The gabbro is typical medium- to coarse-grained hornblende-pyroxene gabbro. Biotite-hornblende tonalite is relatively heterogeneous, foliated, and medium- to coarse-grained hypautomorphic-granular tonalite. Many outcrops of tonalitic rocks have two different planar fabrics, a northwest-striking fabric and an east-striking fabric. Most outcrops of biotite granodiorite appear relatively homogeneous. U-Pb zircon ages for the tonalite are 104 Ma_{id}, 104.1 Ma_{id}, and 101.7 Ma_{ip}. Sr_i of the tonalite is 0.7044 and 0.7047. Granodiorite U-Pb zircon age is 111 Ma_{ip}. The granodiorite has an abnormally high value Sr_i of 0.7076.

Granites of the Riverside area. Discontinuous bodies of biotite granite and local hypersthene and fayalite granite occur in the Riverside area. Although located within the western transition zone and having mostly western transition zone properties, some of these bodies are more typical of western zone plutons based on texture and age. Most of the granitic rocks in the Riverside area are leucocratic, medium- to coarse-grained, massive- to faintly foliated biotite granite that averages 1%–3% biotite. Mafic enclaves are sparse, except locally in some western

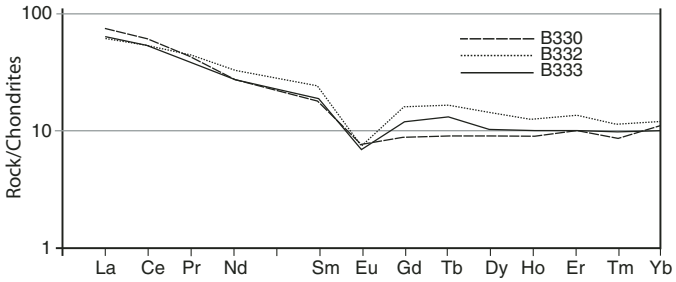

Figure 42. Chondrite-normalized rare earth element (REE) spider diagram for Cajalco pluton, showing relatively uniform, moderately strong negative Eu anomalies. All samples are from the Baird-Welday collection.

exposures, where the granite contains 2%–8% biotite and sparse to abundant xenoliths of quartz diorite, granodiorite, and fine-grained mafic rock. At Mount Rubidoux (Fig. 3), granite contains sparse hypersthene and fayalitic olivine and has a higher concentration of dark-gray, fine-grained enclaves. Also at Mount Rubidoux, a second body, informally named the granite of Mount Rubidoux (Morton and Miller, 2006), is a coarse-grained granite phase that is also characterized by fayalite and hypersthene. This latter granite is massive and heterogranular, with an average grain size of 5 mm, and contains some K-feldspar crystals up to 12 mm in length. Biotite and hornblende aggregate to ~5%, and fayalite and hypersthene are scarce constituents. U-Pb zircon ages are 109.1 Ma_{id} and 106.1 Ma_{ip}. The $^{40}Ar/^{39}Ar$ ages of biotite and of K-feldspar are 98.2 Ma and 95–91 Ma, respectively.

Green Acres gabbro. The Green Acres gabbro is a heterogeneous gabbroic body, the northern half of which consists of intermingled olivine, pyroxene, and hornblende gabbros intruded by biotite-hornblende quartz diorite and tonalite (for a thorough description of the Green Acres gabbro, see Berger, this volume). Within the unit, quartz diorite and tonalite decompose more readily than gabbro, giving rise to slopes covered by gabbro rubble, which in most places masks the presence of the quartz diorite and tonalite. Locally, the unit contains small masses of orbicular gabbro (Fig. 43).

The southern half of the body is mainly olivine gabbro, containing olivine (Fo_{75} to Fo_{87}) that ranges from a few percent to about one third of the rock. Anorthite (An_{90}) makes up 30%–90% of the gabbro as anhedral to subhedral, complexly twinned crystals. Hypersthene and augite are widespread; commonly, augite is mantled with brown and/or green hornblende. Light-green hornblende occurs primarily in kelyphytic reaction rims intergrown with spinel around olivine. Thin, planar, vein-like hornblende-spinel masses are common in gabbro that contains abundant olivine. Protoclastic olivine gabbro (flaser gabbro) occurs locally and contains abundant light-green chlorite. Locally, the rocks consist of nematoblastic hornblende gabbro, which is typically 46% brown hornblende, 7% green hornblende, 9% clinopyroxene, 2% olivine, 34% calcic plagioclase, and 2% opaque minerals. A variety of small gabbroic dikes cut the olivine gabbro. These dikes consist of equigranular fine- to coarse-grained mesocratic to melanocratic hornblende gabbro, porphyritic hornblende-olivine gabbro, and porphyritic anorthite-olivine gabbro.

Two small elliptical masses of distinctive troctolite (Fig. 44) in the southern part of the unit contain ~45% anorthite (An_{90}), 36% olivine (Fo_{85}), 11% clinopyroxene, 3% orthopyroxene, 2% hornblende, 2% spinel, and 5% iddingsite. Kelyphytic rims mantle most olivine crystals, and large subhedral anorthite crystals impart a slightly porphyritic texture to the troctolite. Clinopyroxene and hornblende occur as large poikilitic crystals enclosing large areas of plagioclase and olivine crystals. Locally, masses of leucocratic gabbro consist largely to entirely of labradorite-anorthite with small quantities of olivine and/or pyroxene. This anorthitic gabbro weathers to form gray slopes.

Pegmatite dikes are common in the Green Acres gabbro. Euhedral garnet and tourmaline (schorl) are common accessory minerals; some pegmatite dikes contain andalusite, apparently produced by chemical interaction between pegmatite and gabbro. One pegmatite dike contains a mass of gabbro altered to biotite, hydrobiotite, and vermiculite enclosing individual andalusite crystals up to 6 cm in length. Euhedral dark-blue corundum crystals, up to 1 cm in length, occur in the core of some andalusite crystals. Webb (1943) interpreted this relationship as resulting from the incorporation of metasedimentary rock into the pegmatite, but we interpret it to be the result of interaction between the pegmatite and included masses of olivine gabbro. Some of the pegmatite dikes are mylonitic with very planar fabric and pronounced mineral lineation.

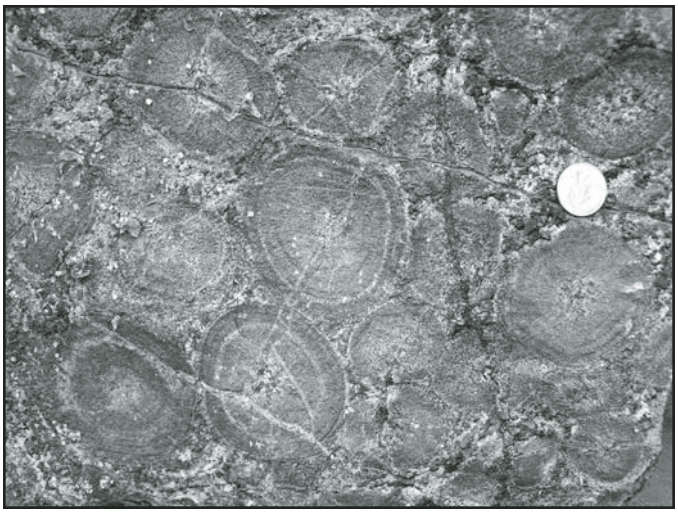

Figure 43. Orbicular gabbro, northeast part of the western transition zone Green Acres gabbro, central Perris block.

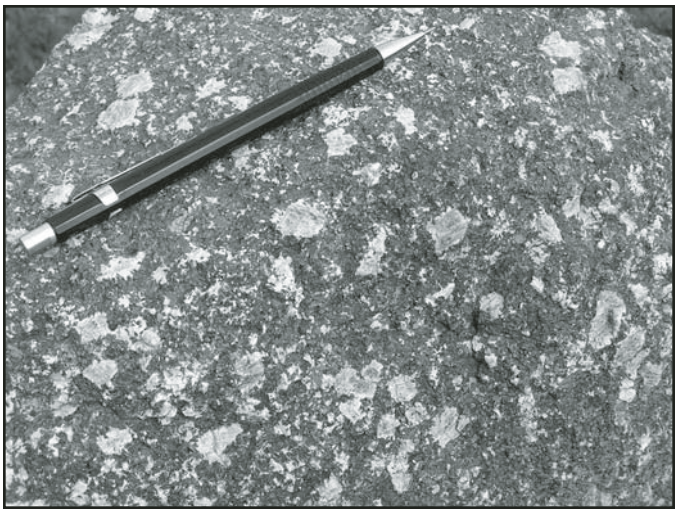

Figure 44. Isotropic-textured troctolite containing large crystals of anorthitic plagioclase, southern part of the Green Acres gabbro, central Perris block.

Mixed granitic rocks at the south end of the Lakeview Mountains pluton contain several small bodies of metamorphosed gabbro apparently derived from the Green Acres gabbro. This metagabbro contains abundant masses of chlorite and blue-green hornblende.

Val Verde pluton. The Val Verde pluton, located along the west side of the western transition zone, extends from south of Perris northward to the Riverside area (Figs. 2 and 45). The pluton is steep walled, exposed at a midcrustal depth, and composed of relatively homogeneous, foliated, medium- to coarse-

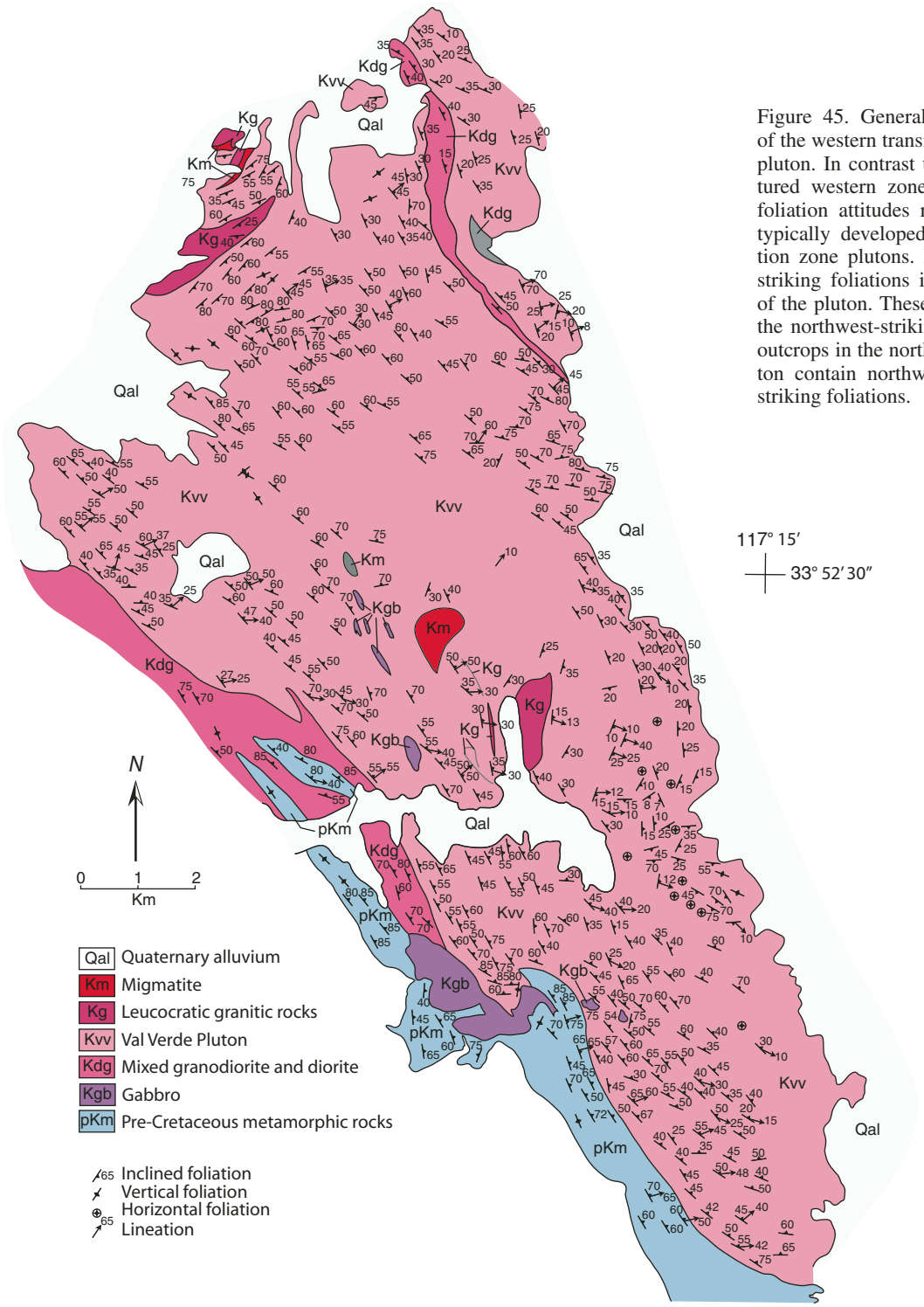

Figure 45. Generalized geologic map of the western transition zone Val Verde pluton. In contrast to the isotropic-textured western zone plutons, abundant foliation attitudes reflect the structure typically developed in western transition zone plutons. Note the northeast-striking foliations in the northern part of the pluton. These foliations postdate the northwest-striking foliations. Some outcrops in the northern part of the pluton contain northwest- and northeast-striking foliations.

grained hypautomorphic-granular biotite-hornblende tonalite. The K-feldspar content is less than 2% for most of the tonalite, except along the west margin of the pluton, where it ranges from 2% to 10%. A number of gabbro and migmatitic bodies and one elongate heterogeneous granodiorite-quartz diorite body are enclosed within the pluton; all of these bodies appear to be older than the Val Verde pluton. Pegmatite dikes are rare, contrasting with the adjacent Box Springs Mountains plutonic complex and the Lakeview Mountains pluton. However, one tabular-shaped pegmatite has a length of 2 km and contains basal aplitic line-rock layering.

Most of the foliation in the tonalite strikes northwest, parallel to the regional structural grain of the batholith, and dips moderately to steeply to the northeast (Fig. 45). In the northern 3 km of the central part of the pluton, east-to-northeast–striking foliations are dominant. To the south, some tonalite outcrops include two planar fabrics, an older northwest-striking foliation cut by a younger east-striking foliation. An elegant investigation of the modal mineralogy and structure of the tonalite through the central part of the pluton, along the Colorado River aqueduct tunnel, was conducted by Osborn (1939). Based on petrofabric analysis, Osborn determined the tonalite had two different planar mineral orientations.

The tonalite contains abundant elliptical to pancake-shaped mafic enclaves parallel to the foliation plane (Fig. 46). Where measured in the northern part of the pluton, the long axes of elongate mafic enclaves are oriented northeast and plunge at moderate angles to the northeast. In the central and southern parts of the pluton, elongate enclaves strike east to southeast and plunge at low to moderate angles to the southeast. In the south-central part of the pluton, much of the rock is massive or has only faint, commonly horizontal, foliation, and the enclaves are less attenuated. In this part of the pluton, there are segregation masses of mesocratic-to-melanocratic tonalite.

Figure 46. Crudely, but pervasively, foliated biotite-hornblende tonalite of the Val Verde pluton, Perris block. Tonalite breaks along foliation that includes elongate E_1 mafic enclaves.

The Val Verde pluton is slightly older than the adjacent Box Springs and Lakeview Mountains plutons. U-Pb zircon ages are 105.7 Ma_{id} and 107.8 Ma_{ip}. The $^{40}Ar/^{39}Ar$ ages of hornblende, biotite, and K-feldspar are 100.5 Ma, 94.7, and 90.3–86.5 Ma, respectively.

Lakeview Mountains pluton. The Lakeview Mountains pluton is a steep-walled, in plan view, teardrop-shaped pluton (Morton, 2003c, 2003d; Morton and Matti, 2001a) exposed at midcrustal depth (Fig. 47). Emplacement of the pluton is interpreted to have been largely forceful. The body is located at a major deflection of the regional northwest structural grain within the batholith. This deflection is interpreted to have been caused by outward growth of the pluton. For a more complete description and chemistry of this pluton, see Morton et al. (this volume).

Mineralogically, the pluton is characterized by extreme heterogeneity produced by ubiquitous schlieren. The pluton consists of foliated biotite-hornblende tonalite, virtually devoid of K-feldspar, which occurs only as rare antiperthite. Schlieren range in composition from leucocratic plagioclase-quartz rock to melanocratic biotite-hornblende rock; in most of the pluton, these schlieren range from a few centimeters to several meters in length (Fig. 48). Typically, schlieren are near-planar, but some are wispy and folded. Locally, alternating sheet-like concentrations of plagioclase-quartz rock and biotite-hornblende rock produce a pronounced layering commonly consisting of juxtaposed leucocratic quartz-plagioclase and melanocratic hornblende-biotite layers. Some hornblende is cored with colorless cummingtonite. Ellipsoidal to pancake-shaped mafic enclaves are common.

Plagioclase-quartz rock and biotite-hornblende rock form mappable-sized (1:24,000 scale) bodies. Except for form and scale, the composition of these bodies is similar to that of the schlieren. Leucocratic rock masses consist of andesine and quartz that have minor amounts of poikilitic biotite and hornblende. Muscovite occurs in these rocks as a rare accessory mineral interstitial to plagioclase. Melanocratic rock masses range in composition from ~50% biotite-hornblende to entirely biotite-hornblende.

An elliptical body of comb-layered gabbro is located along the southwest margin of the pluton. Layering in the gabbro consists of alternating layers of labradorite gabbro and hornblende or augite gabbro. Labradorite crystals are oriented normal to the layering and branch upward from the base of a layer to form feather-like crystals. Folded layering, having fold amplitudes of 1 cm, is common. Concentrated near the center of the pluton are masses of hypersthene gabbro.

Numerous granitic pegmatite dikes are also concentrated in the center of the pluton. Most of the dikes are tabular, steeply dipping, and strike northeast and southwest. A few dikes are bulbous (Jahns, 1955), and a few are thickened at a roll in the dip of the dike. Almost all dikes are symmetrically zoned, compositionally and texturally. Many contain rare earth minerals, both oxides and phosphates.

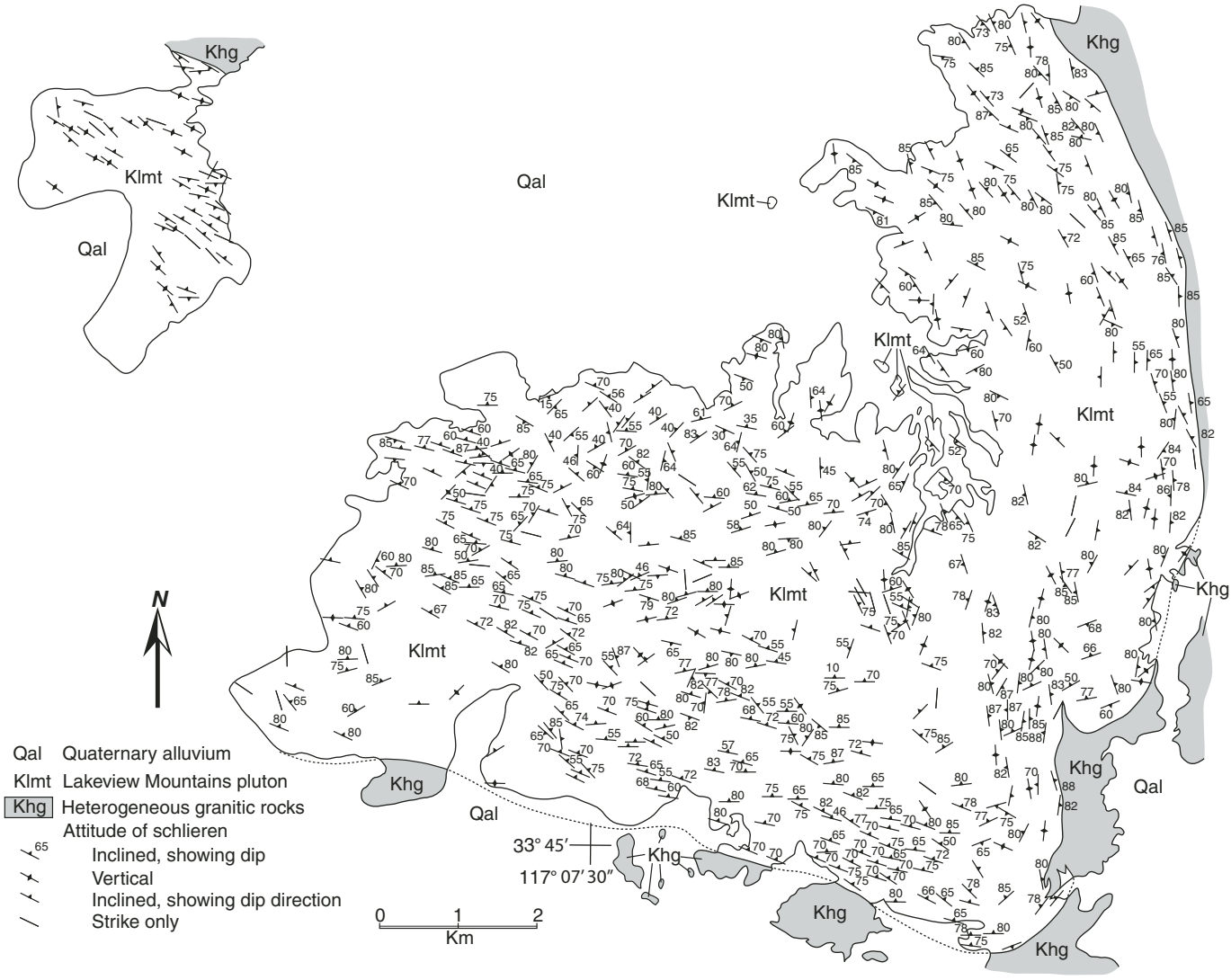

Figure 47. Generalized geologic map of the western transition zone Lakeveiw Mountains pluton showing concordant and discordant northwest- and northeast-oriented schlieren.

Although masked by extreme outcrop-scale chemical variation produced by schlieren, the pluton is chemically and mineralogically zoned (Morton et al., 1969, this volume). Even though the Lakeview Mountains pluton is located in a relatively low-magnetic part of the Peninsular Ranges batholith, the center part of the pluton is more magnetic than any other part of the western transition zone (Langenheim et al., 2004).

U-Pb zircon ages from two samples are 100 Ma_{id}, 97.4 Ma_{ip} and 99.3 Ma_{id} and 98 Ma_{ip}. A third sample has an age of 100.2 Ma_{ip}. The $^{40}Ar/^{39}Ar$ age of hornblende is 98.6 Ma, and the conventional K/Ar age of biotite is 92.4 Ma. The pressure of crystallization of hornblende is 5–5.5 kbar (Smith et al., 1991).

Reinhardt Canyon pluton. An arcuate-shaped tonalite pluton, the Reinhardt Canyon pluton, borders the east side of the Lakeview Mountains pluton. Most tonalite of the Reinhardt Canyon pluton lacks the ubiquitous schlieren of the adjacent Lakeview Mountains pluton, has a well-developed planar fabric parallel to the outline of the body, and contains abundant mafic enclaves that in places are rod-shaped and vertical (Fig. 26). A more extensive description of the pluton is included in the discussion of the Lakeview Mountains pluton (Morton et al., this volume).

Box Springs Mountains plutonic complex. The Box Springs Mountains plutonic complex is elliptical in plan view, flat floored, and compositionally, isotopically, and texturally zoned. It is made up of five major and two minor units (Fig. 49). The core of the complex consists of massive isotropic, high-silica biotite tonalite. Foliated biotite tonalite and granodiorite surround this core, and they are in turn surrounded by a variety of foliated tonalite and granodiorite. Based on a combination of geometry and fabric, the plutonic complex is interpreted as an elongate balloon-like mass having a tapering inflation point near its north end. The outer parts of the complex are in contact with biotite-hornblende

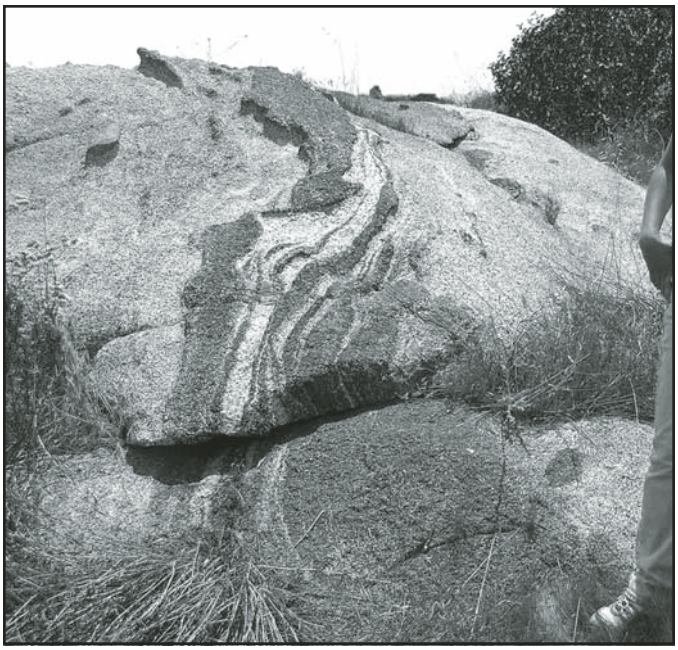

Figure 48. Typical melanocratic biotite-hornblende schlieren, southwestern Lakeview Mountains pluton.

tonalite. All of the units include abundant mafic enclaves, most of which are discoidal to platy in shape.

The southern part of the complex was included by Larsen (1948) in his general Bonsall tonalite unit, but the northern part is located north of his map area. In addition to Larsen's work, the complex has been the subject of several theses (Menzie, 1962; Joshi, 1967; Stock, 1992) and is included in its entirety on a series of detailed 7.5′ quadrangle geologic maps (Morton, 1978; Morton and Cox, 2001a; Morton and Matti, 2001b). The major units of the complex are described here from the core to the outer margin and are shown on Figure 49. In general, this sequence is interpreted as representing the youngest to oldest parts of the complex.

The center of the complex is composed of light-gray, fine- to medium-grained equigranular biotite tonalite (Fig. 50; Kbt on Fig. 49). Unlike other rocks of the complex, the center is massive-textured, and only in the outer part has a crude foliation developed. Lithologically identical tonalite occurs as a small elliptical-shaped body on the summit of Blue Mountain north of the complex core. Compositional layering in the center of the complex is shallow-dipping to horizontal, defining a shallow basin that is horizontally floored. Unlike the core of the complex, the biotite tonalite body on the summit of Blue Mountain has steeply inward-dipping foliation, geometrically defining a funnel-shaped body. Based on the funnel-shaped structure, this body is interpreted as the feeder for the core of the complex.

Much of the center biotite tonalite, the most homogeneous part of the complex, has faint to well-developed primary layering produced by variation in biotite content. Modal mineralogy of this and other units of the Box Springs Mountains plutonic complex is given in Table 4. The tonalite contains scattered, equant subrounded mafic enclaves. The morphology of these enclaves is markedly different from the discoidal to platy mafic enclaves that are common throughout the rest of the complex. U-Pb zircon ages from the core unit are 98.6 Ma_{id} and 98 Ma_{ip}, and the core rocks have a high Pb_i of 19.016.

The massive biotite tonalite (Kbt) is in contact with a biotite granite (Kbgr) on the east and north, a heterogeneous biotite-hornblende tonalite (Kbht) on the west, and appears to grade southward to light-gray, medium- to coarse-grained, foliated biotite tonalite and granodiorite (Fig. 51, Kbfg). The biotite granite (Kbgr) has steeply dipping foliation and occurs north of the core Kbt on Blue Mountain, where it is intruded by Kbt. In the La Loma Hills, in the northwestern part of the complex, the biotite granite is located between two older units, a porphyritic granodiorite and granite (Kbgg) and foliated hornblende tonalite (Kft).

Kbht, which is a light-gray, nonequigranular, medium- to coarse-grained, foliated granitic rock, is restricted to the west side of the core in the northwestern part of the Box Springs Mountains, where it intrudes a foliated biotite-hornblende tonalite (Kbft). The dominant rock type is leucocratic tonalite containing a few percent biotite, which occurs as thin irregular plates that are randomly distributed but crudely aligned to produce a wispy, swirling foliation. Within the leucocratic tonalite, pods and lenses of more mafic tonalite contain ~15% large ragged crystals of biotite. Both the leucocratic and more mafic tonalite contain 30%–40% quartz. Sparse potassium feldspar makes up 1% or less of the rocks. The tonalite contains dispersed, discoidal mesocratic enclaves. Simple granitic pegmatite dikes are abundant within the unit.

The contact between foliated Kbfg and the nonfoliated complex core unit Kbt is drawn on the basis of foliation development because the compositional difference between the two units is not obvious in some places. The inner part of unit Kbfg is tonalite containing minor hornblende and K-feldspar. K-feldspar is extremely variable in the unit, ranging from 1% to 21%, progressively increasing outward, grading from tonalite to granodiorite. Mafic, discoidal enclaves are common but not abundant. The Kbfg unit thins and pinches out along the west side of the core. On the east side of the complex, biotite granodiorite and tonalite are bounded by a unit of similar lithology (Fig. 49, Kbfgi), which contains very abundant discoidal mafic enclaves.

Surrounding Kbfg and the enclave-rich Kbfgi unit, there is a heterogeneous porphyritic granodiorite that locally grades to tonalite (Kbhg). This unit is thickest in the southeast part of the complex, pinches out along the southwest side, and reappears west of the core in conjunction with $Kbhg_1$, a layered version of the porphyritic granodiorite. The porphyritic granodiorite is light gray, medium to coarse grained, and has a well-developed foliation. Heterogeneity in the unit is the result of unevenly distributed mafic minerals. Subhedral tabular K-feldspar phenocrysts are up to 2.5 cm in length. Widespread and common

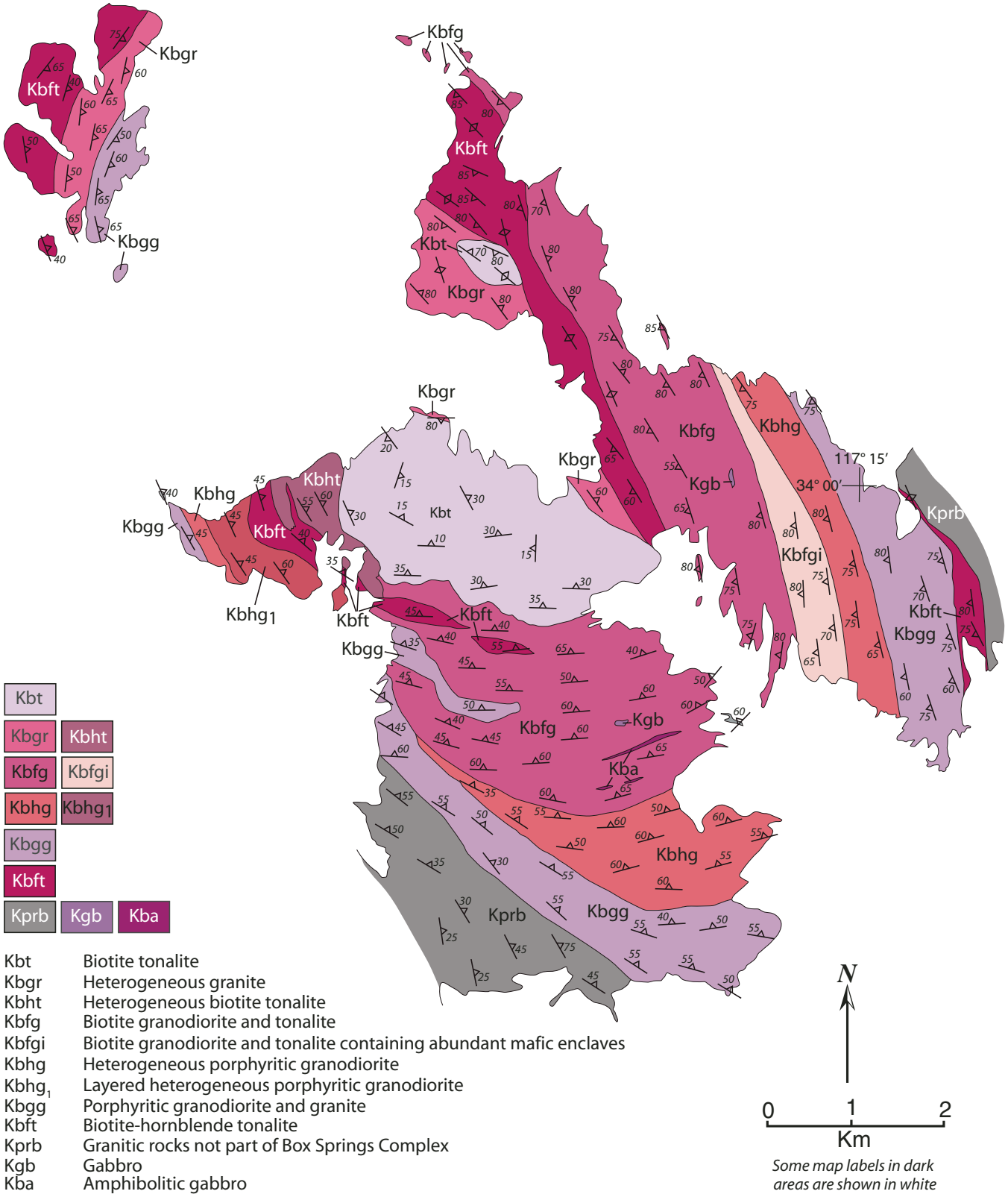

Figure 49. Generalized geologic map of the western transition zone Box Springs Mountains plutonic complex, northern Perris block.

Figure 50. Scattered rounded outcrops and boulders of massive isotropic-textured biotite tonalite (Kbt), which forms the core of the Box Springs Mountains plutonic complex. View looking east from Riverside.

discoidal-shaped mesocratic enclaves are oriented parallel to the foliation. In the west-central part of the complex, this unit has a pronounced layering resulting from systematic layer-by-layer variation in grain size.

The outer part of the Box Springs Mountains plutonic complex consists of a zone of heterogeneous porphyritic biotite granodiorite, lesser amounts of granite, and some biotite tonalite (Kbgg). The biotite granodiorite and subordinate biotite tonalite are light gray, coarse grained, and well foliated. Biotite is the common mafic mineral, but sparse hornblende is present. Mafic minerals are quite evenly distributed, unlike the uneven distribution in the adjacent heterogeneous porphyritic granodiorite. Subhedral K-feldspar phenocrysts are up to 2.5 cm in length. Discoidal mafic enclaves are oriented parallel to foliation. The porphyritic granodiorite grades inward into the heterogeneous porphyritic granodiorite.

Foliated biotite-hornblende tonalite containing minor granite (Kbft) occurs as several discontinuous bodies (1) near the center of the complex, (2) in the northwesternmost part of the complex in the La Loma Hills, and (3) on the east side of the complex. These separate bodies were probably not derived from a single magma source. The tonalite contains 20%–25% quartz and ~25% hornblende and biotite in subequal amounts. Hornblende and biotite occur as ragged crystals. K-feldspar is a sparse constituent, and anhedral interstitial sphene is a conspicuous accessory mineral. The tonalite contains abundant fine-grained ellipsoidal to extremely thin, platy mafic enclaves that are aligned within foliation in the enclosing tonalite (Fig. 52).

Thin elongate bodies of dark-gray to black foliated amphibolitic gabbro occur within biotite granodiorite and tonalite (Fig. 49, unit Kbfg). Only the larger masses are shown on Figure 49, and on the geologic map of the Riverside East 7.5′ quadrangle (Morton and Cox, 2001a). Foliation within the amphibolitic gabbro is parallel to that in the adjacent granodiorite. On the basis of compo-

TABLE 4. MODES OF MAJOR ROCK UNITS, BOX SPRINGS MOUNTAINS PLUTONIC COMPLEX

Sample	Map unit	Kspa. (%)	Plag. (%)	Qtz. (%)	Mafics (%)
BX-1A	kprb	17	41	27	15
BX-1E	kprb	19	39	28	14
BX-1H	kprb	19	41	27	13
BX-2F	Kbgg	15	45	35	5
BX-2C	Kbgg	18	38	38	6
BX-2I	Kbgg	15	41	40	4
BX-3C	Kbgg	28.5	36.5	27	8
BX-3G	Kbgg	4	52	33	11
BX-4D	Kbhg	17	41	32	10
BX-4G	Kbhg	18	42	29	11
BX-5A	Kbhg	1	50	34	15
BX-5B	Kbhg	2	51	34	13
BX-6A	Kbfg	19	40	29	12
BX-6B	Kbfg	16	38	34	12
BX-7A	Kbfg	1	52	37	10
BX-7B	Kbfg	17	43	30	10
BX-8A	Kbfg	4	49	34	13
BX-8B	Kbfg	3	57	26	14
BX-9A	Kbfg	2	54	21	23
BX-9B	Kbfg	1	54	23	22
BX-10A	Kbt	2	50	39	9
BX-10B	Kbt	1	52	37	10
BX-11A	Kbt	2	47	42	9
BX-11B	Kbt	1	51	36	12
BX-12A	Kbft	0	51	24	25
BX-12B	Kbft	0	49	24	27
BX-13A	Kbfg	5	55	28	12
BX-13B	Kbfg	21	38	32	9
BX-14A	Kbfgi	12	45	35	8
BX-14B	Kbfgi	16	44	32	8
BX-15A	Kbhg	22	42	27	9
BX-15B	Kbhg	15	33	41	11
BX-16A	Kbgg	2	54	34	10
BX-16B	Kbgg	17	39	32	12
BX-17A	Kbft	4	48	26	22
BX-17B	Kbft	4	59	18	19
BX-18A	Kprb	14	43	32	11
BX-18B	Kprb	21	36	34	9
BX-19J	Kprb	6	54	25	15
BX-20A	Kbft	4	48	28	20
BX-20B	Kbft	3	49	30	18
BX-21A	Kbgr	27	35	34	4
BX-21B	Kbgr	28	23	46	3
BX-22A	Kbgg	25	33	41	1
BX-22B	Kbgg	29	32	36	3
BX-23A	Kbft	0	53	23	24
BX-23B	Kbft	0	44	34	22
BX-24A	Kbht	0	52	44	4
BX-24B	Kbht	1	51	44	4
BX-25A	Kbht	0	53	30	17
BX-25Z	Kbht	0	49	17	34
BX-26G	Kbht	1	55	41	3
BX-27A	Kbt	3	53	38	6
BX-27B	Kbt	4	54	36	6
BX-1Z1	kprb	14	26	16	44
BX-1Z3	kprb	19	32	6	43
BX-2Z	Kbgg	1	53	33	13
BX-4Z1	Kbhg	0	58	11	31

Note: BX-1Z1 and BX-1Z3 feldspars are concentrated in streaks. Kspa—K-feldpsar; Plag—plagioclase; Qtz—quartz. Refer to text for map units.

Figure 51. North-dipping foliated tonalite-granodiorite (Kbfg, Kbhg, and Kbgg) of the intermediate part of the Box Springs Mountains plutonic complex. View looking west from Moreno Valley.

Figure 52. Well-foliated biotite-hornblende tonalite (Kbft) containing very attenuated E_2 mafic enclaves, southwestern Box Springs Mountains.

sition, the amphibolitic bodies are interpreted to be hornblende gabbro that was deformed and metamorphosed within the granodiorite. In addition to amphibolitic gabbro, several small, less-deformed hornblende gabbro masses occur within biotite granodiorite and tonalite. These small gabbro masses retain a primary gabbroic fabric. In plan view, they are elongate, with the direction of elongation lying within the planar fabric of the enclosing rock.

In addition to the simple granitic-pegmatite dikes found within the heterogeneous Kbht unit, granitic pegmatite dikes occur in the outer parts of the complex. Most dikes are less than a meter thick, and most are less than 10 m in length. Larger dikes are compositionally and texturally zoned. Outer border-wall zones include graphic granite and biotite. Intermediate zones contain schorl, almandine garnet, and muscovite. Giant perthite and quartz crystals occur in the inner part of the intermediate zone. Monazite and columbite-tantalite are accessory minerals. Rarely, the basal area of radiating crystal groups of columbite-tantalite crystals consists of yttrocolumbite-tantalite.

Modes, calculated from point counts on stained slabs, for the major rock units are given in Table 4. To estimate the mineralogic variation at the scale of an outcrop, multiple samples were collected from some outcrops. All of the units, except for the massive tonalite core, are quite heterogeneous. The foliated granodiorite beyond the massive tonalite core is extremely variable in K-feldspar and quite variable in the other mineral contents.

Twenty-seven granitic rock samples, representative of the map units, and their included mafic enclaves, and two amphibolitic gabbros were analyzed (Table 5 [on CD-ROM accompanying this volume and in GSA Data Repository (see footnote 1)]). For six host rock samples, two mafic enclaves were collected and analyzed. Silica content of the mafic enclaves systematically correlates with the silica content of the host rock (Fig. 53). A similar systematic correlation is seen in the comparison of the Fe_2O_3, MgO, and CaO contents of host rocks and their included mafic enclaves.

Averaging the values for each map unit produces a much smoother variation diagram (Fig. 53). Average silica content varies little from the biotite tonalite core to biotite-hornblende tonalite on the outer margin of the complex. Silica content of the granitic host rock is ~10%–12% greater than the silica content of the mafic enclaves (Fig. 53). Average alumina correlates positively between host rock and mafic enclaves. Average alumina content in the host rock ranges from ~12% in the core to 14% in the outer tonalite. Average alumina content in the enclaves is 4% higher than host rock in the core and decreases progressively to 2% higher than host rock in the outer tonalite. Likewise, iron correlates positively between host rock and enclaves (Fig. 53). Iron content in the host rock ranges from ~7.5% in the core to a low of 5.5% in Kbg, but rises to 8% in the outer tonalite. Calcium shows a pattern similar to iron, having a 1.75% core, increasing to 3% in the granodiorite surrounding the core, decreasing to nearly 1% in the outer granodiorite of the complex, and rising to 2.5% in the outer tonalite.

The Na_2O content of enclaves, 3.5% to nearly 4%, correlates negatively with the Na_2O content of the host rock. K_2O progressively increases from 1% in the core to 2.75% in the outer part of the complex. In general, the K_2O content of enclaves is greatest in the core, decreases regularly to the outer granodiorite, and increases slightly in the outer tonalite. There is no systematic correlation in K_2O variation between the host rocks and enclaves.

The relative ages for four of the major units of the complex are reasonably certain. Of the four, Kbt is youngest, Kbfg is older than Kbt and younger than Kbhg, and Kbgg is oldest. The age relations of Kbfg to Kbht and to Kbgr are not clear from intrusive relationships or field exposures. Within the overall complex, Sr_i values range from 0.7048 to 0.7055 (table 6) and have an average value of 0.7051. This 0.0007 range is slightly greater than the 0.0006 range of Sr_i for the Lakeview Mountains pluton. Sr_i values for the constituent units of the complex indicate that it is systematically zoned with respect to Sr_i. Sr_i values for Kbt, Kbfg, Kbhg, and Kbgg correspondingly increase with age from youngest to oldest (Fig. 54A). This progressive increase in Sr_i with age is interpreted to be the result of more interaction of the complex's magmas with older continental materials through

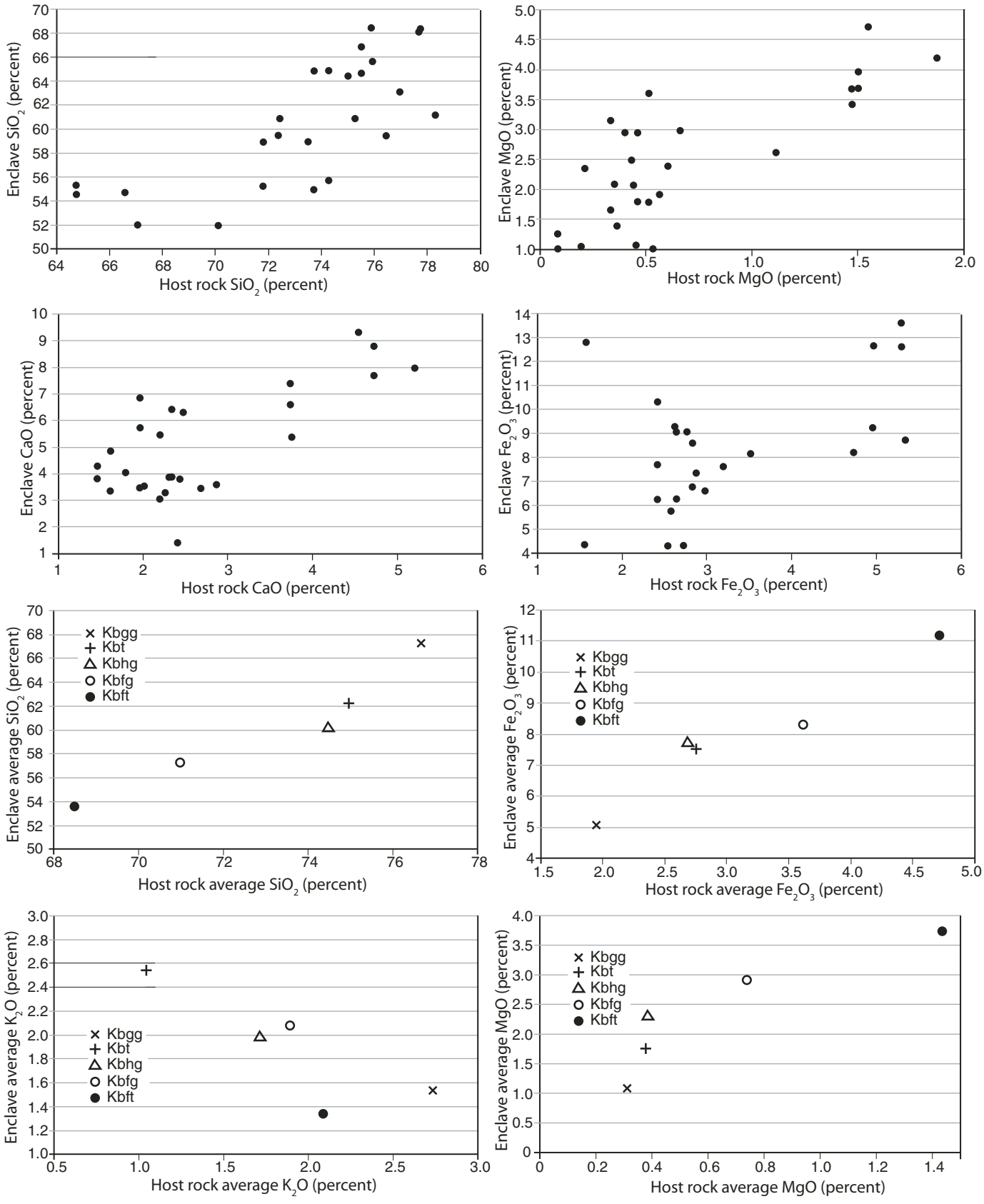

Figure 53. Plots of selected oxides of mafic enclaves and their respective host rock for the major map units, Box Springs Mountains plutonic complex. The upper four plots are all mafic enclaves and their respective host rocks. The lower four plots are the average oxide value for mafic enclaves and their respective host rocks for the major map units of the complex.

TABLE 6. Rb, Sr, AND $^{87}Sr/^{86}Sr$ DATA FOR THE BOX SPRINGS MOUNTAINS PLUTONIC COMPLEX

Specimen	Rb (ppm)	Sr (ppm)	Rb/Sr	$^{87}Rb/^{86}Sr$	$^{87}Sr/^{86}Sr$	$(^{87}Sr/^{86}Sr)$ 99 Ma
B338	95.5	285	0.335	0.969	0.70639	0.7051
BX-1	80.7	195	0.414	1.198	0.70668	0.7050
BX-2	51.7	214	0.242	0.700	0.70637	0.7054
BX-3	80.2	152	0.527	1.525	0.70749	0.7054
BX-4	86.8	172	0.504	1.458	0.70720	0.7052
BX-5	55.3	239	0.231	0.668	0.70611	0.7052
BX-6	70.5	175	0.404	1.169	0.70650	0.7049
BX-7	65.3	224	0.292	0.845	0.70626	0.7051
BX-8	75.8	259	0.292	0.845	0.70625	0.7051
BX-9	45.2	350	0.129	0.373	0.70597	0.7055
BX-10	33.0	403	0.082	0.237	0.70516	0.7048
BX-11	22.9	405	0.057	0.163	0.70501	0.7048
BX-12	43.8	378	0.116	0.336	0.70587	0.7054
BX-13	67.0	237	0.283	0.819	0.70620	0.7051
BX-14	79.7	185	0.432	1.250	0.70676	0.7050
BX-15	62.9	178	0.353	1.021	0.70659	0.7052
BX-16	81.2	183	0.443	1.282	0.70684	0.7050
BX-17	75.1	279	0.269	0.778	0.70653	0.7054
BX-18	68.7	171	0.402	1.163	0.70664	0.7050
BX-19	59.6	226	0.264	0.764	0.70595	0.7049
BX-20	63.9	242	0.263	0.761	0.70628	0.7052
BX-21	97.1	183	0.530	1.533	0.70706	0.7049
BX-22	61.2	196	0.313	0.906	0.70660	0.7053
BX-23	30.2	429	0.070	0.203	0.70574	0.7055
BX-24	12.4	434	0.029	0.083	0.70506	0.7049
BX-25	45.7	373	0.123	0.385	0.70568	0.7051
BX-26	22.6	415	0.055	0.158	0.70521	0.7050
BX-27	26.9	352	0.076	0.221	0.70520	0.7049

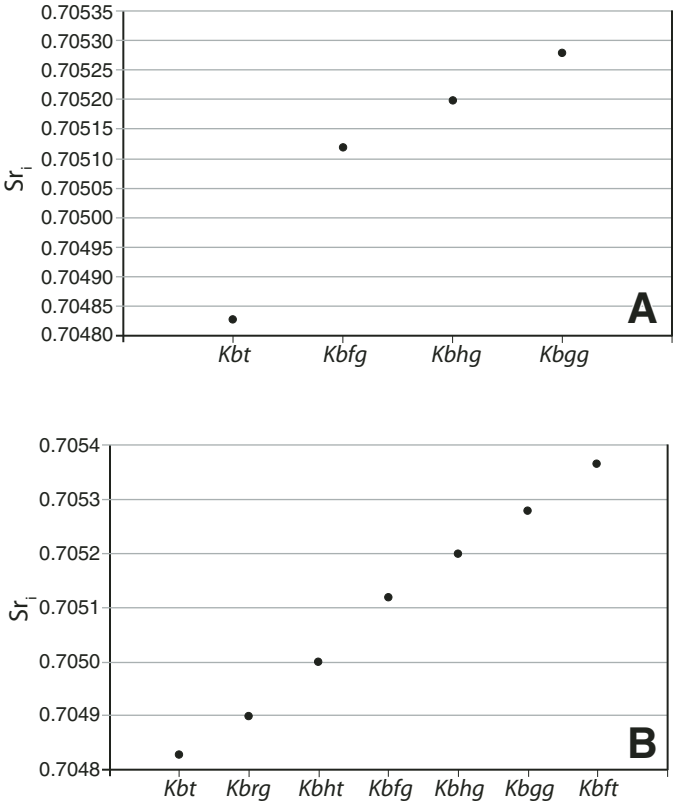

time. Figure 54B shows Sr_i for Kbrg, Kbht, and Kbft in addition to Kbt, Kbfg, Kbhg, and Kbgg. Applying Occam's razor, the ages of Kbgr and Kbht, based on their Sr_i values, should fall between those of Kbt and Kbfg, and Kbft, containing extremely attenuated mafic enclaves, should be the oldest unit of the complex.

Granitic rocks in the Bernasconi Hills area. A wide variety of granitic rocks occurs in the Bernasconi Hills, located between the Lakeview Mountains pluton and the Box Springs Mountains plutonic complex. The monzogranite of Bernasconi Pass (Figs. 2 and 3) underlies the area from the southern part of the Bernasconi Hills to north of Bernasconi Pass. North of Bernasconi Pass, the monzogranite is slightly foliated, contains few mafic enclaves, and weathers to form bold outcrops. South of Bernasconi Pass, porphyritic biotite and biotite-hornblende monzogranite weather to form extremely large outcrops (Figs. 55A and 55B). Unlike the monzogranite north of Bernasconi Pass, much of the latter mon-

Figure 54. (A) Average Sr_i for the four Box Springs Mountains plutonic complex units with known relative ages; Sr_i systematically increases with age. (B) Age of Kbrg and Kbht, relative to each other, is not known. Kbrr and Kbht are older than Kbt and younger than Kbfg. Based on Sr_i values relative to those of Kbt, Kbfg, Kbhg, and Kbgg, Kbrg is interpreted as older than Kbht. Based on its Sr_i value, the relatively older Kbft is considered the oldest unit of the complex.

zogranite contains large quantities of ellipsoidal mafic enclaves. Most of this monzogranite has moderately well-developed planar fabric and includes masses of migmatitic-appearing rock in which the volume of mafic enclaves commonly exceeds the volume of enclosing granitic rock (Fig. 56). On the south side of Bernasconi Pass, a migmatitic zone, mappable at 1:24,000 scale, occurs within the monzogranite and extends both west and east of the Bernasconi Hills. The enclave-rich mafic rocks appear to be the same age as the monzogranite, based on a case of back-veining of a mafic body by the host monzogranite. The relationships among the mafic rocks, mafic enclaves, and granitic rocks have been described by Mason and Cohen (1990).

North of the monzogranite of Bernasconi Pass, brown-weathering sillimanite-cordierite, schist correlated with the rocks of Jacumba Mountains, is intruded by heterogeneous granitic rocks (Khg) and by a series of tonalite plutons comprising the tonalite of Bernasconi Hills (Fig. 2). The tonalite weathers to form distinctive gray bold outcrops; it is relatively fine grained, commonly massive, and has common-to-abundant, small, ellipsoidal mafic enclaves.

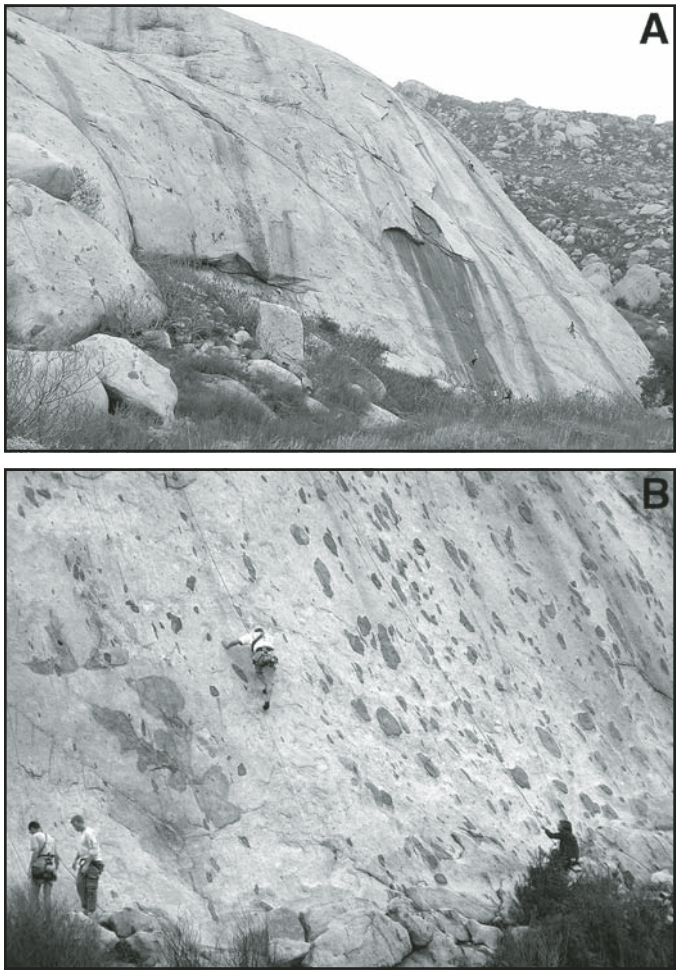

Figure 55. (A) Western transition zone monzogranite of Bernasconi Pass, south of Lake Perris. Rock contains abundant ellipsoidal-shaped E_1 mafic enclaves. (B) Monzogranite of Bernasconi Pass containing abundant E_1 mafic enclaves.

Eastern Transition Zone

Plutons of the eastern transition zone occur primarily south of 33°40′N, but a few relatively sparse exposures are present at the north end of the batholith in the northwestern San Jacinto Mountains, east of the San Jacinto fault zone (Fig. 2). The present level of exposure of eastern transition zone plutons is shallower than western transition zone plutons, as indicated by crystallization pressures of 4.5–6.5 kbar (Ague and Brimhall, 1988; Smith et al., 1991). The eastern transition zone is dominated by the large La Posta–type Coahuila Valley pluton, but unlike other La Posta–type plutons of the eastern zone, it has Sr_i <0.7060 and Pb_i <19. Biotite-hornblende tonalite, characterized by large euhedral biotite and hornblende crystals, is the dominate rock type. Within the eastern transition zone, granodiorite is distinctly subordinate to tonalite, and hornblende gabbro and olivine gabbro are sparse. In contrast to western transition zone plutons, eastern transition zone plutons are noticeably less foliated, and the mafic enclaves less attenuated. Plutonic rocks of the eastern transition zone are generally more homogeneous than those of the western transition zone. Silica content ranges from 42.9% to 77.1% and averages 64.2%. Moreover, pluton emplacement occurred from 99 to 93 Ma. Pluton compositions are isotopically characterized by Sr_i values of 0.7050–0.7054, $\delta^{18}O$ of +7‰ to +10‰, and an average Pb_i value of 18.744. The ε_{Ndi} values are negative (–0.6 to –5), similar to ε_{Ndi} in the eastern zone.

Coahuila Valley pluton. The Coahuila Valley pluton was the name given by Sharp (1967) for a large area underlain by biotite-hornblende and hornblende-biotite tonalite. Within his Coahuila Valley pluton, he distinguished five variations of tonalite. The northern part of the pluton as originally defined by Sharp was

Figure 56. Migmatitic zone within the monzogranite of Bernasconi Pass, west of Lake Perris.

subsequently subdivided into two plutons: the heavily sphene-bearing eastern zone Hemet pluton (Morton and Matti, 2008) and the eastern transition zone Tucalota Valley pluton (Morton and Kennedy, 2005) (Fig. 2). The remaining Coahuila Valley pluton, shown in Figure 2 as the large undifferentiated Kcv + Kt body, probably consists of other discrete plutons. Most of this as-yet-undifferentiated remainder is biotite-hornblende and hornblende-biotite tonalite that contains numerous ellipsoidal-shaped mafic enclaves. At least some of the southeastern part of the Coahuila Valley pluton, where it extends into Coyote Canyon (Fig. 3), is a distinctive tonalite characterized by large euhedral biotite and hornblende crystals. This tonalite has a Sr_i >0.7060 and, based on the Sr_i, is here included in the eastern zone.

The southwestern part of Sharp's Coahuila Valley pluton, in the Chihuahua Valley area, is a classic mineralogically zoned La Posta–type pluton. The outer part of the pluton exposed in Chihuahua Valley consists of biotite-hornblende tonalite containing large euhedral biotite plates and stout euhedral hornblende crystals (Figs. 57A and 57B), and the central part includes a muscovite-biotite granodiorite-tonalite. Abundant schorl-bearing granitic pegmatite dikes are located in the intermediate parts of the pluton and are particularly abundant just west of Chihuahua Valley. Locally, the uppermost part of the pluton is in contact with metasedimentary roof rock where the roof of the pluton includes vuggy greisen composed of muscovite, lepidolite, albite, and minor rubellite tourmaline. Farther south in the metamorphic roof rocks, there is a lithium-bearing pegmatite; a second discrete lithium-bearing pegmatite, the Anita pegmatite, is located in the northern part of the pluton west of Red Mountain (Fig. 3). The pocket-bearing part of the Anita pegmatite is located at a roll in the dip of the dike.

The central part of the Coahuila Valley pluton (Fig. 2) has zircon U-Pb ages of 96.5 Ma_{id} and 95.5 Ma_{ip}. The $^{40}Ar/^{39}Ar$ ages of hornblende and biotite are 94.4 Ma and 91.9 Ma, respectively. Sr_i is 0.7052, and ε_{Nd} is −5.0. A sample from the northwest part of the pluton has zircon ages of 96.5 Ma_{id} and 92.6 Ma_{ip}, and a sphene age of 93.8 Ma.

Tucalota Valley pluton. West of Sharp's Coahuila Valley pluton, the Tucalota Valley pluton (Morton and Kennedy, 2005) is separated from the Coahuila Valley pluton by a septum of amphibolite-facies metamorphic rocks including sillimanite-garnet-biotite schist (Fig. 2). The Tucalota Valley pluton consists of relatively homogeneous biotite-hornblende tonalite that weathers to relatively large core stones. Most of the tonalite is massive to very crudely foliated. Ellipsoidal mafic enclaves are sparse or lacking in much of the pluton.

Tonalite of Lamb Canyon. The Tonalite of Lamb Canyon (Morton and Miller, 2006) is a distinctive sphene-bearing biotite-hornblende tonalite exposed in several noncontiguous exposures surrounded by Tertiary sedimentary rocks in the La Borde and Lamb Canyons area (Fig. 5). Most of the unit is homogeneous-appearing, massive to slightly foliated biotite and hornblende-biotite tonalite that in most places contains large euhedral sphene crystals. Ellipsoidal mafic enclaves are uncommon. Zircon from tonalite at the head of Lamb Canyon yields U-Pb ages of 94 Ma_{id} and 92.8 Ma_{ip}, and the sphene U-Pb age is 92.8 Ma_{id}.

Granite of Mount Eden. The granite of Mount Eden is a small elongate pluton of garnet-muscovite granite that underlies Mount Eden (Fig. 3). Fresh rocks of this pluton are nearly white, but they weather to form very pale-brown bold outcrops. Bright pink garnets impart a distinctive appearance to the otherwise white rock. Grain size in the rock ranges from fine to coarse grained. Adjacent to the pluton, metamorphic rocks contain a number of sills and dikes of the granite. Most of the sills and dikes are foliated, and the foliation is oriented parallel to the enclosing metamorphic rock foliation. Similar, small garnet-muscovite granite plutons occur at several localities in the Bautista complex of Sharp (1967). Except for pegmatite dike rocks, garnet-muscovite–bearing granitic rocks are sparse in the northern Peninsular Ranges batholith.

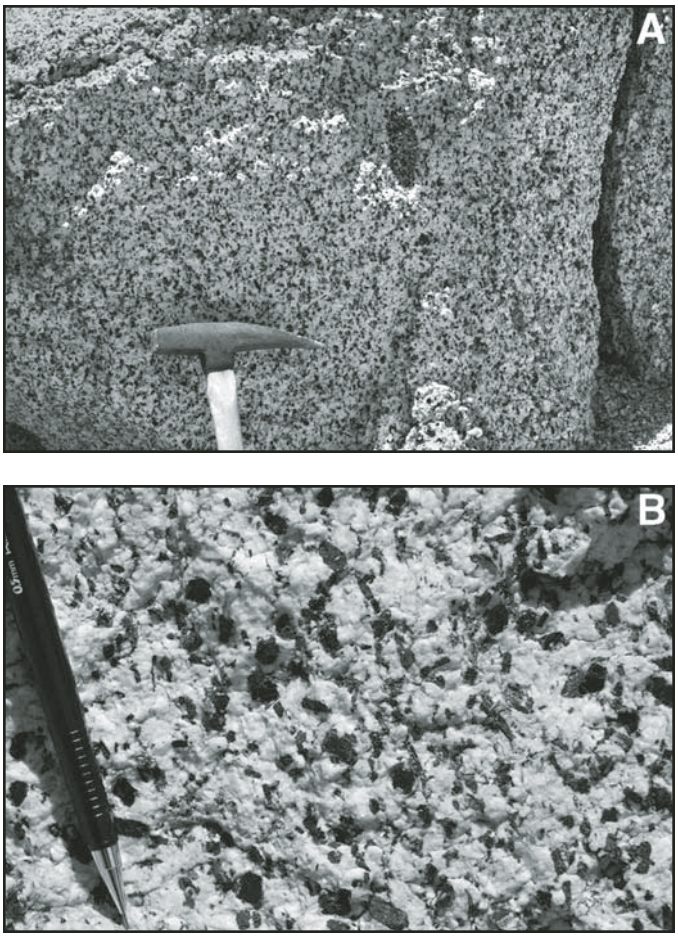

Figure 57. (A) Typical tonalite of the eastern transition zone Coahuila Valley pluton, containing sparse E_1 mafic enclaves, Chihuahua Valley. (B) Euhedral plates of biotite and stubby euhedral hornblende characterize the tonalite of the Coahuila Valley pluton, Chihuahua Valley.

Eastern Zone Plutons

The eastern zone of the batholith is characterized by large tonalitic plutons, most having foliation that is not as well developed as in western transition zone or eastern transition zone plutons. The eastern zone is structurally terminated on the east by the Eastern Peninsular Ranges mylonite zone, and it pinches out at the southeast end of the Buck Ridge pluton located in the southeastern Santa Rosa Mountains. At Coyote Mountain, north of Borrego Springs (Fig. 3), eastern zone rocks are in contact with the Eastern Peninsular Ranges mylonite zone (Fig. 2). West of Borrego Springs, the eastern zone rocks reappear as the Pinyon Ridge pluton (Wagner, 2006), located within an eastern zone inlier on the southeast side of the eastern transition zone; the eastern part of the pluton is deformed by the Eastern Peninsular Ranges mylonite zone.

Plutons in the eastern zone are generally larger than those of the western zone and western transition zone and are characterized by what is commonly termed La Posta–type plutons (e.g., Walawender et al., 1990; Kimbrough et al., 2001). The compositional range of these rocks is narrower than in plutons of the western zone and western transition zone. Sparse occurrences of gabbro occur only in the western part of the eastern zone. Ellipsoidal enclaves are generally less abundant and less attenuated than those in western transition zone and eastern transition zone plutons (Fig. 58). Silica content ranges from 46.8% to 75.8% and averages 67%. Most eastern zone plutons were emplaced between 98 and 91 Ma, with a U-Pb zircon age from an olivine gabbro of 102 Ma. The exposed level of the plutons is shallower than the western transition zone, with most eastern zone plutons crystallizing at pressures of ~4.5 kbar (Ague and Brimhall, 1988; Smith et al., 1991). However, in the eastern part of the eastern zone near the Eastern Peninsular Ranges mylonite zone, pressures of crystallization increase to 5.6 kbar (A. Bern, 2010, personal commun.). Most Sr_i values are 0.7060 to 0.7075, most $\delta^{18}O$ values are +9‰ to +12‰, and Pb_i values average 19.19. Values of ε_{Ndi} range between –2.2 and –3.9.

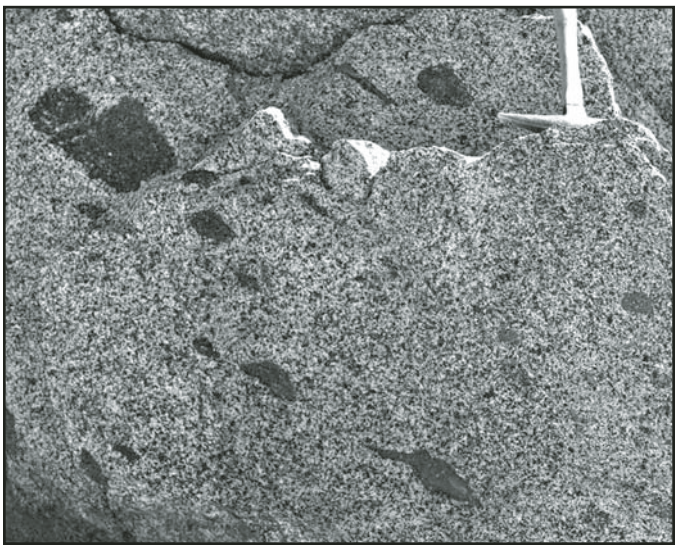

Figure 58. Typical rock of an undifferentiated tonalite unit in the eastern zone containing E_i mafic enclaves, west of Pinyon Flats, southeastern San Jacinto Mountains.

The compositionally zoned San Jacinto pluton is the largest pluton in the eastern zone north of 33°30′N. Sphene is a characterizing accessory mineral in the San Jacinto pluton, as it is in most tonalite plutons in the eastern zone. Sphene commonly occurs as readily visible large euhedral crystals; megascopically visible sphene is uncommon to absent in plutonic rocks of the western zone, western transition zone, and eastern transition zone. Sphene commonly occurs as small groups of crystals in mafic-depleted areas of quartz and feldspar, giving rise to a speckled appearance. In the eastern zone, there are a few garnet and white mica–bearing granitic plutons, a rock type essentially lacking in the western zone and western transition zone. A relatively large body of garnet-bearing granite, the granite of Penrod Canyon, is located in the southern part of the San Jacinto Mountains (Fig. 3). Extensive granodiorite is located in the northernmost part of the eastern zone, and east of the San Jacinto pluton, there is a large area of undifferentiated granodiorite and tonalite (Fig. 2). Biotite-hornblende tonalite just west of the Eastern Peninsular Ranges mylonite zone has U-Pb zircon ages of 97.5 Ma_{id} and 91.3 Ma_{ip}, a U-Pb sphene age of 92 Ma, Sr_i of 0.7074, and ε_{Ndi} of –3.9.

Gabbro is sparse and limited to the western part of the eastern zone, where several olivine-hornblende and hornblende gabbro bodies are located within the Bautista Canyon and Thomas sills of Sharp (1967). An olivine gabbro from Bautista Canyon has a Sr_i of 0.7035. Zircon from olivine gabbro of the Thomas Mountain sill in the southern Thomas Mountains (Fig. 3) has a U-Pb age of 102 Ma (D.L. Kimbrough, 2009, personal commun.). Lithium-bearing pegmatites in the Thomas Mountain gabbro were the source of the first recorded lithium gem tourmaline in California.

In the southeastern part of the pluton, located between the northern part of Coyote Canyon and the Coyote Creek fault (Fig. 3), there is a very distinctive hornblende-biotite tonalite containing large euhedral biotite and hornblende crystals. This distinctive tonalite was included by Sharp (1967) within his Coahuila Valley pluton. Four samples of this tonalite yield U-Pb zircon ages of 96.6, 97.7, 97.8, and 98.2 Ma_{ip}. Sr_i values for the four dated samples have a restricted range of 0.7062–0.7063.

San Jacinto pluton. The San Jacinto pluton (Fig. 59) is an elongate body with a somewhat bulbous northern part, and it consists of three major biotite-hornblende tonalite units. Hill (1984, 1988a, 1988b) provided an in-depth description of the San Jacinto pluton, including chemistry and internal Sr_i and $\delta^{18}O$ variations. All three of his tonalite units, unit I, unit II, and unit III, ranged from mafic tonalite to low-potassium granodiorite. The relatively older units I and II are slightly more mafic than the youngest unit III. Unit I was intruded by unit II before unit I had crystallized completely. The bulbous unit III was emplaced between units I and II before unit II had crystallized completely. Much of unit

III consists of massive to faintly foliated tonalite with few mafic enclaves (Fig. 60). Unit I is in contact with unit II only south of unit III. Mineral layering, foliation, and schlieren are concordant with the plutons external and internal contacts. Schlieren commonly occur as isolated masses within homogeneous tonalite (Figs. 61A and 61B). Hill (1984) interpreted foliation in his unit III as defining a funnel-shaped pluton. Unit III is systematically zoned compositionally, grading from mafic tonalite at the margins to low-potassium granodiorite at the center. Variation in $\delta^{18}O$, caused by contamination from surrounding metamorphic rocks, is limited to a narrow zone at the pluton margin. Synplutonic mafic dikes within the pluton are commonly disaggregated

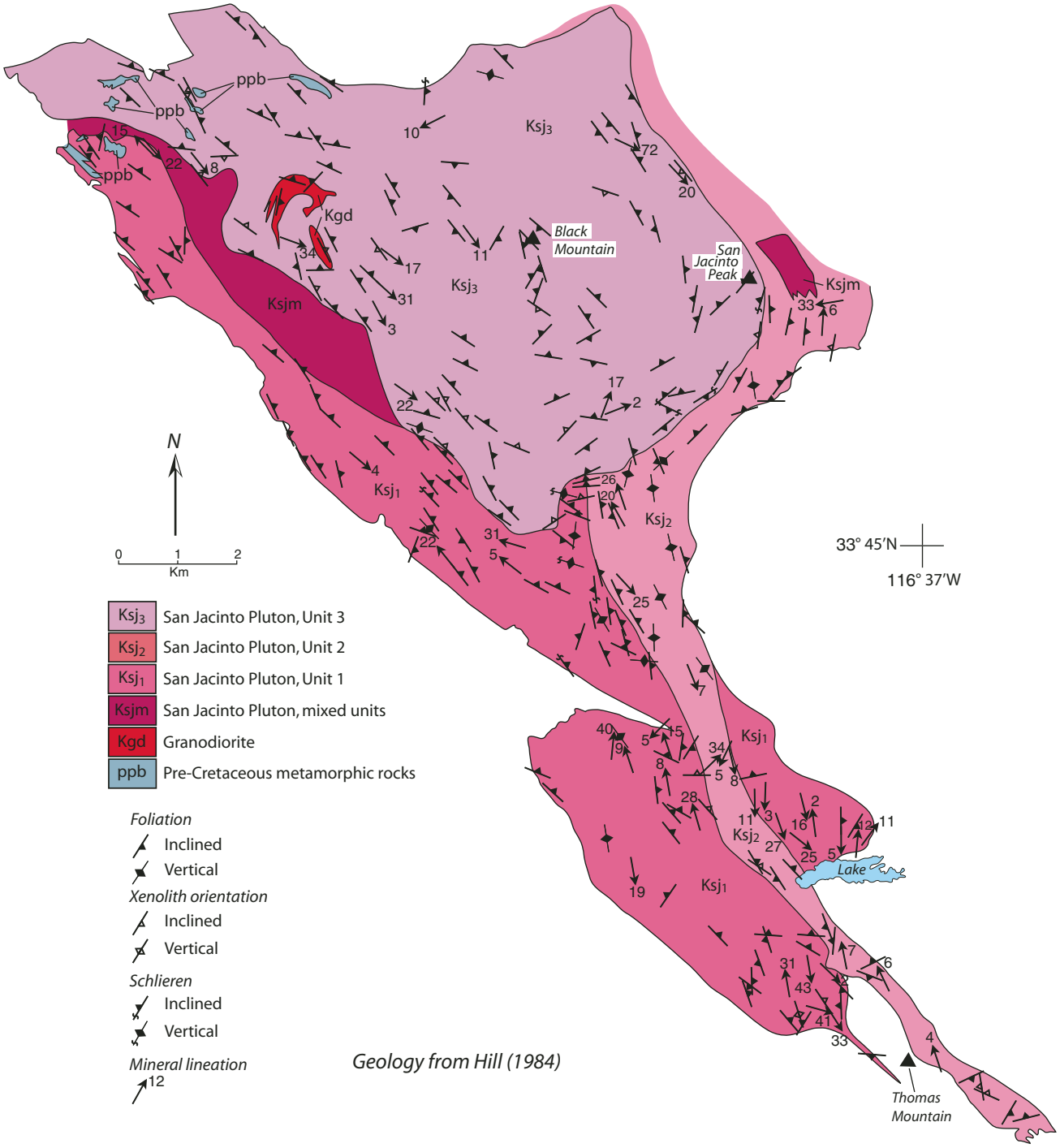

Figure 59. Generalized geologic map of the eastern zone San Jacinto pluton, San Jacinto Mountains. Geology from Hill (1984).

Figure 60. Typical biotite-hornblende tonalite of unit 3, San Jacinto pluton. Tonalite commonly contains few mafic enclaves.

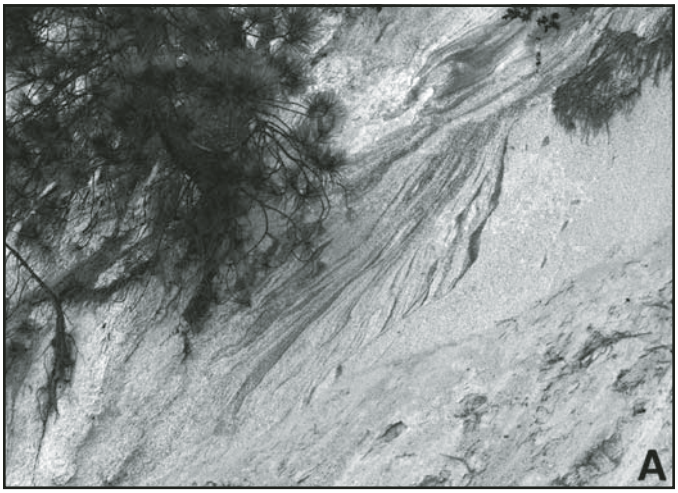

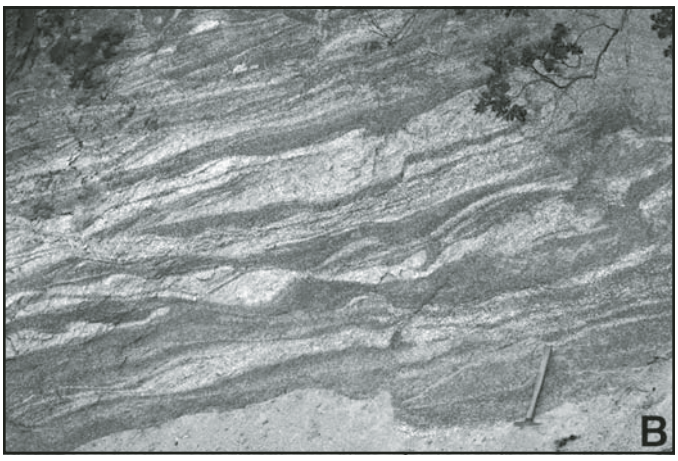

Figure 61. (A) Isolated mass of mafic schlieren-like tonalite within faintly foliated weathered tonalite, unit 3 of the San Jacinto pluton. (B) Close-up of an isolated mass of mafic schlieren-like tonalite; all rock here is deeply weathered unit 3 of the San Jacinto pluton.

to form linear trains of dike fragments (Fig. 62). Minor felsic tonalite differentiates are of granodioritic composition. U-Pb zircon ages from Hill's unit I are 95.3 Ma_{id} and 93.9 Ma_{ip}; U-Pb sphene age is 93.2 Ma. The $^{40}Ar/^{39}Ar$ ages of hornblende and biotite are 91.6 Ma and 92.2 Ma, respectively.

Penrod Canyon pluton. A garnet-bearing granite pluton is located in the southern part of the Garner Valley area, south of the San Jacinto pluton. This body was termed Penrod quartz monzonite by Brown (1968), and granite of Penrod Canyon by Hill (1984). The pluton is ~4 by 9 km and consists of medium-grained, leucocratic biotite-garnet-muscovite granite. Crudely oriented biotite imparts a subtle foliation to the granite. Dark-red garnet occurs in some rocks in amounts up to several percent. Chemistry of the granite is given in Table 2 (on CD-ROM accompanying this volume and in GSA Data Repository [see footnote 1]; B270 and B271). These samples have a Sr_i of 0.7061, which is considerably lower than typical eastern zone plutons.

Hemet pluton. Hornblende-biotite tonalite containing large sphene crystals at the north end of Sharp's (1967) Coahuila Valley pluton has been differentiated as the Hemet pluton (Morton and Matti, 2008). It consists of massive to relatively well-foliated biotite-hornblende tonalite and biotite tonalite, which is noticeably more heterogeneous than the adjacent Coahuila Valley pluton. This tonalite contains only sparse ellipsoidal mafic enclaves. Most of the tonalite contains readily visible subhedral and euhedral sphene. The biotite tonalite is subporphyritic with euhedral biotite up to 1 cm. The texture of biotite tonalite ranges from massive to crudely foliated; however, in many places, the foliation is so indistinct that accurate measurements are not possible. The crude foliation defines a semicircular configuration, apparently the southern part of an elliptical pluton, the northern part of which is covered by alluvium of San Jacinto Valley. The unit contains some layers of brown weathering tonalite that contrasts with typical gray-weathering tonalite. A few simple-mineralogy

Figure 62. Abundant irregularly shaped mafic enclaves, interpreted to be from disaggregated synplutonic mafic dike. Deeply weathered unit 3 of the San Jacinto pluton.

granitic pegmatite dikes are found in the western part of the pluton. One large dike was mined for quartz and K-feldspar.

Tonalite from the north-central part of the pluton has U-Pb zircon ages of 95.9 Ma_{id} and 91.6 Ma_{ip}. Sphene has a U-Pb age of 93.8 Ma. The $^{40}Ar/^{39}Ar$ ages of hornblende and biotite are 92 Ma and 90 Ma, respectively.

Pinyon Ridge pluton. West of Borrego Springs (Fig. 3), in the southeasternmost part of the geologic map shown in Figure 2, there is the eastern zone Pinyon Ridge pluton. The pluton is bordered on the west by western transition zone rocks, on the north by eastern transition zone rocks, and is structurally terminated on the east by the Eastern Peninsular Ranges mylonite zone. Outliers of the pluton occur within metamorphic rocks that enclose it. The 0.7062 value at B450 falls on the small unnamed granite (Kgu) outcrop west of the main Pinyon Ridge body that is probably Pinyon Ridge rock (Fig. 2). The Pinyon Ridge pluton, termed the Pinyon Ridge granodiorite by Wagner (2006), consists mostly of medium-grained biotite-hornblende tonalite, biotite tonalite, and lesser hornblende-biotite tonalite. Some biotite tonalite has small amounts of fine-grained primary muscovite. Accessory minerals are sphene, apatite, zircon, and opaque minerals. Sphene occurs as relatively large euhedral crystals. Common epidote and sparse calcite are secondary minerals. Typical hypautomorphic textured tonalite with common ellipsoidal-shaped mafic enclaves occurs in the western part of the pluton (Fig. 63). In the eastern part, the texture progressively changes near the Eastern Peninsular Ranges mylonite zone, as quartz is intensely undulated, kinks appear in plagioclase, and biotite is highly deformed into kinked and wispy crystals. Moderately strained quartz commonly has fractures that are filled with very fine-grained quartz. Outcrops in the eastern part of the pluton commonly have both an older moderate foliation accompanied by ellipsoidal mafic enclaves, and a younger intense foliation accompanied by extremely attenuated mafic enclaves (Fig. 64). Near the Eastern Peninsular Ranges mylonite zone, foliated tonalite weathers to form shingle-like slopes (Fig. 65). Mylonitic textures are common close to the Eastern Peninsular Ranges mylonite zone. Sr_i values in the pluton ranges from 0.7062 to 0.7072, but most values are around 0.7062.

Figure 63. Typical biotite-hornblende tonalite containing ellipsoidal-shaped E_1 mafic enclaves in the western part of the eastern zone Pinyon Ridge pluton.

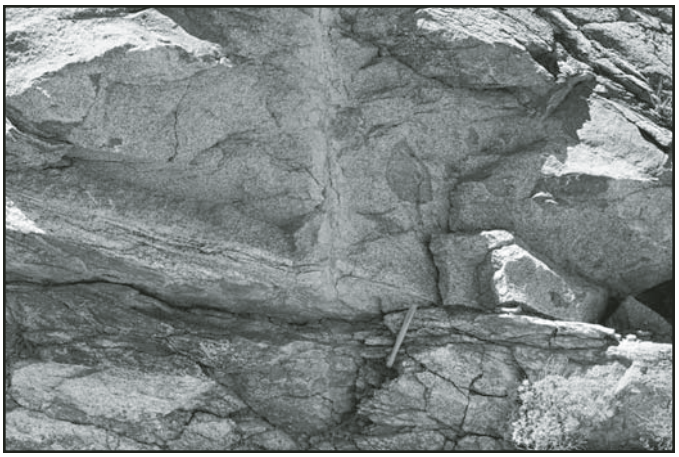

Figure 64. Biotite-hornblende tonalite in the eastern part of the eastern zone Pinyon Ridge pluton, showing an older, faintly foliated fabric containing E_1 mafic enclaves (upper part of photograph), and younger well-foliated fabric containing E_2 mafic enclaves (lower part of photograph). Tonalite having well-foliated fabric with E_2 mafic enclaves is spatially related to the Eastern Peninsular Ranges mylonite zone.

Upper-Plate Zone

Allochthonous granitic rocks, assigned to the Santa Rosa allochthon of Erskine (1986b), constitute the upper-plate zone of the batholith (Fig. 2). The feature separating the eastern zone from the upper-plate zone is a major regional mylonite zone that has been variably termed the Eastern Peninsular Ranges mylonite

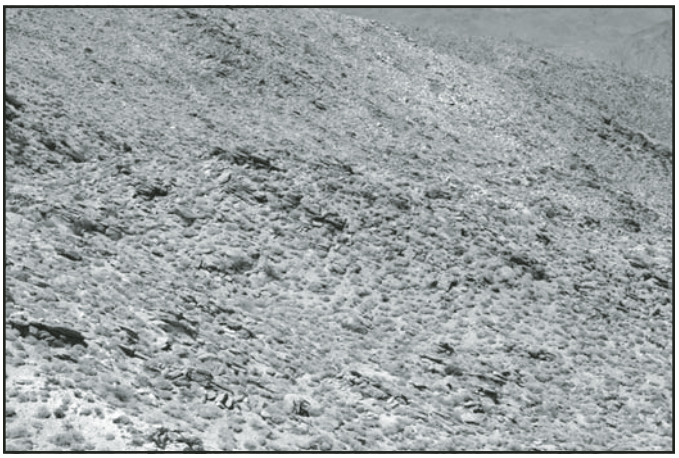

Figure 65. Shingle-like slopes developed from uniformly foliated tonalite containing E_2 mafic enclaves; macroscopic characteristic of Pinyon Ridge pluton rocks near the Eastern Peninsular Ranges mylonite zone, west of Borrego Springs. Field of view across center of photograph is approximately 150 m.

zone (Sharp, 1967, 1979; Todd et al., 1988), Santa Rosa mylonite zone (e.g., Erskine and Wenk, 1985; Wenk and Pannetier, 1990; Goodwin and Wenk, 1995), and Borrego Springs–Santa Rosa mylonite zone (Simpson, 1984); see also Girty et al. (1993). Here, we use the terminology of Sharp, i.e., the Eastern Peninsular Ranges mylonite zone. Within the mylonite zone, shear indicators have been interpreted as showing evidence of east-over-west displacement. Geochemistry and isotopic data also indicate that the upper-plate zone originated east of the autochthonous Peninsular Ranges batholith. Inception of mylonitic deformation has been interpreted to have begun as early as 87 Ma (Cecil, 1990; cited in Wenk, 1998). Goodwin and Renne (1991) interpreted that mylonitization began ca. 80 Ma, and extended to ca. 62 Ma; see also Dokka (1984). The western, structurally lowest, part of the upper-plate zone is dominated by mylonitic fabrics that include pseudotachylyte.

East of the Eastern Peninsular Ranges mylonite zone, the upper-amphibolite-metamorphic-grade Palm Canyon Complex is separated from the mylonite zone by the east-dipping low-angle Palm Canyon fault (Erskine, 1986a, 1986b). Brittle deformation of the Palm Canyon fault contrasts with the ductile deformation of the underlying mylonite zone. The Palm Canyon fault extends from just south of Palm Springs to the southeast end of the Santa Rosa Mountains. It borders the Palm Canyon complex, which consists of anatectic gneiss, orthogneiss, and mylonitic gneiss. In this complex, relatively abundant mylonitic garnet-bearing anatectic gneiss is interlayered with metasedimentary gneiss and orthogneiss. Anatectic metamorphism is interpreted as beginning ca. 110 Ma (Wenk et al., 1998). Structurally above the Palm Canyon complex, there is a second low-angle east-dipping fault, the Asbestos Mountain fault. Above the Asbestos Mountain fault, granitic rocks comprise the allochthonous upper-plate zone of the batholith (Erskine, 1986a; Todd et al., 1988).

In the Pinyon Flats area of the eastern San Jacinto Mountains, a third low-angle fault, the Haystack Mountain fault, is located between granitic sheets within the upper-plate zone. The granitic rocks above the Haystack Mountain fault form a klippe in the Pinyon Flats area. The Asbestos Mountain–Haystack Mountain fault complex is exposed discontinuously southeastward to the end of the Santa Rosa Mountains. For a detailed description and analysis of the upper-plate zone, see Erskine (1986a), Erskine and Wenk (1985), and Todd et al. (1988). Upper-plate granitic rocks are not exposed south of the southeastern end of the Santa Rosa Mountains. The Eastern Peninsular Ranges mylonite zone is offset by branches of the San Jacinto fault zone and is exposed between faults at Coyote Mountain (Theodore, 1967, 1970) north of Borrego Springs, and south of the San Jacinto fault zone west of Borrego Springs. Detailed petrography and structure of the Eastern Peninsular Ranges mylonite zone at Coyote Mountain were given by Theodore (1967, 1970). If upper-plate zone granitic rocks extend south into the Borrego Springs area, they are covered by sedimentary deposits.

Foliated biotite-hornblende granodiorite and tonalite (Fig. 66) containing abundant accessory sphene are the dominant lithologies of the upper-plate zone. Much of the tonalite in the Asbestos Mountain area contains large euhedral sphene crystals (Webb, 1939b). Crude gneissic fabric and ellipsoidal to pancake-shaped mafic enclaves are common throughout the upper-plate zone (e.g., Wenk, 1998) (Fig. 67). Epidote is a common accessory mineral. Magnetite is the common opaque mineral, in contrast to the ilmenite-bearing granitic rocks of the eastern zone.

Ages of most dated upper-plate zone granitic rocks are distinctly younger than those of the eastern zone plutons. Tonalite from the Pinyon Flats area has U-Pb zircon ages of 84.2 Ma_{id} and 85.7 Ma_{ip}, and U-Pb sphene age is 76.9 Ma. The $^{40}Ar/^{39}Ar$ ages of hornblende, biotite, and K-feldspar are 75.3 Ma, 69.8 Ma, and 68–62 Ma, respectively. Pinyon Flats rocks yield Sr_i of 0.7078, $\delta^{18}O$ 8.3 ‰, and ε_{Ndi} of –6.0. Farther east, a tonalite sample yields a U-Pb zircon age of 92.5 Ma_{ip}; the reason for this distinct age reversal is not understood. A sample from Point

Figure 66. Foliated tonalite of the upper-plate zone, east of Pinyon Flats, southeastern San Jacinto Mountains.

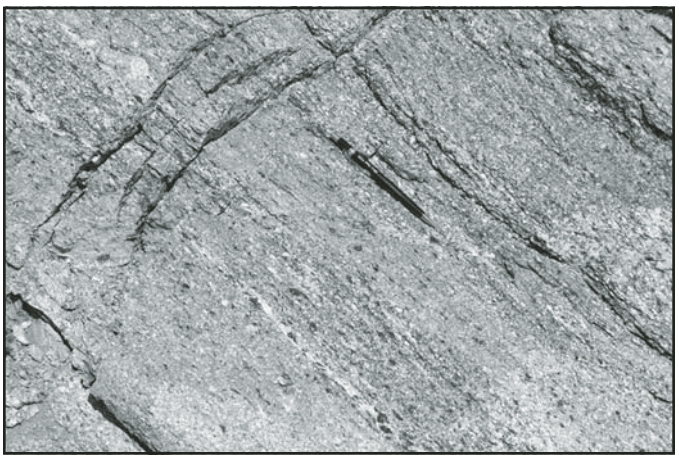

Figure 67. Well-foliated gneissose-textured upper-plate zone granodiorite. East of Pinyon Flats, southeastern San Jacinto Mountains.

Happy (Fig. 2), the easternmost exposure of the upper-plate rocks, gives U-Pb ages of 83 Ma_{id} and 84.5 Ma_{ip} for zircon, and 75.9 Ma for sphene. The $^{40}Ar/^{39}Ar$ ages of hornblende, biotite, and K-feldspar are 71.2 Ma, 63.9 Ma, and 62.5–59 Ma, respectively. A Sr_i value for this rock is 0.7080, and ε_{Ndi} is –7.3. Ague and Brimhall (1988) reported an 87 Ma age for the tonalite. A biotite-hornblende tonalite sample collected south of La Quinta (Fig. 3) has a U-Pb zircon age of 84.4 Ma (D. Kimbrough, 2010, personal commun.).

Upper-plate granitic rocks crystallized at pressures of ~6.0–6.9 kbar (Ague and Brimhall, 1988). The silica range for these granitoids is 60.9%–72.4%, which is a considerably narrower range than that of the other batholith zones. This is, at least to some degree, due to the absence of gabbro in the upper-plate zone. Average silica content of 64.7% is significantly lower than the average of 66.1% for the eastern zone, but it is close to the average of 64.2% for the eastern transition zone. Most Sr_i values are in the range of 0.7077–0.7082, $\delta^{18}O$ values average +8.73‰, and the average Pb_i is 19.336. Based on relatively few samples, all ε_{Ndi} values are negative. At Point Happy, our ε_{Ndi} value is –7.3. DePaolo (1981) reported ε_{Ndi} of –5.9 for the Point Happy rock, but his ε_{Ndi} value was calculated at 100 Ma(?). The Sr_i and Pb_i ratios indicate incorporation of greater amounts of more-evolved continental crust in the pluton-forming magma than the other zones of the batholith (Kistler et al., this volume). Although granitic rocks of the upper-plate zone are magnetite-bearing rocks like those of the western zone, their ages and Sr_i values are entirely different.

REGIONAL GEOCHEMISTRY

Most of our regional geochemical data are from composite samples systematically collected by E.E. Welday and A.K. Baird, Pomona College (Baird et al., 1974, 1979; Baird and Miesch, 1984), from the northern 120 km of the batholith (Fig. 68). These systematically collected samples allow an accurate quantitative estimation of the composition of this part of the Peninsular Ranges batholith. The sample-collection procedure is given in the Appendix. An additional 60 samples were collected in selected areas where greater detail was needed. Chemical analyses are given in Table 2 and Baird-Welday sample locations are given in Figure 68; locations of additional samples are given in Table 2 (on CD-ROM accompanying this volume and in GSA Data Repository [see footnote 1]). All newly collected samples were analyzed, and the Welday-Baird samples reanalyzed, in USGS laboratories, Denver, Colorado, using standard techniques. Major elements were analyzed by X-ray fluorescence, and trace elements were analyzed by ICP analysis. Whole- rock Rb-Sr, U-Pb, and O isotopes were measured in USGS isotope laboratories in Menlo Park, California. Chemistry of the five batholith zones is given in Table 2. Zircon geochronology was obtained in USGS laboratories in Denver, Menlo Park, and Stanford University. Details of analytical procedures are given in the Appendix, in Kistler et al. (this volume), and in Premo et al. (this volume, Chapter 4).

Based on the grid of systematically collected samples, the western zone constitutes 43.7% by area of the northern Peninsular Ranges batholith, western transition zone 12.3%, eastern transition zone 13.3%, eastern zone 22%, and the upper-plate zone 9.7%. Normalized for only the autochthonous part of the batholith, the western zone constitutes 47.9% by area, western transition zone 13.5%, eastern transition zone 14.6%, and the eastern zone 24%. (Note: In both normalizing calculations, the number of eastern zone samples was reduced from 74 to 68 because of the difference in sampling interval in the northern part of the eastern zone.) Alluvial cover in much of the Riverside area, the Perris block, and the Temecula area precludes collection of batholith samples. In spite of the areas of alluvial cover, we consider the systematically collected samples to be a reasonably quantitative representation of the part of the batholith sampled. Several samples shown on Figure 68 that appear to fall within metamorphic units or alluvium actually fall on granitic outcrops too small to show at the scale of the map.

Previous Regional Geochemistry

Systematic west-to-east dichotomy in chemical and isotopic composition of the batholith has long been recognized (e.g., Baird et al., 1974; Gromet and Silver, 1987; Taylor and Silver, 1978; Todd et al., 1988, 2003), and Peninsular Ranges batholith workers now appear to agree on a basic twofold division of the batholith into western and eastern zones (e.g., Taylor and Silver, 1978; Baird and Miesch, 1984; Todd et al., 1988; and various papers in Johnson et al., 2003). The twofold division of the Peninsular Ranges batholith has been variously attributed to be the result of (1) a change in plate-tectonic motions during the Cretaceous (Walawender et al., 1990), (2) two Cretaceous magmatic arcs (Silver and Chappell, 1988; Johnson et al., 1999), and (3) a single Cretaceous arc transitioning from Mesozoic oceanic to continental crust (Thomson and Girty, 1994; Todd et al., 1988, 2003).

Another chemical division of the Peninsular Ranges batholith is based on rare earth element patterns that divide the batholith into three longitudinal zones (Gromet and Silver, 1987). Later, Silver and Chappell (1988) divided the Peninsular Ranges batholith into a western batholith and an eastern batholith and recognized six chemical domains within the two batholiths. Their chemical domains were "…recognized on the basis of a regular linear covariation of Rb and Sr concentrations…." (Silver and Chappell, 1988, p. 110). The northern Peninsular Ranges batholith considered here includes five of the six chemical domains of Silver and Chappell (1988). Except for their chemical domain F, a direct comparison of the chemical domains of Silver and Chappell to our zones is not possible due to their generalized small-scale chemical domain map and lack of sample locations. However, despite the different scale of their study, significant differences are apparent, most notably in some trace elements, and in the average chemistry of their domains, particularly their domain F as compared to our results

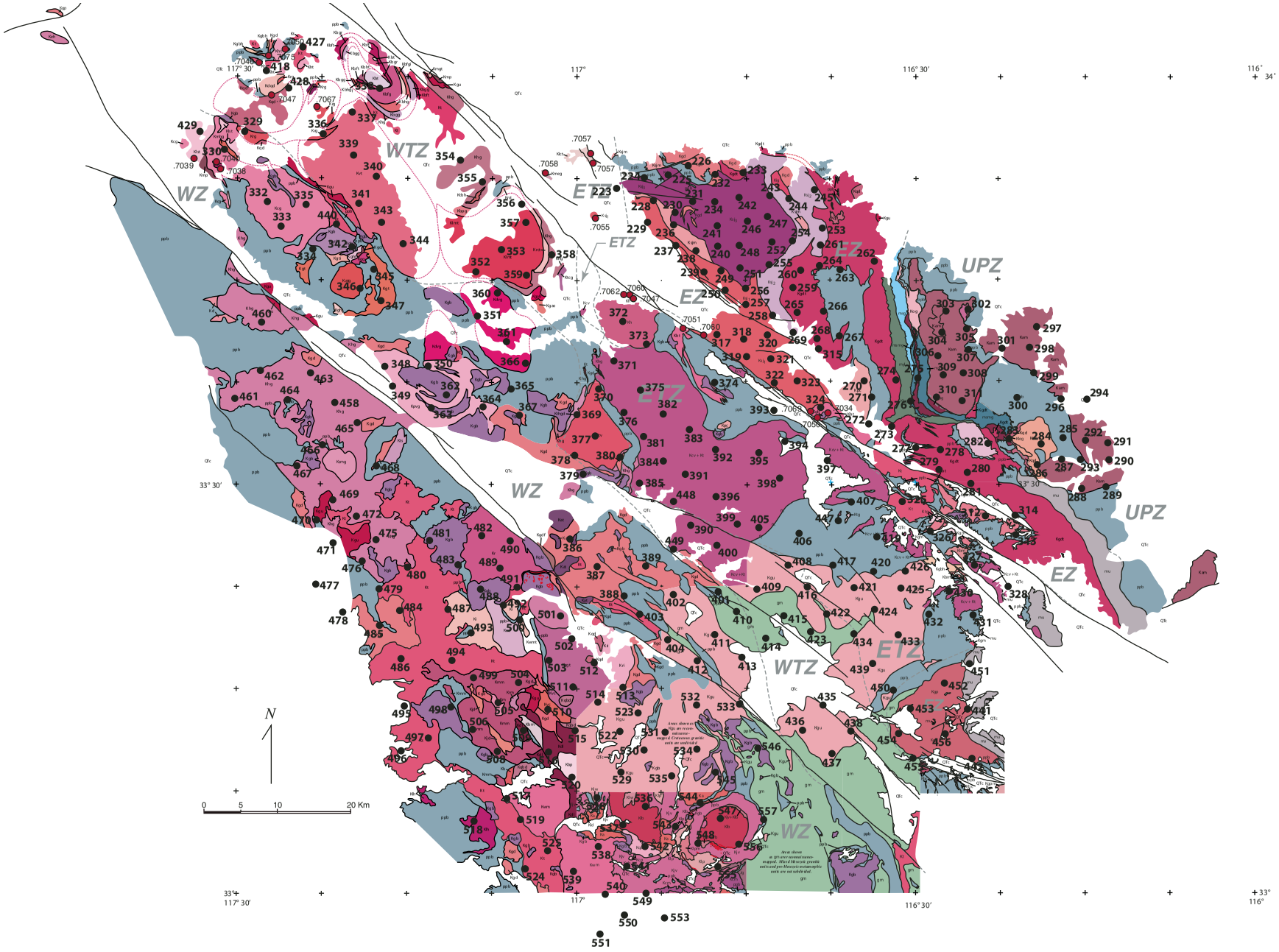

Figure 68. Generalized geologic map of the northern Peninsular Ranges batholith showing Baird-Welday sample localities. An enlargeable version is on accompanying CD (see text footnote 1).

for the upper-plate zone. These differences may be due to differences in sampling or variations in the Peninsular Ranges batholith south of 33°N.

Our western zone and western transition zone in general correspond to the western zone of Todd et al. (2003), and our eastern transition zone and eastern zone correspond to their eastern zone. Upper-plate zone rocks may not occur south of 33°N in the area of Todd et al. (2003). In general, our western zone corresponds to domain B of Silver and Chappell (1988), our transition zones correspond to their domain C, our eastern zone corresponds to their domains D and E, and the upper-plate zone correspond to their domain F. The western REE zone of Gromet and Silver (1987) in general corresponds to our western zone, their intermediate zone corresponds to our transition zones, and their eastern zone corresponds to our eastern zone and upper-plate zone. The western batholith zone of Baird and Miesch (1984) is essentially our western zone and western transition zone, and their eastern batholith zone corresponds to the eastern transition zone, eastern zone, and upper-plate zone.

Regional Geochemistry

Our batholith zones are based on a combination of field and analytical data. Field data include host rock, mode of pluton emplacement, rock fabric, and mineralogy. Analytical data include pluton emplacement age, Sr_i, ε_{Ndi}, Pb_i, whole-rock geochemistry, and aeromagnetic data. A summary of the characteristics of the batholith zones is given in Figure 4. The boundaries between the western zone and the western transition zone, and the western transition zone and the eastern transition zone are based largely on rock fabric, mode of pluton emplacement, aeromagnetic properties, the Sr_i <0.7045 isopleth, and positive ε_{Ndi} values. The change from western zone passively emplaced, massively textured plutons to dynamically emplaced, concordant foliated western transition zone plutons is very noticeable north of 33°22′N, but not to the south (e.g., Todd et al., 2003). Host rocks for the western zone and transition zones plutons are generally quite different, marked by very low metamorphic grade, mostly below greenschist grade in the western zone, and higher amphibolite grade in the transition zones.

Most rocks in western transition zone have Sr_i <0.7055 and a small positive ε_{Ndi}, in contrast with the eastern transition zone, which has Sr_i mostly >0.7055, and a large negative ε_{Ndi}. The eastern transition zone includes large La Posta–type plutons that are not present in the western transition zone. The boundary between the plutons of the western transition zone and eastern transition zone with the eastern zone plutons is less certain based on textural changes, but it is generally more pronounced based on the widespread occurrence of large euhedral sphene in eastern zone rocks. Most of the eastern zone has Sr_i >0.7060 and Pb_i >19. Even though the eastern zone is structurally terminated on the east by the Eastern Peninsular Ranges mylonite zone, the clear eastern zone boundary is the low-angle fault contact above the Eastern Peninsular Ranges mylonite zone that places allochthonous upper-plate zone rocks on autochthonous Peninsular Ranges basement.

Chemical averages for the five zones are summarized here and are given in Figure 69. The compatible elements Fe, Mg, Ca, Sc, V, and Co decrease eastward in the autochthonous zones and increase in the upper-plate zone. K, P, Rb, Sr, Nb, Ba, and light REEs increase from the western zone through the upper-plate zone. As noted by Baird et al. (1974), the increase in K across the batholith is evident, with K_2O increasing from an average of 1.9% to 2.9%. Silica is essentially the same in the western zone and western transition zone, increases slightly in the eastern transition zone, and shows significant increase in the eastern zone, before decreasing in the upper-plate zone. Na_2O increases slightly across the autochthonous batholith from the western zone through the eastern zone and decreases to a low in the upper-plate zone.

As noted by Silver and Chappell (1988), some trace elements have much greater variation across the batholith than major elements. For the autochthonous batholith, average values for Sc, V, Co, Ba, Sr, Nb, La, and Ce change by about a factor of 2. Incompatible trace elements Zn, Rb, Sr, Nb, Ba, Th, and U increase from the western zone through the upper-plate zone (Fig. 69). V, Co, and Mo decrease from the western zone through the eastern zone but increase in the upper-plate zone. REEs show a systematic variation from light REEs to heavy REEs (Gromet and Silver, 1987). Light REEs La, Ce, Pr, Nd, and Eu increase from the western zone through the upper-plate zone, but Tm and Yb decrease east of the western zone.

Harker diagrams for most major elements have a relatively linear pattern. Some dispersion is common for rocks having low SiO_2 and high Fe_2O_3, MgO, and CaO (Figs. 70A–70H). CaO is especially linear, showing only a slight dispersion at the high end of its range. The ratio of Al_2O_3 to SiO_2 increases from the western zone to the eastern zone, but it decreases in the upper-plate zone to the same values seen in the two transition zones, producing an arcuate pattern. Both TiO_2 and P_2O_5 have nonlinear patterns. Reflecting the distribution of apatite, the P_2O_5 pattern is a relatively symmetrical convex arc, having maximum P_2O_5 in intermediate-silica rocks and decreasing in both low-and high-silica rocks. Most low-silica rocks in the western zone have decreased TiO_2, forming an asymmetric pattern.

Rare Earth Elements

Normalized REE patterns are similar to those described by Gromet and Silver (1987) and Todd et al. (2003). Normalized zone-average REE plots show a systematic enrichment in the light REEs from west to east (Fig. 71). Average light REEs are very similar for the western zone, western transition zone, and eastern transition zone, but there is a significant difference between patterns for these three zones and the eastern zone and upper-plate zone. Gabbros have two basic REE patterns, independent of location within the batholith. One pattern, displayed mostly by hornblende gabbros, is nearly flat from light to heavy REEs, but slightly lower toward the heavy REE end (Fig. 21).

	WZ	WTZ	ETZ	EZ	UPZ
SiO_2*	64.0	63.8	64.3	67.1	64.7
Al_2O_3*	15.6	16.2	16.4	15.7	15.8
Fe_2O_3*+	5.7	5.3	4.5	3.8	4.8
MgO*	2.5	2.2	2.0	1.1	1.7
CaO*	5.2	5.1	5.1	3.8	4.2
Na_2O*	3.4	3.3	3.5	3.6	3.2
K_2O*	1.9	2.0	1.9	2.6	2.9
TiO_2*	0.56	0.67	0.68	0.62	0.73
P_2O_5*	0.13	0.15	0.17	0.18	0.22
MnO*	0.09	0.08	0.07	0.06	0.07
Sc	17	15	11	7.1	7.7
V	104	106	85	44	68
Co	15.5	13	10	7	10
Cu	13	8.6	7.5	16	25
Zn	48	64	65	67	72
Rb	59	74	65	89	110
Sr	236	307	402	431	471
Y	23	18	12	17	18
Zr	148	125	130	163	214
Nb	5	5	6	9	15
Mo	2.6	2.0	2.0	2.1	2.8
Cs	2.4	2.6	3.2	2.6	2.3
Ba	557	710	886	1017	1034
La	14.6	15.9	18.7	28.8	44.0
Ce	32.8	34.4	39.2	61.6	90.8
Pr	4.3	4.4	4.9	7.4	10.5
Nd	17.8	18.0	19.6	28.7	38.1
Sm	4.6	4.2	4.2	6.0	7.3
Eu	1.1	1.1	1.2	1.3	1.6
Gd	4.4	3.7	3.4	4.4	5.2
Tb	0.82	0.70	0.51	0.69	0.76
Dy	4.7	3.5	2.7	3.6	4.1
Ho	1.1	0.8	0.6	0.7	0.8
Er	3.1	2.1	1.5	2	2.1
Tm	0.52	0.39	0.23	0.32	0.33
Yb	3.1	1.9	1.3	1.9	1.9
Hf	4.7	3.8	3.9	4.7	5.8
Ta	0.54	0.60	0.61	0.90	1.40
W	0.45	0.36	0.34	0.36	0.43
Th	8.0	8.2	8.5	10.9	20.5
U	1.9	1.8	1.7	2.2	3.0
Zr/Hf	32.1	33.2	33.0	35.0	37.0

Figure 69. Comparisons of zone chemistry, showing major element and rare earth element (REE) averages for the five batholith zones. Asterisk (*) denotes values expressed as percent, Zr/Hf as ratio, all others as parts per million (ppm). Total Fe expressed as Fe_2O_3.

The second gabbro pattern, which includes most pyroxene and/or olivine gabbros, is similar, except for having a positive Eu anomaly. In general, there is less REE enrichment in olivine gabbro than in hornblende gabbros.

Many western zone granitoids are slightly enriched in light REEs and have pronounced low Eu values, especially in what is commonly termed the Woodson Mountain granodiorite (Fig. 27). Most granitoids of the western transition zone and eastern transition zone have a relatively linear pattern, showing moderate enrichment in light REEs, and, with the exception of gabbro, little if any negative Eu. Typical eastern zone granitoids are more enriched in light REEs and more depleted in heavy REEs than western transition zone and eastern transition zone granitoids. Some eastern zone plutons have a slight negative Eu anomaly. White mica– and garnet-bearing leucogranites at Mount Eden and Bautista Canyon have moderate-to-large negative Eu anomalies (Fig. 72). Upper-plate granitoids have patterns similar to the eastern zone granitoids, but they show greater enrichment in La.

Scandium (Fig. 70G) and the heavy REEs decrease progressively from the western zone through the eastern zone, suggesting processes of relatively shallow fractionation in the west to much deeper fractionation in the east, involving garnet and/or clinopyroxene in the thick lower continental crust or upper mantle. Rb, Sr, Nb, Ba, Ta, Th, U, and the light REEs are not sequestered in garnet and/or clinopyroxene. The increase in these elements from the western zone through the upper-plate zone reflects shallow crustal differentiation in the west and much deeper crustal differentiation in the east.

Strontium Isotopes

Our rubidium, strontium, lead, and oxygen isotope data are from the Welday-Baird samples augmented by 104 samples from selected locations. The Sr and Rb data and analytical methods are given in Kistler et al. (2003, this volume). Additional Sr data are given for the Lakeview Mountains pluton (Morton et al., this volume) and the Box Springs Mountains plutonic complex.

Initial strontium isotope variation in the batholith was first described by Early and Silver (1973) and Kistler et al. (1973). Both studies showed a southwest to northeast increase in Sr_i. Samples in Kistler et al. (1973) were from the northern part of the batholith. Early and Silver (1973, p. 494) gave no sample locations other than that the samples were from southern California and Baja California. Their Sr_i values ranged from 0.7033 to 0.7062, except for the "…extreme eastern side of the batholith, initial values are limited to less than 0.7045…." They noted that the "…east-west contrasts appear to relate to a major boundary between pre-batholithic host rocks…. Mesozoic metavolcanics to the west and a metamorphic sedimentary complex of unknown age to the east." A highly diagrammatic depiction of near-linear 0.7040 and 0.7060 Sr_i isopleths from the north end of the batholith southward for 600 km was given by Gromet and Silver (1987). Silver and Chappell (1988), referring to the study of Early and Silver (1973, p. 114), stated, "They found that the rocks of the batholith are characterized in general by a gradient

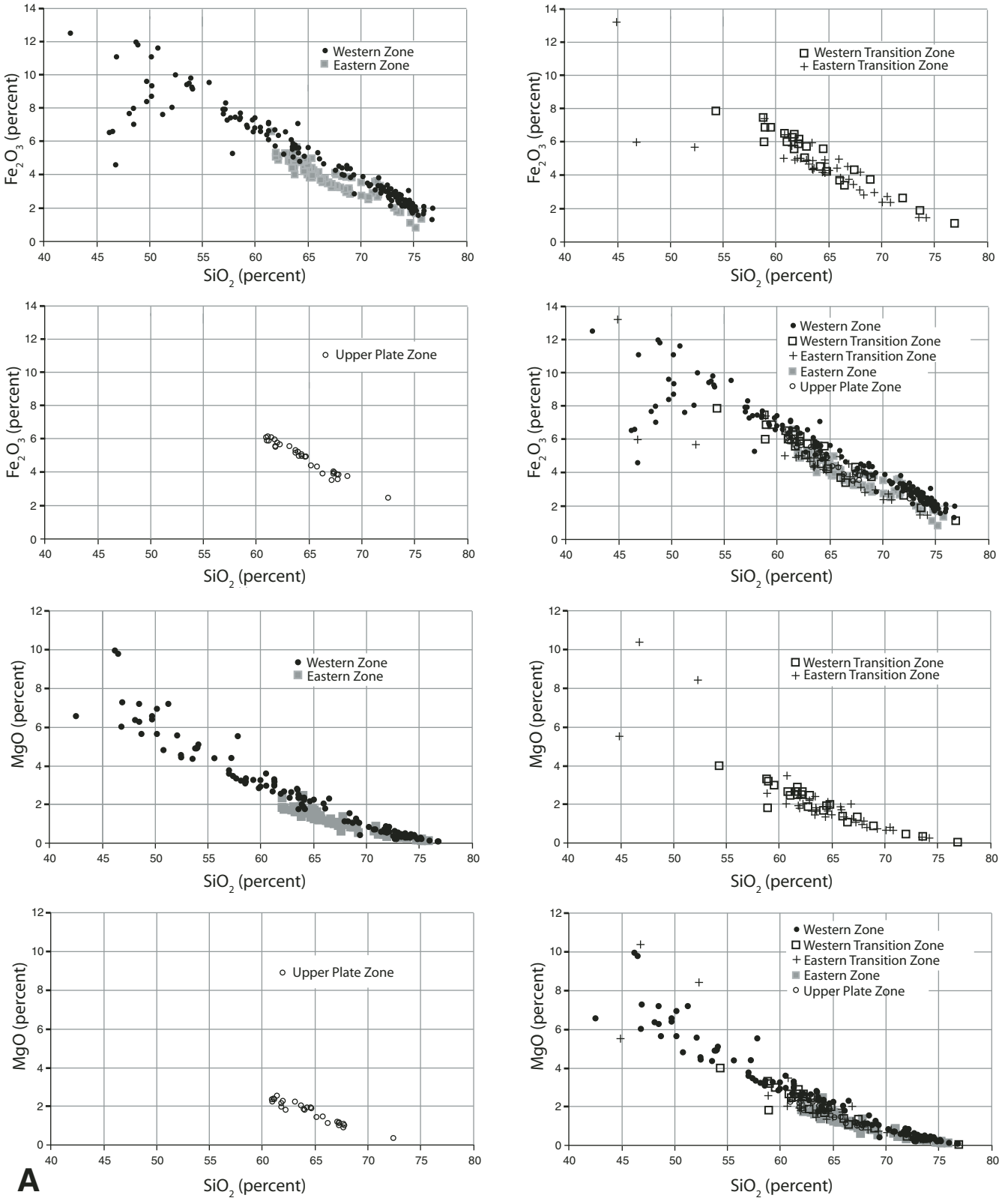

Figure 70 (*Continued on following pages*). Harker diagrams of selected major and trace elements. Diagrams show plots by zones and by all zones combined. Analyzed samples include all Baird-Welday samples, samples collected to augment the Baird-Welday collection, and samples collected primarily for U-Pb isotopes.

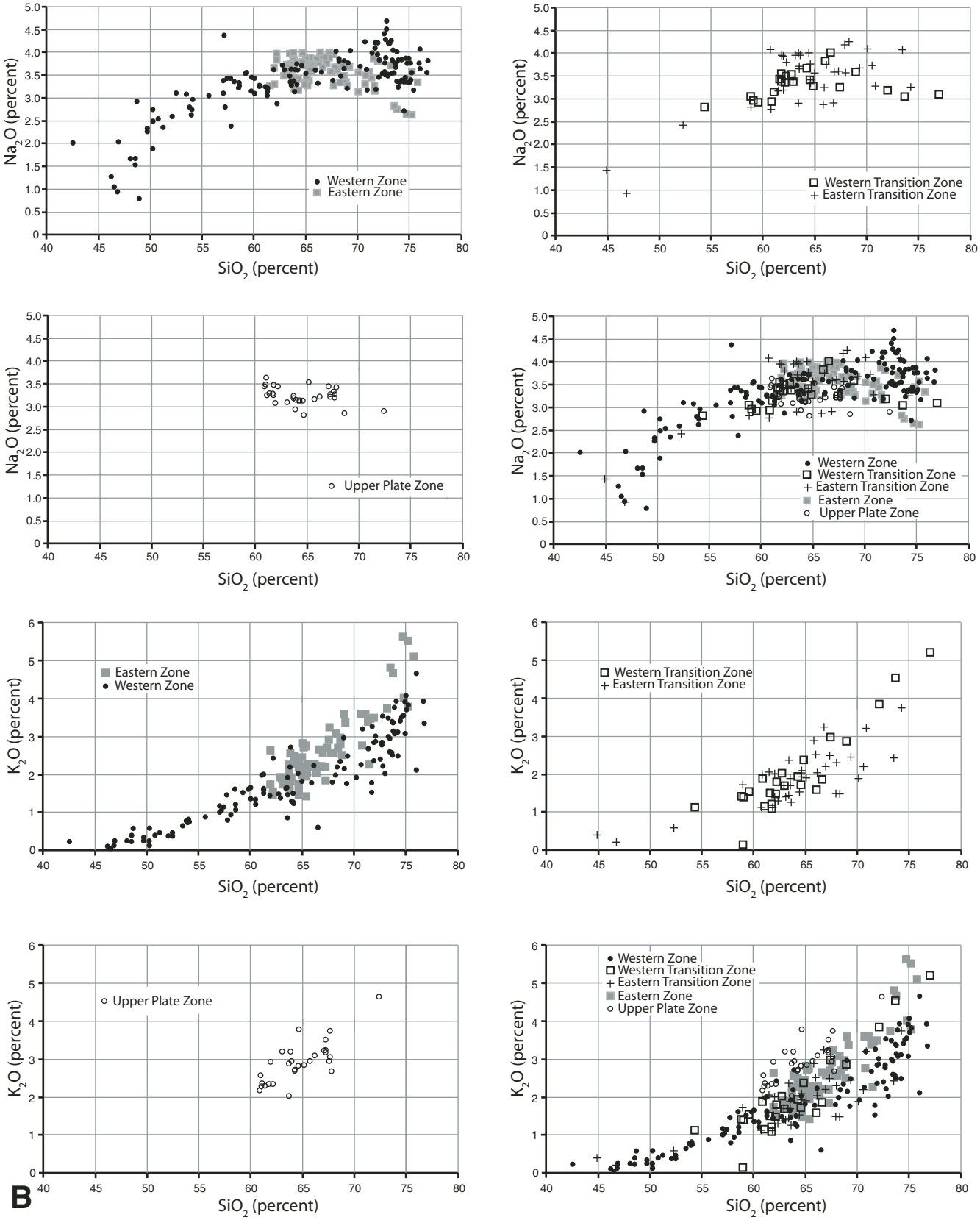

Figure 70 (*Continued*).

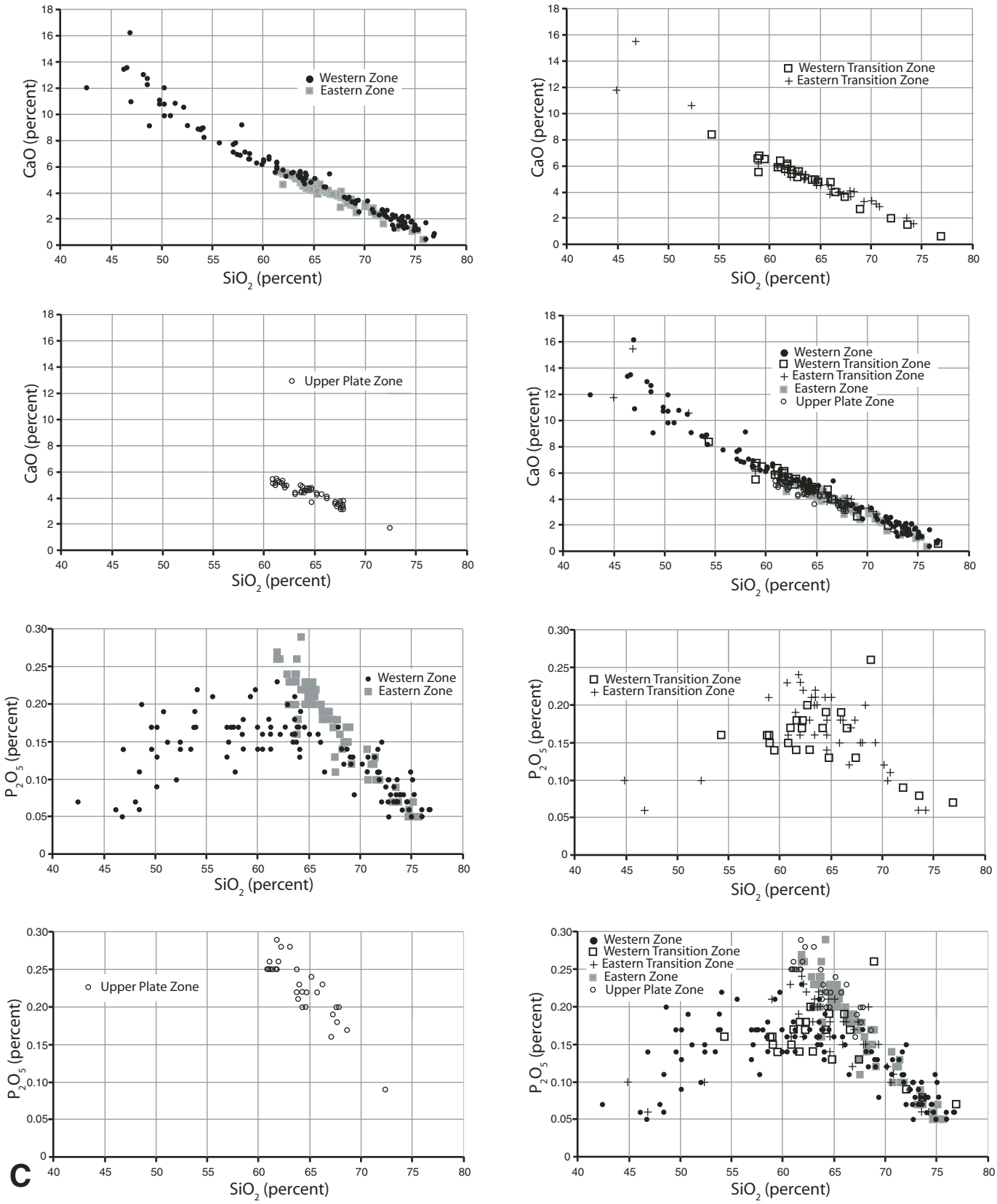

Figure 70 (*Continued*).

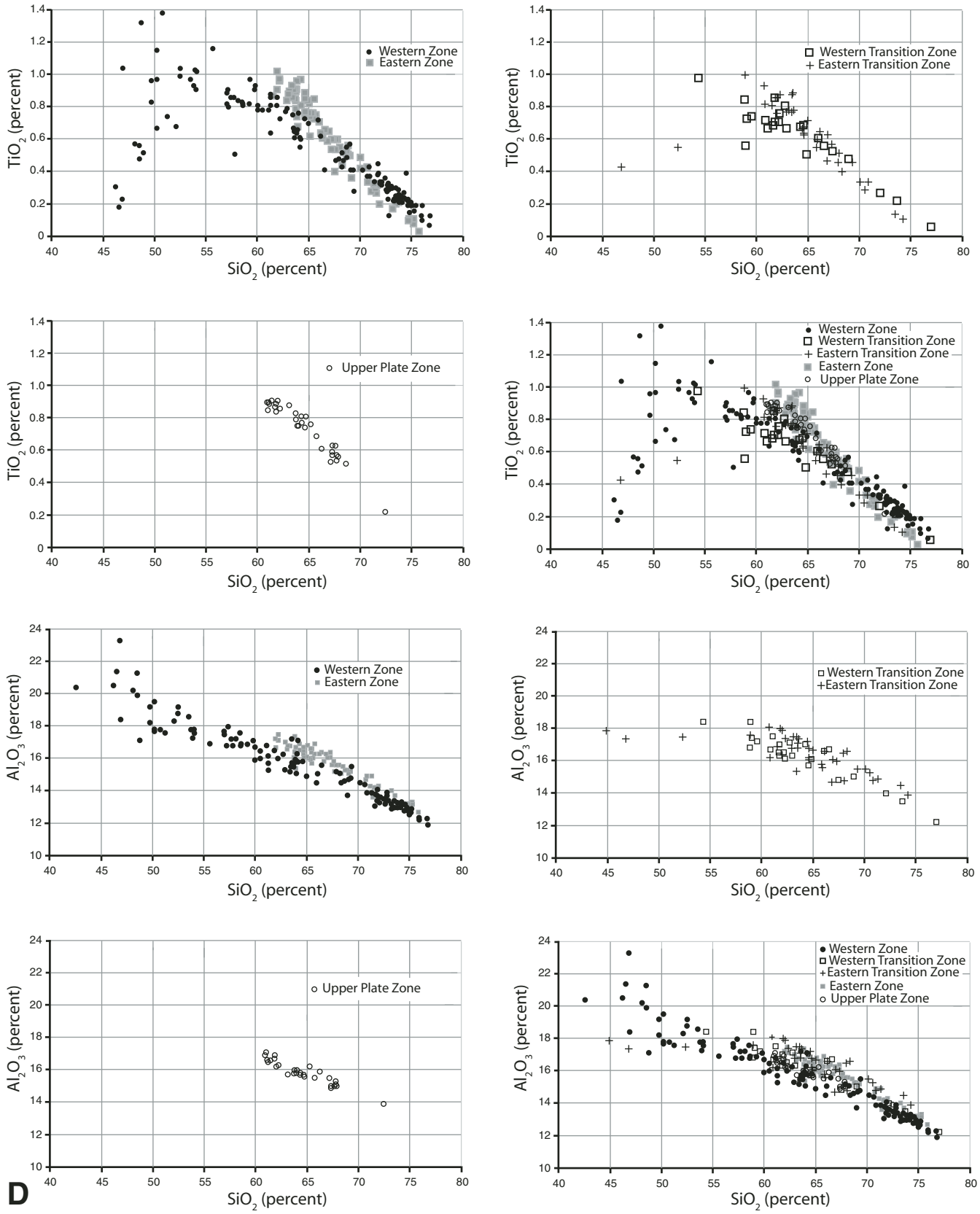

Figure 70 (*Continued*).

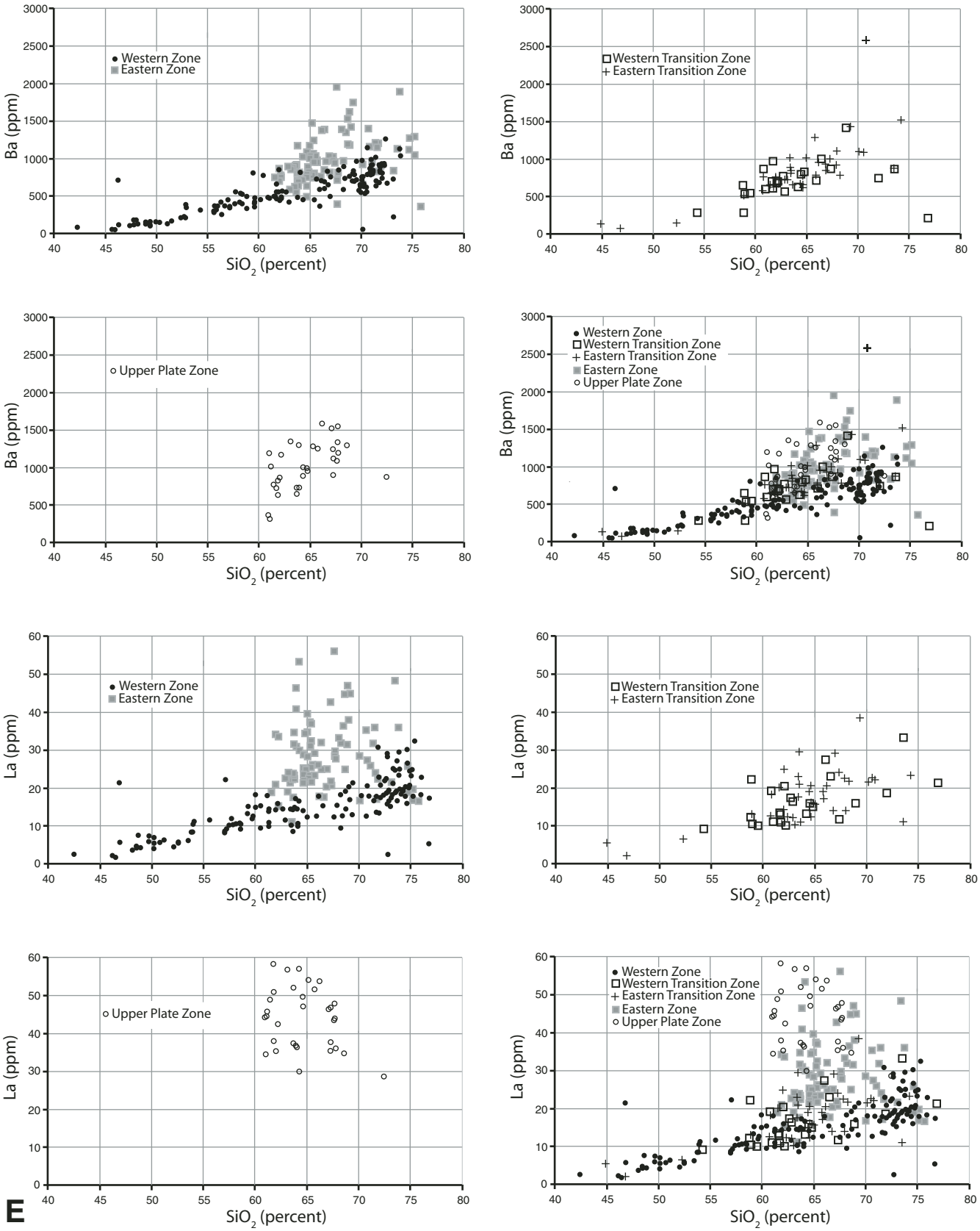

Figure 70 (*Continued*).

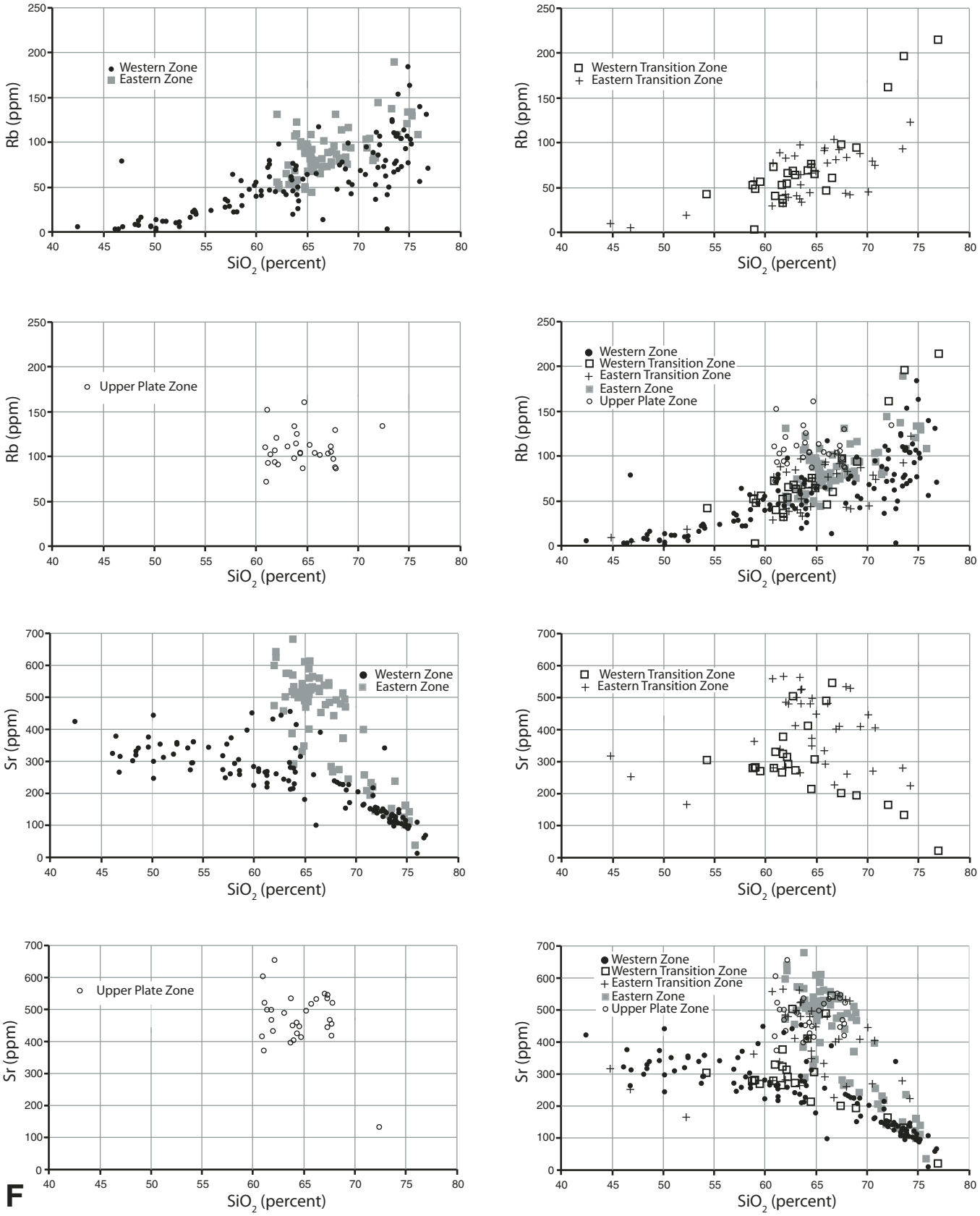

Figure 70 (*Continued*).

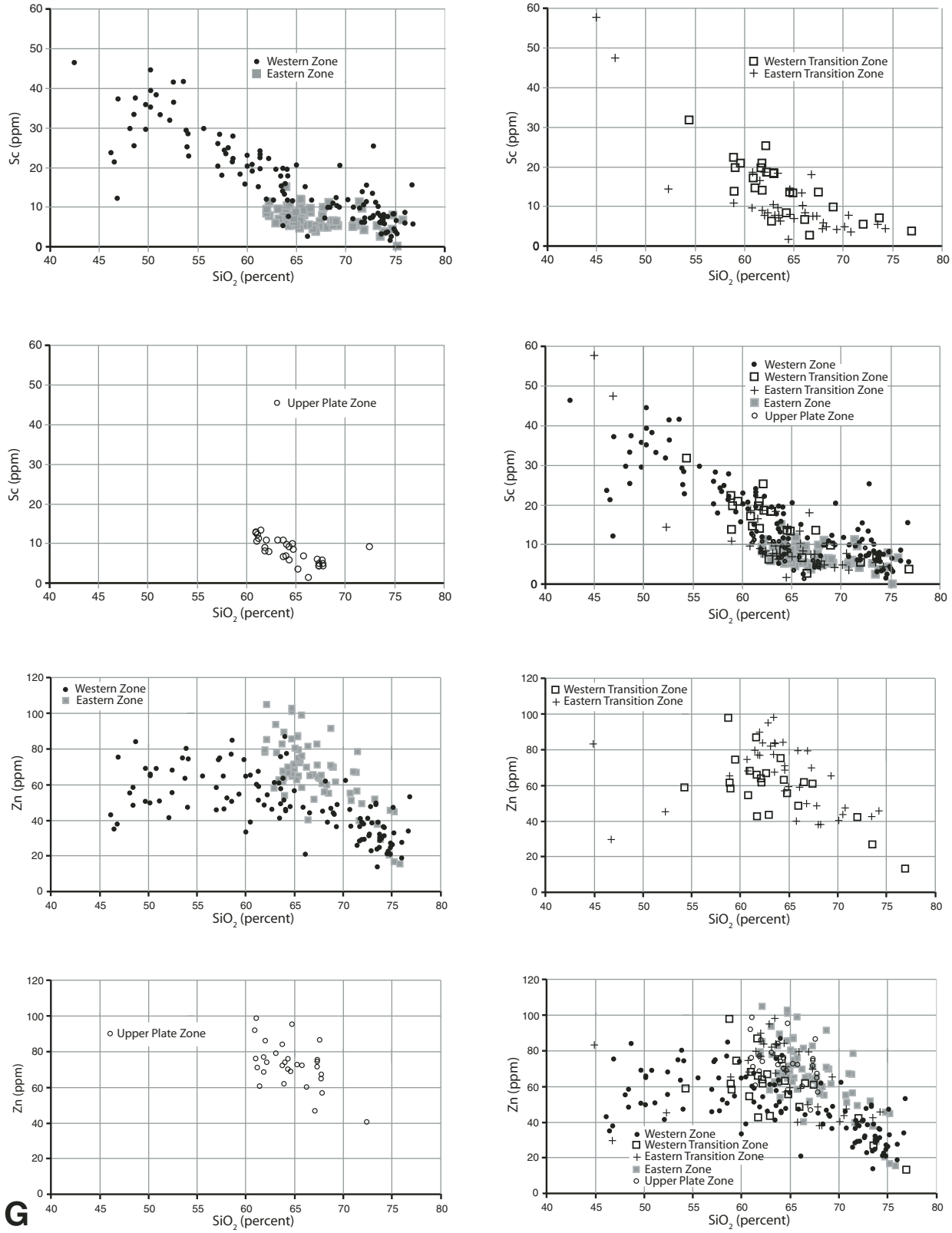

Figure 70 (*Continued*).

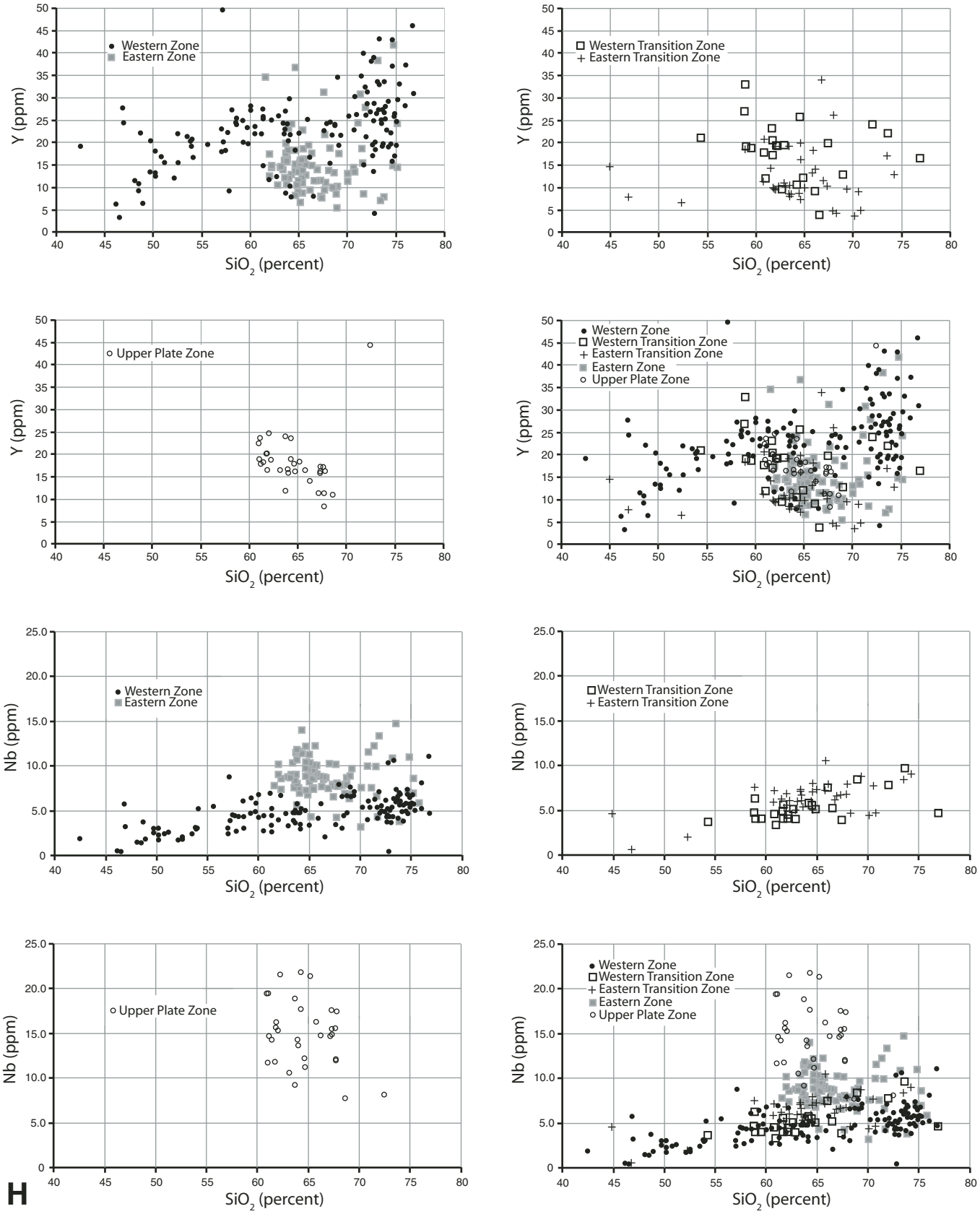

Figure 70 (*Continued*).

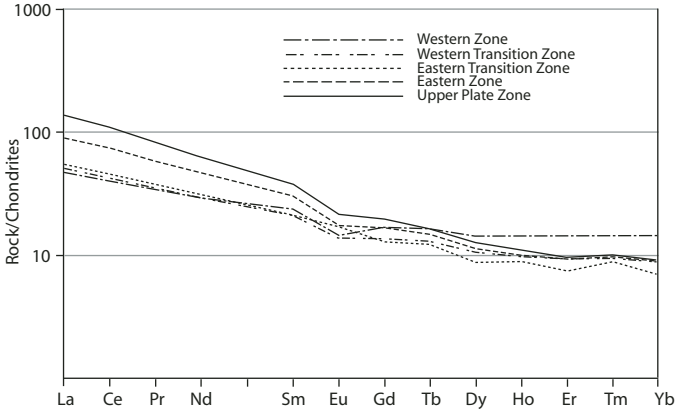

Figure 71. Average chondrite-normalized rare earth elements (REEs) for the five batholith zones. Average light REE values are similar for the western zone, western transition zone, and eastern transition zone, and the eastern zone and upper-plate zone are distinct from each other and from the other zones of the batholith.

from very low values of initial $^{87}Sr/^{86}Sr$ (<0.703) at the western limits, to values as high as 0.7080 at the eastern margin." Kistler and Morton (1994) and Morton and Kistler (1997) discussed preliminary results of investigations of Sr_i variation in the northern Peninsular Ranges batholith between 33°N and 34°N.

Our extensive Sr_i data set for the northern Peninsular Ranges batholith (see also Kistler et al., 2003, this volume) shows considerable geometric complexity in Sr_i isopleths, rather than a uniform gradient. Geometric Sr_i complexities of the 0.7045 and 0.7060 isopleths (Fig. 73) are in part inherent pluton Sr_i variation and in part from offsets on the Neogene Elsinore and San Jacinto fault zones (see also Miller et al., this volume). The Sr_i variation shown in Figure 74 is after 29 km of lateral displacement on the San Jacinto fault zone and 12 km of displacement on the Elsinore fault zone have been restored, so that sample localities have the positions relative to each other that they had at the time of pluton emplacement.

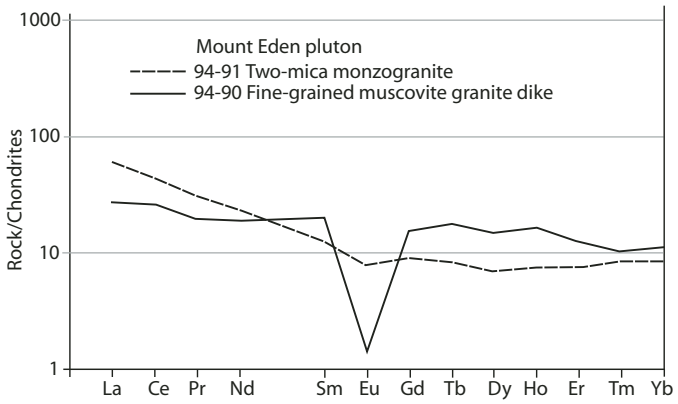

Figure 72. Chondrite-normalized rare earth element (REE) plots for Mount Eden leucogranite and associated fine-grained leucocratic dike.

The average Sr_i for the five zones of the Peninsular Ranges batholith increases systematically from west to east, with a moderate step between the eastern transition zone and the eastern zone (Fig. 75). For the northern Peninsular Ranges batholith, Sr_i is bimodal, with peaks at 0.7038 and 0.7072 (Fig. 76). Only a minor part of the batholith has Sr_i between 0.7056 and 0.7064, with a minimum frequency of samples at 0.7059. Despite considerable sample density, this dearth of samples of Sr_i >0.7056 and <0.7064 and peaks at 0.7038 and 0.7072 clearly define a bimodal character for the batholith. We interpret this bimodal distribution to reflect a relatively sharp boundary between Mesozoic oceanic crust and older continental crust; it is essentially coincident with the western zone and western transition zone boundary, and it is one of the criteria used to establish the boundary.

Sr_i values for western zone samples have an average of 0.7039, with most in the mid-0.7030s and a few in the 0.7040s. The uniformly low Sr_i that characterizes the western zone is notably independent of pluton composition. The Sr_i = 0.7045 isopleth is mostly coincident with the western zone–western transition zone boundary, and at its southern extent also separates highly magnetic rocks on the west from less magnetic rocks on the east. However, in the northern Santa Ana Mountains and the northwestern Perris block, the Sr_i 0.7045 isopleth deviates southwest away from the zone boundary. This deviation is caused by the western zone Gavilan ring complex, which has relatively wide variation in Sr_i ranging from 0.7041 to 0.7062. In the western zone Paloma Valley ring complex, just south of the Gavilan ring complex, most Sr_i values range from 0.7036 to 0.7046, except for one anomalous value of 0.7058. The Sr_i = 0.7045 isopleth bisects the northwest part of the Paloma Valley ring complex mainly because of the anomalous 0.7058 value; lower values typify the southeastern 80% of the complex, and the lone higher value represents the northwestern 20%. The Sr_i heterogeneity of the Gavilan and the Paloma Valley ring complexes is interpreted as a reflection of heterogeneity in the magma sources along the interface between oceanic and continental crust.

For most western transition zone plutons, Sr_i values range from 0.7045 to 0.7050 and average 0.7049. In the Riverside area, a few western transition zone granodiorite and granite samples have Sr_i >0.7060, and in the Jurupa Mountains area, Sr_i is quite variable, with one value of 0.7075. The relatively high Sr_i values in the Riverside–Jurupa Mountains area likely reflect contamination of the magma by abundant Paleozoic(?) prebatholithic rocks in these areas.

Sr_i values of eastern transition zone samples range from 0.7050 to 0.7055 and average 0.7053. The eastern transition zone is dominated by the Coahuila Valley and Tucalota Valley plutons, which have relatively uniform Sr_i values of 0.7048–0.7052. The white mica eastern transition zone Mount Eden granite has Sr_i values of 0.7058 and 0.7059, and a fine-grained leucocratic granite dike of the pluton has Sr_i of 0.7069. Sr_i values of relatively few eastern transition zone gabbros range from 07035 to 0.7050. This range in Sr_i values in eastern transition zone plutons shows a definite link to plutonic rock type, unlike

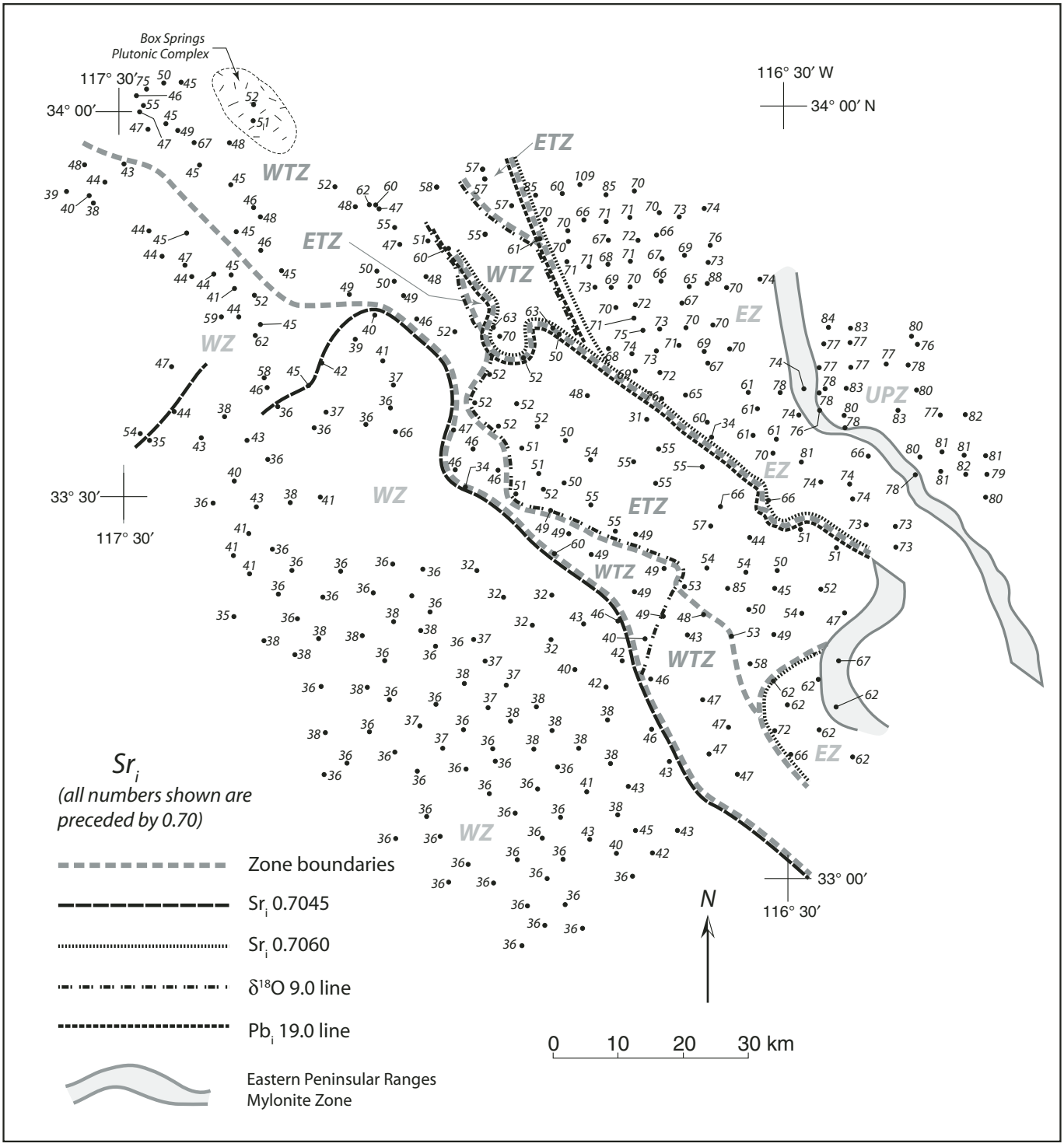

Figure 73. Generalized map showing Sr_i 0.7045 and 0.7060 isopleths and all Sr_i values. Total offset of the Eastern Peninsular Ranges mylonite zone by San Jacinto fault zone is diagrammatically shown as having occurred on a single strand. Major offsets of the Eastern Peninsular Ranges mylonite zone are actually across two stands of the San Jacinto fault zone that are separated by ~7 km at the latitude of the offsets. WZ—western zone; WTZ—western transition zone; ETZ—eastern transition zone; EZ—eastern zone; UPZ—upper-plate zone.

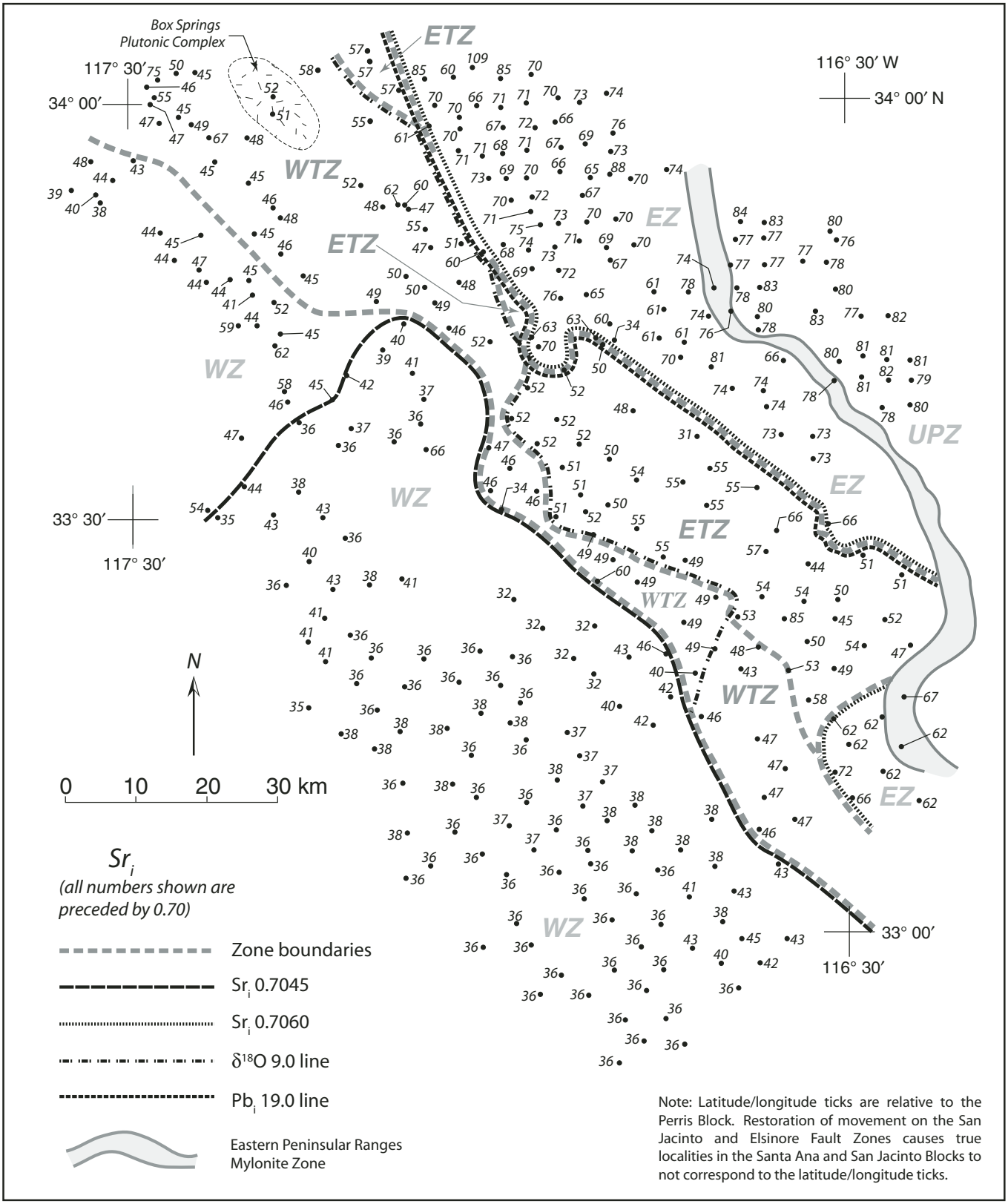

Figure 74. Generalized map showing Sr_i 0.7045 and 0.7060 isopleths and all Sr_i values after restoration of 12 km displacement on the Elsinore fault zone and 29 km displacement on the San Jacinto fault zone. WZ—western zone; WTZ—western transition zone; ETZ—eastern transition zone; EZ—eastern zone; UPZ—upper-plate zone.

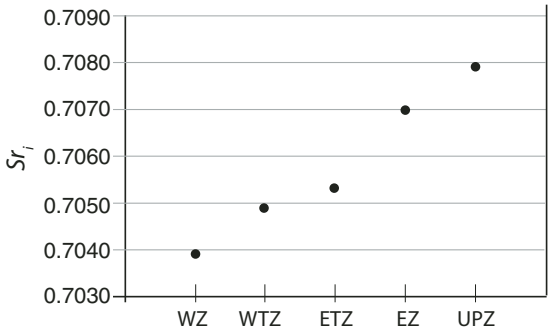

Figure 75. Plot of average Sr_i for the five batholith zones. Note the step between the eastern transition zone and eastern zone. WZ—western zone; WTZ—western transition zone; ETZ—eastern transition zone; EZ—eastern zone; UPZ—upper-plate zone.

western zone plutons, which show little correlation between Sr_i and pluton composition.

For most of its length, the eastern transition zone–eastern zone boundary is essentially coincident with the San Jacinto fault zone (Langenheim et al., 2004), the $Sr_i = 0.7060$ isopleth, and the $Pb_i = 19.0$ isopleth. Most eastern zone granitic rocks have Sr_i values ranging from the mid-0.7060s to the low 0.7070s, but average close to 0.7070, i.e., considerably greater than the average 0.7049 of the western transition zone and 0.7053 of the eastern transition zone. At the north end of the batholith, the $Sr_i = 0.7060$ isopleth is located just east of the San Jacinto fault zone in the northwestern part of the San Jacinto Mountains (Fig. 74). Control at the northern end of the $Sr_i = 0.7060$ isopleth is poor, with only two samples from the Lamb Canyon pluton having Sr_i values of 0.7056 and 0.7057. Upper-plate zone granitic rocks have Sr_i values in the range of 0.7076–0.7084, and they have an average of 0.7079, which is considerably greater than the average of 0.7070 for eastern zone samples.

Lead Isotopes

Silver (1987) and Silver and Chappell (1988) summarized the variation of initial $^{206}Pb/^{204}Pb$ (Pb_i) across the Peninsular Ranges batholith. They described a general gradient of increasing ^{206}Pb from west to east, with Pb_i values of 18.5–18.7 in the western part of the batholith. In the central part of the batholith, at their age step of 105 Ma, Pb_i values were in the range of 18.8–18.9. Values as high as 19.4–19.5 were recorded at the eastern margin of the batholith. Kistler et al. (2003) reported Pb_i values for the northern Peninsular Ranges batholith and gave values as low as 18.4 in the western zone and as high as 19.5 in the upper-plate zone.

The $Pb_i = 19.0$ isopleth is coincident with the $Sr_i = 0.7060$ isopleth (Fig. 77), both of which are generally coincident with the San Jacinto fault zone. All western zone, western transition zone, and eastern transition zone samples have $Pb_i < 19$ (Fig. 77), with the exception of two samples from the eastern transition zone, one sample of the western transition zone Box Springs Mountains pluton, and one sample from the northern Santa Ana Mountains that has an aberrant $\delta^{18}O$ value. Average Pb_i increases systematically from west to east, with a pronounced step between the eastern transition zone and the eastern zone (Fig. 78). Similar to Sr_i, the frequency distribution of Pb_i is bimodal, with a minimum number of samples having Pb_i of 19.05 (Fig. 79). The pronounced step (Fig. 78) and the bimodal minimum at Pb_i of 19.05 are interpreted to reflect the transition of subduction from largely beneath oceanic crust to beneath continental crust.

At ~33°45′N, the eastern transition zone pinches out, and the $Pb_i = 19.0$ isopleth separates the western transition zone from the eastern zone; at ~34°N, the eastern transition zone reappears between the western transition zone and eastern zone. The $Pb_i = 19$ isopleth is one of the criteria used to establish the eastern transition zone–eastern zone boundary.

Oxygen Isotopes

Turi and Taylor (1971) published an early detailed oxygen isotope study on the Domenigoni Valley pluton, but the first detailed investigation of regional oxygen isotope variation of the batholith was by Taylor and Silver (1978). Their work showed a systematic change of $\delta^{18}O$ from 6.0‰ to 7.0‰ in the west to 12.8‰ in the east. They emphasized a near-linear step in $\delta^{18}O$ from 8.5‰ to 9.0‰ isopleths striking southward from the north end of the batholith for over 300 km, well into Baja California. Additional $\delta^{18}O$ data are given in Taylor (1986, 1988). Kistler et al. (2003) showed oxygen isotope variation across the northern part of the batholith and discussed the relationship between $\delta^{18}O$ and Sr_i.

Our oxygen isotope database consists of only 100 samples, 38 from the western zone, 14 from the western transition zone, 9 from the eastern transition zone, 27 from the eastern zone, and 12 from the upper-plate zone. Variation of $\delta^{18}O$ across the northern Peninsular Ranges batholith is depicted in Figure 80, which shows sample locations after restoration of displacement on the Elsinore and San Jacinto fault zones. The average $\delta^{18}O$ values are 7‰ for the western zone, 8.3‰ for the western transition, 10.2‰ for the eastern transition zone, 10.3‰ for the eastern zone, and 8.7‰ for the upper-plate zone, showing a gradual rise in $\delta^{18}O$ values across the autochthonous zones and a notable drop in the

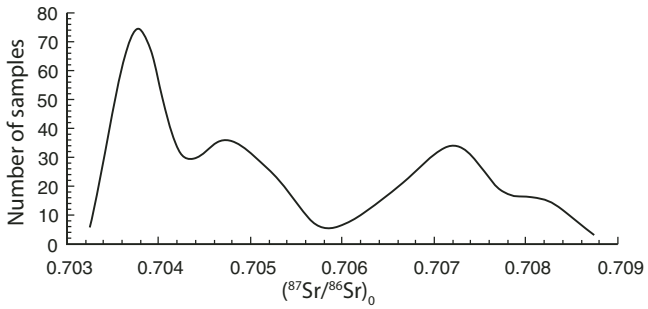

Figure 76. Bimodal frequency distribution of initial $^{87}Sr/^{86}Sr$ for the northern Peninsular Ranges batholith.

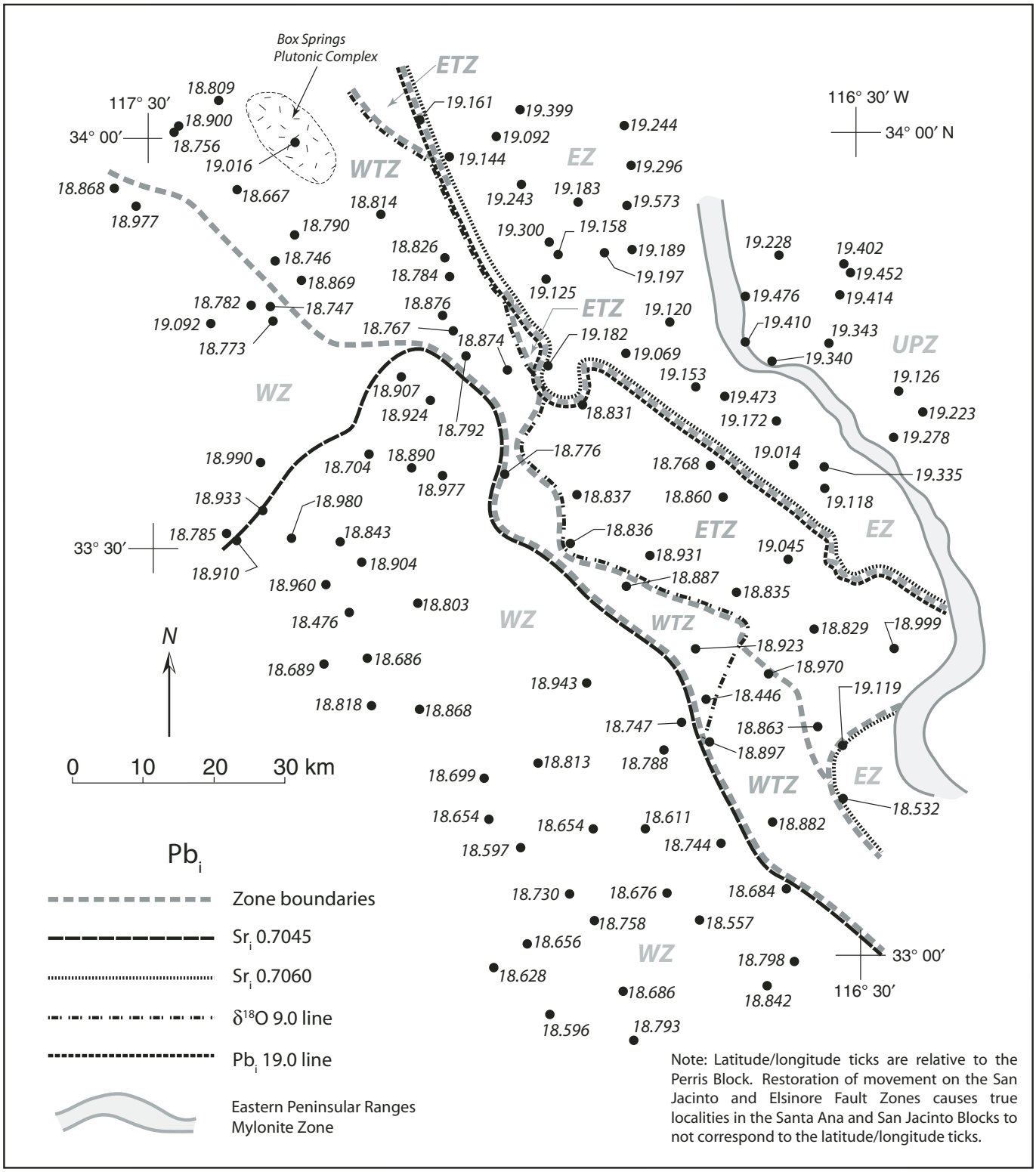

Figure 77. Generalized map showing distribution of lead isotope samples, and initial $^{206}Pb/^{204}Pb$ 19.0 isopleth after restoration of 12 km displacement on the Elsinore fault zone and 29 km displacement on the San Jacinto fault zone. WZ—western zone; WTZ—western transition zone; ETZ—eastern transition zone; EZ—eastern zone; UPZ—upper-plate zone.

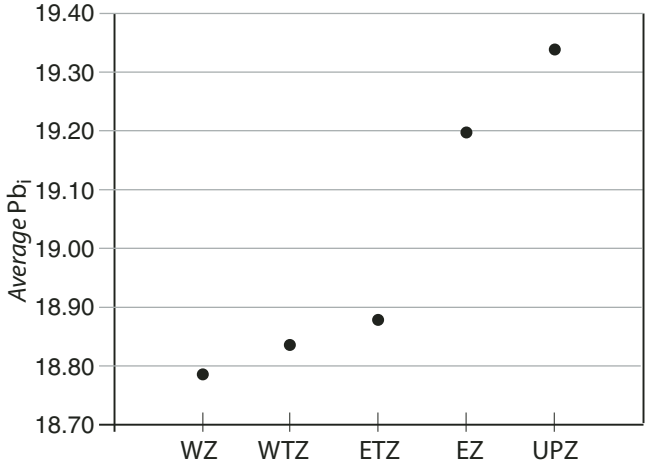

Figure 78. Plot of average Pb_i ($^{206}Pb/^{204}Pb$) for the five batholith zones. There is a much greater step in initial Pb_i values between the eastern transition zone and eastern zone than for initial $^{87}Sr/^{86}Sr$. WZ—western zone; WTZ—western transition zone; ETZ—eastern transition zone; EZ—eastern zone; UPZ—upper-plate zone.

upper-plate zone (Fig. 81). The lower $\delta^{18}O$ values in the upper-plate zone appear coincident with the area of low-$\delta^{18}O$ values in the San Jacinto block reported by Taylor and Silver (1978). The $\delta^{18}O$ map of Taylor and Silver (1978) is reproduced in Silver et al. (1979).

The distribution of $\delta^{18}O$ values within the western zone does not show an even progression from lower values in the western part of the zone to higher values in the eastern part. In places, there are significant reversals or a near randomness to the values. The same absence of an even value-progression is apparent within the combined transition zones, although slightly less pronounced than in the western zone. The internal value distribution within the eastern zone appears to have about the same degree of randomness as the combined transitions. Although it may be partly a result of the limited number of samples, $\delta^{18}O$ values within the upper-plate zone show a regular eastward progression from low to high values. Lackey and coworkers (Lackey et al., 2008, 2112)

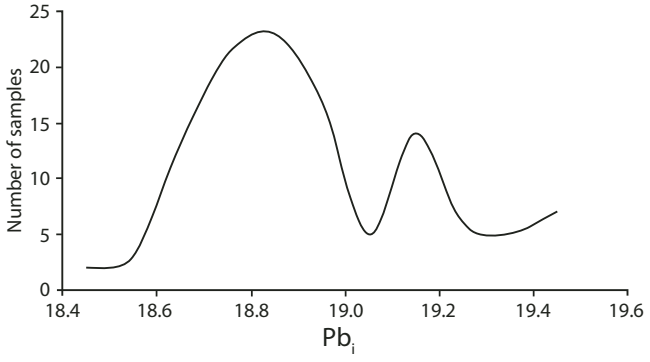

Figure 79. Bimodal frequency distribution of initial Pb_i for the northern Peninsular Ranges batholith.

interpreted $\delta^{18}O$ randomness in the central part of the Cretaceous Sierra Nevada batholith as principally due to variation in the original magma composition and not due to alteration.

Most of the western zone and western transition zone have $\delta^{18}O$ <9‰, and the $\delta^{18}O$ = 9‰ isopleth is essentially coincident with the western transition zone–eastern transition zone boundary, except in the southern part of the area. There, the isopleth diverges from the zone boundary, making a near right-angle turn across the western transition zone, and then follows the western zone–western transition zone boundary to the southern edge of the map. The $\delta^{18}O$ is <9‰ for the western zone, except for a single value of 9.3‰ for the westernmost sample in the northern Santa Ana Mountains (sample HSCZ). The $\delta^{18}O$ values in the eastern transition zone and eastern zone fall between 9.0‰ and 12.8‰, with most between 9.6‰ and 10.6‰.

Geochemical Interpretation

Nearly all current work on the northern part of the Peninsular Ranges batholith appears to substantiate the proposal that relatively uniform west-to-east geochemical and isotopic variations across the batholith reflect a change in magma derivation from oceanic-type lithosphere in the west to derivation from a mix of oceanic-type lithosphere and more-evolved continental lithosphere in the east (e.g., Baird and Miesch, 1984; DePaolo, 1981; Gromet and Silver, 1987; Kistler et al., 2003; Silver and Chappell, 1988; Todd et al., 2003). Baird and Miesch (1984) arrived at this interpretation based on studies of major-element chemistry. Gromet and Silver (1983) based their interpretation on the REE chemistry. Kistler et al. (2003) based their interpretation on a combination of Sr_i, $\delta^{18}O$, and Pb_i isotopes. Silver and Chappell (1988), summarizing various chemical and isotopic data, as did Todd et al. (2003), both arrived at basically the same conclusion.

Uniquely comprehensive geochemical and isotopic data sets are presented here to substantiate and augment the prevailing consensus interpretation for the origin of the northern Peninsular Ranges batholith. West-to-east variations in Sr_i, Pb_i, and ε_{Ndi} and some elements (e.g., Sr, and Ba) support the interpretation of magma emplacement progressing from oceanic to continental lithosphere and forming the five zones of the northern Peninsular Ranges batholith (Figs. 75, 78, and 82). This variation is similar to recent work in the Fine Gold intrusive suite of the central Sierra Nevada batholith (Lackley et al., 2012).

The reversal in trend in average values between the eastern zone and upper-plate zone for $\delta^{18}O$, SiO_2, Fe_2O_3, MgO, and V and the step between the eastern zone and upper-plate zone for other elements (e.g., Th and Ta; Figs. 81and 82) suggest that the magma source for the upper-plate zone was farther east than our designated eastern zone, because its isotopic characteristic suggest greater input of aged North American crust. We are uncertain whether interpretations based on this very detailed data set are applicable to the entire Peninsular Ranges batholith. Our interpretations are linked to the four autochthonous zones of the northern Peninsular Ranges batholith and the criteria used to define

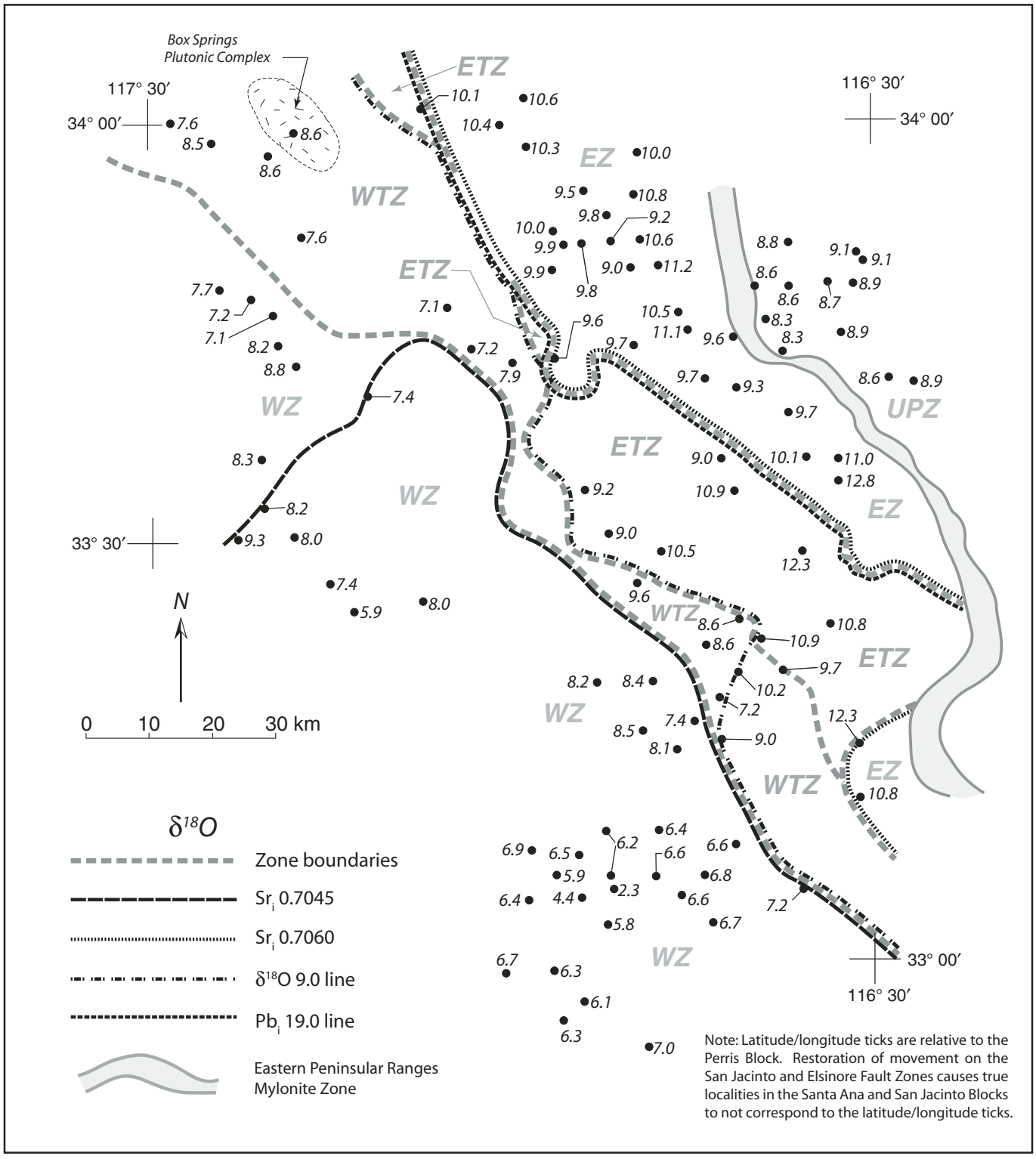

Figure 80. Generalized map showing distribution of oxygen isotope samples, and $\delta^{18}O$ isopleth after restoration of 12 km displacement on the Elsinore fault zone and 29 km displacement on the San Jacinto fault zone. WZ—western zone; WTZ—western transition zone; ETZ—eastern transition zone; EZ—eastern zone; UPZ—upper-plate zone.

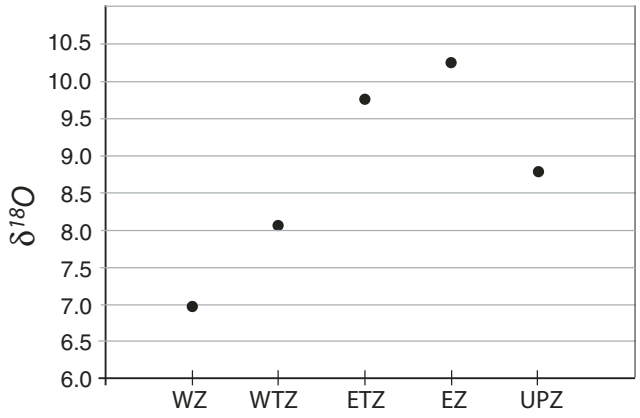

Figure 81. Plot of average $\delta^{18}O$ for the five batholiths zones showing major differences between the eastern zone and upper-plate zone. WZ—western zone; WTZ—western transition zone; ETZ—eastern transition zone; EZ—eastern zone; UPZ—upper-plate zone.

those zones. Variations in major-element chemistry materially support progressively increasing chemical differentiation from west to east. Across the entire autochthonous part of the northern Peninsular Ranges batholith, both major- and trace-element spatial distributions reflect progressive changes from near-juvenile to much more-evolved source materials, reflecting subduction transitioning from oceanic lithosphere to more-evolved subcontinental lithosphere. Major-element chemistry for plutons in both transition zones reflects an intermediate stage of chemical differentiation, as does trace-element distribution.

This chemical progression, however, does not appear to have been a smooth, even process, but in places it shows abrupt changes that, at least in part, are associated with dynamic changes in mode of emplacement and possibly rate of emplacement. In particular, the sharp transition in chemistry, isotopic and magnetic signatures, and rock fabrics from the western zone to western transition zone marks a change consistent with a shift to derivation of magma from more-evolved subcontinental lithosphere in the western transition zone compared with that derived from oceanic lithosphere in the western zone. The notably increased rate of magma emplacement in the eastern part of the Peninsular Ranges batholith, beginning in the eastern transition zone, but especially evident in the eastern zone, as indicated by the size and narrow age range of La Posta–type plutons, does not appear to have any obvious reflection in the major element or REE chemistry.

Source for Granitoids

Sr_i values increase from west to east, reflecting a decrease in mantle component and an increase in continental crustal component. Based on Sr_i values, and assumptions outlined here, an estimate can be made for the proportions of oceanic and continental crust contributions for the five batholith zones. Sr_i values of 0.7040 for juvenile basaltic crust and 0.7140 for continental crust are used in the calculations. Basaltic crust is assumed to have consisted of juvenile island-arc material similar to that in the Marianas and the Fiji-Tonga island arcs. For the Marianas island arc, Sr_i ranges from 0.70263 to 0.70432, averaging 0.7036 (Meijer, 1976). For the Fiji arc, the average Sr_i is 0.7041 (Gill, 1981). There is greater variability for reported Sr_i values of the older continental crust, but a Sr_i of 0.714 appears to be a reasonable average. The western zone batholithic rocks in the northern Peninsular Ranges batholith have an average calculated Sr_i of 0.7039, which is in keeping with oceanic island crust. However, the Sr_i 0.7045 isopleth (Fig. 74) crosses the northern part of the western zone, and that part of the western zone northwest of the isopleth has an average Sr_i of 0.7045, indicating ~93% juvenile component. The bulk of the western zone, southeast of the meandering part of the <0.7045 isopleth, has an average Sr_i of 0.7037, indicating no involvement of ancient continental crust.

The other four batholith zones show a systematic decrease in the island-arc component from west to east (Fig. 83). The western transition zone has an average Sr_i of 0.7049, indicating 91% juvenile component, and the eastern transition zone has an average Sr_i of 0.7053, indicating an 87% juvenile component. As expected, the composition of the eastern zone reflects a major increase (17%) in the ancient continental crust component, having an average 0.7070, which requires 70% juvenile component. The upper-plate zone has an average Sr_i of 0.7079, which indicates a 61% juvenile component. If, however, any juvenile component was derived from anomalously enriched mantle sources, the calculated contributions of evolved crustal components would be smaller. Regardless of these assumptions, some amount of isotopically evolved component (crust or enriched mantle) is required to explain the isotopic signatures of the plutons.

As expected, this west-to-east progression also shows an increase in the incompatible elements (e.g., K, P, Nb, La, Nd, Rb, Ba, Th, U, and Zr) and a decrease in compatible elements (e.g., Ca, Mg, Fe, and Sc). Harker diagrams clearly indicate that, despite the relatively uniform chemistry of the subducting plate component, the magma generated for the eastern granitoids is notably different than that for the western granitoids. This is well illustrated by the Harker diagrams for MgO, Fe_2O_3, TiO_2, Al_2O_3, CaO, and V (Fig. 70).

The discrimination diagram of Ta plotted against Yb (Fig. 84) (Pearce et al., 1984) shows that most of the batholith plots within the volcanic-arc granite field. There is a progressive shift from the western zone to the eastern zone toward the syncollisional granite field. Most of the upper-plate zone falls within the syncollisional granite field. A progressive deepening of the magma source from the west to the east is reflected in the shift in values from the western zone to the eastern zone upward through the volcanic-arc granite field and into the syncollisional granite field in the upper-plate zone.

Based on the correlation of increased alkalinity with depth of magma generation, several variation diagrams indicate that the magma source for the Peninsular Ranges batholith increases in depth from west to east. The Rb (ppm) versus Sr (ppm) plot

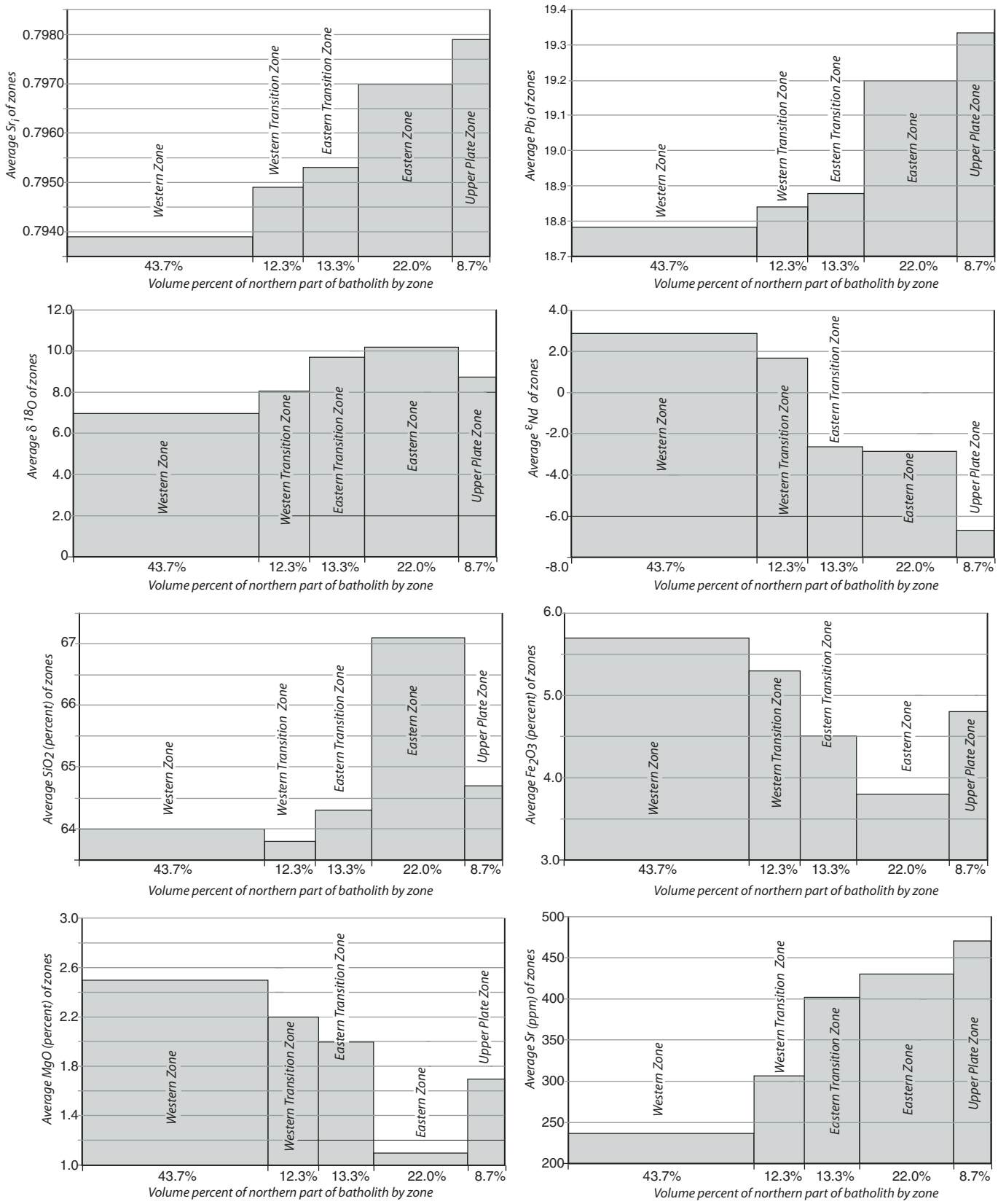

Figure 82 (*Continued on following page*). Plots showing averages of Sr_i, Pb_i, $\delta^{18}O$, ε_{Ndi}, and selected oxides for the five batholith zones. Width of the bars representing each zone is proportionate to its percentage of the batholith based on its areal extent.

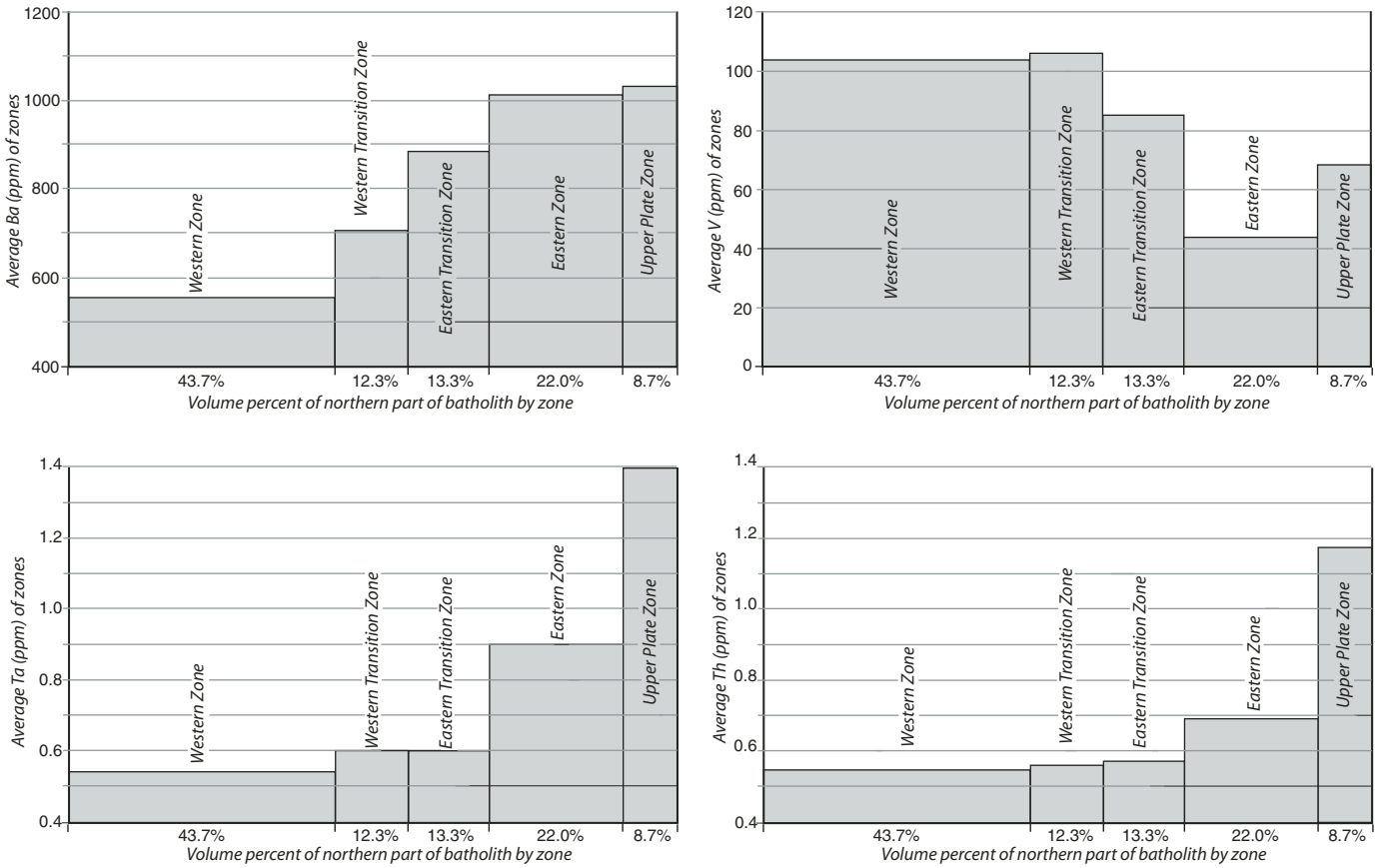

Figure 82 (*Continued*).

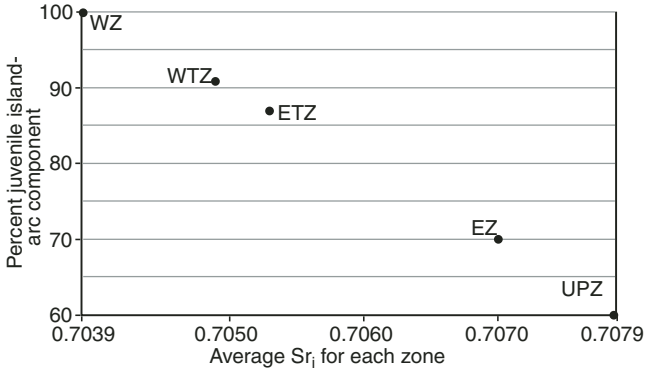

Figure 83. Plot comparing average Sr_i for the five batholith zones with calculated percentage of juvenile island-arc component in the batholith melt. Plot shows progressive decrease in island-arc component from western zone to upper-plate zone, and a major decrease between the eastern transition zone and eastern zone. WZ—western zone; WTZ—western transition zone; ETZ—eastern transition zone; EZ—eastern zone; UPZ—upper-plate zone.

(Fig. 85) and a MALI (modified alkali-lime index) plot (Fig. 86) show that the western part of the batholith is calcic when compared to the eastern, more alkaline part, which is similar to the more alkaline Sierra Nevada batholith (Bateman, 1992). K_2O and Na_2O increase from west to east as the depth of the magma source increases (Fig. 70B). A QAP (quartz, alkali feldspar, and plagioclase feldspar) diagram (Fig. 87) indicates a more calcic differentiation trend for the western part of the batholith than for the eastern part, whereas the differentiation trend for the eastern part of the batholith is similar to that of the Sierra Nevada batholith (Lameyre and Bonin, 1991).

Nb/Yb values systematically increase from the western zone to the upper-plate zone (Fig. 88). For the western zone, Nb/Yb values are quite uniform, mostly 2 or less (Fig. 89; see also Clausen et al., this volume), and they show no increase in values with increase in SiO_2. Nb/Yb values are somewhat less uniform in the western transition zone than in the western zone, with all but seven values in the 1–3 range (Fig. 89). In contrast, most Nb/Yb values in the eastern transition zone and eastern zone are fairly dispersed, mostly ranging in value from 2 to 10, and generally, they show an increase in Nb/Yb with an increase in SiO_2 (Fig. 90). In the upper-plate zone, the values are quite

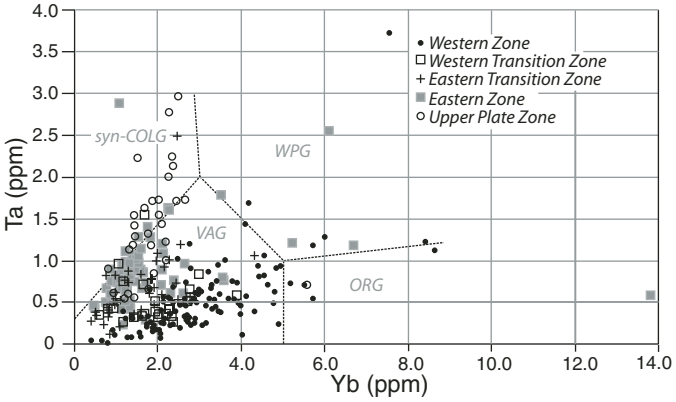

Figure 84. Discrimination diagram of Ta plotted against Yb, northern Peninsular Ranges batholith, showing progression from volcanic-arc granite field (VAG) toward syncollisional granite (syn-COLG) from the western zone to eastern zone. Most of the upper-plate zone is within the syncollisional granite field. WPG—within-plate granite field; ORG—ocean-ridge granite field.

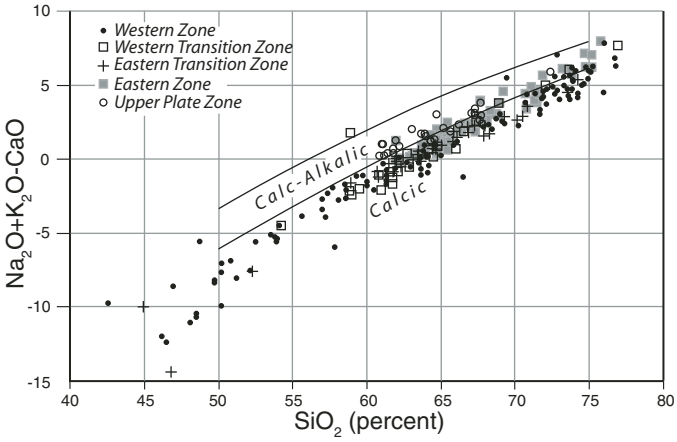

Figure 86. MALI (modified alkali-lime index) plot for northern Peninsular Ranges batholith rocks. The autochthonous zones of the batholith are mostly calcic, and most of the allochthonous upper-plate zone is calc-alkalic.

uniform, with only one aberrant value less than 6 (Fig. 89). This west-to-east dichotomy, due to interaction with continental lithosphere, is also evident from Sr/Y, La/Yb, and Ta/Yb values. Similar to Nb/Yb, average values for La/Yb, Ta/Yb, and Zr/Yb increase from the western zone to upper-plate zone. This increase is interpreted as being due to progressive interaction with continental lithosphere (Figs. 88 and 89).

Garnet

REE spidergrams can be used to estimate the depth at which magma generation occurred. Gromet and Silver (1987) used REE spidergrams to define three north-south–trending depth zones in the batholith, showing that magma was generated at increasingly greater depths eastward. The partition coefficient for garnet changes by three orders of magnitude between the lightest and heaviest REEs for crystallization below the garnet stability pressure of 10–12 kbar (Carroll and Wyllie, 1990; Tepper et al., 1993; Moyen and Stevens, 2006). The gentle slope for the western zone granitoids (Fig. 71) indicates that crystallization occurred at depths less than 30–35 km. Eastern zone plutons have a relatively steeper slope, indicating greater depths.

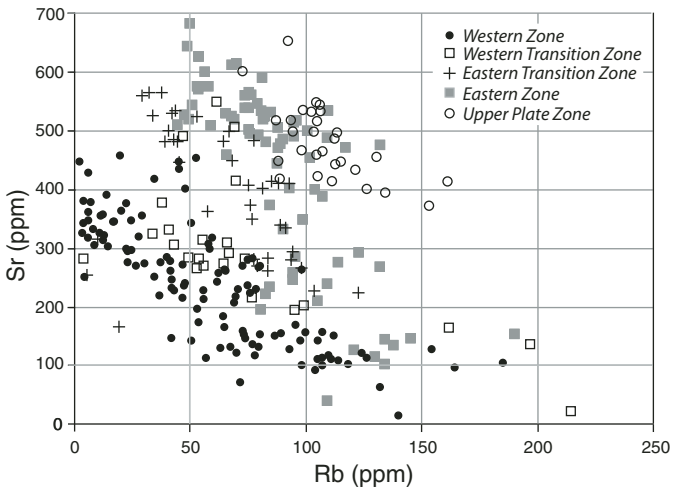

Figure 85. Rubidium plotted against strontium for northern Peninsular Ranges batholith rocks, showing progressive enrichment in Sr from the western zone to upper-plate zone.

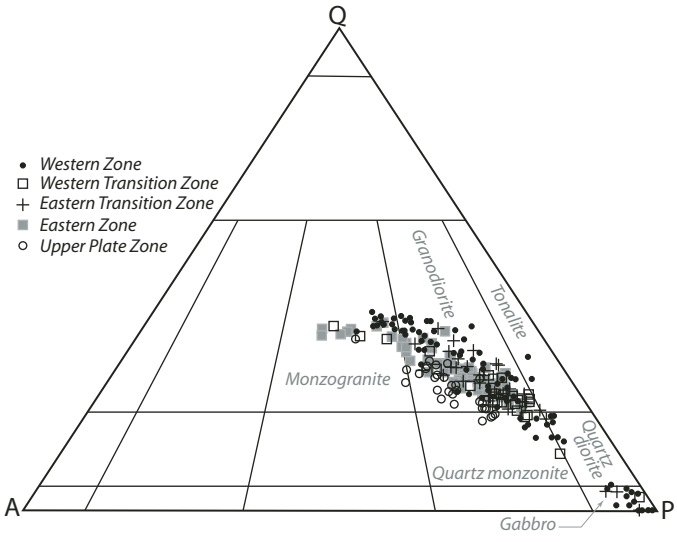

Figure 87. Q-A-P (quartz–alkali feldspar–plagioclase) plot for northern Peninsular Ranges batholith rocks. Because the plot is based on calculated normative values, most rock compositions fall in the granodiorite field. Mineralogically, many northern Peninsular Ranges batholith rock compositions fall within the granodiorite field, but the majority are in the tonalite field. Even though many of the Peninsular Ranges batholith rocks contain almost no K-feldspar, they do contain biotite. In the normative calculation, potassium from the biotite is partitioned to K-feldspar, biasing the plots toward the alkaline corner.

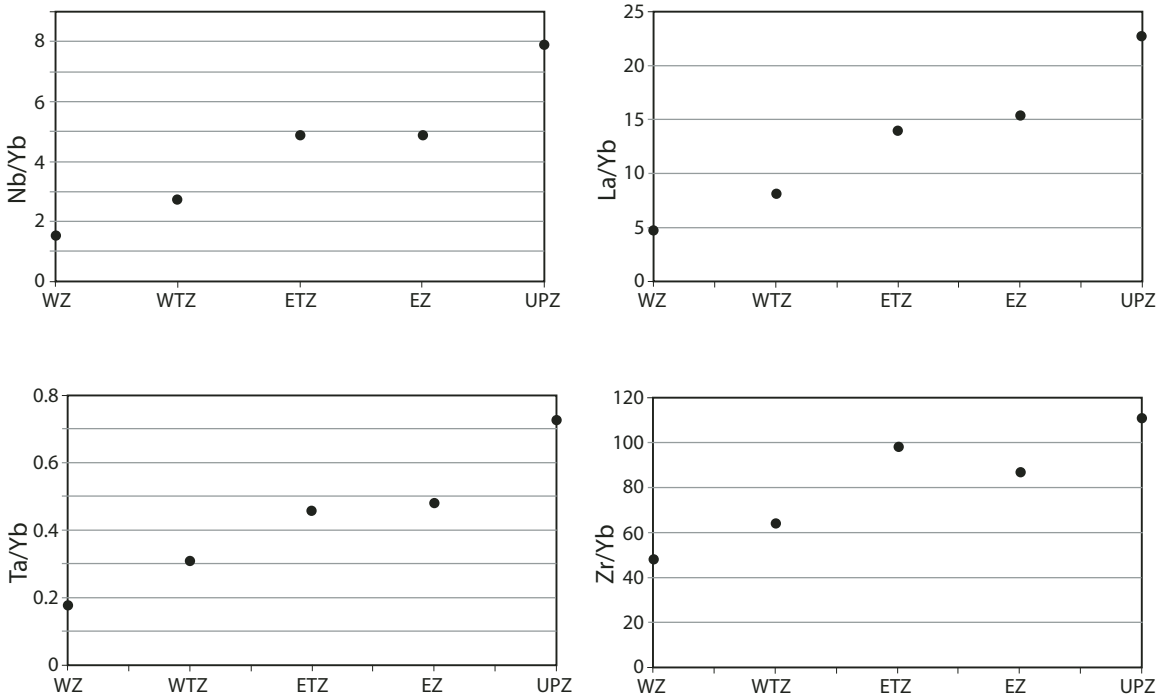

Figure 88. Average Nb/Yb, La/Yb, Ta/Yb, and Zr/Yb values for the five batholith zones showing increases in values from the western zone to the upper-plate zone. The eastern transition zone and eastern zone values are similar, with a step between eastern zone and upper-plate zone values. WZ—western zone; WTZ—western transition zone; ETZ—eastern transition zone; EZ—eastern zone; UPZ—upper-plate zone.

Values for the HREE and LREE ratios, Gd/Yb and La/Sm, respectively, can also be used to estimate depth; Gd/Yb values increase with increasing magma source depth, and La/Sm values increase with fractionation. Most Gd/Yb values are less than 2 for western zone rocks (Fig. 91), but almost all ratios from the eastern transition zone, eastern zone, and upper-plate zone are greater than 2, indicating a relatively deeper source. La/Sm values average ~3.5 for western zone rocks, and, although there is greater scatter for the eastern zone rocks, their average is ~5. With respect to lithology, La/Sm values for western zone plutons increase from an average of ~2.3 for gabbro, to ~2.9 for tonalite, and to ~3.6 for granodiorite.

Sr/Y values summarize the effect of garnet and plagioclase fractionation in a subduction zone. Fractional crystallization at depth in the garnet stability zone, where plagioclase is less stable, separates garnet, Y, and the HREEs from the melt residue, effectively depleting the melt of Y. In the northern Peninsular Ranges batholith, Y averages 23 ppm in the shallow western zone, decreases to 18 in the western transition zone and to 13 in the eastern transition zone, and increases slightly to 16 in the eastern zone. Fractional crystallization at shallower depths where plagioclase is stable and garnet is unstable separates plagioclase, Sr, and Eu from the melt residue and depletes the melt of Sr. Sr concentrations average 227 ppm in the shallow western zone and increase to 283 in the western transition zone, 375 in the eastern transition zone, and 428 in the eastern zone. Sr/Y values reflect depth of differentiation (e.g., Tulloch and Kimbrough, 2003). Shallow differentiation produced granitoids in the western zone with low Sr/Y values that average 13.6 (Fig. 92). In contrast, the deeper level of differentiation that produced rocks of the more easterly batholithic zones resulted in more than double the Sr/Y value, which averages 27.3 for the western transition zone, 41.1 for the eastern transition zone, 33.8 for the eastern zone, and 28.5 for the upper-plate zone.

Magma Mixing

The western zone plutons are interpreted as being derived from three magma groups (see Clausen et al., this volume): (1) gabbros, formed from partial melting of the mantle, (2) granodiorites, formed from partial melting of oceanic crust, and (3) tonalities, interpreted to be the product of mixing of gabbro and granodiorite magmas. This model is discussed in detail by Clausen et al. (this volume) for the low-Sr_i Escondido granitoids.

For granitic rocks, a plot of compatible trace elements against incompatible trace elements on a log base is linear if the rocks were produced by fractional crystallization, and it is concave downward if the rocks were produced by magma mixing (Cocherie, 1986). Plots on a log base of Co versus Ba (Fig. 93), Sr against Rb, and V against Ce are all concave downward, indicating that the chemical variation in the northern Peninsular Ranges batholith is a result of magma mixing. Partial melting would yield a plot with inverse concavity for the magma mixing curve.

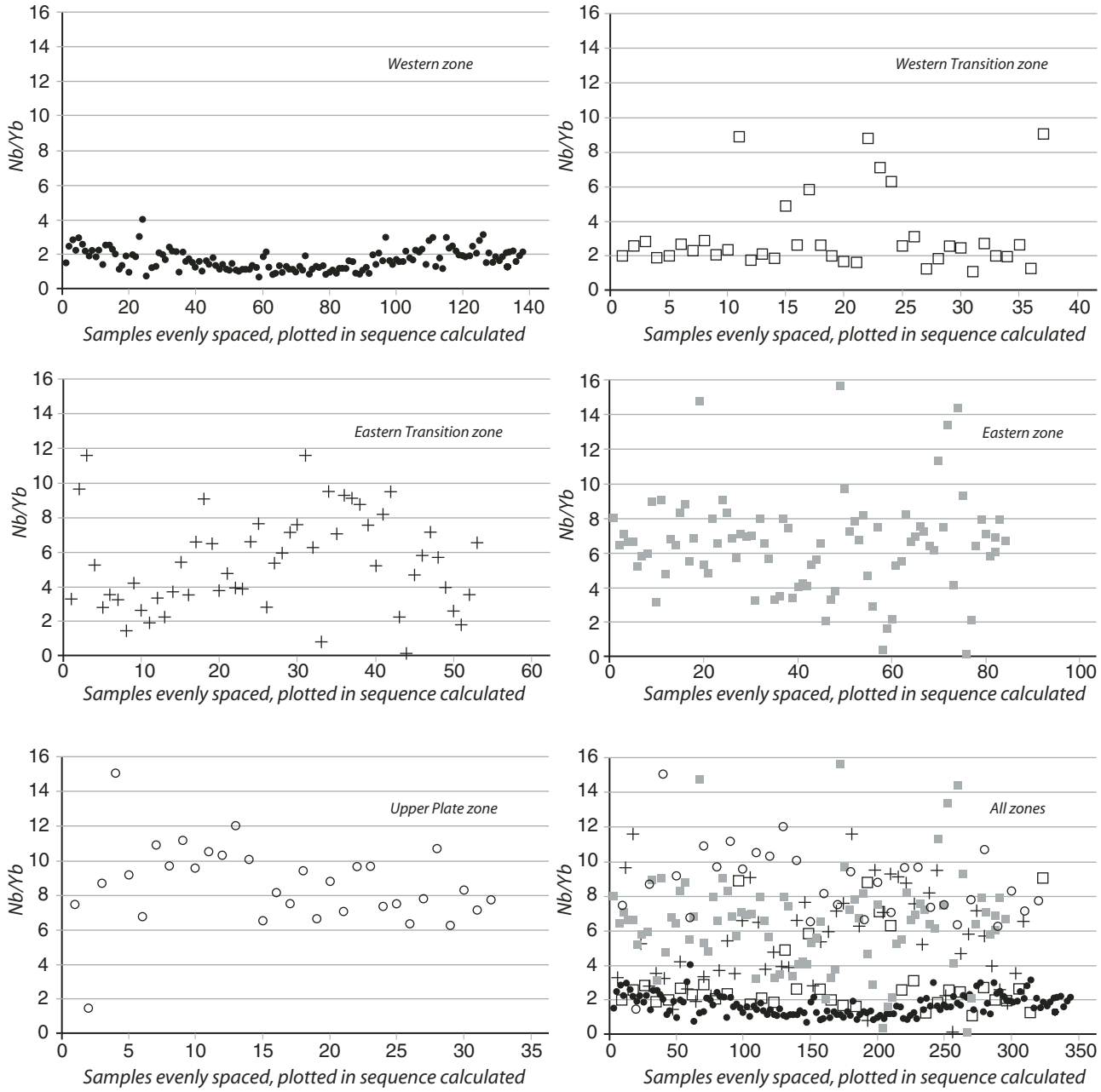

Figure 89. Nb/Yb plots by batholith zones. Nb/Yb plots show progressive increase in value from the western zone to upper-plate zone with very constant values in the western zone, and relatively constant values in the upper-plate zone.

Eichelberger (1978) showed that igneous rocks tend to display a bimodal SiO_2 composition during tectonic extension, whereas intermediate compositions dominate during compression. During tectonic extension in a thin crust, dense basaltic magma from the mantle should have less to inhibit ascent toward the surface, but low-density silicic magma from crustal melting easily ascends with little time for mixing. During tectonic compression and thickening crust, mafic magma from the mantle and felsic magma from partial melting of the lower crust can be trapped and have time to mix and form magmas of intermediate composition.

SUMMARY

The northern Peninsular Ranges batholith includes both autochthonous and allochthonous rocks. Most of the northern Peninsular Ranges batholith is autochthonous, with the allochthonous rocks restricted to the easternmost part. The autochthonous

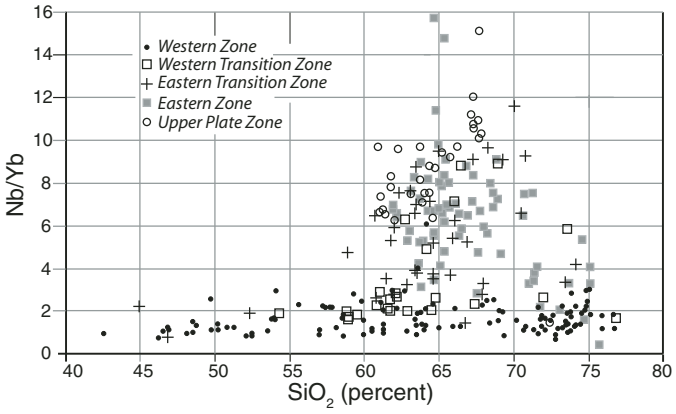

Figure 90. Nb/Yb plotted against SiO_2 showing relatively uniform Nb/Yb values in the western zone, independent of SiO_2 values. Nb/Yb values progressively increase in the western transition zone to upper-plate zone, with a general increase in Nb/Yb values with increasing SiO_2.

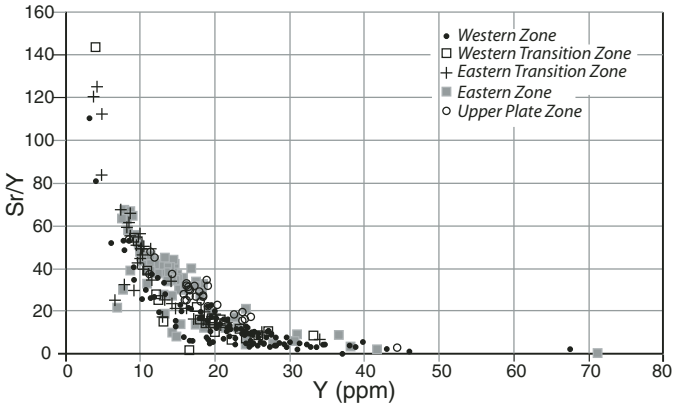

Figure 92. Sr/Y ratio plotted against Y for the northern Peninsular Ranges batholith rocks. The average decrease in Y from the western zone to the eastern zone reflects progressively deeper depth for the batholith melt.

batholithic rocks were emplaced between 126 Ma and 91 Ma. Based on a variety of parameters, the autochthonous northern Peninsular Ranges batholith is divided into four longitudinal zones, a western zone, western transition zone, eastern transition zone, and an eastern zone. In an extensional phase of subduction, highly magnetic western zone plutons were passively emplaced into oceanic Jurassic and Triassic metasedimentary rocks of low metamorphic grade. The western transition zone and eastern transition zone plutons were dynamically emplaced into Mesozoic and Paleozoic (?) rocks of amphibolite facies, and the eastern zone plutons were emplaced into Paleozoic (?) metasedimentary rocks. Rocks of the allochthonous upper-plate zone were thrust into position in the Late Cretaceous. Based on their geochemical nature, the upper-plate zone rocks were derived from east of the eastern zone.

The four autochthonous batholith zones were formed over a 35 m.y. period as subduction progressively transitioned from under oceanic lithosphere to under continental lithosphere. From 126 to 108 Ma, pluton emplacement was passive in an extensional phase of subduction, forming the western 47.6 areal percent of the autochthonous batholith at a rate of 2.6% per million years. By 111 Ma, the subducted plate began to underride continental lithosphere. At this time, the mode of pluton emplacement changed radically from passive to dynamic in a compressional tectonic regime. Dynamically emplaced plutons characterize the two transition zones. The western transition zone formed over a

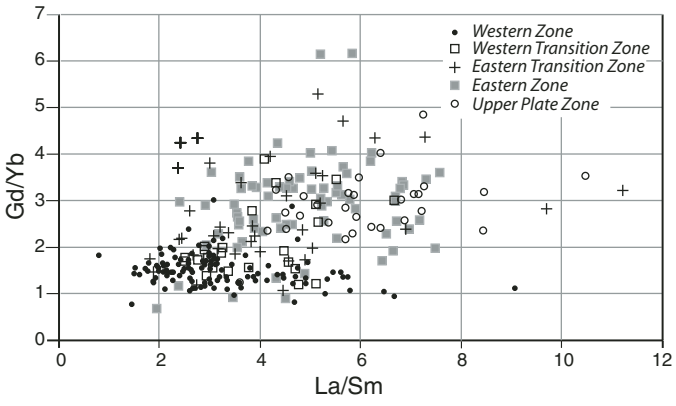

Figure 91. Gd/Yb ratios plotted against La/Sm ratios. The low Gd/Yb ratios, mostly less than 2, for the western zone indicate a relatively shallow source. The higher Gd/Yb ratios in the other zones indicate an increase in source depth.

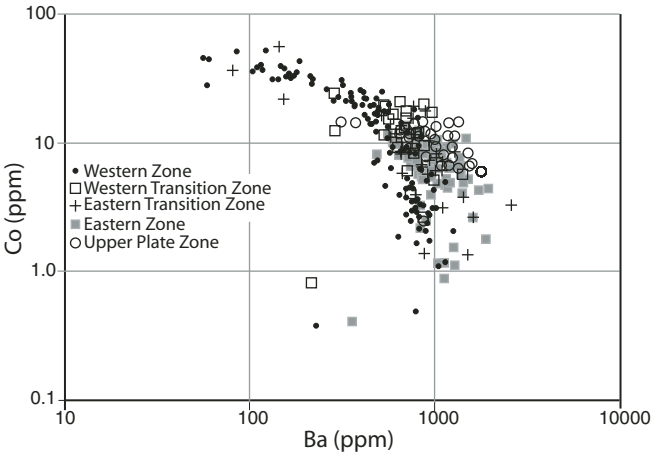

Figure 93. Co plotted against Ba on a log base for the northern Peninsular Ranges batholith rocks. Concave-downward distribution is interpreted to reflect magma mixing. Fractional crystallization would produce a linear array.

period of 11 m.y. and constitutes 13.5% by area of the northern Peninsular Ranges batholith. The western transition zone plutons have geochemical affinities with the western zone plutons. Growth of the northern Peninsular Ranges batholith progressed at a rate of ~1% per million years, with most magma emplacement occurring from 106 to 99 Ma. The 99–93 Ma plutons of the eastern transition zone have geochemical affinities more closely associated with the eastern zone plutons than with the western transition zone plutons. The eastern transition zone plutons form 15% by area of the batholith, with pluton emplacement increasing the size of the northern Peninsular Ranges batholith at a rate of 2.5% per million years. Eastern zone pluton emplacement, 98.5–91 Ma, occurred when the subducted plate was under older continental crust and temporally overlapped plutonism of the eastern transition zone. The eastern zone constitutes 25% by area of the northern Peninsular Ranges batholith, as pluton emplacement increased the northern Peninsular Ranges batholith at a rate of 3.3% per million years. Both the eastern transition zone and eastern zone are dominated by La Posta–type plutons. The combined eastern transition zone and eastern zone formed 40% by area of the batholith in 8 m.y., at a rate of 5% per million years. This rate of magma emplacement from 99 to 91 Ma is similar to the 47% of other parts of the Peninsular Ranges batholith forming in the interval 99–92 Ma calculated by Ortega-Rivera (2003). In the Late Cretaceous, 92–84 Ma granitic rocks were thrust from the east on low-angle faults to form the allochthonous upper-plate zone of the batholith.

Major- and trace-element chemistry shows multiple systematic west-to-east variations across the northern Peninsular Ranges batholith. Compatible elements decrease from west to east, and incompatible elements increase, with some trace elements changing by more than a factor of 2. Geochemical evolution of the northern Peninsular Ranges batholith reflects a shallow and primitive source for the western part of the batholith and a more-evolved, deeper source for the eastern part. Based on geochemistry, the upper-plate zone rocks are distinct from those of the structurally adjacent autochthonous eastern zone.

Three isotopic systems likewise show systematic west-to-east variation. Initial $^{87}Sr/^{86}Sr$ ratios reflect the progressive change in subduction magmatism transitioning from oceanic lithosphere in the west to continental lithosphere in the east. Sr_i is bimodal, with most values between 0.7034 and 0.7040 in the western zone, and slightly higher values of 0.7045–0.7055 in the transition zones. Eastern zone rocks have Sr_i values of 0.7065–0.7080, and the upper-plate zone has Sr_i values of 0.7075–0.7090. Only a very minor part of the batholith has Sr_i >0.7055 and <0.7065, reflecting a relatively abrupt change from pluton emplacement in oceanic lithosphere to emplacement in continental lithosphere. The $^{206}Pb/^{204}Pb$ ratio likewise increases from west to east, with a major step from the transition zones to the eastern zone. The $^{206}Pb/^{204}Pb$ 19.0 isopleth is coincident with the Sr_i 0.7060 isopleth.

Scandium and REE distributions reflect a shallower magma source in the western part of the batholith and a deeper source in the east. Based on the linearity of Harker diagrams and plots of Ba against Co, chemical variation in the batholith is a product of magma mixing. Our data for the northern Peninsular Ranges batholith are best explained by a model involving a single Cretaceous arc that transitioned from Mesozoic oceanic to continental lithosphere. Island arcs and their accretion to continental cratons provide the simplest geochemistry for understanding crust formation (e.g., Leat and Larter, 2003).

ACKNOWLEDGMENTS

The regional geochemistry study would not have been possible if the late Alex Baird had not had the foresight to develop a thorough and systematic regional sampling plan for the northern Peninsular Ranges batholith. The samples would not have been collected except for the sheer tenacity of Ed Welday. The sampling arguably remains the most exhaustive and systematic of any Cordilleran batholith. Many thanks go to U.S. Geological Survey (USGS) analysts Jim Budahn, Fred Lichte, Dave Siems, Jaime Azain, and Dave Detra, for the high quality of chemical analysis. Dave Kimbrough, San Diego State University, Bob Fleck, USGS, and Jade Star Lackey, Pomona College, kindly made available unpublished isotopic data. Thanks also go to Bret Cox, USGS, for the modal analysis of the Box Springs Mountains plutonic complex. Many thanks go to Victoria Todd for numerous conversations regarding the batholith and improving the text of this paper. The paper was greatly improved by thoughtful reviews by Bob Fleck and Jade Star Lackey.

APPENDIX

Batholith Sampling

More than 300 Northern Peninsular Ranges batholith samples were systematically collected by E.E. Welday and A.K. Baird (Baird et al., 1974b, 1979). The resulting sample set is the most systematic geochemical sample set for Cordilleran batholiths assembled to date. The purpose of the sampling was to extract unbiased representative composition of the northern part of the northern Peninsular Ranges batholith that could be used to determine spatial chemical distributions. The sampling method was basically megascale point counting.

A combined large- and small-scale pattern for sampling the northern Peninsular Ranges batholith was developed after a series of sampling studies (Baird et al., 1964, 1967; Morton et al., 1969). Sample localities were spaced ~5 km apart on a grid, and at each locality, eight specimens were collected, two at each of the four corners of a square, 400 ft (120 m) on a side. These eight specimens were separately crushed, and a split was taken from each sample and combined to generate a homogeneous composite sample representative of the sample site. Most sample sites included a single rock type; a few sample sites included multiple rock types. The sampling technique was tested by using a grid offset of half a sample-spacing, and the results were similar. One additional "typical" sample per locality was sectioned and used to determine rock classification (Baird et al., 1979). This determination was based on an older classification system (Bateman et al., 1963).

Note that Ni trace-element concentrations were measured but not tabulated in this paper because of contamination with hardened steel when the samples were plate-pulverized in a ball mill.

Rare Earth Elements: Chondrite Normalization Values for Rare Earth Elements

Rare earth elements were normalized using the following chondrite values.

La = 0.311	Tb = 0.047
Ce = 0.813	Dy = 0.323
Pr = 0.123	Ho = 0.0722
Nd = 0.603	Er = 0.211
Sm = 0.196	Tm = 0.0326
Eu = 0.074	Yb = 0.21
Gd = 0.26	Lu = 0.0323

CIPW Norm Calculations

To plot the granitoid samples on the IUGS (International Union of Geological Sciences) quartz-feldspar (QAP) system, it was necessary to perform CIPW norm calculations on the major-oxide data. Because the oxide data include only Fe_2O_3 total, whereas the norm calculations require both Fe_2O_3 and FeO, the Fe_2O_3/FeO ratios had to be estimated. From Larsen's (1948) data for the eastern Peninsular Ranges batholith, a ratio of 0.3 can be estimated for the gabbros, 0.4 for the tonalites, and 0.5 for the granodiorites. Using the total alkali–silica diagram for volcanic rocks, Middlemost (1989) suggested a ratio of 0.2 for basalt, 0.35 for andesite, 0.4 for dacite, and 0.5 for rhyolite. These two estimates were combined, and the unrealistic discontinuity in ratio at field boundaries was removed by using the following equation to estimate the iron-oxide ratio: $Fe_2O_3/FeO = 0.011 \times SiO_2 - 0.31$. The sum of the albite and anorthite norms was used for the plagioclase composition.

The resulting norms are plotted on the QAP diagram in Figure 87. The gabbro samples fall in the gabbro and quartz diorite fields; the tonalite samples fall in the granodiorite, quartz monzodiorite, quartz diorite, and tonalite fields; and the granodiorite samples fall in the granodiorite and granite fields. This paper uses the generic terms gabbro, tonalite, and granodiorite for the three groups, although the samples do not fit exactly into the corresponding fields in the QAP diagram.

The classification used for these granitoids by Baird et al. (1979) was based on an older QAP system (Bateman et al., 1963). They classified the granitoids as: gabbro, quartz diorite (equivalent to tonalite), and granodiorite plus quartz monzonite (similar to the IUGS granite).

REFERENCES CITED

Ague, J.J., and Brimhall, G.H., 1988, Magmatic arc asymmetry and distribution of anomalous belts in the batholiths of California: Effects of assimilation, crustal thickness, and depth of crystallization: Geological Society of America Bulletin, v. 100, p. 912–927, doi:10.1130/0016-7606(1988)100<0912:MAAADO>2.3.CO;2.

Anderson, C.L., 1991, Zircon Uranium-Lead Isotopic Ages of the Santiago Peak Volcanics and Spatially Related Plutons of the Peninsular Ranges Batholith, Southern California [M.S. thesis]: San Diego, California, San Diego State University, 111 p.

Baird, A.K., and Miesch, A.T., 1984, Batholithic Rocks of Southern California—A Model for the Petrochemical Nature of Their Source Materials: U.S. Geological Survey Professional Paper 1284, 42 p.

Baird, A.K., McIntyre, D.B., Welday, E.E., and Morton, D.M., 1967, A test of chemical variability and field sampling methods, Lakeview Mountain Tonalite, Lakeview Mountains, southern California batholith: California Division of Mines and Geology Special Report 92, p. 11–19.

Baird, A.K., Baird, K.W., and Welday, E.E., 1974, Chemical trends across Cretaceous batholithic rocks of southern California: Geology, v. 2, p. 493–496, doi:10.1130/0091-7613(1974)2<493:CTACBR>2.0.CO;2.

Baird, A.K., Baird, K.W., and Welday, E.E., 1979, Batholithic rocks of the northern Peninsular Ranges, southern California, *in* Abbott, P.L., and Todd, V.R., eds., Mesozoic Crystalline Rocks: San Diego, California, California State University, Department of Geological Sciences, p. 111–132.

Bateman, P.C., 1992, Plutonism in the Central Part of the Sierra Nevada Batholith, California: U.S. Geological Survey Professional Paper 1483, 186 p.

Bateman, P.C., Clark, L.D., Huber, N.K., Moore, J.G., and Rinehart, C.D., 1963, The Sierra Nevada Batholith—A Synthesis of Recent Work across the Central Part: U.S. Geological Survey Professional Paper 414-D, p. D1–D46.

Berger, B.R., 2014, this volume, Petrology and chemistry of the Green Acres gabbro complex near Winchester, Riverside County, California, *in* Morton, D.M., and Miller, F.K., eds., Peninsular Ranges Batholith, Baja California and Southern California: Geological Society of America Memoir 211, doi:10.1130/2014.1211(10).

Brown, A.R., 1968, Geology of a Portion of the Southeastern San Jacinto Mountains, Riverside County, California [M.S. thesis]: Riverside, California, University of California, 95 p.

Burnham, C.W., 1959, Contact metamorphism of magnesian limestones at Crestmore, California: Geological Society of America Bulletin, v. 70, p. 879–920, doi:10.1130/0016-7606(1959)70[879:CMOMLA]2.0.CO;2.

Busby, C., 2004, Continental growth at convergent margins facing large ocean basins: A case study from Mesozoic convergent-margin basins of Baja California, Mexico: Tectonophysics, v. 392, p. 241–277, doi:10.1016/j.tecto.2004.04.017.

Carroll, M.R., and Wyllie, P.J., 1990, The system tonalite-H_2O at 15 kbar and the genesis of calc-alkaline magmas: The American Mineralogist, v. 75, p. 345–357.

Cecil, J.D., 1990, A Study of the Palm Canyon Complex and Related Rocks, Riverside County, California [Senior thesis]: Berkeley, California, University of California–Berkeley.

Clausen, B.L., Morton, D.M., Kistler, R.W., and Lee, C.-T.A., 2014, this volume, Low initial-Sr felsic plutons of the northwestern Peninsular Ranges batholith, southern California, and the role of mafic-felsic magma mixing in continental crust formation, *in* Morton, D.M., and Miller, F.K., eds., Peninsular Ranges Batholith, Baja California and Southern California: Geological Society of America Memoir 211, doi:10.1130/2014.1211(08).

Cocherie, A., 1986, Systematic use of trace element distribution patterns in log-log diagrams for plutonic suites: Geochimica et Cosmochimica Acta, v. 50, p. 2517–2522, doi:10.1016/0016-7037(86)90034-7.

Criscione, J.J., Davis, T.E., and Ehlig, P., 1978, The age of sedimentation/diagenesis for the Bedford Canyon Formation and the Santa Monica Formation in southern California: A Rb/Sr evaluation, *in* Howell, D.G., and McDougall, K.A., eds., Mesozoic Paleogeography of the Western United States: Sacramento, California, Pacific Section, Society of Economic Paleontologists and Mineralogists, Pacific Coast Paleogeography Symposium 2, p. 385.

DePaolo, D.J., 1981, A neodymium and strontium isotopic study of the Mesozoic calc-alkaline granitic batholiths of the Sierra Nevada and Peninsular Ranges, California: Journal of Geophysical Research, v. 86, no. B11, p. 10,470–10,488.

Dockum, M.S., 1982, Greenschist-Facies Carbonates, Eastern Coyote Mountains, Western Imperial County, California [M.S. thesis]: San Diego, California, San Diego State University, 89 p.

Dockum, M.S., and Miller, R.H., 1982, Ordovician conodonts from the greenschist facies carbonates, western Imperial County, California: Geological Society of America Abstracts with Programs, v. 14, p. 160.

Dokka, R.K., 1984, Fission-track geochronological evidence for Late Cretaceous mylonitization and early Paleocene uplift of the northeastern Peninsular Ranges, California: Geophysical Research Letters, v. 11, p. 46–49, doi:10.1029/GL011i001p00046.

Dudley, P.H., 1935, Geology of a portion of the Perris block, southern California: California Journal Mines and Geology, v. 31, p. 487–506.

Early, T.O., and Silver, L.T., 1973, Rb-Sr isotopic systematics in the Peninsular Ranges batholith of southern and Baja California: Eos (Transactions, American Geophysical Union), v. 54, p. 494.

Eichelberger, J.C., 1978, Andesitic volcanism and crustal evolution: Nature, v. 275, p. 21–27, doi:10.1038/275021a0.

Engel, R., 1959, Geology of the Lake Elsinore Quadrangle, California: California Division Mines Bulletin 146, p. 1–59.

Erskine, B.G., 1982, A Paleomagnetic, Rock Magnetic, and Magnetic Mineralogic Investigation of the Northern Peninsular Range Batholith, Southern California [M.S. thesis]: San Diego, California, California State University, 146 p.

Erskine, B.G., 1986a, Mylonitic Deformation and Associated Low-Angle Faulting in the Santa Rosa Mylonite Zone, Southern California [Ph.D. thesis]: Berkeley, California, University of California–Berkeley, 247 p.

Erskine, B.G., 1986b, Syntectic granitic intrusion and mylonitic deformation along the eastern margin of the northern Peninsular Ranges batholith, southern California: Geological Society of America Abstracts with Programs, v. 18, p. 105.

Erskine, B.G., and Wenk, H.-R., 1985, Evidence for Late Cretaceous crustal thinning in the Santa Rosa mylonite zone, southern California: Geology, v. 13, p. 274–277, doi:10.1130/0091-7613(1985)13<274:EFLCCT>2.0.CO;2.

Fife, D.L., Minch, J.A., and Crampton, P.J., 1967, Late Jurassic age of the Santiago Peak volcanics, California: Geological Society of America Bulletin, v. 78, p. 299–304, doi:10.1130/0016-7606(1967)78[299:LJAOTS]2.0.CO;2.

Foord, E.E., London, D., Kampf, A.R., Shigley, and Snee, L.W., 1991, Gem-bearing pegmatites of San Diego County, California, *in* Walawender, M.J., and Hanan, B.B., eds., Geological Excursions in Southern California and Mexico: San Diego, California, San Diego State University, Department of Geological Sciences, p. 128–146.

Gastil, R.G., and Miller, R.H., 1981, Lower Paleozoic strata on the Pacific plate of North America: Nature, v. 292, p. 828–830, doi:10.1038/292828a0.

Gastil, R.G., Diamond, J., Knaack, C., Walawender, M., Marshall, M., Boyles, C., Chadwick, B., and Erskine, B., 1990, The problem of the magnetite-ilmenite boundary in southern and Baja California, *in* Anderson, J.L., ed., The Nature and Origin of Cordilleran Magmatism: Geological Society of America Memoir 174, p. 19–32.

Gill, J.B., 1981, Orogenic Andesites and Plate Tectonics: Berlin, Springer-Verlag, Minerals and Rocks, v. 16, 390 p.

Girty, G.H., Thomson, C.N., Girty, M.S., Miller, J., and Bracchi, K., 1993, The Cuyamaca–Laguna Mountains shear zone, Late Jurassic plutonic rocks and Early Cretaceous extension, Peninsular Ranges, southern California, *in* Abbott, P.L., Sangines, E.M., and Rendina, M.A., eds., Geological Investigations in Baja California, Mexico: Annual Field Trip Guidebook 21: Santa Ana, California, South Coast Geological Society, p. 173–180.

Goodwin, L.B., and Renne, P.R., 1991, Effects of progressive mylonitization on Ar retention in biotites from the Santa Rosa mylonite zone, California, and thermochronologic implications: Contributions to Mineralogy and Petrology, v. 108, p. 283–297, doi:10.1007/BF00285937.

Goodwin, L.B., and Wenk, H.-R., 1995, Development of phyllonite from granodiorite: Mechanisms of grain-size reduction in the Santa Rosa mylonite zone, California: Journal of Structural Geology, v. 17, p. 689–707, doi:10.1016/0191-8141(94)00093-F.

Gray, C.H., Jr., 1961, Geology of the Corona South Quadrangle and the Santa Ana Narrows Area, Riverside, Orange, and San Bernardino Counties, California: California Division of Mines Bulletin 178, 120 p.

Gromet, L.P., and Sliver, L.T., 1983, Rare earth element distributions among minerals in a granodiorite and their petrogenetic implications: Geochimica et Cosmochimica Acta, v. 47, p. 925–939.

Gromet, L.P., and Silver, L.T., 1987, REE variations across the Peninsular Ranges batholith: Implications for batholithic petrogenesis and crustal growth in magmatic arcs: Journal of Petrology, v. 28, p. 75–125, doi:10.1093/petrology/28.1.75.

Hammarstrom, J.M., 1992, Mineral chemistry of Cretaceous plutons: Hornblende geobarometry in southern California and southeastern Alaska: Geological Society of America Abstracts with Programs, v. 24, no. 5, p. 30.

Hanley, J.B., 1951, Economic Geology of the Rincon Pegmatites, San Diego County, California: California Division of Mines Special Report 7-B, 24 p.

Hanna, M.A., 1926, Geology of the La Jolla quadrangle, California: University of California, Department of Geological Sciences Bulletin, v. 16, p. 187–246.

Herzig, C.T., 1991, Petrogenetic and Tectonic Development of the Santiago Peak Volcanics, Northern Santa Ana Mountains, California [Ph.D. thesis]: Riverside, California, University of California, 376 p.

Herzig, C.T., and Kimbrough, D.L., 2014, this volume, Santiago Peak Volcanics: Early Cretaceous arc volcanism of the western Peninsular Ranges batholith, southern California, *in* Morton, D.M., and Miller, F.K., eds., Peninsular Ranges Batholith, Baja California and Southern California: Geological Society of America Memoir 211, doi:10.1130/2014.1211(09).

Hill, R.I., 1984, Petrology and Petrogenesis of Batholithic Rocks, San Jacinto Mountains, Southern California [Ph.D. thesis]: Pasadena, California Institute of Technology, 660 p.

Hill, R.I., 1988a, San Jacinto Intrusive Complex: 1. Geology and mineral chemistry, and a model for intermittent recharge of tonalitic magma chambers: Journal of Geophysical Research, v. 93, no. B9, p. 10,325–10,348, doi:10.1029/JB093iB09p10325.

Hill, R.I., 1988b, San Jacinto Intrusive Complex: 2. Geochemistry: Journal of Geophysical Research, v. 93, no. B9, p. 10,349–10,372, doi:10.1029/JB093iB09p10349.

Hurlbut, C.S., Jr., 1935, Dark inclusions in a tonalite of southern California: The American Mineralogist, v. 20, p. 609–630.

Imlay, R.W., 1963, Jurassic fossils from southern California: Journal of Paleontology, v. 37, p. 97–107.

Imlay, R.W., 1964, Middle and Upper Jurassic fossils from southern California: Journal of Paleontology, v. 38, p. 505–509.

Imlay, R.W., 1980, Jurassic Paleobiogeography of the Conterminous United States in Its Continental Setting: U.S. Geological Survey Professional Paper 1062, 134 p.

Jahns, R.H., 1954, Geology of the Peninsular Ranges Province, southern California and Baja California, *in* Jahns, R.H., ed., Geology of Southern California: California Division Mines Bulletin 170, chapter 2, p. 29–52.

Jahns, R.H., 1955, The study of pegmatites, *in* Bateman, A.M., ed., Economic Geology: Fiftieth Anniversary Volume: Lancaster, Pennsylvania, Society of Economic Geologists, p. 1026–1130.

Jahns, R.H., 1979, Gem bearing pegmatites in San Diego County, California: The Stewart Mine, Pala district, and the Himalaya Mine, Mesa Grande district, *in* Abbott, P.L., and Todd, V.R., eds., Mesozoic Crystalline Rocks: San Diego, California, San Diego State University, Department of Geological Sciences, p. 3–38.

Jahns, R.H., and Wright, L.A., 1951, Gem- and Lithium-Bearing Pegmatites of the Pala District, San Diego County, California: California Division of Mines Special Report 7-A, 72 p.

Jenney, W.W., Jr., 1968, The Structure of a Portion of the Southern California Batholith, Western Riverside County, California [Ph.D. thesis]: Tucson, Arizona, University of Arizona, 137 p.

Johnson, S.E., Tate, M.C., and Fanning, C.M., 1999, New geologic mapping and SHRIMP U-Pb zircon data in the Peninsular Ranges batholith, Baja California, Mexico: Evidence for a suture?: Geology, v. 27, p. 743–746, doi:10.1130/0091-7613(1999)027<0743:NGMASU>2.3.CO;2.

Johnson, S.E., Paterson, S.R., Fletcher, J.M., Girty, G.H., Kimbrough, D.L., and Martín-Barajas, A., 2003, eds., Tectonic Evolution of Northwestern Mexico and the Southwestern USA: Geological Society of America Special Paper 374, 478 p.

Joshi, M.S., 1967, The Genesis of the Granitic and Associated Rocks of the Box Springs Mountains, Riverside, California [Ph.D. thesis]: Riverside, California, University California, 169 p.

Kimbrough, D.L., Smith, D.P., Mahoney, J.B., Moore, T.E., Grove, M., Gastil, R.G., Ortega-Rivera, A., and Fanning, C.M., 2001, Forearc-basin sedimentary response to rapid Late Cretaceous batholith emplacement in the Peninsular Ranges of southern and Baja California: Geology, v. 29, p. 491–494, doi:10.1130/0091-7613(2001)029<0491:FBSRTR>2.0.CO;2.

Kimbrough, D.L., Abbott, P.L., Balch, D.C., Bartling, S.H., Grove, M., Mahoney, J.B., and Donohue, R.F., 2014, this volume, Upper Jurassic Peñasquitos Formation–forearc basin western wallrock of the Peninsular Ranges batholith, *in* Morton, D.M., and Miller, F.K., eds., Peninsular Ranges Batholith, Baja California and Southern California: Geological Society of America Memoir 211, doi:10.1130/2014.1211(19).

Kistler, R.W., and Morton, D.M., 1994, Sr, Rb, Sr_i variation and whole-rock Rb-Sr ages of plutons in the northern Peninsular Ranges batholith, southern California: Geological Society of America Abstracts with Programs, v. 26, no. 2, p. 82.

Kistler, R.W., Peterman, Z.E., Ross, D.C., and Gottfried, D., 1973, Strontium isotopes and the San Andreas fault, *in* Kovach, R.L., and Nur, A., eds., Proceedings of the Conference on the Tectonic Problems of the San Andreas Fault System: Stanford University Publications in Geological Sciences, v. 13, p. 339–347.

Kistler, R.W., Wooden, J.L., and Morton, D.M., 2003, Isotopes and Ages in the Northern Peninsular Ranges Batholith, Southern California: U.S. Geological Survey Open-File Report 03-489, 45 p.

Kistler, R.W., Wooden, J.L., Premo, W.R., and Morton, D.M., 2014, this volume, Pb-Sr-Nd-O isotopic characterization of Mesozoic rocks throughout the northern end of the Peninsular Ranges batholith: Isotopic evidence for the magmatic evolution of oceanic arc–continental margin accretion during the Late Cretaceous of southern California, *in* Morton, D.M., and Miller, F.K., eds., Peninsular Ranges Batholith, Baja California

and Southern California: Geological Society of America Memoir 211, doi:10.1130/2014.1211(07).

Krummenacher, D., Gastil, R.G., Bushee, J., and Doupont, J., 1975, K-Ar apparent ages, Peninsular Ranges batholith, southern California: Geological Society of America Bulletin, v. 86, p. 760–768, doi:10.1130/0016-7606(1975)86<760:KAAPRB>2.0.CO;2.

Lackey, J.S., Valley, J.W., Chen, J.H., and Stockli, D.F., 2008, Evolving magma systems, crustal recycling, and alteration in the central Sierra Nevada batholith: The oxygen isotope record: Journal of Petrology, v. 49, p. 1397–1426, doi:10.1093/petrology/egn030.

Lackey, J.S., Cecil, M.R., Windham, C.J., Frazer, R.E., Bindeman, I.N., and Gehrels, G., 2012, The Fine Gold intrusive suite: The roles of basement terranes and magma source development in the Early Cretaceous Sierra Nevada batholith: Geosphere, v. 8, p. 292–313, doi:10.1130/GES00745.1.

Lameyre, J., and Bonin, B., 1991, Granites in the main plutonic series, *in* Didier, J., and Barbarin, B., eds., Enclaves and Granite Petrology: Developments in Petrology 13: Amsterdam, Elsevier, p. 3–17.

Langenheim, V.E., Jachens, R.C., Morton, D.M., Kistler, R.W., and Matti, J.C., 2004, Geophysical and isotopic mapping of preexisting crustal structures that influenced the location and development of the San Jacinto fault zone, southern California: Geological Society of America Bulletin, v. 116, p. 1143–1157, doi:10.1130/B25277.1.

Langenheim, V.E., Jachens, R.C., and Aiken, C., 2014, this volume, Geophysical framework of the Peninsular Ranges batholith—Implications for tectonic evolution and neotectonics, *in* Morton, D.M., and Miller, F.K., eds., Peninsular Ranges Batholith, Baja California and Southern California: Geological Society of America Memoir 211, doi:10.1130/2014.1211(01).

Larsen, E.S., 1948, Batholith and Associated Rocks of Corona, Elsinore, and San Luis Rey Quadrangles, Southern California: Geological Society of America Memoir 29, 182 p.

Leat, P.T., and Larter, R.D., 2003, Intra-oceanic subduction systems: Introduction, *in* Larter, R.D., and Leat, P.T., eds., Intra-Oceanic Subduction Systems: Tectonic and Magmatic Processes: Geological Society of London Special Publication 219, p. 1–17.

Lee, C-T.A., Morton, D.M., Kistler, R.W., and Baird, A.K., 2007, Petrology and tectonics of Phanerozoic continental formation: From island arcs to accretion and continental arc magmatism: Earth and Planetary Science Letters, v. 263, p. 370–387.

Mason, D.M., and Cohen, L.H., 1990, Field, mineralogical, and mesotextural relationships between mafic dykes, mafic enclaves, and host granitoids in the Bernasconi pluton, Peninsular Ranges batholith, southern California, USA, *in* Parker, A.J., Rickwood, P.C., and Tucker, D.H., eds., Mafic Dykes and Emplacement Mechanisms: Second International Dyke Conference: Rotterdam, Netherlands, A.A. Balkema, p. 461–473.

Meijer, A., 1976, Pb and Sr isotopic data bearing on the origin of volcanic rocks from the Mariana island arc system: Geological Society of America Bulletin, v. 87, p. 1358–1169, doi:10.1130/0016-7606(1976)87<1358:PASIDB>2.0.CO;2.

Menzie, T.E., 1962, The Geology of the Box Springs Mountains, Riverside County, California [M.S. thesis]: Palo Alto, California, Stanford University, 50 p.

Merriam, R.H., 1946, Igneous and metamorphic rocks of the southwestern part of the Ramona quadrangle, San Diego County, California: Geological Society of America Bulletin, v. 57, p. 223–260, doi:10.1130/0016-7606(1946)57[223:IAMROT]2.0.CO;2.

Middlemost, E.A.K., 1989, Iron oxidation ratios, norms, and the classification of volcanic rocks: Chemical Geology, v. 77, p. 19–26.

Miesch, A.T., and Morton, D.M., 1977, Chemical variability in the Lakeview Mountains pluton, southern California batholith—A comparison of the methods of correspondence analysis and extended Q-mode factor analysis: U.S. Geological Survey Journal of Research, v. 5, no. 1, p. 103–116.

Miggins, D.P., Premo, W.R., Snee, L.W., Yeoman, R., Naeser, N.D., Naeser, C.W., and Morton, D.M., 2014, this volume, Thermochronology of Cretaceous batholithic rocks in the northern Peninsular Ranges batholith, southern California: Implications for the Late Cretaceous tectonic evolution of southern California, *in* Morton, D.M., and Miller, F.K., eds., Peninsular Ranges Batholith, Baja California and Southern California: Geological Society of America Memoir 211, doi:10.1130/2014.1211(06).

Miller, F.K., and Morton, D.M., 1980, Potassium-Argon Geochronology of the Eastern Transverse Ranges and Southern Mojave Desert, Southern California: U.S. Geological Survey Professional Paper 1152, 30 p.

Miller, F.K., Morton, D.M., and Premo, W.R., 2014, this volume, Potassium-argon cooling ages in the northern part of the Peninsular Ranges batholith and offsets on the Elsinore and San Jacinto fault zones, *in* Morton, D.M., and Miller, F.K., eds., Peninsular Ranges Batholith, Baja California and Southern California: Geological Society of America Memoir 211, doi:10.1130/2014.1211(05).

Miller, R.H., and Dockum, M.S., 1983, Ordovician conodonts from metamorphosed carbonates of the Salton Trough, California: Geology, v. 11, p. 410–412, doi:10.1130/0091-7613(1983)11<410:OCFMCO>2.0.CO;2.

Miller, W.J., 1946, Crystalline rocks of southern California: Geological Society of America Bulletin, v. 57, p. 457–542, doi:10.1130/0016-7606(1946)57[457:CROSC]2.0.CO;2.

Morton, D.M., 1969, The Lakeview Mountains pluton, southern California batholith: Part I. Petrology and structure: Geological Society of America Bulletin, v. 80, p. 1539–1552, doi:10.1130/0016-7606(1969)80[1539:TLMPSC]2.0.CO;2.

Morton, D.M., 1978, Geologic Map of the San Bernardino South Quadrangle, San Bernardino and Riverside Counties, California: U.S. Geological Survey Open-File Report 78-20, scale 1:24,000.

Morton, D.M., 2001, Preliminary Geologic Map of the Steele Peak 7.5′ Quadrangle, Riverside County, California: U.S. Geological Survey Open-File Report 01-449, scale 1:24,000.

Morton, D.M., 2003a, Preliminary Geologic Map of the Fontana 7.5′ Quadrangle, Riverside and San Bernardino Counties, California: U.S. Geological Survey Open-File Report 03-418, scale 1:24,000.

Morton, D.M., 2003b, Preliminary Geologic Map of the Romoland 7.5′ Quadrangle, Riverside County, California: U.S. Geological Survey Open-File Report 03-102, scale 1:24,000.

Morton, D.M., 2003c, Preliminary Geologic Map of the Winchester 7.5′ Quadrangle, Riverside County, California: U.S. Geological Survey Open-File Report 03-188, scale 1:24,000.

Morton, D.M., 2003d, Preliminary Geologic Map of the Perris 7.5′ Quadrangle, Riverside County, California: U.S. Geological Survey Open-File Report 03-270, scale 1:24,000.

Morton, D.M., and Baird, A.K., 1976, Petrology of the Paloma Valley ring complex, southern California batholith: U.S. Geological Survey Journal of Research, v. 4, no. 1, p. 83–89.

Morton, D.M., and Cox, B.F., 2001a, Preliminary Geologic Map of the Riverside East 7.5′ Quadrangle, Riverside County, California: U.S. Geological Survey Open-File Report 01-452, scale 1:24,000.

Morton, D.M., and Cox, B.F., 2001b, Preliminary Geologic Map of the Riverside West 7.5′ Quadrangle, Riverside County, California: U.S. Geological Survey Open-File Report 01-451, scale 1:24,000.

Morton, D.M., and Kennedy, M.P., 2005, Geologic Map of the Sage 7.5′ Quadrangle, Riverside County, California: U.S. Geological Survey Open-File Report 2005-1285, scale 1:24,000.

Morton, D.M., and Kistler, R.W., 1997, Sr_i variation in the Peninsular Ranges batholith: Geological Society of America Abstracts with Programs, v. 29, no. 6, p. A-69.

Morton, D.M., and Matti, J.C., 1993, Extension and contraction within an evolving divergent strike-slip fault complex: The San Andreas and San Jacinto fault zones at their convergence in southern California, *in* Powell, R.E., Weldon, R.J., II, and Matti, J.C., eds., The San Andreas Fault System: Displacement, Palinspastic Reconstruction, and Geologic Evolution: Geological Society of America Memoir 178, p. 217–230.

Morton, D.M., and Matti, J.C., 2001a, Geologic Map of the Lakeview 7.5′ Quadrangle, Riverside County, California: U.S. Geological Survey Open-File Report 2001-2174, scale 1:24,000.

Morton, D.M., and Matti, J.C., 2001b, Geologic Map of the Sunnymead 7.5′ Quadrangle, Riverside County, California: U.S. Geological Survey Open-File Report 01-450, scale 1:24,000, http://geopubs.wr.usgs.gov/open-file/of01-450.

Morton, D.M., and Matti, J.C., 2008, Preliminary Geologic Map of the Hemet 7.5′ Quadrangle, Riverside County, California: U.S. Geological Survey Open-File Report 2004-1415, scale 1:100,000.

Morton, D.M., and Miller, F.K., 2006, Geologic Map of the San Bernardino and Santa Ana 30′ × 60′ Quadrangles, California: U.S. Geological Survey Open-File Report 2006-1217, scale 1:24,000.

Morton, D.M., and Weber, F.H., Jr., 2001, Geologic Map of the Lake Mathews 7.5′ Quadrangle, Riverside County, California: U.S. Geological Survey Open-File Report 2001-2479, scale 1:24,000.

Morton, D.M., and Weber, F.H., Jr., 2003, Geologic Map of the Elsinore 7.5′ Quadrangle, Riverside County, California: U.S. Geological Survey Open-File Report 03-281.

Morton, D.M., Baird, A.K., and Baird, K.W., 1969, The Lakeview Mountains pluton, southern California batholith: Part II. Chemical composition and

variation: Geological Society of America Bulletin, v. 80, p. 1553–1564, doi:10.1130/0016-7606(1969)80[1553:TLMPSC]2.0.CO;2.

Morton, D.M., Miller, F.K., Kistler, R.W., Premo, W.R., Lee, C-T.A., Langenheim, V.E., Wooden, J.L., Snee, L.W., Clausen, B.L., Cossette, P., 2014, this volume, Framework and petrogenesis of the northern Peninsular Ranges batholith, southern California, *in* Morton, D.M., and Miller, F.K., eds., Peninsular Ranges Batholith, Baja California and Southern California: Geological Society of America Memoir 211, doi:10.1130/2014.1211(03).

Moyen, J.-F., and Stevens, G., 2006, Experimental constraints on TTG petrogenesis: Implications for Archean geodynamics, *in* Benn, K., Mareschal, J.-C., and Condie, K.C., eds., Archean Geodynamics and Environments: American Geophysical Union Geophysical Monograph 164, p. 149–175, doi:10.1029/164GM11.

Murdoch, J., and Webb, R.W., 1942, Notes on some minerals from southern California: The American Mineralogist, v. 27, p. 323–330.

Ortega-Rivera, A., 2003, Geochronological constraints on the tectonic history of the Peninsular Ranges batholith of Alta and Baja California: Tectonic implications for western Mexico, *in* Johnson, S.E., Paterson, S.R., Fletcher, J.M., Girty, G.H., Kimbrough, D.L., and Martín-Barajas, A., eds., Tectonic Evolution of Northwestern Mexico and the Southwestern USA: Geological Society of America Memoir 374, p. 297–335.

Osborn, E.F., 1939, Structural petrology of the Val Verde Tonalite, southern California: Geological Society of America Bulletin, v. 50, p. 921–950.

Pearce, J.A., Harris, N.B.W., and Tindle, A.G., 1984, Trace element discrimination diagrams for the tectonic interpretation of granitic rocks: Journal of Petrology, v. 25, p. 956–983, doi:10.1093/petrology/25.4.956.

Premo, W.R., and Morton, D.M., 2014, this volume, SHRIMP-RG U-Pb ages of provenance and metamorphism from detrital zircon populations and Pb-Sr-Nd signatures of prebatholithic metasedimentary rocks at Searl Ridge, northern Peninsular Ranges batholith, southern California: Implications for their age, origin, and tectonic setting, *in* Morton, D.M., and Miller, F.K., eds., Peninsular Ranges Batholith, Baja California and Southern California: Geological Society of America Memoir 211, doi:10.1130/2014.1211(14).

Premo, W.R., Morton, D.M., Snee, L.W., Naeser, N.D., and Fanning, C.M., 1998, Isotopic Ages, Cooling Histories, and Magmatic Origins for Mesozoic Tonalitic Plutons from the Northern Peninsular Ranges Batholith, Southern California: U.S. Geological Survey Open-File Report 98-0209, 13 p.

Premo, W.R., Morton, D.M., Snee, L.W., and Bern, A.M., 2002, SHRIMP U-Pb ages of provenance from detrital zircons populations of intra-batholithic metasedimentary rocks, n. Peninsular Ranges batholith, southern California: Implications for their tectonic setting: Geological Society of America Abstracts with Programs, v. 34, no. 6, p. 124.

Premo, W.R., Morton, D.M., and Kistler, R.W., 2014, this volume, Chapter 2, Age and isotopic systematics of Cretaceous borehole and surface samples from the greater Los Angeles Basin region: Implications for the types of crust that might underlie Los Angeles and their distribution along late Cenozoic fault systems, *in* Morton, D.M., and Miller, F.K., eds., Peninsular Ranges Batholith, Baja California and Southern California: Geological Society of America Memoir 211, doi:10.1130/2014.1211(02).

Premo, W.R., Morton, D.M., Wooden, J.L., and Fanning, C.M., 2014, this volume, Chapter 4, U-Pb zircon geochronology of plutonism in the northern Peninsular Ranges batholith, southern California: Implications for the Late Cretaceous tectonic evolution of southern California, *in* Morton, D.M., and Miller, F.K., eds., Peninsular Ranges Batholith, Baja California and Southern California: Geological Society of America Memoir 211, doi:10.1130/2014.1211(04).

Rogers, T.H., 1965, Santa Ana Sheet of the Geologic Map of California: San Francisco, California Division Mines and Geology Geologic Map of California, scale 1:250,000.

Sampson, R.J., 1935, Mineral resources of a portion of the Perris block, Riverside County, California: California Journal of Mines and Geology, v. 31, p. 507–521.

Sandy, R.R., and Campbell, K.A., 2003, *Anarhynchia* (Jurassic brachiopoda) in a possible seep deposit from Bedford Canyon, California, USA: Geological Society of America Abstracts with Program, v. 35, no. 6, p. 381.

Schoellhamer, J.E., Vedder, J.G., Yerkes, R.F., and, Kinney, D.M., 1981, Geology of the Northern Santa Ana Mountains, California: U.S. Geological Survey Professional Paper 420-D, 109 p.

Schwarcz, H.P., 1960, I. Geology of the Winchester-Hemet area, Riverside County, California, II. Geochemical Investigations of an Arkosic Quartzite of the Winchester-Hemet Area, California [Ph.D. thesis]: Pasadena, California, California Institute of Technology, 427 p.

Schwarcz, H.P., 1969, Pre-Cretaceous Sedimentation and Metamorphism in the Winchester Area, Northern Peninsular Ranges, California: Geological Society of America Special Paper 100, 63 p.

Sharp, R.V., 1967, San Jacinto fault zone in the Peninsular Ranges of southern California: Geological Society of America Bulletin, v. 78, p. 705–729, doi:10.1130/0016-7606(1967)78[705:SJFZIT]2.0.CO;2.

Sharp, R.V., 1979, Some characteristics of the Eastern Peninsular Ranges mylonite zone, *in* Speed, R., and Sharp, R., co-organizers, Proceedings of Conference VIII—Analysis of Actual Fault Zones in Bedrock: U.S. Geological Survey Open-File Report 79-1239, p. 258–267.

Shaw, S.E., Todd, V.R., and Grove, M., 2003, Jurassic peraluminous gneissic granitics in the axial zone of the Peninsular Ranges, southern California, *in* Johnson, S.E., Paterson, S.R., Fletcher, J.M., Girty, G.H., Kimbrough, D.L., and Martín-Barajas, A., eds., Tectonic Evolution of Northwestern Mexico and the Southwestern USA: Geological Society of America Special Paper 374, p. 157–183.

Silberling, N.J., Schoellhamer, J.E., Gray, C.H., and Imlay, R.W., 1961, Upper Jurassic fossils from Bedford Canyon Formation, southern California: American Association of Petroleum Geologists Bulletin, v. 45, p. 1746–1748.

Silver, L.T., 1979, Peninsular Ranges batholith: A case study in continental margin magmatic arc setting, characteristics and evolution: Geological Society of America Abstracts with Programs, v. 11, no. 2, p. 517.

Silver, L.T., 1987, Lead isotopes and the petrogenesis of Cordilleran batholiths: Geological Society of America Program with Abstracts, v. 19, no. 7, p. 845.

Silver, L.T., and Chappell, B.W., 1988, The Peninsular Ranges batholith: An insight into the evolution of the Cordilleran batholiths of southwestern North America: Transactions of the Royal Society of Edinburgh–Earth Sciences, v. 79, p. 105–121, doi:10.1017/S0263593300014152.

Silver, L.T., Taylor, H.P., Jr., and Chappell, B., 1979, Some petrological, geochemical and geochronological observations of the Peninsular Ranges batholith near the international border of the U.S.A. and Mexico, *in* Abbott, P.L., and Todd, V.R., eds., Mesozoic Crystalline Rocks: San Diego, California, California State University, Department of Geological Sciences, p. 83–110.

Simpson, C., 1984, Borrego Springs–Santa Rosa mylonite zone: A Late Cretaceous west-directed thrust in southern California: Geology, v. 12, p. 8–11, doi:10.1130/0091-7613(1984)12<8:BSRMZA>2.0.CO;2.

Sims, S.J., 1960, Geology of Part of the Santa Rosa Mountains, Riverside County, California [Ph.D. thesis]: Palo Alto, California, Stanford University, 79 p.

Smith, D.K., Morton, D.M., and Miller, F.K., 1991, Hornblende geobarometry and biotite K-Ar ages from the northern part of the Peninsular Ranges batholith, southern California: Geological Society of America Abstracts with Programs, v. 23, no. 5, p. 273.

Stock, J., 1992, Orientation and Shape of Mafic Enclaves in the Box Springs Mountains Pluton, Riverside and San Bernardino Counties, California [M.S. thesis]: Riverside, California, University of California, 248 p.

Taylor, H.P., 1986, Igneous rocks: II. Isotopic case studies of circum-Pacific magmatism, *in* Valley, J.W., Taylor, H.P., and O'Neil, J.R., eds., Stable Isotopes in High Temperature Geological Process: Mineralogical Society of America Reviews in Mineralogy, v. 16, p. 273–317.

Taylor, H.P., 1988, Oxygen, hydrogen, and strontium isotope constraints on the origin of granites: Transactions of the Royal Society of Edinburgh–Earth Sciences, v. 79, p. 317–338, doi:10.1017/S0263593300014309.

Taylor, H.P., Jr., and Silver, L.T., 1978, Oxygen Isotope Relationships in Plutonic Igneous Rocks of the Peninsular Ranges Batholith, Southern and Baja California: U.S. Geological Survey Open-File Report 78-701, p. 423–426.

Tepper, J.H., Nelson, B.K., Bergantz, G.W., and Irving, A.J., 1993, Petrology of the Chilliwack batholith, North Cascades, Washington: Generation of calc-alkaline granitoids by melting of mafic lower crust with variable water fugacity: Contributions to Mineralogy and Petrology, v. 113, p. 333–351, doi:10.1007/BF00286926.

Theodore, T.G., 1967, Structure and Petrology of the Gneisses and Mylonites at Coyote Mountain, Borrego Springs, California [Ph.D. thesis]: Los Angeles, California, University of California, 268 p.

Theodore, T.G., 1970, Petrogenesis of mylonites of high metamorphic grade in the Peninsular Ranges of southern California: Geologi-

cal Society of America Bulletin, v. 81, p. 435–450, doi:10.1130/0016-7606(1970)81[435:POMOHM]2.0.CO;2.

Thomson, C.N., and Girty, G.H., 1994, Early Cretaceous intra-arc ductile strain in Triassic–Jurassic rocks and Cretaceous continental margin arc rocks, Peninsular Ranges, California: Tectonics, v. 13, p. 1108–1119, doi:10.1029/94TC01649.

Todd, V.R., 2004, Preliminary Geologic Map of the El Cajon 30′ × 60′ Quadrangle, Southern California: U.S. Geological Survey Open-File Report 2004-1361, scale 1:100,000.

Todd, V.R., Erskine, B.G., and Morton, D.M., 1988, Metamorphic and tectonic evolution of the northern Peninsular Ranges batholith, *in* Ernst, W.G., ed., Metamorphism and Crustal Evolution of the Western United States (Rubey Volume VII): Englewood Cliffs, New Jersey, Prentice-Hall, p. 894–937.

Todd, V.R., Shaw, S.E., and Hammarstrom, J.M., 2003, Cretaceous plutons of the Peninsular Ranges batholith, San Diego and westernmost Imperial Counties, California: Intrusion across a Late Jurassic continental margin, *in* Johnson, S.E., Paterson, S.R., Fletcher, J.M., Girty, G.H., Kimbrough, D.L., and Martín-Barajas, A., eds., Tectonic Evolution of Northwestern Mexico and the Southwestern USA: Geological Society of America Special Paper 374, p. 185–235.

Todd, V.R., Hernandez, J.L., and Busch, L.L., 2014, this volume, The zoned Ramona plutonic complex: An Early Cretaceous mid-to-upper crustal intrusive sequence, Peninsular Ranges batholith, southern California, *in* Morton, D.M., and Miller, F.K., eds., Peninsular Ranges Batholith, Baja California and Southern California: Geological Society of America Memoir 211, doi:10.1130/2014.1211(17).

Tulloch, A.J., and Kimbrough, D.L., 2003, Paired plutonic belts in convergent margins and the development of high Sr/Y magmatism: Peninsular Ranges batholith of Baja California and Median batholith of New Zealand, *in* Johnson, S.E., Paterson, S.R., Fletcher, J.M., Girty, G.H., Kimbrough, D.L., and Martín-Barajas, A., eds., Tectonic Evolution of Northwestern Mexico and the Southwestern USA: Geological Society of America Special Paper 374, p. 275–295.

Turi, B., and Taylor, H.P., Jr., 1971, An oxygen and hydrogen isotope study of a granodiorite pluton from the southern California batholith: Geochimica et Cosmochimica Acta, v. 35, p. 383–406, doi:10.1016/0016-7037(71)90080-9.

Wagner, D.L., 2006, Geologic Map of the Tubb Canyon 7.5′ Quadrangle, Eastern San Diego County, California: California Geological Survey Open-File Map 96-06, scale 1:24,000.

Walawender, M.J., 2003, Garnet-bearing granitoids and pegmatite dikes in the Indian Hill–Tule Mountain roof pendant: Implications for the origin of gem-bearing pegmatites in southern California, *in* Murbach, M.L., and Hart, M.W., eds., Geology of the Elsinore Fault Zone, San Diego Region: San Diego, California, San Diego Association of Geologists/South Coast Geological Society, publication 31-2003, p. 27–38.

Walawender, M.J., Gastil, R.G., Clinkenbeard, J.P., McCormick, W.V., Eastman, B.G., Wernicke, R.S., Wardlaw, M.S., and Gunn, S.H., 1990, Origin and evolution of the zoned La Posta–type plutons, eastern Peninsular Ranges batholith, southern and Baja California, *in* Anderson, J.L., ed., The Nature and Origin of Cordilleran Magmatism: Geological Society of America Memoir 174, p. 1–18.

Webb, R.W., 1939a, Evidence of the age of a crystalline limestone, southern California: The Journal of Geology, v. 47, p. 198–201, doi:10.1086/624753.

Webb, R.W., 1939b, Large sphene crystals from San Jacinto Mountains, California: The American Mineralogist, v. 24, p. 344–346.

Webb, R.W., 1943, Two andalusite pegmatites from Riverside County, California: The American Mineralogist, v. 28, p. 581–593.

Weber, F.H., Jr., 1963, Geology and Mineral Resources of San Diego County, California: California Division of Mines and Geology County Report 3, 309 p.

Weber, F.H., Jr., 1976, Preliminary Map of Faults of the Elsinore and Chino Fault Zones in Northeastern Riverside County, California, Showing Accompanying Features Related to Character and Recency of Movement: California Division of Mines and Geology Open-File Report 761 LA, scale 1:12,000.

Wenk, H.-R., 1998, Deformation of mylonites in Palm Canyon, California, based on xenolith geometry: Journal of Structural Geology, v. 20, no. 5, p. 559–571, doi:10.1016/S0191-8141(97)00114-4.

Wenk, H.-R., and Pannetier, J., 1990, Texture development in deformed granodiorites from the Santa Rosa mylonite zone, southern California: Journal of Structural Geology, v. 12, p. 177–184, doi:10.1016/0191-8141(90)90003-H.

Wenner, J.M., and Coleman, D.S., 2004, Magma mixing and Cretaceous crustal growth: Geology and geochemistry of granites in the central Sierra Nevada batholith, California: International Geology Review, v. 46, p. 880–903.

Wetmore, P.H., Herzig, C., Alsleben, H., Sutherland, M., Schmidt, K.L., Schultz, P.W., and Paterson, S.R., 2003, Mesozoic tectonic evolution of the Peninsular Ranges of southern and Baja California, *in* Johnson, S.E., Paterson, S.R., Fletcher, J.M., Girty, G.H., Kimbrough, D.L., and Martín-Barajas, A., eds., Tectonic Evolution of Northwestern Mexico and the Southwestern USA: Geological Society of America Special Paper 374, p. 93–116.

Manuscript Accepted by the Society 11 June 2013

Printed in the USA